Anomalous Dissipation in Bose Gases: Analytic Theory of Energy Damping

Rob Glenn McDonald

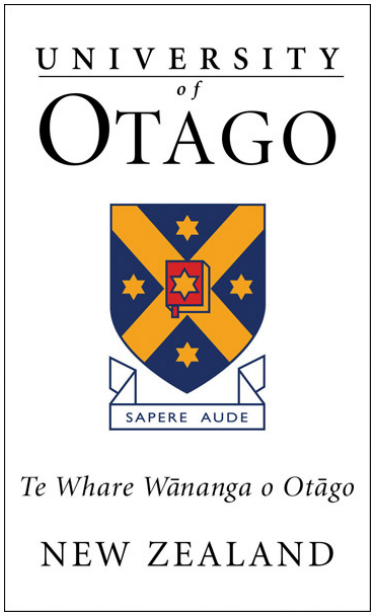

May 2019

A thesis submitted for the degree of

Doctor of Philosophy

at the University of Otago, Dunedin,
New Zealand

Version history

Original version submitted for examination: 31 May, 2019

Revised version submitted following examination: 9 September, 2019

Abstract

The stochastic projected Gross-Pitaevskii equation (SPGPE) is a finite-temperature theory of Bose-Einstein condensate dynamics, utilizing a classical-field approach to describing the dynamics of a low-energy coherent subspace in contact with an incoherent thermal reservoir. Interactions with the reservoir are encapsulated in two distinct processes, known as number damping and energy damping. Historically the energy-damping process has received little attention, at least in part due to difficulty in finding a sufficiently efficient and accurate numerical algorithm for solving the SPGPE. Rooney *et al* [1] developed such an algorithm, providing new opportunities to investigate the energy-damping process. In this work we provide an analytic treatment of the energy-damping process for a range of systems using functional Ito calculus.

We perform a linear fluctuation analysis on the SPGPE for a homogeneous system. We find the dispersion relation to be the usual Bogoliubov dispersion with an additional momentum dependent damping rate. The damping rate is a combination of number- and energy-damping terms with distinct momentum dependence, revealing that each damping process is dominant for excitations of different length scales. We also find the spectra of density and phase fluctuations in momentum space, again with distinct momentum dependence associated with the two damping processes. These results demonstrate that there always exists a regime of length scales where one can expect energy-damping to be the dominant process.

We derive stochastic Ehrenfest relations (SER) from the SPGPE using projected functional change of variables. The SER take the form of stochastic differential equations for matter wave moments of the system and include drift and diffusion terms corresponding to the number- and energy-damping processes. We find that for a well-chosen cutoff the SER can often admit approximate analytic solutions. Analytic solutions of the SER for a quasi-1D Thomas-Fermi system show good agreement with simulations of the 1D SPGPE.

Next, we characterise the centre of mass equilibrium properties of a 3D harmonically trapped finite temperature system in the Thomas-Fermi regime using the SER for position, momentum, and particle number. We find that the energy-damping process is generally dominant over the number-damping process when considering position and momentum fluctuations. Considering the stochastic evolution of particle number in this system, we find that the steady-state fluctuation properties depend only on the number-damping process. This suggests that the effects of each reservoir interaction can be measured individually in the same system, allowing for experimental detection of the energy-damping reservoir interaction.

We finish by considering the motion of a singly-charged quantum vortex confined to a disc trap in an energy-damped system. We find a stochastic differential equation for

the dissipative motion of the vortex. It is revealed that the presence of noise can cause a stabilizing effect on the vortex, extending its lifetime. We also consider the presence of a rotating thermal cloud, a scenario that leads to the vortex becoming the energetically favourable state. This allows for analysis of steady-state stochastic properties of the vortex motion.

Acknowledgements

The completion of this work would not have been possible without the influence of a large number of people. Though I cannot truly convey the depth of each of these individuals contributions in words, I hope to get across some measure of how they have helped me over my time at Otago.

First and foremost, I must extend my gratitude to my supervisor Dr Ashton Bradley. His endless passion for the topic and guidance through the many periods in which I struggled were crucial factors in my ability to continue, and it simply cannot be overstated just how much he helped for this work to reach completion. I could not have hoped for a better supervisor to see me through.

I had many role models in the department throughout my time here, but none more significant than Professor Rob Ballagh. His enthusiasm and encouragement throughout my undergraduate years solidified my desire to carry on and do postgraduate studies in physics. I must also thank him for thinking of me when looking for a demonstrator for PHSI331, a role which I have now enjoyed for a number of years.

I thank the occupants of room 428 for creating a pleasant work environment. There have been many come and go over the last few years, and I will undoubtedly miss someone if I try to list them all, so I will not attempt it. However I will explicitly mention Dr Danny Baillie, Dr Lewis Williamson, Dr Xiaoquan Yu, Dr Matthew Reeves, Dr Samuel Rooney, Dr Luke Symes, and Michael Cawte, for assisting me on a variety of technical problems.

The postgraduate community in the physics department must be one of the best, and made studying here very enjoyable. Again, I cannot possibly mention all the fellow postgraduates who have come through, so I simply extend my thanks to anyone who I have had lunch with! Often I felt like I learned more during our lunchtime discussions than at my desk, and with a healthy dose of humour as well.

When I think about those who have been most significant in my life over my time at university, the first person to come to mind is my good friend Maddy Cormack. These years at university from our Carrington days through to now have been immeasurably improved by your presence, and I feel so lucky to have had such a wonderful person that I can call my friend. I can only hope you feel a fraction of the support from me as I do from you, and I give you my most sincere thanks for your friendship.

I thank my parents, Pam and Glenn, for supporting me in my choice to spend more time at university. They could have quite easily told me to just go get a real job, but they had faith in me that I would carve my own path and for that I am grateful. I also thank my sisters, Kate and Lynn, for their support and encouragement over this time.

Finally to Jay, I don't know that I could have got through this without your constant love and support. There are no words I can find to adequately express just how much it means to me to have had you by my side these last few years. I am truly grateful to you for standing by me through this difficult time, and I am excited to start out on the next phase of our lives together. Also to Subodh and Charu, for accepting me into their family and providing words of encouragement during the latter stages of my studies.

There are many more I have not named here, both in the department and the outside world. To anyone else who has given me kind words or supported me in some way, let it be known that it did not go unnoticed and was very much appreciated.

Contents

Chapter 1

Introduction

1.1 Bose-Einstein condensation

The phenomena now known as Bose-Einstein condensation was first predicted in 1925 by Einstein based on ideas originally developed by Bose for light [3] and extended to bosonic matter by Einstein [4–6]. When a gas of identical bosons is cooled to very low temperatures, a macroscopic amount of identical bosons may transition to the lowest energy mode, forming the Bose-Einstein condensate. This phase transition is purely due to the quantum statistics governing the particles, and is distinct from thermal phase transitions that are due to inter-particle interactions. The Bose-Einstein condensate phase transition is of second order (i.e. the order parameter is continuous across the transition) and occurs when the gas is cooled into the quantum degenerate regime. In an ideal (non-interacting) Bose gas, this occurs when the thermal de-Broglie wavelength of the individual particles becomes comparable to the inter-particle spacing.

The first experimental realization of a Bose-Einstein condensate occurred via the discovery of superfluidity in liquid ^{4}He by Kapitza [7] and Allen and Misener [8], though the connection between Bose-Einstein condensation and superfluidity was not immediately made. Later in the same year, London suggested that the observed superfluid properties of ^{4}He when cooled below the lambda point of $2.17K$ were due to the presence of a Bose-Einstein condensate [9]. Examples of the odd behaviour of superfluids include but are not limited to the fountain effect [10], the existence of quantized vortices [11] and vortex arrays [9], and superfluid creep [12]. Prior to their first experimental realization, quantized vortices in superfluid ^{4}He had been predicted by Onsager [13] and Feynman [14] due to the the irrotational nature of the superfluid velocity field. Quantum vortices are an excellent example of the macroscopic quantum behaviour that is possible due to Bose-Einstein condensates. While the superfluidity of ^{4}He is due to the presence of a Bose-Einstein condensate, and they are certainly related, the superfluid component is not equivalent to the condensate component. At zero temperature ^{4}He is predicted to be entirely superfluid, but

the condensate fraction is only predicted to be ∼8% [15]. The reason for the low condensate fraction is that the strong interactions in ^{4}He gives significant quantum depletion [16]. The low condensate fraction means that superfluid ^{4}He has very limited use as a platform for studying Bose-Einstein condensates, as the non-condensate component is dominant.

1.2 Ultra-cold Bose gases

In 1995, following the advancements in the field of laser cooling throughout the 1980s and 1990s [17–19], Bose-Einstein condensation was achieved in dilute gases of the alkalis rubidium [20], sodium [21], and lithium [22]. In contrast with the strongly interacting ^{4}He, these dilute gases are weakly interacting and thus almost pure condensates can be achieved. The successful formation of Bose-Einstein condensates in these experiments served as a catalyst for the field of ultra-cold Bose gases, stimulating much theoretical and experimental research in the area that continues in earnest to this day. In the intervening years Bose-Einstein condensates have been achieved in dilute gases of many other atomic species, not limited to alkali metals, including ^{1}H [23], ^{85}Rb [24], ^{4}He [25, 26], ^{41}K [27], ^{39}K [28], ^{133}Cs [29], ^{52}Cr [30], ^{40}Ca [31], ^{164}Dy [32], ^{84}Sr [33], ^{86}Sr [34], ^{88}Sr [35], ^{174}Yb [36], ^{170}Yb [37], ^{176}Yb [38], ^{164}Yb [39].

All of the aforementioned examples have concerned condensates formed of single atomic species in a single electronic state. This is by no means the only possible scenario, and indeed there are many examples of Bose-Einstein condensates being formed in more exotic systems. Examples of these include spinor systems [40] used to observe the spin Hall effect [41], two-component systems [42], exciton-polaritons in semiconductor microcavities [43], photons in optical microcavities [44], and magnons in magnetic insulators [45]. The behaviour of these systems are influenced by both the presence of a Bose-Einstein condensate and the exotic nature of the system, making them an interesting area of study in their own right.

The fine control of lasers and magnetic fields possible in modern laboratories allow precise manipulation in dilute gas Bose-Einstein condensate experiments, allowing exploration of a wide range of quantum phenomena. One of the most significant characteristics of Bose-Einstein condensates is the presence of long range quantum coherence[1] [15, 46], a property that was explored in a number of experiments following the initial realization of a Bose-Ein-

[1] In the context of Bose-Einstein condensates, long range quantum coherence manifests as a global phase across the spatial extent of the system.

stein condensate. The presence of long range quantum coherence has been demonstrated via matter wave interference between two expanding condensates [47], coherent four-wave mixing of matter waves [48], and phase-coherent amplification of matter waves [49]. Long range phase coherence has also been measured using Bragg spectroscopy [50] and interference [51], around the Bose-Einstein condensate phase transition [52], and in the phase-fluctuating regime of a quasi-1D condensate [53].

The development of external trapping of dilute gases has been key to the progress of Bose-Einstein condensate research. These traps are typically constructed using magnetic and/or optical techniques [54]. In the past trapping has predominately taken the form of a harmonic potential in three dimensions, but later techniques such as optical painting [55] gave the ability to make essentially custom trapping potentials. As a result the effects of more exotic potentials and geometries can be explored. Dynamics in one or two of the three accessible dimensions can be restricted using very tight confinement, allowing the realization of Bose-Einstein condensation in essentially lower dimensional systems[2] [56]. This has allowed studies of the onset of phase [57] and density [58] fluctuations in one dimension, and of the Berezinskii-Kosterlitz-Thouless transition [59–61] in two dimensions [62–65]. Periodic optical lattices have been used to study many interesting phenomena [66] such as the superfluid to Mott-insulator transition [67] and the collapse and revival of matter waves [68]. The study of persistent superfluid currents is enabled through the realization of toroidal potentials [55, 69–73]. The persistent current itself may be created by angular momentum transfer via Laguerre-Gaussian lasers [74], through the decay of quantum turbulence initiated via stirring [75], or defect formation through the Bose-Einstein condensate phase transition [71]. Homogeneous systems are also accessible through optical box traps [76].

Bose-Einstein condensates in dilute gases provide an excellent platform for the study of dynamical excitations and general condensate dynamics. Experiments have allowed in-depth study of non-equilibrium dynamics associated with condensate growth [77, 78]. Collective modes have been observed, and their frequency at both zero temperature [79] and finite temperate showing damping [80, 81] have been calculated. Various other excitation modes have also been observed, including the scissors mode [82, 83], and quadrupolar and hexadecapolar modes [84].

A Bose-Einstein condensate can also support several types of topological defects. Two prominent examples are vortices [85] and dark solitons [86], which have been observed

[2]The system must retain 3D characteristics such that it can remain globally phase coherent.

in repulsively interacting condensates. Dark solitons were originally created using phase imprinting in an elongated trap [87, 88], and subsequent experiments have explored other methods of formation such as the snake instability [89], formation via flow through a barrier [90], and via the Kibble-Zurek mechanism of defect formation [91]. The dynamical properties of dark solitons have also been explored, including soliton oscillations and interactions [92,93], collisions [94], soliton trains [95], and dark-bright solitons in two-component condensates [96]. In attractively interacting condensates [22] bright solitons have also been observed [97–99].

As evidenced by the number of examples we have listed, which is by no means exhaustive, there are many experimental applications of dilute gas Bose-Einstein condensates, showing that the system provides a unique platform for the observation of many-body quantum phenomena on a macroscopic scale [54]. The theory behind dynamical and equilibrium properties of dilute gas Bose-Einstein condensates is thus an area of great importance. The weak interactions in dilute gases make it feasible to formulate tractable theories from a microscopic derivation that are able to quantitatively describe experimental observations [100]. This gives a significant advantage over other Bose-Einstein condensate systems such as superfluid ^{4}He, where strong interactions make even qualitative comparison between theory and experiment a challenging prospect.

Historically, the usual tool that has been used for the theoretical study of dilute gas Bose-Einstein condensates is the Gross-Pitaevskii equation [101–103]. The Gross-Pitaevskii equation is a mean-field theory for the condensate order parameter ψ, and takes the form of a non-linear partial differential equation

$$i\hbar\frac{\partial\psi(\mathbf{r},t)}{\partial t} = \left(-\frac{\hbar^2\nabla^2}{2m} + V(\mathbf{r},t) + g|\psi(\mathbf{r},t)|^2\right)\psi(\mathbf{r},t) \tag{1.1}$$

where m is the atomic mass, $V(\mathbf{r},t)$ is the external trapping potential, and $g = 4\pi\hbar^2 a_s/m$ parameterizes the strength of two-body interactions, where a_s is the s-wave scattering length which may be positive (repulsive interactions) or negative (attractive interactions).

The Gross-Pitaevskii equation is a generally tractable approach that can be used to describe the coherent evolution of the condensate order parameter. This method assumes that all atoms in the system are represented by a single condensate wave function, and as such the Gross-Pitaevskii equation is only truly valid at zero temperature. In the zero-temperature regime, defined as temperatures significantly below the temperature of the Bose-Einstein condensate transition T_c, the Gross-Pitaevskii equation has been successfully

used to predict a wide range of equilibrium and dynamical properties in trapped dilute gas Bose-Einstein condensate experiments [88, 104, 105].

1.3 Finite temperature regime

Many dilute gas Bose-Einstein condensate experiments are performed in the *finite-temperature* regime, defined as temperatures that are less than but of the same order of magnitude as the Bose-Einstein condensate transition temperature. In this regime there is a significant thermal component present, such that many particles are excited out of the condensate, but the system is still approximately Bose degenerate with an appreciable condensate fraction. This regime can be specified by the condition

$$\epsilon \ll k_B T \tag{1.2}$$

with ϵ the characteristic single-particle energy. For example, in a harmonically trapped system of trapping frequency ω we have $\epsilon = \hbar\omega$. This criterion leads to typical system temperatures of around $0.6T_c$ [106]. In this regime dissipation due to interaction with the thermal component has significant influence on the systems dynamical and equilibrium properties. Experiments commonly consider the dissipative dynamics of Bose-Einstein condensates, such as the decay of collective modes [80], vortex formation and decay [71, 107, 108], condensate growth [77, 78], phase transition dynamics [71], and superfluid turbulence [75].

The highly controllable nature of dilute Bose gas systems make them an excellent platform for investigating finite-temperature dynamics [54]. While the Gross-Pitaevskii equation is extremely useful in the zero-temperature regime, it neglects all the spontaneous and incoherent processes that are significant in the finite-temperature regime. Exact methods may give some insight for very small systems where they are tractable [109], while the positive-P [110] and Monte Carlo [111] techniques may be applied to understand equilibrium properties of larger systems. Developing a quantitative description that may be applied to simulating experiments which incorporates thermal fluctuations and dynamics is a significant challenge [100, 106].

One potential avenue of investigation is the generalization of the Gross-Pitaevskii equation to include a low-energy region consisting of the macroscopically occupied condensate mode in addition to a number of significantly occupied single-particle modes. One of several ways to do this is known as the *classical-field method*, which simulates dynamics of

the low-energy region using the Gross-Pitaevskii equation [112–114]. A more sophisticated approach extends this to include coupling with the higher energy atoms, represented by the addition of noise and damping terms to the Gross-Pitaevskii equation. These stochastic Gross-Pitaevskii equations have seen a range of applications, such as defect formation across phase transitions [71,115–119], decay of vortices [2,120–122] and solitons [123,124], polariton [125] and spinor [126–130] condensates, and equilibrium properties in 3D [131]. The theory has found particular use in lower dimensions where thermal fluctuations may prevent the formation of a true condensate [123,132–142].

While phenomenological arguments can and have been used to obtain a form of stochastic Gross-Pitaevskii equation, it is also possible to derive such an equation from a microscopic theory of the Bose gas. Most prominently such formal derivations have been carried out by the groups of Stoof [132,143,144] and Gardiner [145–147], and have been validated by successfully providing an *ab initio* quantitative and qualitative description of non-equilibrium dynamics.

1.4 Stochastic projected Gross-Pitaevskii equation

In this thesis we make heavy use of the stochastic projected Gross-Pitaevskii equation (SPGPE) as introduced by Gardiner and Davis in 2003 [146]. For simulations we utilize a numerical implementation of the SPGPE devised by Rooney *et al* [1]. The central idea behind the SPGPE is the sub-division of the system into two regions. One is a high-energy region, or *incoherent* region, consisting of modes that are sparsely occupied, while the other is a low-energy region, or *coherent* region, consisting of modes that are significantly occupied and can be treated in a classical field approximation. The low-energy region thus contains not only the condensate, but other modes that are highly Bose degenerate. The high-energy region acts as a thermal reservoir that can exchange energy and particles with the low-energy region and is treated semiclassically. The formalism of the SPGPE makes significant use of the projection operator used to define the two regions; a projection operator appears explicitly in the final equation of motion for the coherent region classical field. The interactions between the coherent and incoherent regions are described by two distinct processes. The *number-damping* process consists of two incoherent region particles interacting and exchanging energy such that one remains in the incoherent region while the other enters the coherent region[3], leading to a change in population of the coherent

[3]The time-reverse process is also included.

region. The *energy-damping* process consists of a particle from each region interacting and exchanging energy such that either both particles stay in the region they began in or they swap regions, such that the population of the coherent region is unchanged. Historically, the number-damping and energy-damping processes have been referred to as growth and scattering processes respectively [146, 148].

The number-damping SPGPE, where the energy-damping process is neglected entirely, was the first to be assigned a numerically tractable method to quantitatively describe finite-temperature dynamics by Bradley *et al* [115], with experimental comparisons quickly following [71]. Methods existing for numerical implementation of the projected Gross-Pitaevskii equation can be relatively easily extended to solve the number-damping SPGPE due to the simplicity of the number damping terms; the damping term is proportional to the Gross-Pitaevskii operator while the noise is additive with local spatial correlations.

The energy-damping terms in the SPGPE present more of a technical challenge. The original derivation of the SPGPE [146] treated the energy-damping terms using a simplified non-local approximation, which was later shown to be exact when the thermal reservoir is treated using a semiclassical approximation [115, 148, 149]. This provided a pathway for the implementation of the energy-damping terms. The challenging nature of the energy-damping is due to the properties of the noise and damping terms; the noise is multiplicative with non-trivial spatial correlations, while the damping term involves a calculation of the current divergence in the coherent region. Neglecting the energy-damping process entirely has been the usual approach, particularly in systems close to equilibrium where it has been argued that the contribution will be small. However it has also been argued that the energy-damping process may have an effect on non-equilibrium scenarios such as condensate growth, vortex dynamics [106], and bright soliton dynamics [150], though to what extent is not clear. Rooney *et al* [1] developed methods for numerically implementing the energy-damping terms, allowing simulation of the full SPGPE.

The main aim of this thesis is to investigate the role energy-damping can play in both equilibrium and non-equilibrium dynamics. Importantly, we approach the SPGPE from an analytic standpoint, gaining insight into the roles of the two damping processes by developing new equations governing the system dynamics. Firstly, we perform a linear fluctuation analysis the SPGPE while retaining the stochastic terms, revealing the roles of the two damping processes in the dispersion, damping, and spectra of density and phase fluctuations. Secondly, we find approximate equations for matter wave moments of the system. In the latter case, the formal elimination of the spatial degree of freedom generally

results in much more simple equations compared to the SPGPE, and approximate analytic solutions may also be found.

1.5 Thesis overview

1.5.1 Aims

- To characterise the effects of the two damping processes, energy-damping and number-damping, by investigating the excitation spectrum and hydrodynamic formulation of the SPGPE. The stochastic nature of the SPGPE is retained in this investigation.

- Extend the method used in our previous work [150] to obtain stochastic Ehrenfest relations for the SPGPE, including both the number-damping and energy-damping processes. The result of this is stochastic equations of motion for several key moments of degenerate Bose gas systems. We use as an example the motion of a quasi-1D harmonically trapped degenerate Bose gas to validate our approach, and use the results to justify a level of approximation that admits analytic solutions.

- To use the stochastic Ehrenfest relations to obtain stochastic equations of motion for moments of some select systems. In particular we fully characterize the centre of mass motion of a harmonically trapped degenerate Bose gas showing the effects of number-damping and energy-damping. We also characterize the motion of a singly-charged vortex in a quasi-2D system.

1.5.2 Outline

- In Chapter 2 we describe the theoretical framework that is used to model finite-temperature Bose-Einstein condensates. This includes the establishment of the various classical-field methods and a description of how they differ in their treatment of reservoir interactions.

- In Chapter 3 we cover our classical-field method of choice, the stochastic projected Gross-Pitaevskii equation. This includes a review of the derivation and a summary of the three distinct sub theories that arise from the consideration of the two reservoir

interaction processes; the SPGPE has both damping processes, the energy-damping SPGPE has only energy-damping, and the number-damping SPGPE has only number-damping. We also consider how to estimate simulation parameters for experimental systems.

- In Chapter 4 we perform a linear fluctuation analysis of the SPGPE for the simple case of a large system of uniform background density. Through this we find the dispersion relation and momentum dependent damping rate, as well as the steady-state fluctuation spectra for density and phase. We consider the relative effects of energy-damping and number-damping.

- In Chapter 5 we develop methods of stochastic projected functional calculus to find stochastic Ehrenfest relations for the SPGPE. We consider a quasi-1D harmonically trapped degenerate Bose gas in the context of these equations, demonstrating how equations of motion for the centre of mass may be found. After justifying the neglect of corrective terms due to the projected formalism, we compare analytic solutions to numerical solutions of the 1D SPGPE.

- In Chapter 6 we use the stochastic Ehrenfest relations for position and momentum to give a complete description of the harmonically trapped Bose gas. We find effective damping rates for the collective motion of the gas corresponding to energy-damping and number-damping. The analytic expressions for the centre of mass position and momentum are found and compared to numerical solutions of the SPGPE. The relative importance of the two damping processes are explored, considering how the values of the rates change for varying experimental parameters. We also consider the steady-state properties of the number of particles in the system. Our collective equations allow a quantitative comparison of the damping rates.

- In Chapter 7 we use the stochastic Ehrenfest relation for angular momentum to characterise the decay of a vortex in a degenerate Bose gas confined to a disc trap. We consider the dissipative effects of the energy-damping reservoir interaction process on the system. We also look at how the predicted motion of the vortex changes upon inclusion of a rotating thermal cloud.

- In Chapter 8 we conclude by summarizing the main results of the thesis and suggesting areas for future research.

Part I

Background

Chapter 2

Classical field theory for finite temperature degenerate Bose gases

2.1 Introduction

The aim of this work is to investigate finite-temperature effects on dynamics and equilibria of Bose degenerate gases using the stochastic projected Gross-Pitaevskii equation (SPGPE), in particular the roles of energy-damping and number-damping. The SPGPE is one of a variety of theoretical methods that extend the Gross-Pitaevskii equation to include finite-temperature effects; an excellent introduction to the many finite-temperature theories is given by Proukakis and Jackson [100]. For the purposes of this thesis, we are interested in the *high-temperature* regime, with temperature approximately in the range $0.6T_c \lesssim T \lesssim 1.1T_c$. Theoretical treatments of dynamics in this regime form two conceptually distinct groups. The classical field methods, of which the SPGPE is one, arise from utilizing a phase-space representation of the many-body quantum field [151]. The second group consists of generalized mean-field theories utilizing a $U(1)$ symmetry-breaking approach. There is also the number-conserving approach [152] which gives a generalized mean-field description while avoiding $U(1)$ symmetry breaking; this falls into neither of the aforementioned groups. In this thesis we concern ourselves predominantly with the classical field methods, introducing the symmetry-breaking and number-conserving approaches as useful points of comparison. In this chapter we summarize classical field theories of the Bose gas. This includes a review of the universal concepts leading to classical field theories and a summary of the differences and applications of the different methods possible from these theories.

We begin in Section 2.2 by considering the effective field theory for a weakly interacting Bose gas and the challenges arising from this description at finite temperatures. Then in Section 2.3 we review the various methods that stem from the classical field approximation. This includes a conceptual overview of the theoretical background of classical field theories

and an outline of the main methods used in practice. In Section 2.4 we briefly summarize the symmetry-breaking and number-conserving approaches and give a comparison with classical field methods. We give a summary of the chapter in Section 2.5.

2.2 Effective field theory for ultra-cold bosons

In this section we introduce the effective field theory for ultra-cold bosons. We consider the cold-collision regime where the two-body interactions are approximated by a delta function potential. This approximation leads to an ultraviolet divergence in the full field theory, and thus necessitates the introduction of an energy cutoff.

2.2.1 Many-body Hamiltonian

We begin with the second quantized Hamiltonian [153] for the Bose field operator $\hat{\Psi}(\mathbf{r},t)$, with commutation relations

$$\left[\hat{\Psi}(\mathbf{r},t),\hat{\Psi}(\mathbf{r}',t)\right]=\left[\hat{\Psi}^{\dagger}(\mathbf{r},t),\hat{\Psi}^{\dagger}(\mathbf{r}',t)\right]=0,\quad\left[\hat{\Psi}(\mathbf{r},t),\hat{\Psi}^{\dagger}(\mathbf{r}',t)\right]=\delta(\mathbf{r}-\mathbf{r}'). \tag{2.1}$$

The many-body Hamiltonian for a system of N particles interacting via a binary interaction is given in second quantized form by [153]

$$\hat{H}=\int d^{3}\mathbf{r}\hat{\Psi}^{\dagger}(\mathbf{r})H_{\rm sp}\hat{\Psi}(\mathbf{r})+\frac{1}{2}\int d^{3}\mathbf{r}\int d^{3}\mathbf{r}'\hat{\Psi}^{\dagger}(\mathbf{r})\hat{\Psi}^{\dagger}(\mathbf{r}')U(\mathbf{r}-\mathbf{r}')\hat{\Psi}(\mathbf{r}')\hat{\Psi}(\mathbf{r}) \tag{2.2}$$

where $U(\mathbf{r}-\mathbf{r}')$ is the two-body interaction potential, and the single-particle Hamiltonian is

$$H_{\rm sp}=-\frac{\hbar^{2}}{2m}\nabla^{2}+V_{\rm ext}(\mathbf{r}), \tag{2.3}$$

which only takes into the account the kinetic energy and effect of the external trapping potential $V_{\rm ext}(\mathbf{r})$ on the individual particles.

2.2.2 Cold-collision regime

The two-body interaction potential $U(\mathbf{r}-\mathbf{r}')$ depends only on the displacement vector between the particles, and the magnitude of the interaction can generally be characterized by some effective range parameter r_0. In a Bose-Einstein condensate of a dilute bosonic

gas, the length scales of interest are much larger than r_0, provided there is no long-range interparticle interactions such as those due to magnetic dipoles, as the de Broglie wavelength becomes much larger than the mean interparticle separation. Thus only low energy binary atomic interactions are important, and the interactions may be characterized by the s-wave scattering length [154–156]. This is known as the *cold-collision* regime, and the two-body interaction potential is approximated by a delta function

$$U(\mathbf{r}-\mathbf{r}') = g\delta(\mathbf{r}-\mathbf{r}') \tag{2.4}$$

where the interaction strength g is

$$g = \frac{4\pi\hbar^2 a_s}{m} \tag{2.5}$$

with a_s the s-wave scattering length and m the atomic mass. The effective Hamiltonian for the cold-collision regime is thus

$$\hat{H} = \int d^3\mathbf{r}\hat{\Psi}^\dagger(\mathbf{r})H_{\rm sp}\hat{\Psi}(\mathbf{r}) + \frac{g}{2}\int d^3\mathbf{r}\hat{\Psi}^\dagger(\mathbf{r})\hat{\Psi}^\dagger(\mathbf{r})\hat{\Psi}(\mathbf{r})\hat{\Psi}(\mathbf{r}). \tag{2.6}$$

The dynamics of the effective field are described by the Heisenberg equation of motion

$$i\hbar\frac{\partial\hat{\Psi}(\mathbf{r})}{\partial t} = H_{\rm sp}\hat{\Psi}(\mathbf{r}) + g\hat{\Psi}^\dagger(\mathbf{r})\hat{\Psi}(\mathbf{r})\hat{\Psi}(\mathbf{r}). \tag{2.7}$$

In principle we are finished: (2.7) can tell us the dynamics of any Bose condensed system in the cold-collisional regime. However the solution in this form is generally intractable, as the Hilbert space is prohibitively large. To understand this, we comment briefly on how we arrive at the effective field theory. We impose an energy cutoff $E_{\rm max}$ on the system, such that all modes outside of a low-energy subspace are neglected. An immediate consequence of this is that the Bose commutation relations are no longer a pure delta function, but instead take the form of a coarse-grained delta

$$\left[\hat{\Psi}(\mathbf{r},t),\hat{\Psi}^\dagger(\mathbf{r}',t)\right] = \delta_\Delta(\mathbf{r},\mathbf{r}') \tag{2.8}$$

where Δ represents the region with modes of energy less than $E_{\max}$. For an effective field theory to be an accurate representation of the system, we require that

$$E_{\max} \ll \frac{\hbar^2}{2mr_0^2}, \tag{2.9}$$

and

$$E_{\max} \gg k_B T, \mu, \tag{2.10}$$

such that using the effective interaction potential (2.4) is valid [106]. The first condition (2.9) allows any effect of short-wavelength components of the wave function that exist in the interaction region to be neglected. The second condition (2.10) ensures that the neglected modes will be sufficiently unpopulated such that they will be unaffected by thermal or interaction effects. Together these conditions allow for a two-body description of the interactions; if these conditions go unsatisfied then a description using a modified many-body T-matrix is required [144].

As a result of imposing these conditions on $E_{\max}$, the size of Δ becomes too large to realistically perform any kind of numerical calculations. When an accurate description of finite-temperature dynamics becomes important this is especially problematic, as there are then many modes within the low-energy subspace that give significant contribution to the overall dynamics and therefore cannot be neglected. The classical field approach provides a numerical method for finding approximate solutions to the Heisenberg equation of motion. In the following section we review this approach.

2.3 Classical field methods

In this section we review the different theories used to describe Bose-Einstein condensates that stem from a classical field approach. These theories arise from a phase-space representation of the effective field theory. First we provide a conceptual overview of phase-space methods, before motivating the use of the classical field approximation. We review the broad theoretical background behind classical field methods, and outline the main methods that are used in practice. Along with this we give a brief review of the key applications of these methods.

2.3.1 Overview

Phase-space methods

Solving the Heisenberg operator equation of motion for the entire many-body quantum field is generally impossible due to the large Hilbert space. Phase-space methods offer a more tractable method for studying the dissipative dynamics of a complete quantum field [157], using the fact that the quantum density operator $\hat{\rho}$ may be represented as a quasi-probability function $P(\mathbf{r}, \mathbf{k})$ of classical phase-space variables. This relationship between quantum and classical variables [158] allows for the existence of an equation of motion for the quasi-probability distribution. The central idea of phase-space methods is that under certain conditions, the equation of motion for the quasi-probability distribution takes the form of a Fokker-Planck equation with a positive-definite diffusion matrix. The Fokker-Planck equation for the quantum phase space distribution may then be mapped to an equivalent stochastic differential equation for a classical field, so that the evolution of the quantum field is described in terms of a classical field equation of motion.

Phase-space methods were originally formulated for quantum optics research, where several approaches have been used that differ in the choice of quasi-probability function representing the quantum field [157]. These approaches, known as the P-, Q-, and Wigner representations, differ by the choice of operator ordering [157]. While the phase-space methods may appear to be classical, in general the equations of motion are driven by stochastic processes representing both thermal and quantum fluctuations of quantum field. Operator averages are obtained by averaging over ensembles of trajectories, such that the ensemble statistics from classical fields correspond to those of the quantum field.

More recently, phase-space methods have been applied to research on Bose-Einstein condensates in the presence of thermal and quantum fluctuations [106, 151, 159]. Utilizing the Wigner representation leads to what is known as the classical field methods. In this group of methods, beyond mean field effects are, to a good approximation, described by a Gross-Pitaevskii equation with additional noise and damping terms. An alternative approach based on the P representation leads to the positive P method [160], which is in principle exact but in practice is numerically unstable.

Motivation for the classical field approximation

Classical field methods utilize a Wigner representation of the quantum field to give dynamics of classically occupied single-particle modes of a finite temperature Bose field. The

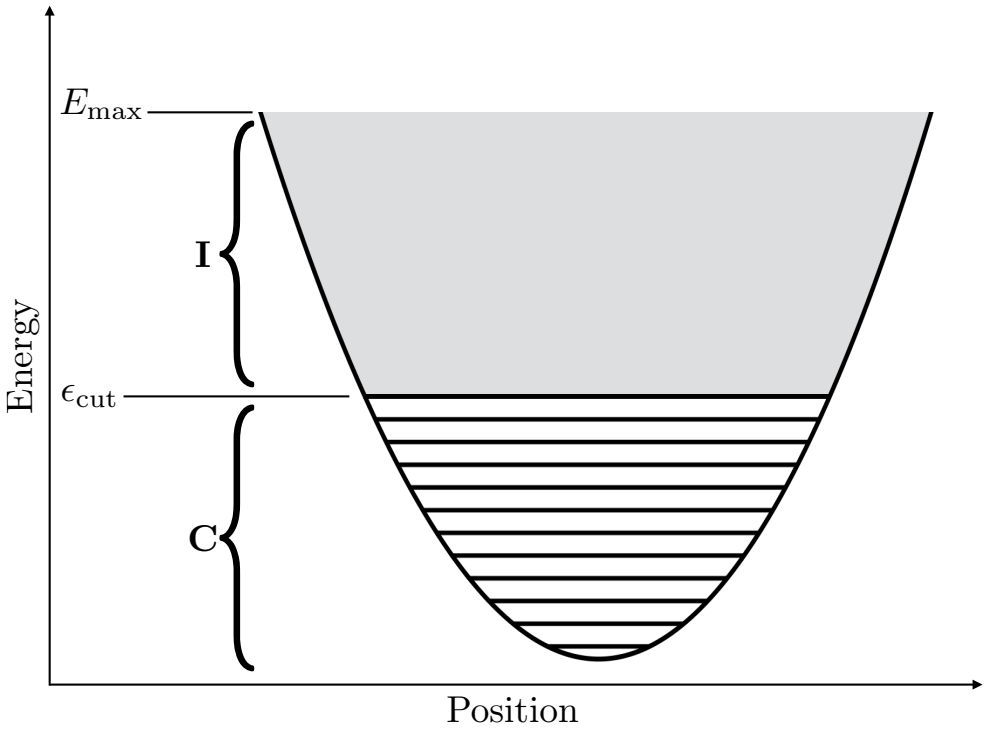

Figure 2.1: A schematic showing the coherent region **C**, incoherent region **I**, and states eliminated to give the effective field theory. In the stochastic Gross-Pitaevskii equation, the coherent region is treated quantum mechanically in a classical field approximation. The incoherent region is treated semiclassically, and is most simply described as a grand canonical reservoir.

foundation of the methods is the separation of the Bose field operator into two regions defined by energy; the separation is formally applied using a projection operator. The low-energy region contains the single-particle modes with significant occupation; this region is known primarily as the *coherent region*, but may also be referred to as the C-region or C-field. The high-energy region contains the single-particle modes with sparse occupation; this region is known primarily as the *incoherent region*, but may also be referred to as the I-region or I-field. A visual representation of the separation may be seen in Fig. 2.1 in the context of single-particle modes of the harmonic oscillator potential. The separation is always introduced in the single-particle basis as the full Hamiltonian is approximately diagonal at high energies for this choice of basis.

An energy cutoff is chosen such that the average occupation of modes in the coherent region is significantly greater than one particle per mode, that is, they are said to be classically occupied. In this regime, the presence of strong interactions and correlations cause

coupling between the single-particle states, and thus in this regime the coherent region can not be understood purely in terms of the the single-particle modes. However, classical occupation of the single-particle modes allows the neglect of quantum fluctuations; the non-trivial dynamics and correlations in the coherent region are predominantly due to interaction between the various modes rather than any effects due to quantization of the low-energy modes. This neglect of quantum fluctuations in the coherent region is what is known as the *classical field approximation*, and leads to a tractable Gross-Pitaevskii like description of the coherent region dynamics where interactions are treated non-perturbatively. The range of classical field methods have different regimes of validity, but all share the basic treatment of a Gross-Pitaevskii equation describing evolution of a set of highly occupied low-energy modes; what distinguishes the various methods is the way in which the reservoir interactions are treated.

2.3.2 Classical field theory

The field operator is expanded on a basis of single-particle states

$$\hat{\Psi}(\mathbf{r}) = \sum_n \hat{a}_n \chi_n(\mathbf{r}) \tag{2.11}$$

where the single-particle eigenstates $\chi_n(\mathbf{r})$ are solutions of

$$\epsilon_n \chi_n(\mathbf{r}) = H_{\rm sp} \chi_n(\mathbf{r}), \tag{2.12}$$

the operators $\hat{a}_n$ obey the Bose commutation relations

$$[\hat{a}_n, \hat{a}_m^\dagger] = \delta_{nm}, \tag{2.13}$$

n represents all quantum numbers required to fully define the single-particle states, and the summation includes all single-particle states with energy less than the effective-field theory energy cutoff $E_{\rm max}$. The system is formally split into the coherent and incoherent regions using projection operators, or *projectors*, defined by

$$\mathcal{P}\left\{F(\mathbf{r})\right\} \equiv \sum_{n\in\mathbf{C}} \chi_n(\mathbf{r}) \int d^3\mathbf{r}' \chi_n^*(\mathbf{r}') F(\mathbf{r}) \tag{2.14}$$

$$\mathcal{Q}\left\{F(\mathbf{r})\right\} \equiv \sum_{n\in\mathbf{I}} \chi_n(\mathbf{r}) \int d^3\mathbf{r}' \chi_n^*(\mathbf{r}') F(\mathbf{r}), \tag{2.15}$$

where the regions are defined by

$$\mathbf{C} = \{n : \epsilon_n \leq \epsilon_{\rm cut}\} \tag{2.16}$$

$$\mathbf{I} = \{n : \epsilon_{\rm cut} < \epsilon_n \leq E_{\rm max}\} \tag{2.17}$$

where $\epsilon_{\rm cut}$ is the single-particle cutoff energy. The projectors have the following properties

$$\mathcal{P}\{\mathcal{Q}\{F(\mathbf{r})\}\} = \mathcal{Q}\{\mathcal{P}\{F(\mathbf{r})\}\} = 0 \tag{2.18}$$

$$\mathcal{P}\{\mathcal{P}\{F(\mathbf{r})\}\} = \mathcal{P}\{F(\mathbf{r})\} \tag{2.19}$$

$$\mathcal{P}\{F(\mathbf{r})\} + \mathcal{Q}\{F(\mathbf{r})\} = F(\mathbf{r}). \tag{2.20}$$

The field operator (2.11) can now be decomposed into coherent ($\hat{\psi}$) and incoherent ($\hat{\phi}$) field operators using the projectors

$$\hat{\Psi}(\mathbf{r}) = \hat{\psi}(\mathbf{r}) + \hat{\phi}(\mathbf{r}) \tag{2.21}$$

where

$$\hat{\psi}(\mathbf{r}) = \mathcal{P}\left\{\hat{\Psi}(\mathbf{r})\right\} = \sum_{n\in\mathbf{C}} \hat{a}_n \chi_n(\mathbf{r}), \tag{2.22}$$

$$\hat{\phi}(\mathbf{r}) = \mathcal{Q}\left\{\hat{\Psi}(\mathbf{r})\right\} = \sum_{n\in\mathbf{I}} \hat{a}_n \chi_n(\mathbf{r}), \tag{2.23}$$

are the coherent region field operator and incoherent region field operator respectively. At times it is helpful to represent the projector as an operator

$$\hat{\mathcal{P}} = \sum_{n\in\mathbf{C}} |n\rangle\langle n| \tag{2.24}$$

where $\langle \mathbf{r}|n\rangle = \chi_n(\mathbf{r})$ are the single particle basis kets. Substituting the separated field operator (2.21) into the cold-collisional Hamiltonian (2.6) allows us to decompose it into three terms

$$\hat{H} = \hat{H}_0 + \hat{H}_{\mathbf{I}} + \hat{H}_{\rm int}, \tag{2.25}$$

where $\hat{H}_0$ comprises all terms containing solely coherent region operators[1], $\hat{H}_{\mathbf{I}}$ comprises all terms containing solely incoherent region operators, and $\hat{H}_{\text{int}}$ comprises all terms containing both coherent and incoherent region operators and thus describes the interactions between the two regions. The purpose of the classical field methods is to describe evolution of the coherent region. In the following three sections we will discuss three different classical field methods, all differing based on the treatment of the interaction Hamiltonian term $\hat{H}_{\text{int}}$ [106].

2.3.3 Truncated Wigner Gross-Pitaevskii equation

The truncated Wigner method is a natural starting point for discussion of the classical field methods, as it provides the foundation of all classical field methods. This method provides a description of quantum fluctuations on sparsely occupied modes, and was the first successful application of the Wigner representation to describe quantum dynamics in Bose-Einstein condensates [151].

The truncated Wigner method includes the effects of vacuum noise on a cold condensate by evolving an ensemble of trajectories of the Gross-Pitaevskii equation. In the language of our projected field theory, the coherent region is evolved in isolation, with no dynamic effects from interaction with the incoherent region included. Instead, beyond mean-field effects arise from initial fluctuations that are seeded into the system. Essential to this method is the accurate sampling of the initial Wigner distribution of the system. In practice, this is done by seeding the single-particle or Bogoliubov modes [161–163] with an average of half a quantum per mode to represent quantum fluctuations [106, 164].

This approach may be formally obtained by consideration of a master equation for the coherent region density operator only under the action of the Hamiltonian H_0. This is then followed by the usual phase-space procedure, where the density operator is represented by the Wigner quasi-probability distribution. This leads to an equation of motion for the Wigner function. This equation of motion does not take the form of a Fokker-Planck equation as it contains third order derivatives of the distribution. Neglecting the third order derivatives is known as the *truncated-Wigner approximation*, valid when the coherent region modes are highly occupied, and it is an essential component of all classical field methods utilizing the Wigner representation. Applying this approximation leaves us with

[1]Note that $\hat{H}_0$ does not include all Hamiltonian evolution of the coherent region, as there is a forward scattering contribution due to interaction with the thermal cloud. This is accounted for in the coherent region Hamiltonian $\hat{H}_{\mathbf{C}}$, which we define in the next chapter.

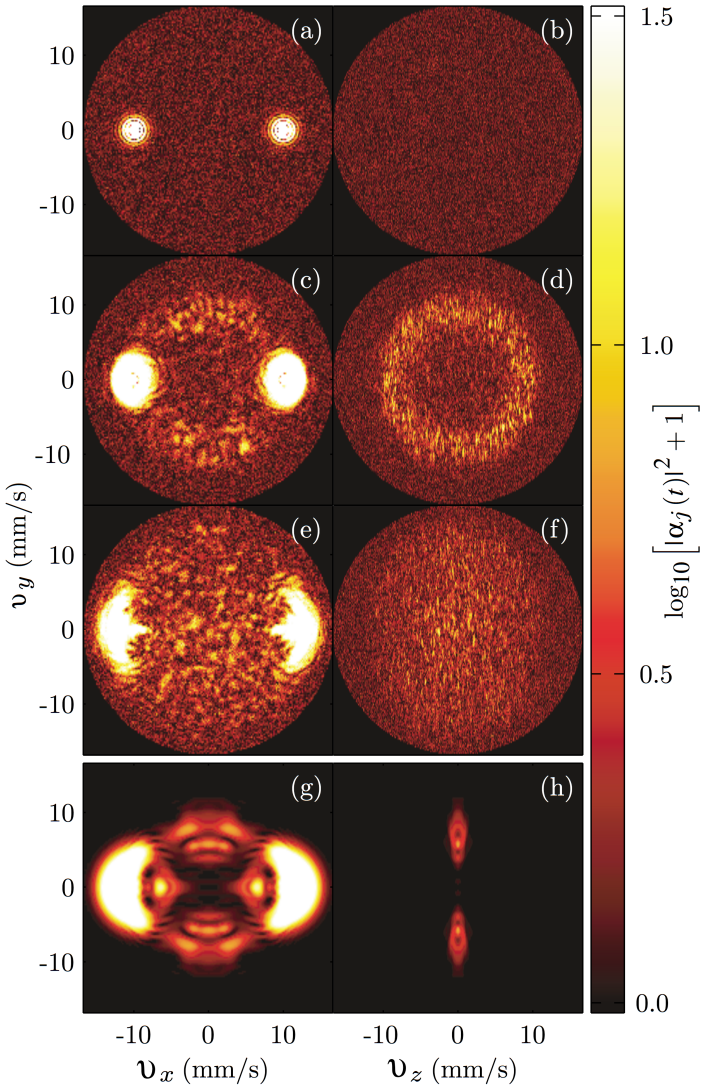

Figure 2.2: (a)-(f) Velocity mode populations on the planes $v_z = 0$ (left) and $v_x = 0$ (right) for the condensate collision described in the text at $t = 0$ (top), $t = 0.5$ ms (middle), and $t = 2.0$ ms (bottom). The spherical momentum cutoff is clearly visible in the upper plots due to the presence of quantum fluctuations. (g)-(h) Mode populations at $t = 2.0$ ms for an identical collision excluding vacuum noise. Reproduced from [165].

a Fokker-Planck equation, which can then be mapped to an equation of motion for the classical field. This equation is known as the *truncated-Wigner Gross-Pitaevskii equation*, a somewhat misleading name as the equation itself is exactly the classical Gross-Pitaevskii equation; the distinction lies in the use of an ensemble of specific initial conditions.

The applicability of the truncated-Wigner Gross-Pitaevskii equation in the finite-temperature regime may be questioned, as the method includes single-particle modes with vacuum occupation. An argument for the validity of the truncated-Wigner approximation

is presented by Norrie *et al* [166]; the method is valid in the regime where the spatial condensate density is very large compared to the density of the added quantum fluctuations. The truncated-Wigner approximation also arises as the first quantum correction to the classical Gross-Pitaevskii equation [167]. When using the truncated-Wigner Gross-Pitaevskii equation, one must take care when when considering evolution over long time scales, as virtual particles may cause spurious thermalization of the classical field under Gross-Pitaevskii evolution [164].

The first application of the truncated-Wigner Gross-Pitaevskii equation was by Steel *et al* [151], who considered a one-dimensional homogeneous condensate. Since then this method has found application in many systems where beyond mean-field effects are important. An excellent example of a system where there is a clear departure from the mean-field theory is the collision of two Bose-Einstein condensates. This was studied using the truncated-Wigner Gross-Pitaevskii equation by Norrie *et al* [165, 166], where this was also compared to simulations using the mean-field theory. In a collision between two condensates, atom pairs are scattered onto a spherical shell in momentum space creating an S-wave halo where energy are conserved. The halo arises due to incoherent and spontaneous scattering and is therefore not able to be replicated by a mean-field description. In Fig. 2.2 the result of Norrie *et al* [165] is shown, where as predicted the halo is only present in truncated-Wigner simulations.

The truncated-Wigner Gross-Pitaevskii equation has been used to describe a variety of systems and phenomena including three-body recombination [168], condensate reflection [169], quantum de Laval nozzles [170], supersonic condensate transport [171], atom chip interferometry [172], collapsing condensates [173], vortex lattice formation [174, 175], and dark solitons [176, 177]. The study of bright solitons has utilized distinct approaches for sampling of the initial Wigner function, such as assuming a coherent initial state [178] or sampling of Bogoliubov modes [179]. The effect of quantum fluctuations on bright solitons has been studied by sampling initial fluctuations in the soliton centre of mass distribution [180, 181].

2.3.4 Projected Gross-Pitaevskii equation

The *projected Gross-Pitaevskii equation* results from a treatment of the coherent region in isolation while the incoherent mode is neglected entirely, that is, there is no interaction between the two regions. This approach, as described by Davis and others [112, 182–184], is valid in the classical regime where all modes in the coherent region are macroscopi-

cally occupied. Svistunov first suggested the use of a Gross-Pitaevskii method to describe degenerate finite-temperature systems in 1991 [185], and this was followed by several theoretical [186–188] and numerical [182, 189] works further developing the idea.

The projected Gross-Pitaevskii equation can be obtained by replacing the coherent region field operator (2.22) with a classical field, that is, making the substitution

$$\hat{\psi}(\mathbf{r},t) \to \psi(\mathbf{r},t) = \sum_{n\in\mathbf{C}} c_n(t)\chi_n(\mathbf{r}). \tag{2.26}$$

Ultimately, the substitution consists of replacing the set of operators $\{\hat{a}_n\}$ with complex numbers $\{c_n\}$, the magnitude of which gives the occupancy of the modes. Applying (2.26) to the coherent region Hamiltonian H_0 gives the Gross-Pitaevskii energy functional, then taking the projected functional derivative[2] of this gives the projected Gross-Pitaevskii equation

$$\frac{\partial\psi(\mathbf{r},t)}{\partial t} = \mathcal{P}\left\{\left(H_{\rm sp} + g\left|\psi(\mathbf{r},t)\right|^2\right)\psi(\mathbf{r},t)\right\}. \tag{2.27}$$

The projected Gross-Pitaevskii equation can also can be found using the Wigner representation of the coherent region. In the classical limit the third-order derivative terms in the Wigner distribution equation of motion identically go to zero. Furthermore, in this limit the commutation relations may be neglected. Clearly the truncated Wigner approximation is valid in this case, and the resulting truncated-Wigner Gross-Pitaevskii equation is identical to the projected Gross-Pitaevskii equation.

The projected Gross-Pitaevskii equation gives a microcanonical description of coherent region dynamics. The evolution of the classical field is formally Hamiltonian, and all first integrals of the system are conserved (e.g. normalization, energy, momentum) [112, 183, 184]. The nonlinear interactions between modes in the coherent region generate ergodic dynamics, allowing the projected Gross-Pitaevskii equation to describe the complex interactions of fluctuating coherent region atoms non-perturbatively [106]. The projected Gross-Pitaevskii equation is thus able to give a quantitatively accurate description of finite temperature systems in or near equilibrium, with the caveat that the reservoir interaction is insignificant. Significantly, the projected Gross-Pitaevskii equation was shown to accurately replicate the departure of the critical temperature in a harmonically trapped Bose gas from the ideal gas prediction [190].

[2] This modification of functional differentiation is defined in Section 3.4.1.

The projected Gross-Pitaevskii equation has seen wide application over a variety of systems. Early studies considered the thermalization and equilibrium properties of homogeneous Bose gases [112, 184, 191]. This was followed by the application of the method to trapped systems [192, 193], where many quantities of interest were explored including two-point correlations [194], critical properties [195], and temporal coherence [196]. It has been shown that the nonlinear classical field dynamics includes a full account of many-body processes within the classical field approximation [197]. Studies of Bose gas dynamics have considered collective modes [198], vortex nucleation [175], and the rotating to non-rotating transition [197].

A crucial aspect of the projected Gross-Pitaevskii equation is the formal implementation of the projector in terms of the single-particle modes. There have been other implementations of the Hamiltonian classical-field method without such a formal implementation, however the use of a finite grid [199] means that an implicit projection is still incorporated. Such an approach has been used to consider quadrupole oscillations in three dimensions [200] and spontaneous soliton formation is a quasi-1D system [201].

2.3.5 Stochastic Gross-Pitaevskii theory

The inclusion of interactions between the incoherent and coherent regions leads to what is known as *stochastic Gross-Pitaevskii theory*, where the equation of motion takes the form of a stochastic differential equation for the classical field. There are two distinct methods that fall under this banner. The *stochastic projected Gross-Pitaevskii equation*, introduced by Gardiner and others [145–147, 149], stems from utilizing a phase-space method, while the *Stoof stochastic Gross-Pitaevskii equation* of Stoof *et al* [144] utilizes the Keldysh path-integral formalism.

Stochastic projected Gross-Pitaevskii equation: Phase-space approach

The stochastic projected Gross-Pitaevskii equation (SPGPE) is a grand-canonical theory of finite temperature Bose gases that makes use of the truncated Wigner approximation and extends the projected Gross-Pitaevskii equation to include the interactions between the incoherent and coherent regions. The interaction is treated using standard methods of open quantum systems [157, 202], with the incoherent region is treated as a thermal reservoir in equilibrium with temperature T and chemical potential μ. In these methods the reservoir degrees of freedom are traced out and a phase-space approach leads to a

stochastic differential equation for the classical field.

The seeds of the theory that would become the SPGPE are present in a series of seven papers by Gardiner *et al* regarding the quantum kinetic theory of Bose-Einstein condensation [203–209], an approach that successfully replicated observations of condensate formation and growth in select experimental systems [210, 211]. The use of the random phase approximation in quantum kinetic theory, essentially neglecting coherences between low energy modes, imposes significant restrictions on the range of validity. In particular, in regimes where quasi-condensation may be important, the application of quantum kinetic theory could not accurately predict experimentally observed condensate growth [78].

Instead of the random phase approximation, the SPGPE as formulated by Gardiner *et al* [145–147,149] relies on the truncated-Wigner approximation, and as such is valid for high temperature systems. The method is a unification of the reservoir treatment considered in the quantum kinetic theory and the projected Gross-Pitaevskii equation. Ultimately the SPGPE takes the form of the projected Gross-Pitaevskii equation with additional noise and damping terms. Thus the method serves as an extension of the projected Gross-Pitaevskii equation allowing the quantitative description of non-equilibrium dynamics. Treating the incoherent region as a semiclassical thermal reservoir allows the damping rates to be analytically calculated, and thus an *ab initio* description of non-equilibrium dissipative dynamics is possible. Temperature and chemical potential are control parameters in the theory, thus equilibrium states are more easily produced compared to the projected Gross-Pitaevskii equation [2], and as such the SPGPE is also useful for studying equilibrium properties of the coherent region.

There are two distinct dissipative processes describing interactions between the reservoir and coherent region, shown in Fig. 2.3, each giving a noise term and a damping term in the SPGPE. The *number-damping* process involves the interaction between two incoherent region particles where energy and momenta are exchanged such that one of the particles enters the coherent region. The reverse process is also included, where there is net particle loss in the coherent region. The *energy-damping* process involves the interaction between one incoherent region particle and one coherent region particle where energy and momenta are exchanged such that there is no net transfer of particles between the regions. The particles may remain in the respective region they began in, or they may exchange places. One might suggest that there is a third reservoir interaction process, where two coherent region particles interact resulting in one particle entering the incoherent region, however

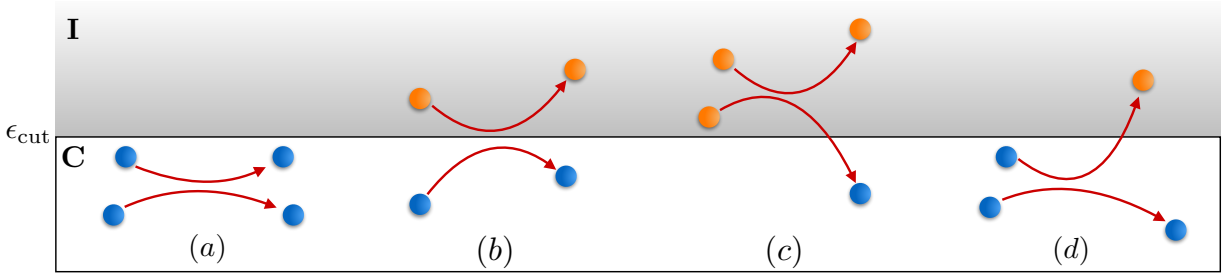

Figure 2.3: A schematic describing the various interparticle interactions accounted for in the SPGPE, where $\epsilon_{\rm cut}$ is the energy cutoff defining the coherent (**C**) and incoherent (**I**) regions. The incoherent region is considered to be a thermal reservoir defined by the temperature T and chemical potential μ. (a) Non-linear mixing interaction in the coherent region. This is the result of Hamiltonian evolution of the coherent region. There is no transfer of energy, momenta, or particles between the two regions. (b) The energy-damping process, where one particle from the coherent region interacts with one particle from the reservoir resulting in energy and momenta exchange such that there is no net movement of particles between the regions, The two particles may swap regions. (c) The number-damping process, where two particles from the reservoir interact resulting in energy and momenta exchange such that one of the particles enters the coherent region. The reverse process also occurs.(d) A third reservoir interaction process, where two particles from the coherent region interact resulting in energy and momenta exchange such that one particle enters the reservoir. The rate of this process is formally zero.

the rate of this process is formally zero[3]. In the literature the number-damping process has frequently been referred to as the *growth* process, while the energy-damping process has been referred to as the *scattering* process [146, 148]. This is a misleading terminology, as both processes are fundamentally scattering processes, and so we eschew this in favor of the number-damping/energy-damping terminology.

Historically, most studies utilizing simulations of the SPGPE have neglected the energy-damping terms. The resulting equation is most commonly known as the *simple-growth SPGPE*, however we will refer to it as the *number-damping SPGPE* to keep in line with our terminology. This sub-theory of the SPGPE is closely related to Ginzburg-Landau ϕ^4 theory [212, 213]. The use of the number-damping SPGPE as opposed to the full SPGPE has been justified using several lines of reasoning:

(i) The number-damping process is a grand canonical reservoir interaction, and so equilibrium states of the number-damping SPGPE sample the same grand canonical ensemble as the the full SPGPE. On the other hand, the energy-damping process is a canonical reservoir interaction, and so should have no effect on the grand canonical

[3] See Section 3.3.3.

equilibrium achieved in the full SPGPE.

(ii) The damping term relating to the energy-damping process is (approximately) proportional to the divergence of the coherent region current, which is expected to be small near equilibrium.

(iii) The inclusion of energy-damping may not qualitatively effect the observed physics of the system. In quantum kinetic theory, an energy-damping process was seen to have a quantitative effect on condensate growth dynamics, but this could also be accounted for by renormalizing the rate of number-damping [208, 214].

(iv) The numerical implementation of the energy-damping terms is rather technically challenging. This is due to the dependence on the divergence of the coherent region current in the damping term, and also the multiplicative nature of the noise. In contrast, the number-damping process is fairly simple to implement, with the damping term being proportional to the Gross-Pitaevskii operator and the noise being additive. This is possibly the most significant reason for the use of the number-damping SPGPE.

The number-damping SPGPE was first numerically implemented to study vortex lattice formation following condensation of a rotating thermal cloud [115], and has since seen significant use in a wide range of systems. Examples include spontaneous vortex formation via the Kibble-Zurek mechanism [71], vortex decay [2, 120], equilibrium properties in 1D [140] and 3D [131], and the study of dipolar systems [215].

There are however a variety of systems and scenarios where the neglect of energy-damping terms is not justified. Since the deterministic energy-damping term is dependent on the coherent region current divergence, it is likely that energy-damping is important in non-equilibrium systems. Energy-damping has been shown to lead to phase diffusion [216], has been been identified as the driver of superfluid internal convection [217] and dissipation in negative differential conductivity experiments [218], and may play a central role in vortex decay [122]. More recent studies utilizing the SPGPE have included the effects of energy-damping, both in addition to number-damping [119, 122, 148] or in systems where number-damping is neglected [150]. The full SPGPE including the energy-damping terms was first numerically implemented by Rooney *et al* [1, 148], who showed that the evolution to equilibrium is significantly altered from the number-damping only case.

Stochastic Gross-Pitaevskii equation: Keldysh path-integral approach

An alternative method for including the stochastic interactions between the thermal reservoir and condensate was formulated by Stoof *et al* [144]. In this approach a Fokker-Planck equation for the probability distribution of the condensate order parameter is derived within the Keldysh path-integral framework, which is then mapped to a stochastic Gross-Pitaevskii equation for the order parameter. We refer to the resulting equation of motion as the *Stoof stochastic Gross-Pitaevskii equation* or Stoof SGPE. This method has seen considerable use in one dimension, describing phenomena such as reversible formation of condensates [132], calculation of collective-mode damping rates [133] and spatial correlations [135], the interplay of density and phase fluctuations [134], and quasicondensate growth on an atom chip [136]. Equilibrium properties of the Stoof SGPE have been compared with the number-conserving Bogoliubov approach [138], and also with experimental observations with respect to density profiles and fluctuations [139] and temperature dependence of phase coherence [141].

The Keldysh path-integral approach is very closely related to the phase-space approach, as both result in a stochastic differential equation for a classical field with a reservoir interaction driving dissipation. There is a technical difference in the Wigner phase-space representation used in the SPGPE, but this is not physically significant. There are however several key conceptual differences between the two theories. In the Keldysh path-integral approach the cutoff defining the reservoir is relatively low, such that the reservoir contains all modes with energy larger than the chemical potential. Consequently, the contact interaction approximation in the cold-collision regime is inappropriate and a full many-body T-matrix must be used to calculate self-energy functions appearing in the Fokker-Planck equation. Furthermore the classical field then contains significantly fewer modes than in the SPGPE, typically just the condensate mode and only a few low-energy excitations; in the projected formalism the classical field typically contains $10^3 - 10^4$ single-particle modes [193] corresponding to a cutoff of around 3μ [106]. The Stoof SGPE only includes a number-damping reservoir interaction; the energy-damping process cannot be consistently included as a result of the low-energy cutoff.

It is unclear how important the conceptual differences between the two approaches are in practice. Evidence suggests that the two theories will closely agree in equilibrium [219]. Numerical results of both theories have been compared favorably to experiments involving quasi-1D Bose gases [140, 142, 220], corroborating the equilibrium convergence of the two theories, at least in the one dimensional regime. Indeed, both approaches are functionally

equivalent when both the projector and energy-damping process are neglected [100]. In higher dimensions beyond 1D, the inclusion of the projector is essential in treatment of the ultraviolet divergence [146] and cannot be neglected. Also, the role of energy-damping in finite temperature dynamics is yet to be fully understood; investigating the importance of these terms may give insight into the differences between the SPGPE and the Stoof SGPE.

Damped Gross-Pitaevskii equation: a limiting case

Dynamics of finite temperature-Bose-Einstein condensates have commonly been described using a purely deterministic equation of motion. When applying this approach to the SPGPE or the Stoof SGPE, this amounts to neglecting the noise terms associated with reservoir interactions while retaining the deterministic terms. Both the number-damping SPGPE and Stoof SGPE reduce to the same equation of motion under this approximation: the *damped Gross-Pitaevskii equation* (dGPE). The dGPE was originally proposed using phenomenological arguments [221]. It can also be obtained via a Wick rotation, introducing a small imaginary time component to the non-linear GPE evolution. The dGPE has been used to study vortex lattice formation [222–224], two-dimensional quantum turbulence [75, 225, 226], and vortex chain formation in a spin-1 condensate [227].

A significant advantage of using the dGPE as opposed to one of the stochastic equations of motion is the potential for analytical insights. One can also use the physically appropriate damping rate obtained from the SPGPE, such that the dGPE can give a realistic description of the dissipative dynamics in regimes where the noise is negligible. Such regimes may exist when the system is far from equilibrium or at relatively low temperature. These physically consistent damping rates have been used to describe the dissipative dynamics of a single vortex [228], and also for dark solitons [123] where the Stoof SGPE was also used to show that the mean stochastic trajectories agreed with the analytic predictions from the dGPE. It has been shown in a different study of single vortex decay [2] that at higher temperatures the inclusion of noise can introduce both qualitative and quantitative differences compared to the dGPE; in such regimes a stochastic theory is essential.

2.3.6 Importance of the projector

We have repeatedly mentioned the use of the projector (2.14) as a crucial aspect of the SPGPE and other classical field theories. The formal separation of the system into the coherent and incoherent region must be performed in a particular way in order to obtain

quantitative results from numerical simulations. In this subsection we outline the various reasons justifying this careful approach.

The classical-field methods hinge on the use of the classical-field approximation. The assumption behind this is that the single-particle modes of the coherent region are appreciably occupied such that the truncated Wigner approximation is valid. The use of a formal projector ensures that the division of the system is such that this is indeed the case.

An important aspect of the projector is that it is defined in terms of single-particle basis states. If one instead uses a momentum space basis in a trapped system, then the energy cutoff becomes spatially dependent, and as a result the separation of the coherent and incoherent regions is ill-defined. Using the single-particle basis ensures that the separation of the two regions is well defined. The cutoff energy must also be physically appropriate; too high and modes in the coherent region will be sparsely occupied, but too low and modes in the incoherent region will be classically occupied. In practice the appropriate cutoff is on the order of three times the chemical potential ($\epsilon_{\rm cut} \approx 3\mu$). As a result of this appropriate cutoff, the many-body Hamiltonian will be approximately diagonal at the cutoff energy. This allows the incoherent region to be treated semiclassically [115] as a thermal reservoir. The thermodynamic properties of the reservoir are simple to calculate, and a quantitative description of the full system can be found.

The use of a projector also ensures that the energy-damping process can be represented. This process is thought to be significant in non-equilibrium systems [106], but is frequently neglected. As mentioned earlier, the energy-damping process is formally absent in the Stoof SGPE due to the lack of a high-energy cutoff.

In numerical simulations, it is crucial that all modes in the coherent region are evolved accurately. Regular cartesian grid methods are sufficient in zero-temperature simulations of the Gross-Pitaevskii equation, as all high-energy modes are sparsely occupied and have little to no effect on the system dynamics. In classical-field simulations, the significant occupancy of higher energy modes combined with the non-linearity can generate momentum components several times larger than those in the coherent region [229]. The projected Gross-Pitaevskii equation provides a spectral method for propagation that ensures these components do not lead to spurious aliasing. In the plane wave basis description of a system without confinement this is done by evaluating the nonlinear interaction term on a grid with twice the points as the wave function grid, extending the momentum cutoff to twice that of the wave function [184]. This is easily extended to other bases [115, 192], where the order of the grid is again twice that of the mode space.

2.3.7 Positive P method

While classical-field methods based on the Wigner representation of the density operator have been very successful in describing finite temperature Bose-Einstein condensates, these methods rely on the use of the truncated Wigner approximation. This many be seen as unsatisfactory, as the neglected third order derivative terms may be significant in some regimes. An alternative method using the Glauber-Sudarshan P-representation is based on normally-ordered operator averages [230, 231]. In this approach there are formally no third order derivative terms in the equation of motion for the distribution and thus no truncation is required; the equation of motion is already in the form of a Fokker-Planck equation. However, this representation allows the distribution function to take on negative values and delta function singularities, and thus the diffusion matrix is not positive semi-definite and there is no mapping to an equivalent stochastic differential equation.

A solution to this problem was found by Drummond and Gardiner, who considered a variety of generalized P-representations [160]. One of these, the positive P-representation, is particularly useful in the field of ultra-cold atoms. This method considers a phase-space that has twice the dimensionality of the usual classical phase-space [160, 232, 233]. The result of this is that the diffusion matrix in the Fokker-Planck equation becomes strictly positive semi-definite, and an equivalent stochastic differential equation for the classical phase-space variables may be found that exactly represents the quantum dynamics. Because there is no truncation of higher order terms, the positive P-representation is valid in regimes where the truncated Wigner approach fails, in particular allowing the study of strongly correlated systems.

The downside of the positive P-representation is the technical challenges associated with numerical implementation. Because the dimensionality of the phase-space has been doubled, there is increased sensitivity to sampling errors. Over long times these sampling errors grow exponentially, so while positive P-representation simulations are well defined over very short times, convergence is difficult to achieve for longer simulations [233].

Because the validity of the positive P-representation is restricted to relatively short times compared to the more robust SPGPE, its use in studying the dissipative dynamics of Bose-Einstein condensates is somewhat limited. Despite the limitations there are many examples of the positive P-representation being used to study dynamics in such systems, including studies of condensate formation [234], spin squeezing in two-component condensates [235], correlation dynamics in uniform systems [236], and dynamics and correlations of Bose-Einstein condensates formed via dissociation of molecules [237–240]. These exam-

ples are all limited to short time scales and weak interactions. In general the utility of the positive P-representation in quantum optics can be traced to stronger interactions and weaker damping compared to Bose-Einstein condensates.

2.4 Alternative finite-temperature methods

In this section we review two alternative methods used to describe finite temperature Bose-Einstein condensates. The first method is based on the Beliaev broken symmetry approach, where the field operator is separated into condensate and non-condensate contributions. This approach follows a theoretical framework traditionally used in condensed matter physics, and leads to theories describing physics beyond the predictions of Gross-Pitaevskii theory [100]. In particular we focus on the method of Zaremba, Nikuni, and Griffin (ZNG), who utilize a kinetic desription of the thermal cloud coupled to a dissipative Gross-Pitaevskii equation. The second method avoids the use of symmetry-breaking, and results in a number-conserving theory.

2.4.1 Symmetry-breaking methods: Zaremba-Nikuni-Griffin

System Separation

Just as in the classical field methods, the starting point for the symmetry breaking approach is the effective field theory described in Section 2.2. The field operator $\hat{\Psi}(\mathbf{r})$ is decomposed into the expectation of the field operator and a fluctuation operator

$$\hat{\Psi}(\mathbf{r}) = \langle\hat{\Psi}(\mathbf{r})\rangle + \hat{\delta}(\mathbf{r}). \tag{2.28}$$

The fluctuation operator is the difference between the field operator and its expectation $\hat{\delta}(\mathbf{r}) \equiv \hat{\Psi}(\mathbf{r}) - \langle\hat{\Psi}(\mathbf{r})\rangle$; from this definition the fluctuation operator expectation is clearly zero ($\langle\hat{\delta}(\mathbf{r})\rangle = 0$). The expectation is identified as the condensate contribution $\langle\hat{\Psi}(\mathbf{r})\rangle \equiv \hat{\phi}(\mathbf{r}) \neq 0$ (assumed to be non-zero), while the fluctuation operator represents all non-condensed atoms and thus accounts for all quantum fluctuations, thermally excited atoms, or excited atoms due to interaction effects. The field operator decomposition can then be expressed as

$$\hat{\Psi}(\mathbf{r}) = \hat{\phi}(\mathbf{r}) + \hat{\delta}(\mathbf{r}) = \hat{a}_c\phi_c(\mathbf{r}) + \sum_{n\neq c}\hat{a}_n\phi_n(\mathbf{r}), \tag{2.29}$$

where $\hat{a}_n$ obey the Bose commutation relations and $\phi_n(\mathbf{r})$ are a complete set of single-particle eigenstates, found in practice by diagonalizing the one-body density matrix introduced by Penrose and Onsager [15]

$$\rho(\mathbf{r},\mathbf{r}') = \langle \hat{\Psi}^\dagger(\mathbf{r}')\hat{\Psi}(\mathbf{r})\rangle. \tag{2.30}$$

The condensate mode $\phi_c(\mathbf{r})$ is defined as the eigenstate of the one-body density matrix with the largest eigenvalue; the value of the eigenvalue N_c gives the occupation of the condensate mode. Assuming a well defined condensate exists, the condensate operator $\hat{a}_c$ can be replaced by the complex number $\sqrt{N_c}e^{i\Theta}$ with Θ the phase. The field operator is then

$$\hat{\Psi}(\mathbf{r}) = \phi(\mathbf{r}) + \hat{\delta}(\mathbf{r}), \tag{2.31}$$

where all operator dependence is now given by the fluctuation operator. The replacement $\hat{\phi}(\mathbf{r}) \to \phi(\mathbf{r}) \equiv \sqrt{N_c}e^{i\Theta}\phi_c(\mathbf{r})$ is what gives the symmetry-breaking approach its name, as this gives the condensate a determinate phase, breaking the $U(1)$ gauge symmetry of the cold-collision Hamiltonian (2.6).

Hamiltonian and equations of motion

Under substitution of the separated field operator (2.31), the cold-collision Hamiltonian (2.6) may be written as

$$\hat{H} + H_0 + \hat{H}_1 + \hat{H}_2 + \hat{H}_3 + \hat{H}_4 \tag{2.32}$$

where the subscript denotes the number of occurrences of the fluctuation operator in each term. Averaging of the Heisenberg equation of motion leads to the generalized Gross-Pitaevskii equation [241]

$$i\hbar\frac{\partial\phi(\mathbf{r})}{\delta t} = \left(H_{\rm sp} + g(n_c(\mathbf{r}) + 2\bar{n}(\mathbf{r}))\right)\phi(\mathbf{r}) + g\bar{m}(\mathbf{r})\phi^*(\mathbf{r}) + g\langle\hat{\delta}^\dagger(\mathbf{r})\hat{\delta}(\mathbf{r})\hat{\delta}(\mathbf{r})\rangle, \tag{2.33}$$

with $n_c(\mathbf{r}) = |\phi(\mathbf{r})|^2$ the condensate density, $\bar{n}(\mathbf{r}) = \langle\hat{\delta}^\dagger(\mathbf{r})\hat{\delta}(\mathbf{r})\rangle$ the non-condensate density, and $\bar{m}(\mathbf{r}) = \langle\hat{\delta}(\mathbf{r})\hat{\delta}(\mathbf{r})\rangle$ the anomalous average. This equation of motion is generally intractable, and as such approximations are essential to gaining a useful description of the system.

Hartree-Fock-Bogoliubov approximation

One of the common approximations applied to the generalized GPE is the neglect of the triplet correlation function $\langle\hat{\delta}^\dagger(\mathbf{r})\hat{\delta}(\mathbf{r})\hat{\delta}(\mathbf{r})\rangle$ in (2.33), known as the Hartree-Fock-Bogoliubov (HFB) approximation [242]. This approximation leads to population conservation of the condensate, as the triplet correlation function is the only source term in the generalized GPE. The HFB approximation also leads to some unphysical behavior, due to the inconsistent treatment of the condensate and non-condensate particles [163, 242]. This may be remedied in a variety of ways.

Neglecting the anomalous average in the HFB approximation [242] is known as the *Popov approximation*. The result is a more tractable description of the condensate and non-condensate interactions. This is often used in static form, where thermal cloud fluctuations are also neglected ($\bar{n}(\mathbf{r},t) = \bar{n}(\mathbf{r},0)$). The physical interpretation of this is that the condensate atoms are moving in a static Hartree-Fock field resulting from non-condensate atoms. Dynamics of the non-condensate density can also be included [243]. Calculations within the Popov approximation have shown agreement with experiment, however the neglect of high oder fluctuation operators limits its regime of validity to low temperatures.

The triplet correlation function can also be included. This term allows the description of particle transfer between the condensate and non-condensate, as well as interactions between non-condensate particles. The inclusion is possible via a kinetic theory treatment of the scattering dynamics [244, 245]. The triplet term contributions have been combined with the HFB formalism by perturbatively including the difference between the full Hamiltonian (2.32) and the HFB Hamiltonian including all fluctuation operator terms up to second order [246–248]. The inclusion of these high order terms allows a description of high-temperature dynamics, however their implementation in the HFB formalism is technically challenging.

Zaremba-Nikuni-Griffin approach

An effective solution to the challenge of including high order terms in the HFB formalism was formulated by Zaremba, Nikuni, and Griffin, known as the Zaremba-Nikuni-Griffin (ZNG) approach [249]. The ZNG approach combines the Popov approximation with a perturbative description of the triplet terms, allowing for a full description of thermal

collisions. The condensate equation of motion is

$$i\hbar\frac{\partial\phi(\mathbf{r},t)}{\partial t} = \left(H_{\rm sp} + g(n_c(\mathbf{r},t) + 2\bar{n}(\mathbf{r},t)) - iR(\mathbf{r},t)\right)\phi(\mathbf{r},t). \tag{2.34}$$

The term $iR(\mathbf{r},t)$ is a contribution from the triplet term, a non-Hermitian source term describing particle exchange between the condensate and thermal cloud.

In the ZNG approach the thermal cloud is treated with a Wigner distribution $f(\mathbf{p},\mathbf{r},t)$ within a local semiclassical approximation. Using a phase-space distribution function results in the kinetic equations from the perturbative treatment of the fluctuation operators becoming numerically tractable; this is in direct contrast to the perturbative treatments of [246–248]. The equation of motion for the thermal cloud is a quantum Boltzmann equation

$$\frac{\partial f}{\partial t} + \frac{\mathbf{p}}{m}\cdot\nabla_{\mathbf{r}} f - (\nabla_{\mathbf{r}} U_{\rm HF})\cdot(\nabla_{\mathbf{p}} f) = C_{12}(f,\phi) + C_{22}(f) \tag{2.35}$$

with the generalized mean-field potential

$$U_{\rm HF} = V_{\rm ext}(\mathbf{r}) + 2g(n_c(\mathbf{r}) + \bar{n}(\mathbf{r})). \tag{2.36}$$

The terms on the right hand side of (2.35) are collisional integrals, with C_{12} representing collisions between condensate and non-condensate particles leading to particle transfer, and C_{22} representing collisions between two non-condensate particles.

The ZNG method gives a self-consistent approach to treating thermal cloud dynamics via the Boltzmann equation (2.35), which is coupled to condensate dynamics via the collisional integrals C_{12} and C_{22}, and the growth term $R(\mathbf{r},t)$. The major strength of the ZNG approach is the ability to give a quantitative description of thermal cloud dynamics in addition to the dynamics of the condensate. Application of the ZNG method has been used to study collective mode oscillations at finite temperature [250–253], hydrodynamic regimes [254, 255], surface mode damping in a rotating thermal cloud [256], dark soliton decay [257, 258], and vortex decay [259, 260]. However, ZNG is not a true reservoir theory, as it lacks any noise that would allow satisfaction of the fluctuation-dissipation theorem. Furthermore, ZNG cannot easily describe systems involving fragmented condensates, or the formation of topological excitations during the BEC phase transition.

2.4.2 Number-conserving approach: beyond symmetry-breaking

There are some issues in the symmetry-breaking approach that can be problematic in some regimes. Particle number is not explicitly conserved, and the condensate and symmetry-broken non-condensate operator are not orthogonal. As a result of this, there is some ambiguity in defining the condensate and non-condensate, which is a concern in systems where the coupled condensate and non-condensate dynamics are significant [152]. This is the case in non-equilibrium systems at cold temperatures, where the presence of a large condensate contribute significantly to the dynamics. Also, the HFB and ZNG approaches are not valid in this low-temperature non-equilibrium regime, as there the anomalous average is significant.

In the number-conserving approach, the global $U(1)$ symmetry of the many-body Hamiltonian is preserved [161–163, 261]. The formalism initially follows that of the symmetry-breaking method, with the condensate being identified using the Penrose-Onsager criterion, with the key differences being that the condensate mode is in operator form and the fluctuation operator is defined such that it commutes with the total particle number operator. It is not surprising that this results in a theory that is much greater in complexity compared to the theories resulting from the symmetry-breaking approach. Nevertheless, formalism has been developed to describe time dependence in finite temperature systems [261, 262].

Fully dynamical implementations of the number-conserving method are rare [152, 263]. The number-conserving approach has been used to study condensate excitations [264], and non-equilibrium dynamics of a δ-kicked-rotor Bose-Einstein condensate at finite temperature [152].

2.4.3 Comparison with the SPGPE

We finish this section by comparing the SPGPE and ZNG methodologies. In particular we will outline the key differences between the two theories. There have been very few studies comparing the classical-field and symmetry breaking methods [122], however both have seen questions arise about their validity [265, 266]. The number-conserving approach is appropriate to low-temperature regimes, and so is not directly comparable to the high-temperature SPGPE method.

The most significant advantage of the ZNG method is the inclusion of a fully dynamical thermal cloud. While the SPGPE does include some thermal dynamics in the coherent

region, the omission of high-energy thermal cloud dynamics is the main limitation. While there is no current dynamical description of a thermal cloud in the SPGPE theory, this is not fundamentally impossible to include [106].

In the symmetry breaking approach, a macroscopically occupied single-particle mode is identified corresponding to the condensate. At this point a mean-field description of the condensate mode is enforced. While this is useful for immediate access to the condensate order parameter and related properties, the choice of a single coherent mode assumes that the condensate has no fluctuations or non-trivial correlations with thermal particles. This is problematic in many scenarios. Around the BEC transition the condensate will be small and fluctuations necessarily large in comparison, in the high-temperature regime there are large fluctuations in the condensate population in equilibrium [195, 197], and in dimensionally reduced systems enhanced fluctuations lead to a significant difference in the condensate and superfluid densities [61]. These regimes are of experimental interest but all outside the validity of the symmetry breaking approach.

In the classical-field approach, the classical-field includes many low-energy modes in addition to the condensate mode. Separating the system into a coherent region and incoherent region, as opposed to a condensate mode and thermal cloud, obscures the role of the condensate in the system and has been called *ad hoc* [266]. However the system separation is based on the choice of a physically consistent energy cutoff such that the modes in the classical-field are classically occupied. There is some freedom in the choice of cutoff within this regime, and any results should be independent of the exact cutoff provided it meets this criteria. A significant advantage in the classical-field approach is that the existence of a condensate not necessary; in general the condensate must be extracted from the one-body density matrix approach of Penrose and Onsager [15]. All interactions between classically occupied modes are also included non-perturbatively. The classical-field approach is thus valid in systems with large fluctuations, and in non-equilibrium systems.

It is apparent that each method is valid in regimes where the other is not, and as such may be viewed as complementary methods rather than than alternative methods. ZNG is the more appropriate method when thermal cloud dynamics are important in highly condensed systems, while the SPGPE is more suited to systems where the temperature is high such that the reservoir is highly populated and rapidly thermalizes, or in highly non-equilibrium systems.

2.5 Summary

In this chapter we have described the classical-field methods for describing degenerate Bose gases at finite temperature, providing a conceptual background and discussion of the validity and limitations of the resulting theories.

We introduced the effective field theory essential to the development of the classical-field method, where the infinite dimensional energy space is restricted to a finite subspace. The use of a consistent projector was discussed, a crucial element of the classical-field method, and how this leads to a treatment of reservoir interactions that can be used to describe finite temperature dynamics. We gave a brief survey of several classical-field theories including the precise way in which the reservoir interactions are accounted for, the regime in which they may be applied, and examples of their use in the literature. Finally, we introduced possible alternative approaches for describing finite temperature degenerate Bose gases, and discussed how they compare with the classical-field approach.

In the remainder of this thesis we focus on the classical-field method known as the stochastic projected Gross-Pitaevskii equation. In particular we are interested in the role of energy-damping in system dynamics and equilibrium, as this process is formally absent in all the other theories we have described.

Chapter 3

Stochastic projected Gross-Pitaevskii equation

3.1 Introduction

The main tool we use in this work is the stochastic projected Gross-Pitaevskii equation (SPGPE), one of several classical field methods that describe the dynamics of finite temperature Bose-Einstein condensates. The SPGPE is derived via a microscopic treatment of reservoir interactions, and is thus a first-principles approach to describing evolution of dissipative superfluid systems. Here we outline the derivation of the SPGPE for a single component bose gas, as well as how it may be used to perform simulations of finite-temperature dynamics. We endeavour to present this derivation with a level of clarity such that a doctoral level student can follow with little difficulty.

The outline of the chapter is as follows. In Section 3.2 we separate the system by performing a projection of the quantum field and review the resulting Hamiltonian terms including reservoir interactions. In Section 3.3 we give a theoretical treatment of the reservoir interaction terms. Section 3.4 sets out the Fokker-Planck equation for the Wigner representation of the quantum field. In Section 3.5 we arrive at the full form of the single component SPGPE; we also comment on extensions of this to multi-component, spinor, and effective low-dimensional systems. Section 3.6 considers different sub-theories of the SPGPE that arise from neglecting different reservoir processes. In Section 3.7 we outline how one may estimate SPGPE parameters for the purposes of performing numerical simulations of experimental systems. We conclude in Section 3.8 by briefly commenting on the numeric method used in this work, and the computing resources that were required.

3.2 System separation

We begin with the second-quantised cold-collision Hamiltonian for the effective field operator

$$\hat{H} = \int d^3\mathbf{r}\, \hat{\Psi}^\dagger(\mathbf{r}) H_{\rm sp} \hat{\Psi}(\mathbf{r}) + \frac{g}{2} \int d^3\mathbf{r}\, \hat{\Psi}^\dagger(\mathbf{r}) \hat{\Psi}^\dagger(\mathbf{r}) \hat{\Psi}(\mathbf{r}) \hat{\Psi}(\mathbf{r}), \tag{3.1}$$

where the interaction strength is parameterised by

$$g = \frac{4\pi\hbar^2 a_s}{m}, \tag{3.2}$$

with a_s the s-wave inter-particle scattering length, m the particle mass, and

$$H_{\rm sp} = -\frac{\hbar^2}{2m}\nabla^2 + V_{\rm ext}(\mathbf{r}) \tag{3.3}$$

the single particle Hamiltonian. The single-particle states of the system are separated into a low-energy coherent region (or **C**-field) and a high-energy incoherent region (or **I**-field); the energy defining the two regions is known as the *cutoff energy* $\epsilon_{\rm cut}$. The field operator is decomposed into

$$\hat{\Psi}(\mathbf{r}) = \hat{\psi}(\mathbf{r}) + \hat{\phi}(\mathbf{r}), \tag{3.4}$$

where

$$\hat{\psi}(\mathbf{r}) = \mathcal{P}\left\{\hat{\Psi}(\mathbf{r})\right\}, \tag{3.5}$$

$$\hat{\phi}(\mathbf{r}) = \mathcal{Q}\left\{\hat{\Psi}(\mathbf{r})\right\}, \tag{3.6}$$

are field operators for the coherent region and incoherent region respectively. Here we have introduced the projection operators, or *projectors*, which have the following properties

$$\mathcal{P}\left\{\mathcal{Q}\left\{F(\mathbf{r})\right\}\right\} = \mathcal{Q}\left\{\mathcal{P}\left\{F(\mathbf{r})\right\}\right\} = 0, \tag{3.7}$$

$$\mathcal{P}\left\{\mathcal{P}\left\{F(\mathbf{r})\right\}\right\} = \mathcal{P}\left\{F(\mathbf{r})\right\}, \tag{3.8}$$

$$\mathcal{P}\left\{F(\mathbf{r})\right\} + \mathcal{Q}\left\{F(\mathbf{r})\right\} = F(\mathbf{r}). \tag{3.9}$$

The cold-collision Hamiltonian can then be written as

$$\hat{H} = \hat{H}_0 + \hat{H}_{\mathbf{I}} + \hat{H}_{\rm int}, \tag{3.10}$$

where

$$\hat{H}_0 = \int d^3\mathbf{r}\hat{\psi}^\dagger(\mathbf{r})H_{\rm sp}\hat{\psi}(\mathbf{r}) + \frac{g}{2}\int d^3\mathbf{r}\hat{\psi}^\dagger(\mathbf{r})\hat{\psi}^\dagger(\mathbf{r})\hat{\psi}(\mathbf{r})\hat{\psi}(\mathbf{r}), \tag{3.11}$$

is the Hamiltonian for the coherent region in isolation

$$\hat{H}_{\mathbf{I}} = \int d^3\mathbf{r}\hat{\phi}^\dagger(\mathbf{r})H_{\rm sp}\hat{\phi}(\mathbf{r}) + \frac{g}{2}\int d^3\mathbf{r}\hat{\phi}^\dagger(\mathbf{r})\hat{\phi}^\dagger(\mathbf{r})\hat{\phi}(\mathbf{r})\hat{\phi}(\mathbf{r}), \tag{3.12}$$

is the Hamiltonian for the incoherent region in isolation and

$$\hat{H}_{\rm int} = \hat{H}^{(1)}_{\rm int} + \hat{H}^{(2)}_{\rm int} + \hat{H}^{(3)}_{\rm int} \tag{3.13}$$

is the Hamiltonian for reservoir interactions resulting in energy and/or particle transfer between the two regions. The terms in the reservoir interaction Hamiltonian have been grouped by how many coherent region field operators are present, indicated by the superscript number. The contributions to the reservoir interaction Hamiltonian are

$$\hat{H}^{(1)}_{\rm int} = g\int d^3\mathbf{r}\left[\hat{\psi}^\dagger(\mathbf{r})\hat{\phi}^\dagger(\mathbf{r})\hat{\phi}(\mathbf{r})\hat{\phi}(\mathbf{r}) + \hat{\phi}^\dagger(\mathbf{r})\hat{\phi}^\dagger(\mathbf{r})\hat{\phi}(\mathbf{r})\hat{\psi}(\mathbf{r})\right], \tag{3.14}$$

$$\hat{H}^{(2)}_{\rm int} = \frac{g}{2}\int d^3\mathbf{r}\left[\hat{\psi}^\dagger(\mathbf{r})\hat{\psi}^\dagger(\mathbf{r})\hat{\phi}(\mathbf{r})\hat{\phi}(\mathbf{r}) + \hat{\phi}^\dagger(\mathbf{r})\hat{\phi}^\dagger(\mathbf{r})\hat{\psi}(\mathbf{r})\hat{\psi}(\mathbf{r}) + 4\hat{\psi}^\dagger(\mathbf{r})\hat{\phi}^\dagger(\mathbf{r})\hat{\phi}(\mathbf{r})\hat{\psi}(\mathbf{r})\right], \tag{3.15}$$

$$\hat{H}^{(3)}_{\rm int} = g\int d^3\mathbf{r}\left[\hat{\phi}^\dagger(\mathbf{r})\hat{\psi}^\dagger(\mathbf{r})\hat{\psi}(\mathbf{r})\hat{\psi}(\mathbf{r}) + \hat{\psi}^\dagger(\mathbf{r})\hat{\psi}^\dagger(\mathbf{r})\hat{\psi}(\mathbf{r})\hat{\phi}(\mathbf{r})\right]. \tag{3.16}$$

Note that mixed terms of the coherent and incoherent region operator and the single particle Hamiltonian are zero by definition

$$\int d^3\mathbf{r}\,\hat{\psi}^\dagger(\mathbf{r})H_{\rm sp}\hat{\phi}(\mathbf{r}) = \int d^3\mathbf{r}\,\hat{\phi}^\dagger(\mathbf{r})H_{\rm sp}\hat{\psi}(\mathbf{r}) = 0. \tag{3.17}$$

3.3 Microscopic treatment of reservoir interactions

In this section we describe how we microscopically account for the reservoir interactions between the incoherent and coherent regions, following the derivations presented in [145–147, 149]. This involves the derivation of an equation of motion for the coherent region density operator using master equation techniques [157, 158, 202].

3.3.1 Master equation

The system evolves according to the von Neumann equation of motion for the density operator

$$\dot{\rho} = -\frac{i}{\hbar}\left[\hat{H}_0 + \hat{H}_{\mathbf{I}} + \hat{H}_{\mathrm{int}}, \rho\right], \tag{3.18}$$

or equivalently

$$\dot{\rho} = \left(\mathcal{L}_0 + \mathcal{L}_{\mathbf{I}} + \mathcal{L}_{\mathrm{int}}\right)\rho, \tag{3.19}$$

where the $\mathcal{L}$ are Louivillian superoperators. We now trace out the incoherent region degrees of freedom to obtain an equation of motion for the coherent field density operator

$$\rho_{\mathbf{C}} = \mathrm{Tr}_{\mathbf{I}}\left(\rho\right). \tag{3.20}$$

We define a new pair of projectors[1] $\mathcal{P}$ and $\mathcal{Q}$ such that

$$v(t) = \mathcal{P}\rho = \rho_{\mathbf{I}} \otimes \mathrm{Tr}_{\mathbf{I}}\left(\rho\right) = \rho_{\mathbf{I}} \otimes \rho_{\mathbf{C}}, \tag{3.21}$$

$$w(t) = \mathcal{Q}\rho = \left(1 - \mathcal{P}\right)\rho = \rho_{\mathbf{IC}}, \tag{3.22}$$

so

$$\rho = v(t) + w(t) = \rho_{\mathbf{I}} \otimes \rho_{\mathbf{C}} + \rho_{\mathbf{IC}} \tag{3.23}$$

[1] Note that the projectors $\mathcal{P}$ and $\mathcal{Q}$ are not the same as the projectors $\mathcal{P}\{\cdot\}$ and $\mathcal{Q}\{\cdot\}$ we defined earlier to separate the system into the two regions.

where $\rho_{\mathbf{I}} \otimes \rho_{\mathbf{C}}$ is the part of the total density operator where the coherent and incoherent regions are uncorrelated and $\rho_{\mathbf{IC}}$ is the part of the total density operator where the coherent and incoherent regions are correlated. The von Neumann equation then gives

$$\dot{v}(t) = \mathcal{P}\left[\left(\mathcal{L}_0 + \mathcal{L}_{\mathbf{I}} + \mathcal{L}_{\text{int}}\right)\left(v(t) + w(t)\right)\right], \tag{3.24}$$

$$\dot{w}(t) = \mathcal{Q}\left[\left(\mathcal{L}_0 + \mathcal{L}_{\mathbf{I}} + \mathcal{L}_{\text{int}}\right)\left(v(t) + w(t)\right)\right]. \tag{3.25}$$

It is easiest to manipulate these equations using the Laplace transform, defined by

$$\tilde{f}(s) = \int_0^\infty e^{-st} f(t) dt. \tag{3.26}$$

The equations of motion are now

$$s\tilde{v}(s) - v(0) = \mathcal{P}\left[\left(\mathcal{L}_0 + \mathcal{L}_{\mathbf{I}} + \mathcal{L}_{\text{int}}\right)\left(\tilde{v}(s) + \tilde{w}(s)\right)\right], \tag{3.27}$$

$$s\tilde{w}(s) = \mathcal{Q}\left[\left(\mathcal{L}_0 + \mathcal{L}_{\mathbf{I}} + \mathcal{L}_{\text{int}}\right)\left(\tilde{v}(s) + \tilde{w}(s)\right)\right], \tag{3.28}$$

where we have assumed that the coherent and incoherent regions are initially uncorrelated and so $w(0) = 0$. We now introduce the superoperators

$$\mathcal{L}_{\mathbf{C}} \equiv \mathcal{L}_0 + \mathcal{P}\mathcal{L}_{\text{int}}\mathcal{P}, \tag{3.29}$$

$$\mathcal{L}_{\mathbf{IC}} \equiv \mathcal{L}_{\text{int}} - \mathcal{P}\mathcal{L}_{\text{int}}\mathcal{P}, \tag{3.30}$$

such that $\mathcal{L}_0 + \mathcal{L}_{\text{int}} = \mathcal{L}_{\mathbf{C}} + \mathcal{L}_{\mathbf{IC}}$. The superoperator $\mathcal{L}_{\mathbf{C}}$ has been defined such that it contains the mean-field contribution of scattering from the incoherent region, known as *forward scattering*. Thus $\mathcal{L}_{\mathbf{C}}$ accounts for all terms that contribute to the Hamiltonian evolution of the coherent region. The evolution equations are now

$$s\tilde{v}(s) - v(0) = \mathcal{P}\left[\left(\mathcal{L}_{\mathbf{C}} + \mathcal{L}_{\mathbf{I}} + \mathcal{L}_{\mathbf{IC}}\right)\left(\tilde{v}(s) + \tilde{w}(s)\right)\right], \tag{3.31}$$

$$s\tilde{w}(s) = \mathcal{Q}\left[\left(\mathcal{L}_{\mathbf{C}} + \mathcal{L}_{\mathbf{I}} + \mathcal{L}_{\mathbf{IC}}\right)\left(\tilde{v}(s) + \tilde{w}(s)\right)\right]. \tag{3.32}$$

We can simplify this by using the following properties [267]:

- The superoperator $\mathcal{L}_{\mathbf{C}}$ evolves the coherent region only. Applying this to the uncor-

related part $\tilde{v}(s)$ thus cannot cause any correlations to form. Therefore

$$\mathcal{P}\mathcal{L}_{\mathbf{C}}\tilde{v}(s) = \mathcal{L}_{\mathbf{C}}\tilde{v}(s), \tag{3.33}$$
$$\mathcal{Q}\mathcal{L}_{\mathbf{C}}\tilde{v}(s) = 0. \tag{3.34}$$

- The term $\mathcal{P}\mathcal{L}_{\mathbf{IC}}\mathcal{P}$ is zero by the construction of $\mathcal{L}_{\mathbf{IC}}$, so

$$\mathcal{P}\mathcal{L}_{\mathbf{IC}}\tilde{v}(s) = 0, \tag{3.35}$$
$$\mathcal{Q}\mathcal{L}_{\mathbf{IC}}\tilde{v}(s) = \mathcal{L}_{\mathbf{IC}}\tilde{v}(s). \tag{3.36}$$

- We enforce a thermal equilibrium incoherent density operator

$$\rho_{\mathbf{I}} = \exp\left[-\beta\hat{H}_{\mathbf{I}}\right] / \mathrm{Tr}_{\mathbf{I}}\left\{\exp\left[-\beta\hat{H}_{\mathbf{I}}\right]\right\}, \tag{3.37}$$

  such that $\mathcal{L}_{\mathbf{I}}\rho_{\mathbf{I}} = \rho_{\mathbf{I}}$. Then

$$\mathcal{Q}\mathcal{L}_{\mathbf{I}}\tilde{v}(s) = 0. \tag{3.38}$$

- The projector $\mathcal{P}$ also has the property $\mathcal{P}\mathcal{L}_{\mathbf{I}} = \mathcal{L}_{\mathbf{I}}\mathcal{P} = 0$. This gives

$$\mathcal{P}\mathcal{L}_{\mathbf{I}}\tilde{v}(s) = 0, \tag{3.39}$$
$$\mathcal{P}\mathcal{L}_{\mathbf{I}}\tilde{w}(s) = 0, \tag{3.40}$$
$$\mathcal{Q}\mathcal{L}_{\mathbf{I}}\tilde{v}(s) = 0, \tag{3.41}$$
$$\mathcal{Q}\mathcal{L}_{\mathbf{I}}\tilde{w}(s) = \mathcal{L}_{\mathbf{I}}\tilde{w}(s). \tag{3.42}$$

- Furthermore, $\mathcal{P}$ and $\mathcal{L}_{\mathbf{C}}$ commute ($\mathcal{P}\mathcal{L}_{\mathbf{C}} = \mathcal{L}_{\mathbf{C}}\mathcal{P}$) , so

$$\mathcal{P}\mathcal{L}_{\mathbf{C}}\tilde{w}(s) = 0, \tag{3.43}$$
$$\mathcal{Q}\mathcal{L}_{\mathbf{C}}\tilde{w}(s) = \mathcal{L}_{\mathbf{C}}\tilde{w}(s). \tag{3.44}$$

Applying these leads to

$$s\tilde{v}(s) - \tilde{v}(0) = \mathcal{L}_{\mathbf{C}}\tilde{v}(s) + \mathcal{P}\mathcal{L}_{\mathbf{IC}}\tilde{w}(s), \tag{3.45}$$
$$s\tilde{w}(s) = \left(\mathcal{L}_{\mathbf{C}} + \mathcal{L}_{\mathbf{I}} + \mathcal{Q}\mathcal{L}_{\mathbf{IC}}\right)\tilde{w}(s) + \mathcal{L}_{\mathbf{IC}}\tilde{v}(s). \tag{3.46}$$

We may eliminate $\tilde{w}(s)$ using

$$\tilde{w}(s) = \left[s - \mathcal{L}_{\mathbf{C}} - \mathcal{L}_{\mathbf{I}} - \mathcal{Q}\mathcal{L}_{\mathbf{IC}}\right]^{-1} \mathcal{L}_{\mathbf{IC}}\tilde{v}(s), \tag{3.47}$$

so

$$s\tilde{v}(s) - v(0) \quad = \quad \mathcal{L}_{\mathbf{C}}\tilde{v}(s) + \mathcal{P}\mathcal{L}_{\mathbf{IC}}\left[s - \mathcal{L}_{\mathbf{C}} - \mathcal{L}_{\mathbf{I}} - \mathcal{Q}\mathcal{L}_{\mathbf{IC}}\right]^{-1} \mathcal{L}_{\mathbf{IC}}\tilde{v}(s). \tag{3.48}$$

Inverting the Laplace transform and using its properties with respect to convolutions

$$\dot{v}(t) = \mathcal{L}_{\mathbf{C}}v(t) + \mathcal{P}\mathcal{L}_{\mathbf{IC}}\left\{\int_0^t d\tau \exp\left[(\mathcal{L}_{\mathbf{C}} + \mathcal{L}_{\mathbf{I}} + \mathcal{Q}\mathcal{L}_{\mathbf{IC}})\tau\right] u(\tau)\mathcal{L}_{\mathbf{IC}}\right\} v(t-\tau), \tag{3.49}$$

with $u(\tau)$ the Heaviside step function. We now make two physical approximations. The first is that $\mathcal{L}_{\mathbf{C}}$ and $\mathcal{L}_{\mathbf{I}}$ are dominant over $\mathcal{L}_{\mathbf{IC}}$, which acts only as a weak coupling over the time scale of the integrand, so we may neglect the final term in the argument of the exponential

$$\dot{v}(t) = \mathcal{L}_{\mathbf{C}}v(t) + \left\{\mathcal{P}\mathcal{L}_{\mathbf{IC}}\int_0^t d\tau \exp\left[(\mathcal{L}_{\mathbf{C}} + \mathcal{L}_{\mathbf{I}})\tau\right] \mathcal{L}_{\mathbf{IC}}\right\} v(t-\tau). \tag{3.50}$$

Secondly we use the Markov approximation [157], assuming that the correlation times of the incoherent region are very small compared to those of the coherent region. The energy cutoff is chosen fairly high, so this approximation is justified. In this case we can set $v(t-\tau) \to v(t)$ and the integration limit to ∞

$$\dot{v}(t) = \mathcal{L}_{\mathbf{C}}v(t) + \left\{\mathcal{P}\mathcal{L}_{\mathbf{IC}}\int_0^\infty d\tau \exp\left[(\mathcal{L}_{\mathbf{C}} + \mathcal{L}_{\mathbf{I}})\tau\right] \mathcal{L}_{\mathbf{IC}}\right\} v(t). \tag{3.51}$$

It will be convenient to modify the variable of integration $\tau \to -\tau$ such that the argument of the exponential is negative

$$\dot{v}(t) = \mathcal{L}_{\mathbf{C}}v(t) + \left\{\mathcal{P}\mathcal{L}_{\mathbf{IC}}\int_{-\infty}^0 d\tau \exp\left[-(\mathcal{L}_{\mathbf{C}} + \mathcal{L}_{\mathbf{I}})\tau\right] \mathcal{L}_{\mathbf{IC}}\right\} v(t). \tag{3.52}$$

3.3.2 Hamiltonian terms

The Hamiltonian terms arise from the $\mathcal{L}_{\mathbf{C}}v(t)$ term of (3.52)

$$\dot{\rho}_{\mathbf{C}}|_H = \mathcal{L}_{\mathbf{C}}\rho_{\mathbf{C}} = -\frac{i}{\hbar}\left[H_{\mathbf{C}}, \rho_{\mathbf{C}}\right], \tag{3.53}$$

where

$$\hat{H}_{\mathbf{C}} = \hat{H}_0 + \hat{H}_F. \tag{3.54}$$

Here we have defined the *forward-scattering* Hamiltonian[2] as

$$\hat{H}_F = 2g\int d^3\mathbf{r} n_{\mathbf{I}}(\mathbf{r})\hat{\psi}^\dagger(\mathbf{r})\hat{\psi}(\mathbf{r}), \tag{3.55}$$

with the incoherent region density

$$n_{\mathbf{I}}(\mathbf{r}) = \mathrm{Tr}_{\mathbf{I}}\left[\rho_{\mathbf{I}}\hat{\phi}^\dagger(\mathbf{r})\hat{\phi}(\mathbf{r})\right] = \langle\hat{\phi}^\dagger(\mathbf{r})\hat{\phi}(\mathbf{r})\rangle. \tag{3.56}$$

The forward-scattering term takes into account the influence of the average incoherent region density, taking the form of a Hartree-Fock term. It is convenient to include this term by defining an effective potential

$$V_{\mathrm{eff}}(\mathbf{r}) \equiv V_{\mathrm{ext}}(\mathbf{r}) + 2gn_{\mathbf{I}}(\mathbf{r}), \tag{3.57}$$

which then defines the *effective single-particle Hamiltonian*

$$H_{\mathrm{sp}}^{\mathrm{eff}} = -\frac{\hbar^2}{2m}\nabla^2 + V_{\mathrm{eff}}(\mathbf{r}). \tag{3.58}$$

3.3.3 Reservoir interaction terms

The second part of (3.52) accounts for interactions between the coherent and incoherent regions. We expand $\mathcal{L}_{\mathbf{IC}}$ as

$$\mathcal{L}_{\mathbf{IC}} \equiv \mathcal{L}_{\mathbf{IC}}^{(1)} + \mathcal{L}_{\mathbf{IC}}^{(2)} + \mathcal{L}_{\mathbf{IC}}^{(3)}, \tag{3.59}$$

[2] See appendix A.

then

$$\dot{\rho}_{\mathbf{C}}|_{\mathbf{IC}} = \dot{\rho}_{\mathbf{C}}|_{(1)} + \dot{\rho}_{\mathbf{C}}|_{(2)} + \dot{\rho}_{\mathbf{C}}|_{(3)}, \tag{3.60}$$

where

$$\dot{\rho}_{\mathbf{C}}|_{(1)} = \mathrm{Tr}_{\mathbf{I}}\left[\left\{\mathcal{P}\mathcal{L}^{(1)}_{\mathbf{IC}}\int_{-\infty}^{0} d\tau \exp\left[-(\mathcal{L}_{\mathbf{C}}+\mathcal{L}_{\mathbf{I}})\tau\right]\mathcal{L}^{(1)}_{\mathbf{IC}}\right\}\rho_{\mathbf{C}}(t)\otimes\rho_{\mathbf{I}}\right], \tag{3.61}$$

$$\dot{\rho}_{\mathbf{C}}|_{(2)} = \mathrm{Tr}_{\mathbf{I}}\left[\left\{\mathcal{P}\mathcal{L}^{(2)}_{\mathbf{IC}}\int_{-\infty}^{0} d\tau \exp\left[-(\mathcal{L}_{\mathbf{C}}+\mathcal{L}_{\mathbf{I}})\tau\right]\mathcal{L}^{(2)}_{\mathbf{IC}}\right\}\rho_{\mathbf{C}}(t)\otimes\rho_{\mathbf{I}}\right], \tag{3.62}$$

$$\dot{\rho}_{\mathbf{C}}|_{(3)} = \mathrm{Tr}_{\mathbf{I}}\left[\left\{\mathcal{P}\mathcal{L}^{(3)}_{\mathbf{IC}}\int_{-\infty}^{0} d\tau \exp\left[-(\mathcal{L}_{\mathbf{C}}+\mathcal{L}_{\mathbf{I}})\tau\right]\mathcal{L}^{(3)}_{\mathbf{IC}}\right\}\rho_{\mathbf{C}}(t)\otimes\rho_{\mathbf{I}}\right]. \tag{3.63}$$

There are no terms like (3.61) that involve cross-terms between the interaction terms, for example $\mathcal{L}^{(1)}_{\mathbf{IC}}$ and $\mathcal{L}^{(2)}_{\mathbf{IC}}$. This is because no non-zero contributions remain after Hartree-Fock factorization of the reservoir correlation functions stemming from these cross-terms for a thermalised incoherent region[3].

To evaluate these terms, we introduce the following definitions and notation. For a general function $f(\mathbf{r})$, we have

$$e^{-(\mathcal{L}_{\mathbf{C}}+\mathcal{L}_{\mathbf{I}})\tau}f(\mathbf{r}) = e^{i\hat{H}_{\mathbf{C}}\tau/\hbar}e^{i\hat{H}_{\mathbf{I}}\tau/\hbar}f(\mathbf{r})e^{-i\hat{H}_{\mathbf{C}}\tau/\hbar}e^{-i\hat{H}_{\mathbf{I}}\tau/\hbar}. \tag{3.64}$$

To simplify the formalism we will use interaction picture operators, defined as

$$\hat{\psi}(\mathbf{r},t) = e^{i\hat{H}_{\mathbf{C}}t/\hbar}\hat{\psi}(\mathbf{r})e^{-i\hat{H}_{\mathbf{C}}t/\hbar} = e^{-\mathcal{L}_{\mathbf{C}}t}\hat{\psi}(\mathbf{r}), \tag{3.65}$$

$$\hat{\phi}(\mathbf{r},t) = e^{i\hat{H}_{\mathbf{I}}t/\hbar}\hat{\phi}(\mathbf{r})e^{-i\hat{H}_{\mathbf{I}}t/\hbar} = e^{-\mathcal{L}_{\mathbf{I}}t}\hat{\phi}(\mathbf{r}). \tag{3.66}$$

Number damping process: One-field terms

The one-field terms (3.61) refer to the reservoir interaction terms in (3.52) that contain one instance of the coherent region field operator. These terms correspond physically to the *number-damping* process, interactions between two reservoir atoms that result in an energy exchange where one atom loses sufficient energy that it moves into the coherent region, as well as the reverse process. Evaluating (3.61) using (3.64) gives[4]

[3] See appendix B.1.
[4] See appendix B.2.

$$\begin{aligned}\dot{\rho}_{\mathbf{C}}|_{(1)} &= \frac{g^2}{\hbar^2}\int d^3\mathbf{r}\int d^3\mathbf{r}'\int_{-\infty}^{0} d\tau\Big\{ \\ &\langle\hat{\phi}^\dagger(\mathbf{r}',\tau)\hat{\phi}^\dagger(\mathbf{r}',\tau)\hat{\phi}(\mathbf{r}',\tau)\hat{\phi}^\dagger(\mathbf{r},0)\hat{\phi}(\mathbf{r},0)\hat{\phi}(\mathbf{r},0)\rangle\left[\hat{\psi}^\dagger(\mathbf{r},0),\rho_{\mathbf{C}}\hat{\psi}(\mathbf{r}',\tau)\right] \\ &+\langle\hat{\phi}^\dagger(\mathbf{r}',\tau)\hat{\phi}(\mathbf{r}',\tau)\hat{\phi}(\mathbf{r}',\tau)\hat{\phi}^\dagger(\mathbf{r},0)\hat{\phi}^\dagger(\mathbf{r},0)\hat{\phi}(\mathbf{r},0)\rangle\left[\hat{\psi}(\mathbf{r},0),\rho_{\mathbf{C}}\hat{\psi}^\dagger(\mathbf{r}',\tau)\right] \\ &+\langle\hat{\phi}^\dagger(\mathbf{r},0)\hat{\phi}^\dagger(\mathbf{r},0)\hat{\phi}(\mathbf{r},0)\hat{\phi}^\dagger(\mathbf{r}',\tau)\hat{\phi}(\mathbf{r}',\tau)\hat{\phi}(\mathbf{r}',\tau)\rangle\left[\hat{\psi}^\dagger(\mathbf{r}',\tau)\rho_{\mathbf{C}},\hat{\psi}(\mathbf{r},0)\right] \\ &+\langle\hat{\phi}^\dagger(\mathbf{r},0)\hat{\phi}(\mathbf{r},0)\hat{\phi}(\mathbf{r},0)\hat{\phi}^\dagger(\mathbf{r}',\tau)\hat{\phi}^\dagger(\mathbf{r}',\tau)\hat{\phi}(\mathbf{r}',\tau)\rangle\left[\hat{\psi}(\mathbf{r}',\tau)\rho_{\mathbf{C}},\hat{\psi}^\dagger(\mathbf{r},0)\right]\Big\},\end{aligned} \tag{3.67}$$

where we have used

$$\langle\hat{\mathcal{R}}[\hat{\phi}^\dagger(\mathbf{r}',\tau),\hat{\phi}(\mathbf{r}',\tau),\hat{\phi}^\dagger(\mathbf{r},0),\hat{\phi}(\mathbf{r},0)]\rangle = \mathrm{Tr}_{\mathbf{I}}\left[\hat{\mathcal{R}}[\hat{\phi}^\dagger(\mathbf{r}',\tau),\hat{\phi}(\mathbf{r}',\tau),\hat{\phi}^\dagger(\mathbf{r},0),\hat{\phi}(\mathbf{r},0)]\rho_{\mathbf{I}}\right], \tag{3.68}$$

with $\hat{\mathcal{R}}[\hat{\phi}^\dagger(\mathbf{r}',\tau),\hat{\phi}(\mathbf{r}',\tau),\hat{\phi}^\dagger(\mathbf{r},0),\hat{\phi}(\mathbf{r},0)]$ a product of the incoherent field operators.

Energy damping process: Two-field terms

The two-field terms (3.62) refer to the reservoir interaction terms in (3.52) that contain two instances coherent region field operator. These terms correspond physically to the *energy-damping* process, interactions between one coherent region atom and one reservoir atom that result in an energy exchange such that there is no net change in particle number for either the coherent region or the reservoir. Evaluating (3.62) using (3.64) gives[5]

$$\begin{aligned}\dot{\rho}_{\mathbf{C}}|_{(2)} &= \frac{4g^2}{\hbar^2}\int d^3\mathbf{r}\int d^3\mathbf{r}'\int_{-\infty}^{0} d\tau\Big\{ \\ &\langle\hat{\phi}^\dagger(\mathbf{r}',\tau)\hat{\phi}(\mathbf{r}',\tau)\hat{\phi}^\dagger(\mathbf{r},0)\hat{\phi}(\mathbf{r},0)\rangle\left[\hat{n}(\mathbf{r},0),\rho_{\mathbf{C}}\hat{n}(\mathbf{r}',\tau)\right] \\ &+\langle\hat{\phi}^\dagger(\mathbf{r},0)\hat{\phi}(\mathbf{r},0)\hat{\phi}^\dagger(\mathbf{r}',\tau)\hat{\phi}(\mathbf{r}',\tau)\rangle\left[\hat{n}(\mathbf{r}',\tau)\rho_{\mathbf{C}},\hat{n}(\mathbf{r},0)\right]\Big\},\end{aligned} \tag{3.69}$$

where we have introduced the coherent region number density operator

$$\hat{n}(\mathbf{r},t) = \hat{\psi}^\dagger(\mathbf{r},t)\hat{\psi}(\mathbf{r},t). \tag{3.70}$$

[5] See appendix B.3.

Here we have neglected all terms that contain the anomalous field operator pairings $\hat{\psi}^\dagger\hat{\psi}^\dagger$, $\hat{\psi}\hat{\psi}$, $\hat{\phi}^\dagger\hat{\phi}^\dagger$, and $\hat{\phi}\hat{\phi}$. The terms we have retained are know as *resonant* terms, while those we neglected are *non-resonant*. When neglecting the condensate energy relative to the reservoir, the non-resonant terms violate energy conservation, hence their non-inclusion.

Three-field terms

The entirety of (3.63) are also neglected, since they do not lead to processes that conserve energy and momentum [146]. This can be seen by following the procedure used for the one and two-field terms in Sections 3.3.5 and 3.3.6. For the case of $\mathcal{L}^{(3)}_{\mathbf{IC}}$, the resulting Wigner function phase space integral [compare with (3.88)] is formally zero, otherwise the delta-function term would violate energy conservation[6].

3.3.4 Reservoir correlation functions

Hartree-Fock factorization

We treat the incoherent region as fully thermalized, so we may assume that the incoherent region density operator is quantum Gaussian. This allows us to factorize the reservoir correlation functions using *Hartree-Fock factorization*. This leads to a sum of all possible factorizations into pair averages in which the order of the operators in the individual pair averages is the same as within the many-operator average [267]. The Hartree-Fock factorization of six operators is

$$\begin{aligned}\langle ABCDEF\rangle \;=\; &\langle AB\rangle\langle CD\rangle\langle EF\rangle + \langle AB\rangle\langle CE\rangle\langle DF\rangle + \langle AB\rangle\langle CF\rangle\langle DE\rangle \\ &+\langle AC\rangle\langle BD\rangle\langle EF\rangle + \langle AC\rangle\langle BE\rangle\langle DF\rangle + \langle AC\rangle\langle BF\rangle\langle DE\rangle \\ &+\langle AD\rangle\langle BC\rangle\langle EF\rangle + \langle AD\rangle\langle BE\rangle\langle CF\rangle + \langle AD\rangle\langle BF\rangle\langle CE\rangle \\ &+\langle AE\rangle\langle BC\rangle\langle DF\rangle + \langle AE\rangle\langle BD\rangle\langle CF\rangle + \langle AE\rangle\langle BF\rangle\langle CD\rangle \\ &+\langle AF\rangle\langle BC\rangle\langle DF\rangle + \langle AF\rangle\langle BD\rangle\langle CE\rangle + \langle AF\rangle\langle BE\rangle\langle CD\rangle, \end{aligned} \tag{3.71}$$

while for four operators

$$\langle ABCD\rangle \;=\; \langle AB\rangle\langle CD\rangle + \langle AC\rangle\langle BD\rangle + \langle AD\rangle\langle BC\rangle. \tag{3.72}$$

[6] See appendix B.4.

Since the incoherent region is approximated as a non-interacting thermal distribution the anomalous averages $\langle\hat{\phi}^\dagger\hat{\phi}^\dagger\rangle$ and $\langle\hat{\phi}\hat{\phi}\rangle$ are zero, and furthermore we neglect terms like $\langle\hat{\phi}^\dagger(\mathbf{r}',\tau)\hat{\phi}(\mathbf{r}',\tau)\rangle$ where the position and time are equal as they do not conserve energy. So for example the first term in (3.67) is

$$\begin{aligned}\langle\hat{\phi}^\dagger(\mathbf{r}',\tau)\hat{\phi}^\dagger(\mathbf{r}',\tau)\hat{\phi}(\mathbf{r}',\tau)\hat{\phi}^\dagger(\mathbf{r},0)\hat{\phi}(\mathbf{r},0)\hat{\phi}(\mathbf{r},0)\rangle \;&=\; 2\langle\hat{\phi}^\dagger(\mathbf{r}',\tau)\hat{\phi}(\mathbf{r},0)\rangle \\ &\quad\times\langle\hat{\phi}^\dagger(\mathbf{r}',\tau)\hat{\phi}(\mathbf{r},0)\rangle \\ &\quad\times\langle\hat{\phi}(\mathbf{r}',\tau)\hat{\phi}^\dagger(\mathbf{r},0)\rangle, \qquad (3.73)\end{aligned}$$

and we can factorize the remaining correlations of (3.67) and (3.69) in the same manner.

Semiclassical Wigner representation

The one-body correlations can be approximated using the one-body Wigner function [267]

$$W(\mathbf{r},\mathbf{k}) = \int d^3\mathbf{v}\langle\hat{\phi}^\dagger(\mathbf{r}+\mathbf{v}/2)\hat{\phi}(\mathbf{r}-\mathbf{v}/2)\rangle e^{i\mathbf{k}\cdot\mathbf{v}}, \qquad (3.74)$$

so the incoherent region particle density can be recovered by integrating over the distribution

$$n_{\mathbf{I}}(\mathbf{r}) \equiv \langle\hat{\phi}^\dagger(\mathbf{r})\hat{\phi}(\mathbf{r})\rangle = \frac{1}{(2\pi)^3}\int_{\mathbf{I}} d^3\mathbf{k}\, W(\mathbf{r},\mathbf{k}). \qquad (3.75)$$

If the incoherent region is in a state of thermal equilibrium, it can be accurately described using a semiclassical approximation. For a reservoir in equilibrium with temperature T and chemical potential μ, and employing the local-density approximation, the Wigner function is simply given by the Bose-Einstein distribution [268]

$$W(\mathbf{r},\mathbf{k}) = \frac{1}{\exp\left[\beta\left(\hbar\omega(\mathbf{r},\mathbf{k})-\mu\right)\right]-1}, \qquad (3.76)$$

where the semiclassical energy is

$$\hbar\omega(\mathbf{r},\mathbf{k}) = \frac{\hbar^2\mathbf{k}^2}{2m} + V(\mathbf{r}). \qquad (3.77)$$

Approximate correlation functions

We are now able to evaluate the one-body correlations within a semiclassical approximation. Defining $\mathbf{u} = (\mathbf{r} + \mathbf{r}')/2$ and $\mathbf{v} = \mathbf{r} - \mathbf{r}'$, the pair correlations are approximated over the reservoir correlation times by

$$\langle \hat{\phi}^\dagger(\mathbf{r},0)\hat{\phi}(\mathbf{r}',\tau)\rangle \approx \int_{\mathbf{I}} \frac{d^3\mathbf{k}}{(2\pi)^3} W(\mathbf{u},\mathbf{k}) e^{-i\mathbf{k}\cdot\mathbf{v} - i\omega(\mathbf{u},\mathbf{k})\tau}, \tag{3.78}$$

$$\langle \hat{\phi}(\mathbf{r},0)\hat{\phi}^\dagger(\mathbf{r}',\tau)\rangle \approx \int_{\mathbf{I}} \frac{d^3\mathbf{k}}{(2\pi)^3} \left[1 + W(\mathbf{u},\mathbf{k})\right] e^{i\mathbf{k}\cdot\mathbf{v} + i\omega(\mathbf{u},\mathbf{k})\tau}, \tag{3.79}$$

$$\langle \hat{\phi}(\mathbf{r}',\tau)\hat{\phi}^\dagger(\mathbf{r},0)\rangle \approx \int_{\mathbf{I}} \frac{d^3\mathbf{k}}{(2\pi)^3} \left[1 + W(\mathbf{u},\mathbf{k})\right] e^{-i\mathbf{k}\cdot\mathbf{v} - i\omega(\mathbf{u},\mathbf{k})\tau}, \tag{3.80}$$

$$\langle \hat{\phi}^\dagger(\mathbf{r}',\tau)\hat{\phi}(\mathbf{r},0)\rangle \approx \int_{\mathbf{I}} \frac{d^3\mathbf{k}}{(2\pi)^3} W(\mathbf{u},\mathbf{k}) e^{i\mathbf{k}\cdot\mathbf{v} + i\omega(\mathbf{u},\mathbf{k})\tau}, \tag{3.81}$$

where the subscript $\mathbf{I}$ on the integration limit represents the semiclassical incoherent region of phase space $\mathbf{I} = \{\hbar\omega(\mathbf{r},\mathbf{k}) > \epsilon_{\text{cut}}\}$.

3.3.5 Master equation for number damping terms

Applying the Hartree-Fock factorization (3.71) to the number-damping terms (3.67) leads to

$$\begin{aligned}
\dot{\rho}_{\mathbf{C}}|_{(1)} = \frac{2g^2}{\hbar^2} \int d^3\mathbf{r} \int d^3\mathbf{r}' \int_{-\infty}^{0} d\tau \Big\{ & \\
& \langle \hat{\phi}^\dagger(\mathbf{r}',\tau)\hat{\phi}(\mathbf{r},0)\rangle \langle \hat{\phi}^\dagger(\mathbf{r}',\tau)\hat{\phi}(\mathbf{r},0)\rangle \langle \hat{\phi}(\mathbf{r}',\tau)\hat{\phi}^\dagger(\mathbf{r},0)\rangle \left[\hat{\psi}^\dagger(\mathbf{r},0), \rho_{\mathbf{C}}\hat{\psi}(\mathbf{r}',\tau)\right] \\
& + \langle \hat{\phi}^\dagger(\mathbf{r}',\tau)\hat{\phi}(\mathbf{r},0)\rangle \langle \hat{\phi}(\mathbf{r}',\tau)\hat{\phi}^\dagger(\mathbf{r},0)\rangle \langle \hat{\phi}(\mathbf{r}',\tau)\hat{\phi}^\dagger(\mathbf{r},0)\rangle \left[\hat{\psi}(\mathbf{r},0), \rho_{\mathbf{C}}\hat{\psi}^\dagger(\mathbf{r}',\tau)\right] \\
& + \langle \hat{\phi}^\dagger(\mathbf{r},0)\hat{\phi}(\mathbf{r}',\tau)\rangle \langle \hat{\phi}^\dagger(\mathbf{r},0)\hat{\phi}(\mathbf{r}',\tau)\rangle \langle \hat{\phi}(\mathbf{r},0)\hat{\phi}^\dagger(\mathbf{r}',\tau)\rangle \left[\hat{\psi}^\dagger(\mathbf{r}',\tau)\rho_{\mathbf{C}}, \hat{\psi}(\mathbf{r},0)\right] \\
& + \langle \hat{\phi}^\dagger(\mathbf{r},0)\hat{\phi}(\mathbf{r}',\tau)\rangle \langle \hat{\phi}(\mathbf{r},0)\hat{\phi}^\dagger(\mathbf{r}',\tau)\rangle \langle \hat{\phi}(\mathbf{r},0)\hat{\phi}^\dagger(\mathbf{r}',\tau)\rangle \left[\hat{\psi}(\mathbf{r}',\tau)\rho_{\mathbf{C}}, \hat{\psi}^\dagger(\mathbf{r},0)\right] \Big\}.
\end{aligned} \tag{3.82}$$

We now rewrite this equation in terms of the approximate reservoir correlation functions (3.78)-(3.81). This leads to the expression

$$\begin{aligned}
\dot{\rho}_{\mathbf{C}}|_{(1)} &= \frac{g^2}{(2\pi)^8\hbar^2}\int_{\mathbf{I}}d^3\mathbf{k}_1\int_{\mathbf{I}}d^3\mathbf{k}_2\int_{\mathbf{I}}d^3\mathbf{k}_3\int d^3\mathbf{u}\int d^3\mathbf{v}\Big\{ \\
&\Big[\hat{\psi}^\dagger(\mathbf{u}+\mathbf{v}/2),\rho_{\mathbf{C}}\Big\{\left[1+W(\mathbf{u},\mathbf{k}_1)\right]W(\mathbf{u},\mathbf{k}_2)W(\mathbf{u},\mathbf{k}_3)e^{i(\mathbf{k}_1-\mathbf{k}_2-\mathbf{k}_3)\cdot\mathbf{v}} \\
&\times\delta(\hat{L}_{\mathbf{C}}/\hbar+\omega(\mathbf{u},\mathbf{k}_1)-\omega(\mathbf{u},\mathbf{k}_2)-\omega(\mathbf{u},\mathbf{k}_3))\hat{\psi}(\mathbf{u}-\mathbf{v}/2)\Big\}\Big] \\
&+\Big[\hat{\psi}(\mathbf{u}+\mathbf{v}/2),\rho_{\mathbf{C}}\Big\{W(\mathbf{u},\mathbf{k}_1)\left[1+W(\mathbf{u},\mathbf{k}_2)\right]\left[1+W(\mathbf{u},\mathbf{k}_3)\right]e^{i(\mathbf{k}_1-\mathbf{k}_2-\mathbf{k}_3)\cdot\mathbf{v}} \\
&\times\delta(-\hat{L}_{\mathbf{C}}/\hbar+\omega(\mathbf{u},\mathbf{k}_1)-\omega(\mathbf{u},\mathbf{k}_2)-\omega(\mathbf{u},\mathbf{k}_3))\hat{\psi}^\dagger(\mathbf{u}-\mathbf{v}/2)\Big\}\Big] \\
&+\Big[\Big\{\left[1+W(\mathbf{u},\mathbf{k}_1)\right]W(\mathbf{u},\mathbf{k}_2)W(\mathbf{u},\mathbf{k}_3)e^{i(\mathbf{k}_1-\mathbf{k}_2-\mathbf{k}_3)\cdot\mathbf{v}} \\
&\times\delta(-\hat{L}_{\mathbf{C}}/\hbar+\omega(\mathbf{u},\mathbf{k}_1)-\omega(\mathbf{u},\mathbf{k}_2)-\omega(\mathbf{u},\mathbf{k}_3))\hat{\psi}^\dagger(\mathbf{u}-\mathbf{v}/2)\Big\}\rho_{\mathbf{C}},\hat{\psi}(\mathbf{u}+\mathbf{v}/2)\Big] \\
&+\Big[\Big\{W(\mathbf{u},\mathbf{k}_1)\left[1+W(\mathbf{u},\mathbf{k}_2)\right]\left[1+W(\mathbf{u},\mathbf{k}_3)\right]e^{i(\mathbf{k}_1-\mathbf{k}_2-\mathbf{k}_3)\cdot\mathbf{v}} \\
&\times\delta(\hat{L}_{\mathbf{C}}/\hbar+\omega(\mathbf{u},\mathbf{k}_1)-\omega(\mathbf{u},\mathbf{k}_2)-\omega(\mathbf{u},\mathbf{k}_3))\hat{\psi}(\mathbf{u}-\mathbf{v}/2)\Big\}\rho_{\mathbf{C}},\hat{\psi}^\dagger(\mathbf{u}+\mathbf{v}/2)\Big]\Big\},
\end{aligned} \tag{3.83}$$

where we have defined the coherent region operator

$$\hat{L}_{\mathbf{C}}\hat{\psi}(\mathbf{r}) = \left[\hat{\psi}(\mathbf{r}),\hat{H}_{\mathbf{C}}\right], \tag{3.84}$$

and noted that this leads to

$$\hat{\psi}(\mathbf{r},t) = e^{-i\hat{L}_{\mathbf{C}}t/\hbar}\hat{\psi}(\mathbf{r}), \tag{3.85}$$

$$\hat{\psi}^\dagger(\mathbf{r},t) = e^{-i\hat{L}_{\mathbf{C}}t/\hbar}\hat{\psi}^\dagger(\mathbf{r}). \tag{3.86}$$

In (3.83) we have ignored the principal value of the time integral

$$\int_{-\infty}^{0}d\tau e^{-i\omega\tau} = \pi\delta(\omega)+iP(1/\omega)\approx\pi\delta(\omega), \tag{3.87}$$

a physically appropriate approximation as it ensures that scattering events between coherent region and incoherent region atoms conserve energy. We now define the *number-damp-*

ing amplitudes

$$G^{(+)}(\mathbf{u},\mathbf{v},\epsilon) = \frac{g^2}{(2\pi)^8\hbar^2}\int_{\mathbf{I}} d^3\mathbf{k}_1 \int_{\mathbf{I}} d^3\mathbf{k}_2 \int_{\mathbf{I}} d^3\mathbf{k}_3 \left[1+W(\mathbf{u},\mathbf{k}_1)\right] W(\mathbf{u},\mathbf{k}_2)W(\mathbf{u},\mathbf{k}_3) \times e^{i(\mathbf{k}_1-\mathbf{k}_2-\mathbf{k}_3)\cdot\mathbf{v}}\delta(\epsilon/\hbar+\omega(\mathbf{u},\mathbf{k}_1)-\omega(\mathbf{u},\mathbf{k}_2)-\omega(\mathbf{u},\mathbf{k}_3)), \tag{3.88}$$

$$G^{(-)}(\mathbf{u},\mathbf{v},\epsilon) = \frac{g^2}{(2\pi)^8\hbar^2}\int_{\mathbf{I}} d^3\mathbf{k}_1 \int_{\mathbf{I}} d^3\mathbf{k}_2 \int_{\mathbf{I}} d^3\mathbf{k}_3 W(\mathbf{u},\mathbf{k}_1)\left[1+W(\mathbf{u},\mathbf{k}_2)\right]\left[1+W(\mathbf{u},\mathbf{k}_3)\right] \times e^{i(\mathbf{k}_1-\mathbf{k}_2-\mathbf{k}_3)\cdot\mathbf{v}}\delta(\epsilon/\hbar+\omega(\mathbf{u},\mathbf{k}_1)-\omega(\mathbf{u},\mathbf{k}_2)-\omega(\mathbf{u},\mathbf{k}_3)), \tag{3.89}$$

such that the number-damping master equation terms can be written in the much more elegant form

$$\begin{aligned}\dot{\rho}_{\mathbf{C}}|_{(1)} = \int d^3\mathbf{u}\int d^3\mathbf{v}\Big\{ &\Big[\hat{\psi}^\dagger(\mathbf{u}+\mathbf{v}/2),\rho_{\mathbf{C}}\Big\{G^{(+)}(\mathbf{u},\mathbf{v},\hat{L}_{\mathbf{C}})\Big\}\hat{\psi}(\mathbf{u}-\mathbf{v}/2)\Big]\\ &+\Big[\hat{\psi}(\mathbf{u}+\mathbf{v}/2),\rho_{\mathbf{C}}\Big\{G^{(-)}(\mathbf{u},\mathbf{v},-\hat{L}_{\mathbf{C}})\Big\}\hat{\psi}^\dagger(\mathbf{u}-\mathbf{v}/2)\Big]\\ &+\Big[\Big\{G^{(+)}(\mathbf{u},\mathbf{v},-\hat{L}_{\mathbf{C}})\Big\}\hat{\psi}^\dagger(\mathbf{u}-\mathbf{v}/2)\rho_{\mathbf{C}},\hat{\psi}(\mathbf{u}+\mathbf{v}/2)\Big]\\ &+\Big[\Big\{G^{(-)}(\mathbf{u},\mathbf{v},\hat{L}_{\mathbf{C}})\Big\}\hat{\psi}(\mathbf{u}-\mathbf{v}/2)\rho_{\mathbf{C}},\hat{\psi}^\dagger(\mathbf{u}+\mathbf{v}/2)\Big]\Big\}.\end{aligned} \tag{3.90}$$

3.3.6 Master equation for energy damping terms

Applying the Hartree-Fock factorization (3.72) to the energy-damping terms (3.69) leads to

$$\begin{aligned}\dot{\rho}_{\mathbf{C}}|_{(2)} = \frac{4g^2}{\hbar^2}\int d^3\mathbf{r}\int d^3\mathbf{r}'\int_{-\infty}^{0} d\tau\Big\{ &\langle\hat{\phi}^\dagger(\mathbf{r}',\tau)\hat{\phi}(\mathbf{r},0)\rangle\langle\hat{\phi}(\mathbf{r}',\tau)\hat{\phi}^\dagger(\mathbf{r},0)\rangle\left[\hat{n}(\mathbf{r},0),\rho_{\mathbf{C}}\hat{n}(\mathbf{r}',\tau)\right]\\ &+\langle\hat{\phi}^\dagger(\mathbf{r},0)\hat{\phi}(\mathbf{r}',\tau)\rangle\langle\hat{\phi}(\mathbf{r},0)\hat{\phi}^\dagger(\mathbf{r}',\tau)\rangle\left[\hat{n}(\mathbf{r}',\tau)\rho_{\mathbf{C}},\hat{n}(\mathbf{r},0)\right]\Big\}.\end{aligned} \tag{3.91}$$

Just as we did for the number-damping terms, we rewrite the equation in terms of the approximate reservoir correlation functions (3.78)-(3.81) and neglect the principal part of

the time integral (3.87). This leads to the expression

$$\begin{aligned}\dot{\rho}_{\mathbf{C}}|_{(2)} &= \frac{2g^2}{\hbar^2(2\pi)^5}\int_{\mathbf{I}} d^3\mathbf{k}_1 \int_{\mathbf{I}} d^3\mathbf{k}_2 \int d^3\mathbf{u} \int d^3\mathbf{v}\Big\{ \\ &\Big[\hat{n}(\mathbf{u}+\mathbf{v}/2), \rho_{\mathbf{C}}\Big\{W(\mathbf{u},\mathbf{k}_1)\left[1+W(\mathbf{u},\mathbf{k}_2)\right] e^{i(\mathbf{k}_1-\mathbf{k}_2)\cdot\mathbf{v}} \\ &\times\delta(\omega(\mathbf{u},\mathbf{k}_1)-\omega(\mathbf{u},\mathbf{k}_2)-\hat{L}_{\mathbf{C}}/\hbar)\hat{n}(\mathbf{u}-\mathbf{v}/2)\Big\}\Big] \\ &+\Big[\Big\{W(\mathbf{u},\mathbf{k}_1)\left[1+W(\mathbf{u},\mathbf{k}_2)\right] e^{i(\mathbf{k}_1-\mathbf{k}_2)\cdot\mathbf{v}} \\ &\times\delta(\omega(\mathbf{u},\mathbf{k}_1)-\omega(\mathbf{u},\mathbf{k}_2)+\hat{L}_{\mathbf{C}}/\hbar)\hat{n}(\mathbf{u}-\mathbf{v}/2)\Big\}\rho_{\mathbf{C}}, \hat{n}(\mathbf{u}+\mathbf{v}/2)\Big]\Big\}, \end{aligned} \tag{3.92}$$

from which we define the *energy-damping amplitude*

$$\begin{aligned}M(\mathbf{u},\mathbf{v},\epsilon) &= \frac{2g^2}{\hbar^2(2\pi)^5}\int_{\mathbf{I}} d^3\mathbf{k}_1 \int_{\mathbf{I}} d^3\mathbf{k}_2 W(\mathbf{u},\mathbf{k}_1)\left[1+W(\mathbf{u},\mathbf{k}_2)\right] \\ &\times e^{i(\mathbf{k}_1-\mathbf{k}_2)\cdot\mathbf{v}}\delta(\omega(\mathbf{u},\mathbf{k}_1)-\omega(\mathbf{u},\mathbf{k}_2)-\epsilon/\hbar), \end{aligned} \tag{3.93}$$

leading to the simplified expression for the energy-damping master equation terms

$$\begin{aligned}\dot{\rho}_{\mathbf{C}}|_{(2)} &= \int d^3\mathbf{u}\int d^3\mathbf{v}\Big\{\Big[\hat{n}(\mathbf{u}+\mathbf{v}/2), \rho_{\mathbf{C}}\Big\{M(\mathbf{u},\mathbf{v},\hat{L}_{\mathbf{C}})\hat{n}(\mathbf{u}-\mathbf{v}/2)\Big\}\Big] \\ &+\Big[\Big\{M(\mathbf{u},\mathbf{v},-\hat{L}_{\mathbf{C}})\hat{n}(\mathbf{u}-\mathbf{v}/2)\Big\}\rho_{\mathbf{C}}, \hat{n}(\mathbf{u}+\mathbf{v}/2)\Big]\Big\}. \end{aligned} \tag{3.94}$$

3.3.7 High temperature regime master equation

We are interested in the high-temperature regime, where the eigenvalues of the coherent region operator $\hat{L}_{\mathbf{C}}$ are very small compared to the temperature, that is

$$\epsilon_n \ll k_B T \tag{3.95}$$

with ϵ_n the eigenvalues of $\hat{L}_{\mathbf{C}}$.

Forward-backward relations

If the reservoir is in thermal equilibrium, then the Wigner function takes the semiclassical form (3.76) and the number-damping and energy-damping amplitudes satisfy what is known as the *forward-backward relations*. The two number-damping amplitudes are related

by

$$G^{(-)}(\mathbf{u},\mathbf{v},\epsilon) = e^{\beta(\epsilon-\mu)}G^{(+)}(\mathbf{u},\mathbf{v},\epsilon), \tag{3.96}$$

while the energy-damping amplitude satisfies

$$M(\mathbf{u},\mathbf{v},\epsilon) = e^{-\beta\epsilon}M(\mathbf{u},\mathbf{v},-\epsilon). \tag{3.97}$$

In the high-temperature regime we can linearize the forward-backward relations with respect to the energy ϵ.

Number-damping terms

We assume that the local condensate energy is small compared to the energy of the scattering process represented in (3.88) [269], allowing us to the neglect the coherent region energy, that is

$$G^{(+)}(\mathbf{u},\mathbf{v},\epsilon) \approx G^{(+)}(\mathbf{u},\mathbf{v},0). \tag{3.98}$$

Using this and linearizing (3.96) leads to

$$G^{(-)}(\mathbf{u},\mathbf{v},\epsilon) \approx \left(1-\frac{\mu-\epsilon}{k_BT}\right)G^{(+)}(\mathbf{u},\mathbf{v},0). \tag{3.99}$$

Recognising that the number-damping amplitudes (3.88) and (3.89) are sharply peaked functions of $\mathbf{v}$, we are able to approximate that

$$\hat{\psi}(\mathbf{u}+\mathbf{v}/2) \approx \hat{\psi}(\mathbf{u}) \tag{3.100}$$

in the number-damping master equation terms (3.90). We can then write the number-damping master equation terms as

$$\begin{aligned}\dot{\rho}_{\mathbf{C}}|_{(1)} \;=\; & \int d^3\mathbf{u}G(\mathbf{u})\Big\{\Big[\Big[\hat{\psi}(\mathbf{u}),\rho_{\mathbf{C}}\Big],\hat{\psi}^\dagger(\mathbf{u})\Big]+\Big[\hat{\psi}(\mathbf{u}),\Big[\rho_{\mathbf{C}},\hat{\psi}^\dagger(\mathbf{u})\Big]\Big] \\ & -\frac{1}{k_BT}\left(\Big[\Big(\mu-\hat{L}_{\mathbf{C}}\Big)\hat{\psi}(\mathbf{u})\rho_{\mathbf{C}},\hat{\psi}^\dagger(\mathbf{u})\Big]+\Big[\hat{\psi}(\mathbf{u}),\rho_{\mathbf{C}}\Big(\mu+\hat{L}_{\mathbf{C}}\Big)\hat{\psi}^\dagger(\mathbf{u})\Big]\right)\Big\}.\end{aligned} \tag{3.101}$$

where

$$G(\mathbf{u}) \equiv \int d^3\mathbf{v} G^{(+)}(\mathbf{u},\mathbf{v},0). \tag{3.102}$$

Energy-damping terms

The linearization of (3.97) leads to

$$M(\mathbf{u},\mathbf{v},\epsilon) \approx \left(1-\frac{\epsilon}{2k_BT}\right) M(\mathbf{u},\mathbf{v},0). \tag{3.103}$$

We are unable to treat the energy-damping as a local process as we did for the number-damping, due to the form of the energy-damping amplitude (3.93). We are able to reduce $M(\mathbf{u},\mathbf{v},0)$ to a nonlocal form [146]

$$M(\mathbf{u},\mathbf{v},0) = \frac{k_BT}{\hbar}\varepsilon(\mathbf{r}-\mathbf{r}') \tag{3.104}$$

as shown in appendix C.2. We will discuss the specific form of $\varepsilon(\mathbf{r}-\mathbf{r}')$ after we have obtained the final equation of motion, for now we retain the general form. The energy-damping master equation is now

$$\begin{aligned}\dot{\rho}_{\mathbf{C}}|_{(2)} = &-\int d^3\mathbf{r}\int d^3\mathbf{r}'\varepsilon(\mathbf{r}-\mathbf{r}')\left\{\frac{k_BT}{\hbar}\left[\hat{n}(\mathbf{r}),[\hat{n}(\mathbf{r}'),\rho_{\mathbf{C}}]\right]\right.\\ &\left.+\frac{1}{2\hbar}\left[\hat{n}(\mathbf{r}),\left[\hat{L}_{\mathbf{C}}\hat{n}(\mathbf{r}'),\rho_{\mathbf{C}}\right]_+\right]\right\}.\end{aligned} \tag{3.105}$$

where $[\hat{A},\hat{B}]_+ \equiv \hat{A}\hat{B}+\hat{B}\hat{A}$ is the anticommutator.

High temperature regime master equation

The final master equation for the coherent region density operator, valid in the high temperature regime, is

$$\dot{\rho}_{\mathbf{C}} \approx \dot{\rho}_{\mathbf{C}}|_H + \dot{\rho}_{\mathbf{C}}|_{(1)} + \dot{\rho}_{\mathbf{C}}|_{(2)}, \tag{3.106}$$

with $\dot{\rho}_{\mathbf{C}}|_{H_{\mathbf{C}}}$ given by (3.53), $\dot{\rho}_{\mathbf{C}}|_{(1)}$ given by (3.101), and $\dot{\rho}_{\mathbf{C}}|_{(2)}$ given by (3.105). The master equation in this form can be mapped to a Fokker-Planck equation using a Wigner representation of the density operator.

3.4 Fokker-Planck equation

We use phase-space methods to represent the coherent region density operator with the Wigner quasi-probability distribution [270]. In this section we derive a Fokker-Planck equation for evolution of the Wigner function.

3.4.1 Multimode Wigner representation

Representation of the coherent region

In projected classical field theory, the coherent region field operator is expanded in terms of eigenstates of the single-particle Hamiltonian, that is

$$\hat{\psi}(\mathbf{r}) = \sum_{n\in\mathbf{C}} \hat{a}_n \chi_n(\mathbf{r}), \tag{3.107}$$

where the $\hat{a}_n$ are mode operators obeying the usual Bose commutation relations

$$[\hat{a}_n, \hat{a}_m] = \left[\hat{a}_n^\dagger, \hat{a}_m^\dagger\right] = 0, \quad \left[\hat{a}_n, \hat{a}_m^\dagger\right] = \delta_{mn}, \tag{3.108}$$

and the $\chi_n(\mathbf{r})$ are eigenstates of the single-particle Hamiltonian (3.3)

$$H_{\rm sp}\chi_n(\mathbf{r}) = \epsilon_n \chi_n(\mathbf{r}), \tag{3.109}$$

with the index of summation n being a shorthand for all quantum numbers required to specify the eigenstate. The summation in (3.107) is restricted to eigenstates in the coherent region

$$\mathbf{C} = \left\{n : \epsilon_n \leq \epsilon_{\rm cut}\right\}, \tag{3.110}$$

with $\epsilon_{\rm cut}$ the cutoff energy defining the two regions. The projectors introduced in Section 3.2 can be defined in terms of the eigenstates

$$\mathcal{P}\left\{F(\mathbf{r})\right\} = \sum_{n\in\mathbf{C}} \chi_n(\mathbf{r}) \int d^3\mathbf{r}' \chi_n^*(\mathbf{r}') F(\mathbf{r}'), \tag{3.111}$$

$$\mathcal{Q}\left\{G(\mathbf{r})\right\} = \sum_{n\in\mathbf{I}} \chi_n(\mathbf{r}) \int d^3\mathbf{r}' \chi_n^*(\mathbf{r}') G(\mathbf{r}'), \tag{3.112}$$

where $F(\mathbf{r})$ and $G(\mathbf{r})$ are general functions, and the summation in (3.112) is restricted to eigenstates in the incoherent region

$$\mathbf{I} = \{n : \epsilon_{\text{cut}} < \epsilon_n \leq E_{\text{max}}\}, \tag{3.113}$$

with E_{max} the energy cutoff that defines the effective field theory defined in Section 2.2.2. The projector can also be equivalently written as

$$\mathcal{P}\{F(\mathbf{r})\} \equiv \int d^3\mathbf{r}' \delta(\mathbf{r}, \mathbf{r}') F(\mathbf{r}'), \tag{3.114}$$

where

$$\delta(\mathbf{r}, \mathbf{r}') = \sum_{n \in \mathbf{C}} \chi_n(\mathbf{r}) \chi_n^*(\mathbf{r}') \tag{3.115}$$

is the commutator of the coherent region field operators

$$\left[\hat{\psi}(\mathbf{r}), \hat{\psi}^\dagger(\mathbf{r}')\right] = \delta(\mathbf{r}, \mathbf{r}'), \tag{3.116}$$

known as the *projected delta function*. In the limit of infinitely high ϵ_{cut}, we recover the true Dirac delta

$$\lim_{\epsilon_{\text{cut}} \to \infty} \delta(\mathbf{r}, \mathbf{r}') = \delta(\mathbf{r} - \mathbf{r}'). \tag{3.117}$$

Multimode Wigner distribution

The multimode Wigner distribution for a system of M modes, easily obtained as a generalization of the single mode Wigner distribution [157, 229], is given by

$$W(\boldsymbol{\alpha}, \boldsymbol{\alpha}^*) = \frac{1}{\pi^{2M}} \int \prod_{n=1}^{M} d^2\lambda_n \exp\left(\sum_{m=1}^{M} \lambda_m^* \alpha_m - \lambda_m \alpha_m^*\right) \chi_W(\boldsymbol{\lambda}, \boldsymbol{\lambda}^*), \tag{3.118}$$

where $\boldsymbol{\lambda} = (\lambda_1, \lambda_2, ..., \lambda_M)$ is a vector of complex variables and the $\boldsymbol{\alpha} = (\alpha_1, \alpha_2, ..., \alpha_M)$ are the complex amplitudes of the modes. The function $\chi_W(\boldsymbol{\lambda}, \boldsymbol{\lambda}^*)$, defined as

$$\chi_W(\boldsymbol{\lambda}, \boldsymbol{\lambda}^*) \equiv \text{Tr}\left\{\hat{\rho} \exp\left(\sum_{n=1}^{M} \lambda_n \hat{a}_n^\dagger - \lambda_n^* \hat{a}_n\right)\right\}, \tag{3.119}$$

is the symmetrically ordered quantum characteristic function for a multimode bosonic field with density operator $\hat{\rho}$ and mode operators $\hat{a}_n$. General operators are expressed in terms of the mode operators $\hat{a}_n$, with the observables given by

$$\int d^2\boldsymbol{\alpha}\,(\alpha_m^*)^p(\alpha_n)^q W(\boldsymbol{\alpha},\boldsymbol{\alpha}^*) = \left\langle \left\{(\hat{a}_m^\dagger)^p(\hat{a}_n)^q\right\}_S\right\rangle. \tag{3.120}$$

Here the curly braces $\{\cdot\}_S$ denotes the symmetrically ordered product of the arguments. For example for the number density operator $\hat{a}_n^\dagger\hat{a}_n$ for mode n

$$\left\{\hat{a}_n^\dagger\hat{a}_n\right\}_S = \frac{1}{2}\left(\hat{a}_n^\dagger\hat{a}_n + \hat{a}_n\hat{a}_n^\dagger\right), \tag{3.121}$$

and the quantum expectation is determined by

$$\int d^2\boldsymbol{\alpha}\,\alpha_n^*\alpha_n W(\boldsymbol{\alpha},\boldsymbol{\alpha}^*) = \frac{1}{2}\langle\hat{a}_n^\dagger\hat{a}_n + \hat{a}_n\hat{a}_n^\dagger\rangle = \langle\hat{a}_n^\dagger\hat{a}_n\rangle + \frac{1}{2}. \tag{3.122}$$

Note that we pick up an extra term due to the symmetrically ordered product, representing half a virtual particle per mode [151]. In the regime of validity for the SPGPE the extra term is much smaller than the operator expectation, and it is thus safely neglected.

Operator correspondences

A central component of phase-space methods is the *operator correspondences*. These correspondences allow the action of a quantum operator on the density matrix to be mapped to the action of a classical operator on a quasi-probability distribution, in this case the Wigner distribution. That is, we can map from a quantum representation of the system to an equivalent classical representation.

The classical field representation of the coherent region quantum field (3.107) is

$$\psi(\mathbf{r}) = \sum_{n\in\mathbf{C}} \alpha_n\chi_n(\mathbf{r}), \tag{3.123}$$

where again the α_n are the complex amplitudes of the modes; we have effectively made the replacements $\hat{\psi}(\mathbf{r}) \to \psi(\mathbf{r})$ and $\hat{a}_n \to \alpha_n$. The quantum to classical functional operator

correspondences for the Wigner distribution are [157, 229]

$$\hat{\psi}(\mathbf{r})\rho_{\mathbf{C}} \longleftrightarrow \left(\psi(\mathbf{r}) + \frac{1}{2}\frac{\bar{\delta}}{\bar{\delta}\psi^*(\mathbf{r})}\right) W, \tag{3.124}$$

$$\hat{\psi}^\dagger(\mathbf{r})\rho_{\mathbf{C}} \longleftrightarrow \left(\psi^*(\mathbf{r}) - \frac{1}{2}\frac{\bar{\delta}}{\bar{\delta}\psi(\mathbf{r})}\right) W, \tag{3.125}$$

$$\rho_{\mathbf{C}}\hat{\psi}(\mathbf{r}) \longleftrightarrow \left(\psi(\mathbf{r}) - \frac{1}{2}\frac{\bar{\delta}}{\bar{\delta}\psi^*(\mathbf{r})}\right) W, \tag{3.126}$$

$$\rho_{\mathbf{C}}\hat{\psi}^\dagger(\mathbf{r}) \longleftrightarrow \left(\psi^*(\mathbf{r}) + \frac{1}{2}\frac{\bar{\delta}}{\bar{\delta}\psi(\mathbf{r})}\right) W, \tag{3.127}$$

where we have introduced the *projected functional derivatives* [146]

$$\frac{\bar{\delta}}{\bar{\delta}\psi(\mathbf{r})} \equiv \sum_{n\in\mathbf{C}} \chi_n^*(\mathbf{r})\frac{\partial}{\partial\alpha_n}, \tag{3.128}$$

$$\frac{\bar{\delta}}{\bar{\delta}\psi^*(\mathbf{r})} \equiv \sum_{n\in\mathbf{C}} \chi_n(\mathbf{r})\frac{\partial}{\partial\alpha_n^*}. \tag{3.129}$$

Other useful mappings stemming from (3.124)-(3.127) include the commutator mappings

$$\left[\hat{\psi}(\mathbf{r}), \rho_{\mathbf{C}}\right] \longleftrightarrow \frac{\bar{\delta}}{\bar{\delta}\psi^*(\mathbf{r})} W, \tag{3.130}$$

$$\left[\hat{\psi}^\dagger(\mathbf{r}), \rho_{\mathbf{C}}\right] \longleftrightarrow -\frac{\bar{\delta}}{\bar{\delta}\psi(\mathbf{r})} W, \tag{3.131}$$

and repeated instances of the field operator stack in the way one would naively expect, for example

$$\hat{\psi}^\dagger(\mathbf{r})\hat{\psi}(\mathbf{r})\rho_{\mathbf{C}} \longleftrightarrow \left(\psi^*(\mathbf{r}) - \frac{1}{2}\frac{\bar{\delta}}{\bar{\delta}\psi(\mathbf{r})}\right)\left(\psi(\mathbf{r}) + \frac{1}{2}\frac{\bar{\delta}}{\bar{\delta}\psi^*(\mathbf{r})}\right) W. \tag{3.132}$$

We now use the operator correspondences to map the master equation (3.106) for the coherent region density matrix $\rho_{\mathbf{C}}$ to an equivalent equation of motion for the Wigner function W of the classical field $\psi(\mathbf{r})$.

3.4.2 Wigner evolution equation

Hamiltonian terms

Using the operator correspondences we map the Hamiltonian master equation (3.53) to a Wigner function evolution equation; the equation of motion is

$$\left.\frac{\partial W}{\partial t}\right|_H = \int d^3\mathbf{r}\left[\frac{ig}{4\hbar}\frac{\bar{\delta}^{(2)}}{\bar{\delta}\psi(\mathbf{r})\bar{\delta}\psi^*(\mathbf{r})}\psi^*(\mathbf{r})\frac{\bar{\delta}}{\bar{\delta}\psi^*(\mathbf{r})} + \text{c.c}\right]W + \int d^3\mathbf{r}\left[\frac{i}{\hbar}\frac{\bar{\delta}}{\bar{\delta}\psi(\mathbf{r})}\left\{H_{\text{sp}} + g|\psi(\mathbf{r})|^2\right\}\psi(\mathbf{r}) + \text{c.c}\right]W. \tag{3.133}$$

In principle this is solvable, however the phase-space occupied by the Wigner function is rather large. In addition to this, the third-order derivative term cannot be represented by an equivalent diffusion process that would allow a formulation in terms of a stochastic differential equation. In fact, in order to be mapped to a stochastic differential equation, the Wigner evolution equation must take the form of a Fokker-Planck equation, with derivatives up to second order and a positive-definite diffusion matrix [271, 272]. To this end we neglect the third order derivative term in (3.133), employing the *truncated Wigner approximation*. Then

$$\left.\frac{\partial W}{\partial t}\right|_H \approx \int d^3\mathbf{r}\left[\frac{i}{\hbar}\frac{\bar{\delta}}{\bar{\delta}\psi(\mathbf{r})}L\psi(\mathbf{r}) + \text{c.c}\right]W, \tag{3.134}$$

where we have introduced the Gross-Pitaevskii classical-field operator

$$\mathcal{P}\left\{L\psi(\mathbf{r})\right\} \equiv \frac{\bar{\delta}E}{\bar{\delta}\psi^*(\mathbf{r})} \tag{3.135}$$

$$= \mathcal{P}\left\{\left(H_{\text{sp}} + g|\psi(\mathbf{r})|^2\right)\psi(\mathbf{r})\right\}, \tag{3.136}$$

with E the Gross-Pitaevskii energy functional

$$E = \int d^3\mathbf{r}\left[\frac{\hbar^2}{2m}|\nabla\psi(\mathbf{r})|^2 + V(\mathbf{r})|\psi(\mathbf{r})|^2 + \frac{g}{2}|\psi(\mathbf{r})|^4\right]. \tag{3.137}$$

The approximate Wigner evolution equation (3.134) is a Fokker-Planck equation with no diffusion. It may appear that there is no stochasticity in this equation due to the absence of a diffusion term; in fact the stochastic nature comes from the initial conditions sampling

the Wigner distribution.

Number-damping terms

Mapping the number-damping master equation (3.101) to a Wigner evolution equation give the Fokker-Planck equation

$$\left.\frac{\partial W}{\partial t}\right|_{\gamma} = \int d^3\mathbf{r}\, G(\mathbf{r}) \left[-\frac{\bar{\delta}}{\bar{\delta}\psi(\mathbf{r})}\frac{(\mu - L)\,\psi(\mathbf{r})}{k_B T} + \frac{\bar{\delta}^{(2)}}{\bar{\delta}\psi(\mathbf{r})\bar{\delta}\psi^*(\mathbf{r})} + \text{c.c}\right] W, \tag{3.138}$$

where in contrast to the Hamiltonian Fokker-Planck equation (3.134) there is now a diffusion term. When the incoherent region is near equilibrium and well described by a single-particle Wigner function in the local density approximation, the function $G(\mathbf{r})$ is approximately constant over the spatial extent of the condensate [115]. The value of $G(\mathbf{r})$ can then be calculated explicitly[7]

$$G(\mathbf{r}) \approx \frac{k_B T}{\hbar}\gamma = \frac{k_B T}{\hbar}\gamma_0 \sum_{j=1}^{\infty} \frac{e^{\beta\mu(j+1)}}{e^{2\beta\epsilon_{\text{cut}} j}} \Phi\left[\frac{e^{\beta\mu}}{e^{\beta\epsilon_{\text{cut}}}}, 1, j\right]^2, \tag{3.139}$$

where $\gamma_0 = 8a_s^2/\lambda_{dB}^2$, with $\beta = 1/k_B T$, $\lambda_{dB} = \sqrt{2\pi\hbar^2/m k_B T}$ the thermal de Broglie wavelength, and $\Phi[z, x, a] = \sum_{k=0}^{\infty} z^k/(a+k)^x$ the Lerch transcendent. With this (3.138) becomes

$$\left.\frac{\partial W}{\partial t}\right|_{\gamma} = \int d^3\mathbf{r} \left[-\frac{\bar{\delta}}{\bar{\delta}\psi(\mathbf{r})}\frac{\gamma}{\hbar}(\mu - L)\,\psi(\mathbf{r}) + \frac{\gamma k_B T}{\hbar}\frac{\bar{\delta}^{(2)}}{\bar{\delta}\psi(\mathbf{r})\bar{\delta}\psi^*(\mathbf{r})} + \text{c.c}\right] W. \tag{3.140}$$

Energy-damping terms

Finally, mapping the energy-damping master equation (3.105) to Wigner evolution equation gives the Fokker-Planck equation

$$\begin{aligned}\left.\frac{\partial W}{\partial t}\right|_{\varepsilon} = \frac{k_B T}{\hbar}\int d^3\mathbf{r} \int d^3\mathbf{r}'\, \varepsilon(\mathbf{r}-\mathbf{r}') \Bigg[&-\frac{\bar{\delta}}{\bar{\delta}\psi(\mathbf{r}')}\frac{i\hbar\nabla\cdot\mathbf{j}(\mathbf{r})\psi(\mathbf{r}')}{k_B T} + \text{c.c} \\ &+\frac{\bar{\delta}}{\bar{\delta}\psi(\mathbf{r}')}\psi(\mathbf{r}')\frac{\bar{\delta}}{\bar{\delta}\psi^*(\mathbf{r})}\psi^*(\mathbf{r}) - \frac{\bar{\delta}}{\bar{\delta}\psi(\mathbf{r}')}\psi(\mathbf{r}')\frac{\bar{\delta}}{\bar{\delta}\psi(\mathbf{r})}\psi(\mathbf{r}) + \text{c.c}\Bigg] W,\end{aligned} \tag{3.141}$$

[7] See appendix C.1.

where we have used that

$$\psi^*(\mathbf{r})L\psi(\mathbf{r}) - \psi(\mathbf{r})L\psi^*(\mathbf{r}) \quad = \quad i\hbar\nabla\cdot\mathbf{j}(\mathbf{r}), \tag{3.142}$$

with

$$\mathbf{j}(\mathbf{r}) = \frac{i\hbar}{2m}\left[\psi(\mathbf{r})\nabla\psi^*(\mathbf{r}) - \psi^*(\mathbf{r})\nabla\psi(\mathbf{r})\right] \tag{3.143}$$

the coherent region current. The drift term can be expressed in terms of an effective potential

$$V_\varepsilon(\mathbf{r}) = -\hbar\int d^3\mathbf{r}'\varepsilon(\mathbf{r}-\mathbf{r}')\nabla'\cdot\mathbf{j}(\mathbf{r}) \tag{3.144}$$

leading to

$$\begin{aligned}\left.\frac{\partial W}{\partial t}\right|_\varepsilon \quad = \quad & \frac{k_BT}{\hbar}\int d^3\mathbf{r}\int d^3\mathbf{r}'\,\varepsilon(\mathbf{r}-\mathbf{r}')\left[\frac{\bar\delta}{\bar\delta\psi(\mathbf{r}')}\psi(\mathbf{r}')\frac{\bar\delta}{\bar\delta\psi^*(\mathbf{r})}\psi^*(\mathbf{r}) + \text{c.c}\right]W \\ & -\frac{k_BT}{\hbar}\int d^3\mathbf{r}\int d^3\mathbf{r}'\,\varepsilon(\mathbf{r}-\mathbf{r}')\left[\frac{\bar\delta}{\bar\delta\psi(\mathbf{r}')}\psi(\mathbf{r}')\frac{\bar\delta}{\bar\delta\psi(\mathbf{r})}\psi(\mathbf{r}) + \text{c.c}\right]W \\ & +\int d^3\mathbf{r}\left[\frac{i}{\hbar}\frac{\bar\delta}{\bar\delta\psi(\mathbf{r})}V_\varepsilon(\mathbf{r})\psi(\mathbf{r}) + \text{c.c}\right]W.\end{aligned} \tag{3.145}$$

3.5 Stochastic projected Gross-Pitaevskii equation

We now have the Wigner evolution equation in the form of a Fokker-Planck equation

$$\frac{\partial W}{\partial t} = \left.\frac{\partial W}{\partial t}\right|_H + \left.\frac{\partial W}{\partial t}\right|_\gamma + \left.\frac{\partial W}{\partial t}\right|_\varepsilon \tag{3.146}$$

with the Hamiltonian, number-damping, and energy-damping terms given by (3.134), (3.140), and (3.145) respectively. At this point we are able to map the Wigner evolution equation to an equivalent stochastic differential equation for $\psi(\mathbf{r})$[8] [272].

[8] See appendix D.

3.5.1 Equation of motion

The SPGPE is given by [145–147, 149]

$$(\mathbf{S})d\psi = d\psi|_H + d\psi|_\gamma + (\mathbf{S})d\psi|_\varepsilon\,, \tag{3.147}$$

where

$$d\psi|_H \equiv \mathcal{P}\left\{-\frac{i}{\hbar}\left(L-\mu\right)\psi dt\right\}, \tag{3.148}$$

$$d\psi|_\gamma \equiv \mathcal{P}\left\{\frac{\gamma}{\hbar}\left(\mu-L\right)\psi dt + dW(\mathbf{r},t)\right\}, \tag{3.149}$$

$$(\mathbf{S})d\psi|_\varepsilon \equiv \mathcal{P}\left\{-\frac{i}{\hbar}V_\varepsilon(\mathbf{r},t)\psi dt + i\psi dU(\mathbf{r},t)\right\}, \tag{3.150}$$

and the (**S**) in (3.150) denotes that the equation is in *Stratonovich form*[9]. The individual terms are as follows:

Hamiltonian term

The Hamiltonian term (3.148) describes evolution of the coherent region under the coherent region GPE operator L, as defined in (3.136). The Hamiltonian term in isolation is known as the projected GPE (PGPE), as described in Section 2.3.4, encapsulating the interactions between the low energy modes. Note that we have also transformed to a rotating frame with reference energy given by the chemical potential μ, the result of which is the the chemical potential appearing explicitly in this term.

Number-damping term

The term describing the number-damping process (3.149) takes the form of a drift term characterized by the rate γ (3.139) and a diffusion (noise) term $dW(\mathbf{r},t)$. The non-zero correlations of the Gaussian complex noise are

$$\langle dW^*(\mathbf{r},t)dW(\mathbf{r}',t)\rangle = \frac{2\gamma k_B T}{\hbar}\delta(\mathbf{r},\mathbf{r}')dt, \tag{3.151}$$

where $\delta(\mathbf{r},\mathbf{r}')$ is the coherent region delta function (3.115).

[9]Note that a distinction between the Ito and Stratonovich forms exists only for multiplicative noise. We thus only denote which form an equation is in when multiplicative noise is involved.

Energy-damping term

The term describing the energy-damping process (3.150) takes the form of a drift term characterized by the effective potential $V_\varepsilon(\mathbf{r})$ (3.144) and a diffusion (noise) term $dU(\mathbf{r},t)$. The noise is multiplicative and real with non-zero correlations

$$\langle dU(\mathbf{r},t)dU(\mathbf{r}',t)\rangle = \frac{2k_BT}{\hbar}\varepsilon(\mathbf{r}-\mathbf{r}')dt, \tag{3.152}$$

where the *epsilon function* is given by

$$\varepsilon(\mathbf{r}) = \frac{\mathcal{M}}{(2\pi)^3}\int d^3\mathbf{k}\frac{e^{i\mathbf{k}\cdot\mathbf{r}}}{|\mathbf{k}|}, \tag{3.153}$$

with[10]

$$\mathcal{M} \equiv \frac{16\pi a_s^2}{e^{(\epsilon_{\rm cut}-\mu)/k_BT}-1}. \tag{3.154}$$

The domain of integration for the epsilon function (3.153) is over all $\mathbf{k}$, though there is an implicit cutoff as it inevitably is associated with a projected function. The object $\mathcal{M}$ is sometimes referred to as the energy-damping rate, in direct analogy to the number-damping rate γ, however this terminology is somewhat misleading; while both are directly related to the strength of the corresponding process, the two processes are so functionally distinct that it is not clear that comparing the sizes of $\mathcal{M}$ and γ will give any physical insight. In fact the two rates do not even share the same units; $\mathcal{M}$ has units of length squared while γ is dimensionless.

3.5.2 Formal properties

The SPGPE describes a coherent region with coupling to a thermal reservoir, with which can be exchanged energy and particles. Thus the SPGPE gives a grand canonical description of the coherent region. Regardless of the values of γ and $\mathcal{M}$, or indeed the actual forms of the functions $G(\mathbf{r})$ and $\varepsilon(\mathbf{r})$, the SPGPE evolves any initial condition towards samples of the grand canonical ensemble[11], with equilibrium probability $P(\psi) \propto \exp(-K/k_BT)$,

[10] See appendix C.2.

[11] This is only true if $G(\mathbf{r}) > 0$; we clarify this case in the next section.

where $K \equiv E - \mu N$ is the grand canonical Hamiltonian and

$$E = \int d^3\mathbf{r}\psi^*(\mathbf{r})H_{\rm sp}\psi(\mathbf{r}) + \frac{g}{2}\int d^3\mathbf{r}|\psi(\mathbf{r})|^4, \tag{3.155}$$

$$N = \int d^3\mathbf{r}|\psi(\mathbf{r})|^2 \tag{3.156}$$

are the coherent region energy and particle number respectively.

3.6 Sub-theories of the SPGPE

A range of sub-theories of the SPGPE may be obtained by neglecting various terms. These sub-theories can be useful for gaining insight into the effect of the individual terms of the SPGPE. Two of these sub-theories, the PGPE and the number-damping SPGPE[12], have seen extensive use in the past. The energy-damping SPGPE has only recently been attracting more interest. Here we give a brief overview of the properties of these three sub-theories.

3.6.1 Projected GPE

The PGPE (see Section 2.3.4) is given by (3.148), with the latter two terms neglected. Formally, this may be thought of as setting the rates γ and $\mathcal{M}$ both to zero. It can be shown explicitly that the PGPE is both number-conserving and energy-conserving for any energy cutoff $\epsilon_{\rm cut}$ and single-particle basis, that is,

$$\left.\frac{dN}{dt}\right|_H = \left.\frac{dE}{dt}\right|_H = 0. \tag{3.157}$$

Thus the PGPE equilibrium states are drawn from the microcanonical ensemble [106].

3.6.2 Number-damped SPGPE

The number-damped SPGPE is given by

$$d\psi|_{H+\gamma} = d\psi|_H + d\psi|_\gamma\,, \tag{3.158}$$

[12] More commonly referred to as the simple growth SPGPE in the literature.

or by formally setting the rate $\mathcal{M}$ to zero while keeping γ non-zero (and positive) in the SPGPE (3.147). The number-damping drift term is proportional to the PGPE, and the noise is additive and weak. As a result, numerical implementation of the number-damped SPGPE is of a similar computational expense to the PGPE [273], and a high order Runge-Kutta algorithm can be used [115, 274].

The quiet number-damped SPGPE, obtained by neglecting the noise ($dW \equiv 0$), is equivalent to the *damped PGPE* [221–224]. This equation of motion evolves the particle number N to equilibrium as

$$\left.\frac{dN}{dt}\right|_{H+\gamma,\text{quiet}} = -\frac{2\gamma}{\hbar}\left[\bar{\mu}(t) - \mu\right] N, \tag{3.159}$$

with $\bar{\mu}(t) = N^{-1}\int d^3\mathbf{r}\psi^* L\psi$ the instantaneous chemical potential. The grand canonical energy K evolves to equilibrium as

$$\left.\frac{dK}{dt}\right|_{H+\gamma,\text{quiet}} = -\frac{2\gamma}{\hbar}\int d^3\mathbf{r}\left|\mathcal{P}\left\{\left(\mu - L\right)\psi\right\}\right|^2, \tag{3.160}$$

a monotonic decay that minimizes K and damps out thermal fluctuations. The equilibrium state is the zero temperature ground state of the PGPE (3.148), that is the solution of $\mu\psi_0 = \mathcal{P}\left\{L\psi_0\right\}$.

When the noise is retained, the number-damped SPGPE samples the grand canonical distribution. The grand canonical energy $K\left[\psi\right] > K\left[\psi_0\right]$ for any sample ψ, however all equilibrium properties are independent of the value of γ. This property provides a good test when numerically implementing the number-damped SPGPE.

3.6.3 Energy-damped SPGPE

The energy-damped SPGPE is given by

$$(\mathbf{S})\, d\psi|_{H+\varepsilon} = d\psi|_H + (\mathbf{S})\, d\psi|_\varepsilon, \tag{3.161}$$

or by formally setting the rate γ to zero while keeping $\mathcal{M}$ non-zero (and positive) in the SPGPE (3.147). The energy-damped SPGPE is number-conserving, and thus samples the canonical distribution with probability $P(\psi) \propto \exp\left(-E/k_B T\right)$.

Numerical implementation of this sub-theory is much more technically challenging than

for the number-damped case due to the nature of the terms in $d\psi|_{\varepsilon}$. The noise is multiplicative, requiring a semi-implicit vector Euler algorithm for stochastic integration. The semi-implicit vector Euler algorithm is first order in the weak sense of convergence [272], and so is much more inefficient in terms of computing resources than the high order Runge-Kutta algorithms available for the number-damped SPGPE. Furthermore, the deterministic term $V_{\varepsilon}(\mathbf{r},t)$ (3.144) requires calculation of the coherent region current divergence, and the noise dU has non-local spatial correlations. A numerical method for implementing the energy-damped SPGPE (and with it the full SPGPE) was developed by Rooney *et al* [1] based on techniques used for solving the PGPE with dipole-dipole interactions [275]. We give an overview of this method in appendix F.

The quiet energy-damped SPGPE, obtained by neglecting the noise ($dU \equiv 0$), may also be referred to as the *energy-damped PGPE*. The deterministic term $V_{\varepsilon}(\mathbf{r},t)$ takes the form of an effective potential that coherently damps the energy of the coherent region by

$$\left.\frac{dK}{dt}\right|_{H+\varepsilon,\text{quiet}} = \left.\frac{dE}{dt}\right|_{H+\varepsilon,\text{quiet}} = \int d^3\mathbf{r}\, V_{\varepsilon}(\mathbf{r},t)\nabla\cdot\mathbf{j}(\mathbf{r},t) \tag{3.162}$$

$$= -\hbar\mathcal{M}\int d^3\mathbf{k}|\mathbf{k}|^{-1}\left|\mathbf{k}\cdot\tilde{\mathbf{j}}(\mathbf{k},t)\right|^2. \tag{3.163}$$

This is negative semi-definite, causing the energy of the coherent region to monotonically decrease. This property provides a good test when numerically implementing the energy-damped SPGPE.

When the noise is retained, we have $E[\psi] > E[\psi_0]$ for any sample ψ, however all equilibrium properties are independent of the value of $\mathcal{M}$, also a convenient test when attempting numerical implementation. Under the assumed equivalence of the canonical and grand canonical ensembles, the equilibrium state of the energy-damped SPGPE must share the same equilibrium properties with the equilibrium state of the number-damped SPGPE for the same final particle number and energy.

3.7 Estimating parameters for experiments

As a result of the first principles microscopic treatment of the reservoir interactions, the SPGPE allows for *ab initio* numerical simulations that may be directly compared to experiments. For this, the control parameters T, μ, and ϵ_{cut} must be appropriately chosen. The rates (3.139) and (3.154) of each damping process can then be calculated. Also, the

properties of the incoherent region can be found; this is crucial as generally experiments will measure the total particle number.

Here we outline the incoherent region properties, then review a method for estimating SPGPE parameters for a harmonically trapped three-dimensional system [2]. We finish by comparing the values the SPGPE parameters for given T and N_T, in addition to the values of the two rates γ and $\mathcal{M}$.

3.7.1 Properties of the incoherent region

The incoherent region density is given by semi-classical description using the single-particle Wigner function (3.76). The incoherent region density is [115]

$$n_{\mathbf{I}}(\mathbf{r}) = \frac{1}{(2\pi)^3}\int_{\mathbf{I}} d^3\mathbf{k} W(\mathbf{r},\mathbf{k}) \tag{3.164}$$

$$= \frac{1}{(2\pi)^3}\sum_{n=1}^{\infty} e^{\beta(\mu - V_{\rm ext}(\mathbf{r}))}\int_{K_{\mathbf{I}}(\mathbf{r})}^{\infty} dk k^2 e^{-n\beta\hbar^2k^2/2m}, \tag{3.165}$$

with $W(\mathbf{r},\mathbf{k})$ given by (3.76) and the lower integration limit

$$\frac{\hbar^2 K_{\mathbf{I}}^2(\mathbf{r})}{2m} \equiv \max\left\{\epsilon_{\rm cut} - V_{\rm ext}(\mathbf{r}), 0\right\}. \tag{3.166}$$

The incoherent region density (3.164) can also be expressed as

$$n_{\mathbf{I}}(\mathbf{r}) = \frac{g_{3/2}\left(e^{\beta(\mu - V_{\rm ext}(\mathbf{r}))}, \beta\hbar^2K_{\mathbf{I}}^2(\mathbf{r})/2m\right)}{\lambda_{dB}^3}, \tag{3.167}$$

where $g_\nu(z,y)$ is the incomplete Bose-Einstein function[13]

$$g_\nu(z,y) \equiv \frac{1}{\Gamma(\nu)}\int_y^\infty dx \frac{x^{\nu-1}}{e^x/z - 1}, \tag{3.168}$$

with $\Gamma(\nu)$ the gamma function. The incoherent region particle number is then

$$N_{\mathbf{I}} = \frac{g_3\left(e^{\beta\mu}, \beta\epsilon_{\rm cut}\right)}{\left(\beta\hbar\omega\right)^3}, \tag{3.169}$$

where $\omega \equiv (\omega_x\omega_y\omega_z)^{1/3}$ is the geometric mean of the harmonic trapping frequencies.

[13] Also commonly known as the incomplete polylogarithm function, denoted $\mathrm{Li}_\nu(y,z)$.

3.7.2 Parameter estimation for a trapped system

We need to find an estimate for the chemical potential μ such that the total particle number

$$N_T = \langle N \rangle + N_{\mathbf{I}} \tag{3.170}$$

is matched accurately with experiment, where $\langle N \rangle$ is the ensemble average of the coherent region particle number given by (3.156) and the incoherent region particle number is given by (3.169). The energy cutoff $\epsilon_{\rm cut}$ must also then be chosen such that cutoff occupation is appreciable to validate the truncated Wigner approximation, typically $n_{\rm cut} \approx 1 - 3$ [106].

We utilise the Hartree-Fock approach developed by Rooney *et al* [2] to find estimates of μ and $\epsilon_{\rm cut}$. In this method the coherent region is treated using the Thomas-Fermi approximation, such that the number of particles in the coherent region determines the value of μ. The thermal particles comprising the incoherent region are treated with a semiclassical Hartree-Fock description, with energy

$$E_{\rm HF}(\mathbf{r}, \mathbf{k}) \equiv \frac{\hbar^2 \mathbf{k}^2}{2m} + V_{\rm ext}(\mathbf{r}) + 2gn(\mathbf{r}), \tag{3.171}$$

where $n(\mathbf{r})$ is the Thomas-Fermi particle density. The density of states from (3.171) can be treated semi-analytically for a harmonically trapped system [276], allowing one to determine self-consistently the values of μ and $\epsilon_{\rm cut}$ for a given total particle number N_T. The resulting SPGPE equilibrium states from these estimates gives final total particle numbers within a few percent of the desired value [2]. The numerical implementation of this method is shown in detail in appendix E.

3.7.3 Comparison of energy-damping and number-damping rates

It can be of interest to compare the values of γ and $\mathcal{M}$. We consider the ratio of γ and $\mathcal{M}/a_\omega^2$, with $a_\omega \equiv \sqrt{\hbar/m\omega}$ the geometric mean harmonic oscillator length scale, included here to ensure the ratio is dimensionless. The ratio is

$$\frac{\mathcal{M}}{\gamma a_\omega^2} = 2\pi \left(\frac{\lambda_{dB}}{a_\omega}\right)^2 \frac{1}{e^{\beta(\epsilon_{\rm cut}-\mu)} - 1} \left(\sum_{j=1}^{\infty} \frac{e^{\beta\mu(j+1)}}{e^{2\beta\epsilon_{\rm cut} j}} \Phi\left[\frac{e^{\beta\mu}}{e^{\beta\epsilon_{\rm cut}}}, 1, j\right]^2 \right)^{-1}. \tag{3.172}$$

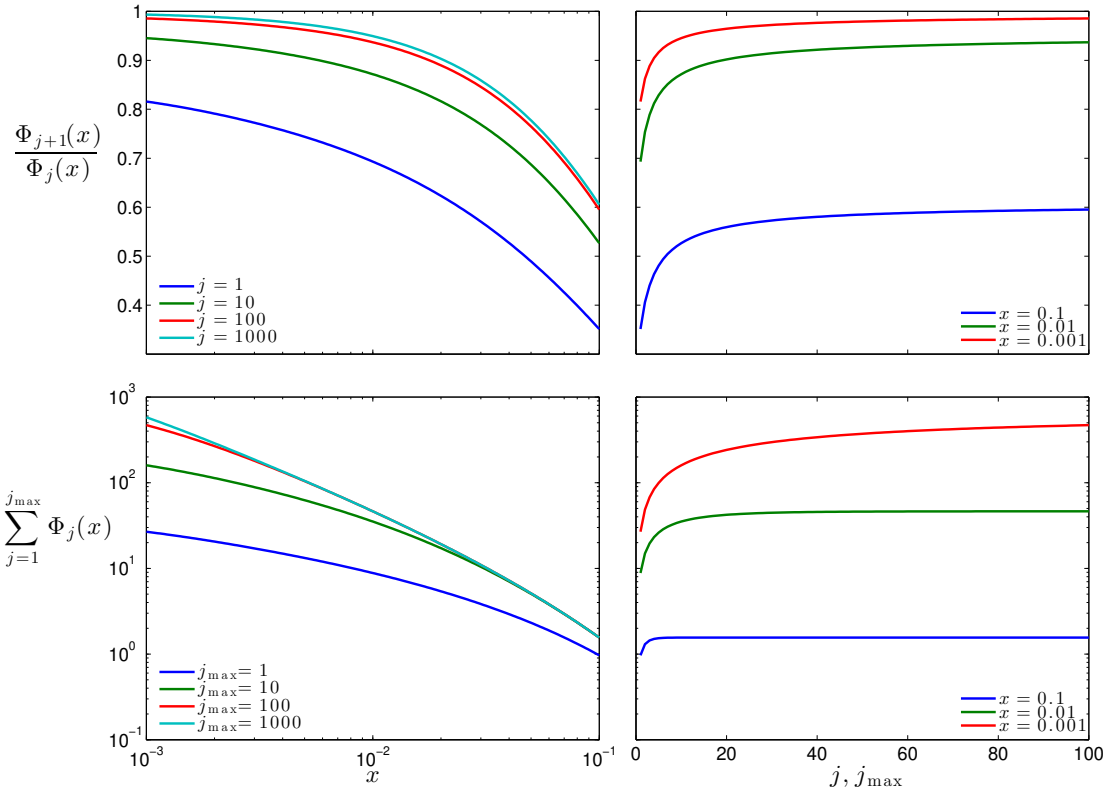

Figure 3.1: Measures of convergence for (3.173). The top row is the ratio $\Phi_{j+1}(x)/\Phi_j(x)$ with varying $x \equiv \beta\mu$ for several values of j (top left), and varying j for several values of x (top right). The bottom row is the truncated sum $\sum_{j=1}^{j_{\max}} \Phi_j(x)$ with varying x for several values of $j_{\max}$ (bottom left), and varying $j_{\max}$ for several values of x (bottom right).

To gain some insight, we consider a typical energy cutoff of $\epsilon_{\rm cut} = 3\mu$ and assume $k_B T \gg \mu$. The summation

$$\Phi_0(\beta\mu) \equiv \sum_{j=1}^{\infty} e^{-\beta\mu(5j-1)} \Phi\left[e^{-2\beta\mu}, 1, j\right]^2 = \sum_{j=1}^{\infty} \Phi_j(\beta\mu) \tag{3.173}$$

does not have a linear approximation with respect to $\beta\mu$ as the Lerch transcendent diverges when the first argument goes to unity.

In Fig. 3.1, we consider the convergence properties of $\Phi_0(x)$. When considering the ratio $\Phi_{j+1}(x)/\Phi_j(x)$ we see that for $x \gtrsim 10^{-2}$ the ratio converges to less than 1, indicating that the sum should converge. This is supported by considering the truncated sum $\sum_{j=1}^{j_{\max}} \Phi_j(x)$, where we see that for $x \gtrsim 10^{-2}$ the sum converges to a finite value relatively quickly. For $x \lesssim 10^{-3}$ the convergence is less clear, however this is well below the values of $\beta\mu$ appropriate to the SPGPE formulation. For typical values of $\beta\mu \sim 10^{-1}$, the value of

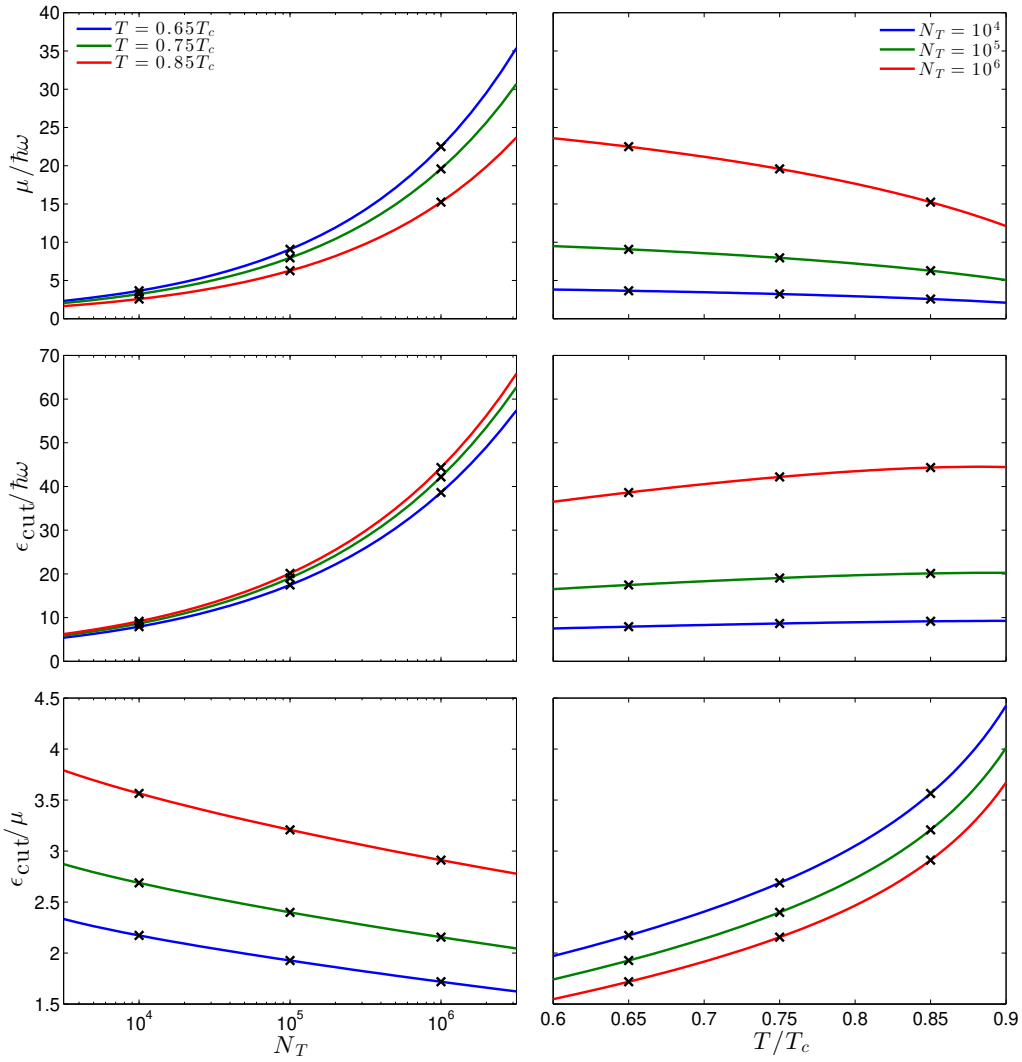

Figure 3.2: Estimates of the chemical potential μ (top row), energy cutoff $\epsilon_{\rm cut}$ (middle row), and the ratio of the two (bottom row) obtained using the Hartree-Fock parameter estimation scheme [2] for various experimentally accessible parameters of total particle number N_T and temperature T. The black crosses indicate the parameters considered in Chapter 6.

$\Phi_0(\beta\mu)$ is on the order of unity. The damping rate ratio is then approximately

$$\frac{\mathcal{M}}{\gamma x_0^2} \approx \frac{\pi}{\Phi_0(\beta\mu)} \left(\frac{\lambda_{dB}}{x_0}\right)^2 \frac{k_B T}{\mu}. \tag{3.174}$$

It is common in experiments to access regimes where $\lambda_{dB} \sim a_\omega$ for temperatures near the critical temperature, and so this figure of merit indicates that the energy-damping rate

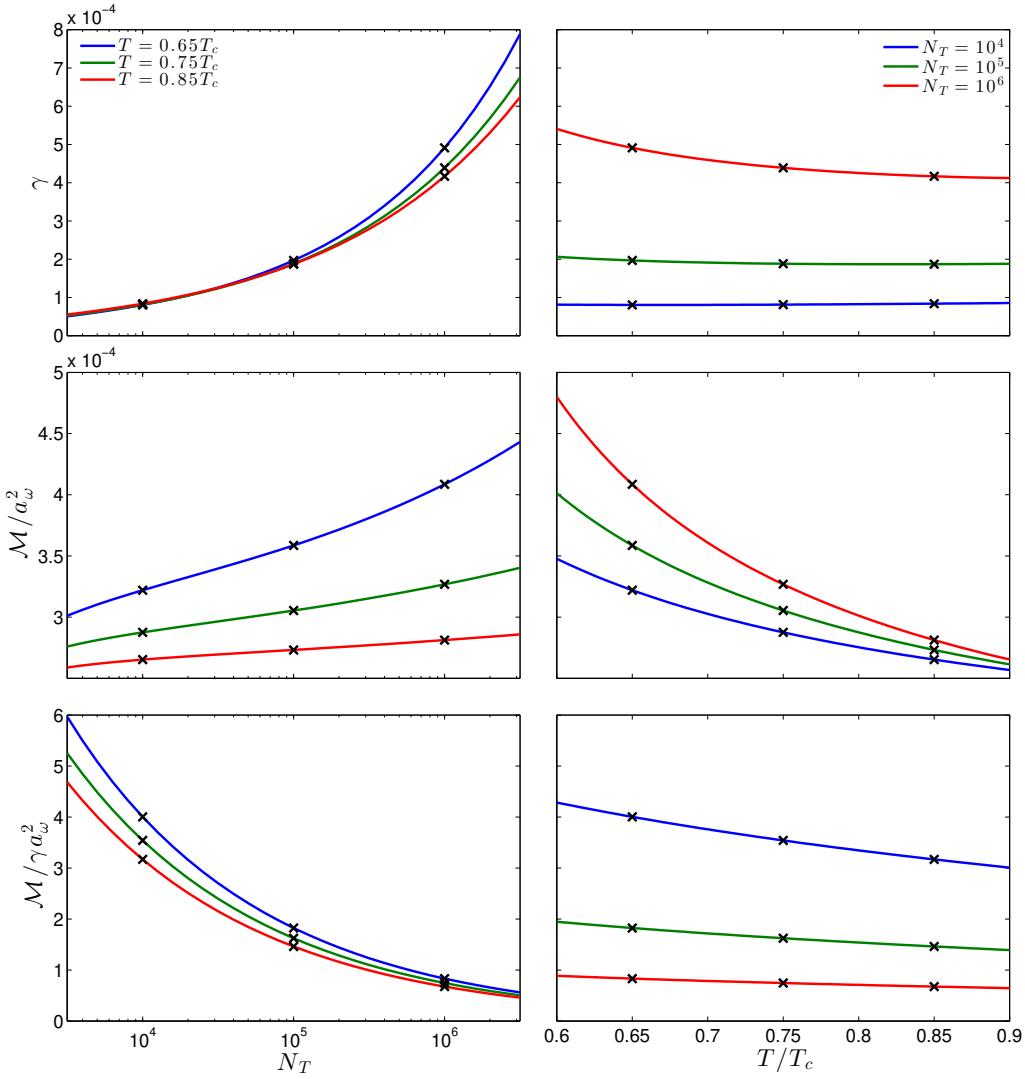

Figure 3.3: Estimates of the number-damping rate γ (top row), dimensionless energy-damping rate $\mathcal{M}/a_\omega^2$ (middle row), and the ratio of the two (bottom row) obtained using the Hartree-Fock parameter estimation scheme [2] for various experimentally accessible parameters of total particle number N_T and temperature T. The black crosses indicate the parameters considered in Chapter 6.

may be comparable to or even dominant over the number-damping rate. While (3.174) seems to imply a linear relationship with temperature, we must keep in mind that the chemical potential μ is also dependent on temperature, so the true temperature dependence is obscured.

For a more quantitative comparison, we use the Hartree-Fock parameter estimation

scheme to obtain SPGPE parameters for an isotropic harmonically trapped system with $\omega = 2\pi \times 10$ Hz for a range of total particle numbers $N_T \in \left[10^4, 10^6\right]$ and ratios of the temperature to critical temperature $T/T_c \in [0.5, 0.9]$. In Fig. 3.2 we show the estimated values of the chemical potential μ and energy cutoff ϵ_{cut}. We see that μ increases with total particle number but decreases with temperature, while ϵ_{cut} increases with both total particle number and temperature. The ratio of ϵ_{cut} and μ decreases slowly with increasing total particle number and increases with increasing temperature. The ratio is in the expected range, staying below $\epsilon_{\text{cut}} = 4.5\mu$ and only just dropping below $\epsilon_{\text{cut}} = 1.5\mu$ at the extremes of temperature. In Fig. 3.3 we show the estimated values of the number-damping rate γ and dimensionless energy-damping rate $\mathcal{M}/a_\omega^2$, where $a_\omega \equiv \sqrt{\hbar/(m\omega)}$ is the harmonic oscillator length. We see that γ increases with increasing total particle number but only has a weak dependence on temperature, showing a slow decrease. Similar behaviour is seen for $\mathcal{M}$, increasing with N_T and decreasing with T/T_c, though with a stronger dependence on the latter than for γ. The ratio of the two decreases with increasing total particle number and also with increasing temperature, though the dependence on temperature is weaker than that on total particle number. The value of the ratio only just drops below $\mathcal{M}/a_\omega^2 = \gamma$ and reaches as high as $\mathcal{M}/a_\omega^2 = 5\gamma$ at the extremes, thus indicating that the energy-damping rate is generally comparable to the number-damping rate. In Fig. 3.2 and Fig. 3.3 we also indicate the parameters we have used when considering the 3D harmonically trapped system in Chapter 6.

While we have shown that the number-damping and energy-damping rates are comparable, the two processes manifest in such different forms that simply comparing the respective multiplicative factors is insufficient for making any conclusions at this stage. The energy-damping takes the form of an effective potential related to the coherent region current, while the number-damping is, up to a multiplicative factor, given by the projected Gross-Pitaevskii operator. In the main results of this thesis, we show for specific systems how one can directly compare the two processes, and use this to make conclusions about their respective significance.

3.8 Numerically solving the SPGPE

Finding numeric solutions of the SPGPE is a highly non-trivial process, mainly due to two technical challenges. Firstly, all moderately occupied low-energy modes play a significant role in finite-temperature non-equilibrium dynamics. Thus we must propagate all modes

beneath an appropriately chosen cutoff to a high degree of accuracy. Secondly, the deterministic term arising from the energy-damping reservoir interactions is non-local, and furthermore the noise is multiplicative and has non-local spatial correlations. Efficiently and accurately accounting for the energy-damping contributions is thus very challenging. Previous works have shown how a spectral approach [277, 278] can be used for numerically solving the PGPE [192], providing a method of accurately propagating the low energy coherent modes for a Bose gas with both contact [273] and dipolar [275] interactions. The numerical method used in this work was developed by Rooney *et al* for a three-dimensional harmonically trapped system [1], and is an extension of the spectral-Galerkin method previously developed for evaluating the SPGPE number-damping terms [115]. The core principle of the algorithm exploits that the basis states of the harmonic oscillator are Gauss-Hermite functions, and so many of the spatial integrals can be evaluated exactly using Gauss-Hermite quadrature. The finer details of this method are presented in appendix F.

We do wish to point out two errors that appear in the literature surrounding the numerical method we have used. Firstly, in [1, 275] it is erroneously stated that both the spectral and auxiliary basis states are eigenstates of the Fourier transform, giving an incorrect quadrature rule for the energy-damping potential. This error is present in the text only; the code developed in those works and used in this work has the correct quadrature rule. Secondly, in [1] it is stated that the correlations of the energy-damping noise are anti-diagonal in momentum space. This is not so much an error as it is an oversimplification. The correlations in the traditional sense, where we take the complex conjugate of the second noise are diagonal

$$\langle dU(\mathbf{k},t)dU^{*}(\mathbf{k}',t)\rangle \propto \delta(\mathbf{k},\mathbf{k}'), \tag{3.175}$$

but if we do not take the conjugate of the second noise the correlations are indeed anti-diagonal

$$\langle dU(\mathbf{k},t)dU(\mathbf{k}',t)\rangle \propto \delta(\mathbf{k},\mathbf{k}'). \tag{3.176}$$

This is a consequence of the energy-damping noise being real in position space.

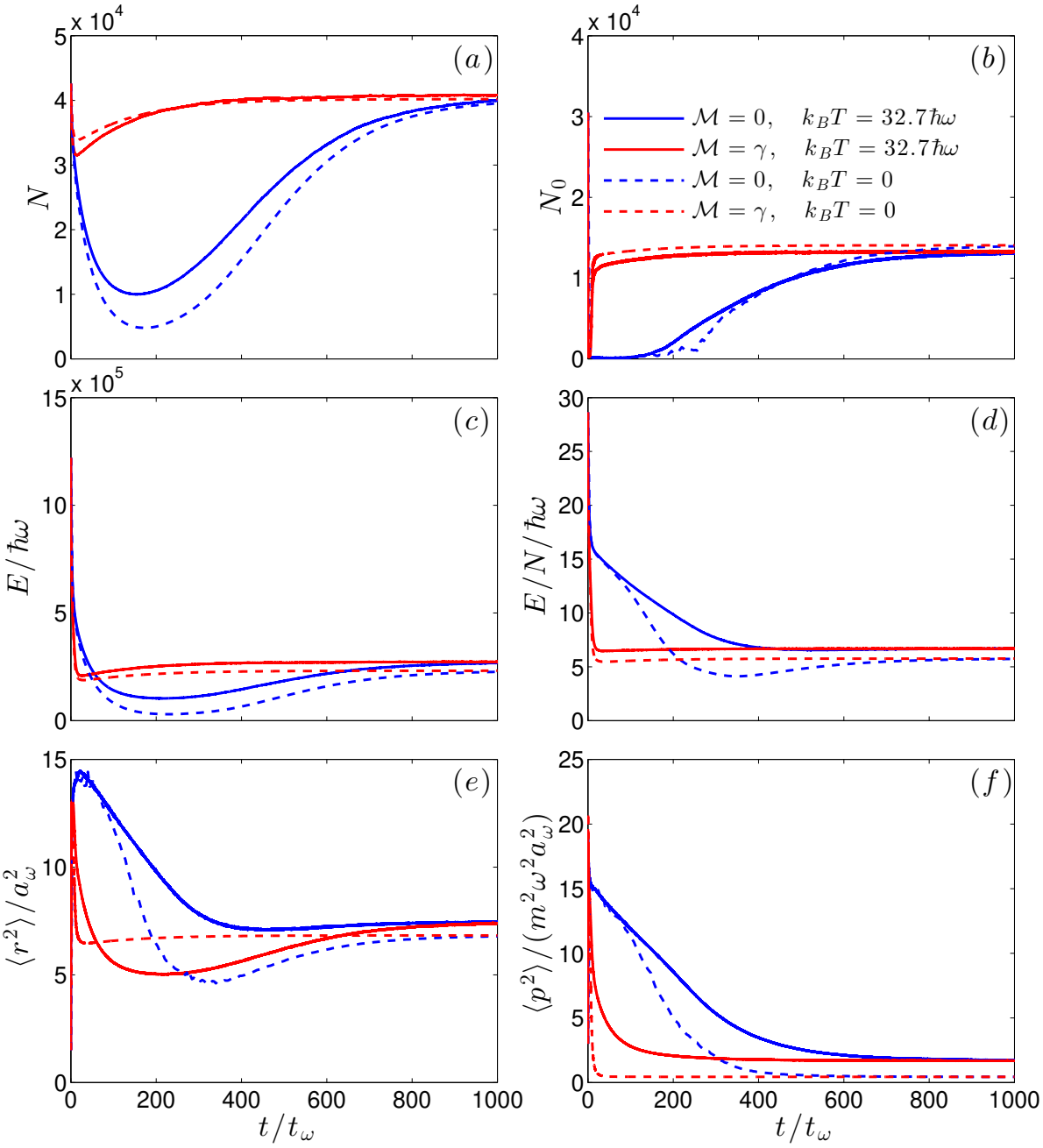

Figure 3.4: Ensemble averages of (a) normalization, (b) condensate number, (c) energy, (d) energy per particle, (e) position squared, and (f) momentum squared for evolution of a breathing mode to equilibrium by numerically propagating the SPGPE over 100 trajectories.

3.8.1 Equilibrium state

We perform a basic check of the algorithm by evolving some initial state to equilibrium. We consider evolution to equilibrium of a breathing mode

$$\psi(\mathbf{r},0)=\frac{\sqrt{N_i}}{(\pi\sigma^2)^{3/4}}e^{-r^2/2\sigma^2+i\kappa r^2/2}, \tag{3.177}$$

in an isotropic harmonic trap of frequency ω. We consider four parameter sets; a quiet system with number-damping only, a quiet system with both number-damping and energy-damping, a noisy system with number-damping only, and a noisy system with both number-damping and energy-damping. The parameters are $\omega = 2\pi \times 10$ Hz, $N_i = 4.3 \times 10^4$, $\sigma = a_\omega$, $\kappa = a_\omega^{-2}$, $\mu = 7.9\hbar\omega$, $\epsilon_{\rm cut} = 19.1\hbar\omega$, $\gamma = 1.9 \times 10^{-4}$, $k_BT = 0$ or $k_BT = 32.7\hbar\omega$, and $\mathcal{M} = 0$ or $\mathcal{M} = \gamma$. In Fig. 3.4 we show the ensemble averages of normalization N, condensate number N_0, energy E, energy per particle E/N, position squared $\langle r^2\rangle$, and momentum squared $\langle p^2\rangle$ over 1000 oscillator time periods. The time axis is scaled by γ^{-1}, as this determines the timescale of equilibration. We see that for each observable the inclusion of energy-damping provides a quicker route to equilibrium. In Fig. 3.4 we see that the coherent region loses $\sim$ %75 of the initial particles before reaching equilibrium when only number-damping is present, but when energy-damping is included the loss is only $\sim$ %25, indicating that the energy-damping provides a more coherent route to equilibrium. However the presence of the energy-damping does not influence the equilibrium values reached for any of these measurements. This is true for both quiet and noisy systems, though the presence of noise does change the equilibrium values as one would expect. These effects due to energy-damping have previously been demonstrated [148].

3.9 Computing resources

In this section we briefly discuss the computing resources we used when obtaining the numerical data in this thesis. The vast majority of the data was obtained using the University of Otago's thunderbird machines. These machines each contain twelve to twenty Intel Core i7 CPUs, ranging from 3.2 to 3.7 GHz clock rates.

In Chapter 5 we use the 1D SPGPE, allowing us to easily vectorize the code such that multiple trajectories are performed in parallel. The increase in computing time with trajectories is slower than linear, so obtaining large ensembles is not too time consuming. The main set of data in Chapter 5 is an ensemble of 5000 trajectories, which took $\sim$ 940

hours of computing time to simulate.

In Chapter 6 we use the 3D SPGPE, and as such we are unable to vectorize the code to perform trajectories in parallel. The total computing time thus scales linearly with the number of trajectories. Furthermore, the number of modes needed to be accurately propagated scales like the cutoff energy cubed, so considering larger systems quickly increases the required computing time. The individual trajectories in Chapter 6 ranged from ~ 2 hours of computing time for an energy cutoff of $\epsilon_{\text{cut}} = 7.9$ to ~ 80 hours for $\epsilon_{\text{cut}} = 44$. The main set of data in Chapter 6 is the ensembles of 100 trajectories for each of the 9 parameter sets, which took a total of ~ 14000 hours, or ~ 570 days, of computing time to simulate. In general one would desire more trajectories for analysing a system, preferably by an order of magnitude, but in our timeframe we were unable to do this while still having some exploration of the parameter space. Potential future work is the modelling of a particular experiment using the SPGPE; in that case we would focus on a single parameter set and acquire more trajectories.

Part II

Results

Chapter 4

SPGPE linear fluctuation analysis

4.1 Introduction

While giving a simple figure of merit, comparing values of the damping rates does not give a complete picture, as the way they manifest in the equation of motion is not equivalent. Number-damping is simply a constant multiplied by the Gross-Pitaevskii operator, while the energy-damping is given by an effective potential related to the divergence of the coherent region superfluid current, thus the detailed dynamics matter in setting the relative importance of the two non-linear dissipative mechanisms. The noises are also distinct, with number-damping being additive, complex and local, while energy-damping is multiplicative, real, and non-local. The importance to dynamics of each process is thus not initially clear. Equilibrium system properties can become clearer by performing a linear fluctuation analysis. Linear fluctuation analysis is a commonly used technique that generally results in obtaining the dispersion relation and momentum dependent damping rates for the system under consideration. The technique is closely related to the analysis of Bogoliubov modes of a system.

In this chapter we perform linear fluctuation analysis of the SPGPE, assuming a 3D homogeneous system and considering density and phase fluctuations. This analysis reveals a number of key properties of the system. Neglecting the noise allows us to obtain the dispersion relation and momentum-dependant damping for the SPGPE. This damping has distinct dependences on both number-damping and energy-damping. Retaining the noise then leads us to the steady-state variances and spectra for the fluctuations, further revealing the significant role that energy-damping plays in the equilibrium properties of the system.

In Section 4.2 we find the linearized form of the SPGPE in momentum space, utilising a hydrodynamic approximation and neglecting projector effects. In Section 4.3 we find analytic expressions for various properties of density and phase fluctuations around a homogeneous background. We consider the dispersion relation, damping, and fluctuation

spectra, in particular with respect to the two reservoir interaction processes. In Section 4.4 we conclude.

4.2 Linearized hydrodynamic SPGPE in k-space

Here we show step by step how to obtain a form of the SPGPE that allows us to perform the linear fluctuation analysis. First we recast the SPGPE in a hydrodynamic form by writing the wave function ψ in terms of the probability density n and phase θ, giving a pair of coupled stochastic differential equations for n and θ. We then linearize the equations around the equilibrium background density $\bar{n}$ and phase $\bar{\theta}$, giving a pair of coupled stochastic differential equations for the fluctuations in density δn and phase $\delta\theta$. Finally, we transform these equations to momentum space, where each of the noise terms have delta correlations. This final form of the SPGPE allows us to analyse the properties of the density and phase fluctuations.

4.2.1 Hydrodynamic form

The SPGPE (3.147)-(3.150) may be written as a single equation

$$(\mathbf{S})d\psi(\mathbf{r},t) = \mathcal{P}\left\{\frac{i}{\hbar}\left[(1-i\gamma)\left(\mu - L\right)dt - V_{\varepsilon}(\mathbf{r},t)dt + \hbar dU(\mathbf{r},t)\right]\psi(\mathbf{r},t) + dW(\mathbf{r},t)\right\}. \quad (4.1)$$

If we neglect the projector, we can write the SPGPE as

$$\begin{aligned}(\mathbf{S})d\psi(\mathbf{r},t) \;=\; & \frac{i}{\hbar}(1-i\gamma)\left(-\frac{\hbar^2}{2m}\nabla^2 + V_{\text{ext}}(\mathbf{r}) + V_{\varepsilon}(\mathbf{r},t) + g|\psi(\mathbf{r},t)|^2 - \mu\right)\psi(\mathbf{r},t)dt \\ & -i\psi(\mathbf{r},t)dU(\mathbf{r},t) - \sqrt{\frac{\gamma k_B T}{\hbar}}dW_1(\mathbf{r},t) - i\sqrt{\frac{\gamma k_B T}{\hbar}}dW_2(\mathbf{r},t), \end{aligned} \quad (4.2)$$

where we have decomposed the number-damping noise into real and imaginary parts

$$dW = \sqrt{\frac{\gamma k_B T}{\hbar}}\left(dW_1(\mathbf{r},t) + i\,dW_2(\mathbf{r},t)\right), \quad (4.3)$$

where the $dW_i(\mathbf{r},t)$ are increments of real Wiener processes with true delta correlations

$$\langle dW_i(\mathbf{r},t)dW_j(\mathbf{r}',t)\rangle = \delta(\mathbf{r}-\mathbf{r}')\delta_{ij}dt, \quad (4.4)$$

consistent with the neglect of the projector. In (4.2) we have used that $\gamma V_\varepsilon(\mathbf{r},t) \propto \gamma\mathcal{M} \approx 0$ to bring the the energy-damping potential $V_\varepsilon(\mathbf{r},t)$ into the first term with common factor $(1-i\gamma)$. The SPGPE is in Stratonovich form so we are free to proceed using standard calculus. We use the Madelung transformation

$$
\begin{aligned}
n &= |\psi|^2, && (4.5)\\
(\mathbf{S})dn &= \psi^* d\psi + \psi d\psi^* = 2\mathrm{Re}\left(\psi^* d\psi\right), && (4.6)\\
\theta &= -\frac{i}{2}\log\left(\frac{\psi}{\psi^*}\right), && (4.7)\\
(\mathbf{S})d\theta &= -\frac{i}{2}\left(\frac{d\psi}{\psi} - \frac{d\psi^*}{\psi^*}\right) = \mathrm{Im}\left(\frac{d\psi}{\psi}\right), && (4.8)
\end{aligned}
$$

to recast the SPGPE in hydrodynamic form. This leads to

$$
\begin{aligned}
(\mathbf{S})dn(\mathbf{r},t) &= \frac{2\gamma\mu}{\hbar}n(\mathbf{r},t)dt - \frac{2\gamma g}{\hbar}n(\mathbf{r},t)^2dt - \frac{2\gamma}{\hbar}V_{\mathrm{ext}}(\mathbf{r})n(\mathbf{r},t)dt - \frac{2\gamma}{\hbar}V_\varepsilon(\mathbf{r},t)n(\mathbf{r},t)dt\\
&\quad -\frac{\gamma\hbar}{4m}\frac{|\nabla n(\mathbf{r},t)|^2}{n(\mathbf{r},t)}dt - \frac{\gamma\hbar}{m}n(\mathbf{r},t)|\nabla\theta(\mathbf{r},t)|^2dt + \frac{\gamma\hbar}{2m}\nabla^2 n(\mathbf{r},t)dt\\
&\quad -\frac{\hbar}{m}\nabla n(\mathbf{r},t)\cdot\nabla\theta(\mathbf{r},t)dt - \frac{\hbar}{m}n(\mathbf{r},t)\nabla^2\theta(\mathbf{r},t)dt\\
&\quad +\sqrt{\frac{4\gamma k_B T n(\mathbf{r},t)}{\hbar}}\cos\theta(\mathbf{r},t)dW_1(\mathbf{r},t)\\
&\quad +\sqrt{\frac{4\gamma k_B T n(\mathbf{r},t)}{\hbar}}\sin\theta(\mathbf{r},t)dW_2(\mathbf{r},t), && (4.9)\\
(\mathbf{S})d\theta(\mathbf{r},t) &= \frac{\mu}{\hbar}dt - \frac{g}{\hbar}n(\mathbf{r},t)dt - \frac{1}{\hbar}V_{\mathrm{ext}}(\mathbf{r})dt - \frac{1}{\hbar}V_\varepsilon(\mathbf{r},t)dt - \frac{\hbar}{8m}\frac{|\nabla n(\mathbf{r},t)|^2}{n(\mathbf{r},t)^2}dt\\
&\quad -\frac{\hbar}{2m}|\nabla\theta(\mathbf{r},t)|^2dt + \frac{\hbar}{4m}\frac{\nabla^2 n(\mathbf{r},t)}{n(\mathbf{r},t)}dt + \frac{\gamma\hbar}{2m}\frac{\nabla n(\mathbf{r},t)\cdot\nabla\theta(\mathbf{r},t)}{n(\mathbf{r},t)}dt\\
&\quad +\frac{\gamma\hbar}{2m}\nabla^2\theta(\mathbf{r},t)dt + dU(\mathbf{r},t) - \sqrt{\frac{\gamma k_B T}{\hbar n(\mathbf{r},t)}}\sin\theta(\mathbf{r},t)dW_1(\mathbf{r},t)\\
&\quad +\sqrt{\frac{\gamma k_B T}{\hbar n(\mathbf{r},t)}}\cos\theta(\mathbf{r},t)dW_2(\mathbf{r},t). && (4.10)
\end{aligned}
$$

Note that if we neglect the presence of noise the hydrodynamic form of the SPGPE becomes

$$\frac{\partial n(\mathbf{r},t)}{\partial t} = -\nabla\cdot(n(\mathbf{r},t)\mathbf{v}(\mathbf{r},t)) + \frac{2n(\mathbf{r},t)\gamma\mu}{\hbar}\left(\mu - V_{\rm eff}(\mathbf{r},t)\right), \tag{4.11}$$

$$m\frac{\partial \mathbf{v}(\mathbf{r},t)}{\partial t} = -\nabla\left(V_{\rm eff}(\mathbf{r},t) - \frac{\hbar\gamma}{2n(\mathbf{r},t)}\nabla\cdot(n(\mathbf{r},t)\mathbf{v}(\mathbf{r},t))\right), \tag{4.12}$$

where we have used the standard definition for the superfluid velocity

$$\mathbf{v}(\mathbf{r},t) = \frac{\hbar}{m}\nabla\theta(\mathbf{r},t), \tag{4.13}$$

and the effective potential $V_{\rm eff}(\mathbf{r},t)$ is

$$V_{\rm eff}(\mathbf{r},t) = \frac{m\mathbf{v}(\mathbf{r},t)^2}{2} + V_{\rm ext}(\mathbf{r}) + V_\varepsilon(\mathbf{r},t) + gn(\mathbf{r},t) - \frac{\hbar^2}{2m}\frac{\nabla^2\sqrt{n(\mathbf{r},t)}}{\sqrt{n(\mathbf{r},t)}}. \tag{4.14}$$

We have thus recovered the quantum Euler equations for a superfluid with damping γ and trapping $V(\mathbf{r},t) = V_{\rm ext}(\mathbf{r}) + V_\varepsilon(\mathbf{r},t)$. Evidently (4.9) and (4.10) may be considered stochastic versions of the standard quantum Euler equations.

4.2.2 Linearized homogeneous system

We consider a homogeneous system with $V_{\rm ext}(\mathbf{r}) = 0$ and linearize about the Thomas-Fermi ground state. That is, we set

$$n(\mathbf{r},t) = \bar{n} + \delta n(\mathbf{r},t), \tag{4.15}$$

$$\theta(\mathbf{r},t) = \bar{\theta} + \delta\theta(\mathbf{r},t), \tag{4.16}$$

where $\mu = g\bar{n}$. Note that we are free to set $\bar{\theta} = 0$ given it is a global phase and thus does not have any physical meaning. The hydrodynamic form of the SPGPE then becomes

$$\begin{aligned} d\delta n(\mathbf{r},t) = &-\frac{2\gamma\mu}{\hbar}\delta n(\mathbf{r},t)dt + \frac{\gamma\hbar}{2m}\nabla^2\delta n(\mathbf{r},t)dt \\ &-\frac{\hbar\bar{n}}{m}\nabla^2\delta\theta(\mathbf{r},t)dt + \sqrt{\frac{4\gamma k_B T\bar{n}}{\hbar}}dW_1(\mathbf{r},t), \end{aligned} \tag{4.17}$$

$$\begin{aligned} d\delta\theta(\mathbf{r},t) = &-\frac{g}{\hbar}\delta n(\mathbf{r},t)dt - \frac{1}{\hbar}V_\varepsilon(\mathbf{r},t)dt + \frac{\hbar}{4m\bar{n}}\nabla^2\delta n(\mathbf{r},t)dt \\ &+\frac{\gamma\hbar}{2m}\nabla^2\delta\theta(\mathbf{r},t)dt + dU(\mathbf{r},t) + \sqrt{\frac{\gamma k_B T}{\hbar\bar{n}}}dW_2(\mathbf{r},t). \end{aligned} \tag{4.18}$$

Note that we have not yet applied the linearization to the effective energy-damping potential $V_\varepsilon(\mathbf{r},t)$; it is simpler to leave this until we have transformed to momentum space. We have also dropped the (S) denoting that the SDE is of the Stratonovich form; as we no longer have multiplicative noise there is no difference of consequence between the Ito and Stratonovich forms.

4.2.3 Momentum space

We progress by transforming to k-space using

$$\delta n(\mathbf{r},t) = \frac{1}{(2\pi)^{3/2}}\int d^3\mathbf{k}\delta n(\mathbf{k},t)e^{i\mathbf{k}\cdot\mathbf{r}}, \tag{4.19}$$

$$\delta\theta(\mathbf{r},t) = \frac{1}{(2\pi)^{3/2}}\int d^3\mathbf{k}\delta\theta(\mathbf{k},t)e^{i\mathbf{k}\cdot\mathbf{r}} \tag{4.20}$$

or equivalently

$$\delta n(\mathbf{r},t) = \mathcal{F}^{-1}\left[\delta n(\mathbf{k},t)\right], \tag{4.21}$$

$$\delta\theta(\mathbf{r},t) = \mathcal{F}^{-1}\left[\delta\theta(\mathbf{k},t)\right] \tag{4.22}$$

The noises in momentum space

$$dW_1(\mathbf{k},t) = \frac{1}{(2\pi)^{3/2}}\int d^3\mathbf{r}\, dW_1(\mathbf{r},t)e^{-i\mathbf{k}\cdot\mathbf{r}} \tag{4.23}$$

$$dW_2(\mathbf{k},t) = \frac{1}{(2\pi)^{3/2}}\int d^3\mathbf{r}\, dW_2(\mathbf{r},t)e^{-i\mathbf{k}\cdot\mathbf{r}} \tag{4.24}$$

$$dU(\mathbf{k},t) = \frac{1}{(2\pi)^{3/2}}\int d^3\mathbf{r}\, dU(\mathbf{r},t)e^{-i\mathbf{k}\cdot\mathbf{r}} \tag{4.25}$$

are now complex with correlations

$$\langle dW_i(\mathbf{k},t)dW_j^*(\mathbf{k}',t)\rangle = \delta(\mathbf{k}-\mathbf{k}')\delta_{ij}dt \tag{4.26}$$

$$\langle dU(\mathbf{k},t)dU^*(\mathbf{k}',t)\rangle = \frac{2\mathcal{M}k_BT}{\hbar k}\delta(\mathbf{k}-\mathbf{k}')dt. \tag{4.27}$$

We rescale the energy-damping noise $dU(\mathbf{k},t)$ to have unit correlations

$$dU(\mathbf{k},t) \equiv \sqrt{\frac{2\mathcal{M}k_BT}{\hbar k}}dW_3(\mathbf{k},t), \tag{4.28}$$

where $dW_3(\mathbf{k},t)$ is also the Fourier transform of a real Wiener process with correlations given by (4.26). Note that the linearized form of the energy-damping potential is

$$V_\varepsilon(\mathbf{r},t) \approx \frac{\bar{n}\hbar^2\mathcal{M}}{m}\mathcal{F}^{-1}\left[k\delta\theta(\mathbf{k},t)\right]. \tag{4.29}$$

Transforming to k-space then leads to

$$\begin{aligned} d\delta n(\mathbf{k},t) &= -\frac{2\gamma\mu}{\hbar}\delta n(\mathbf{k},t)dt - \frac{\gamma\hbar k^2}{2m}\delta n(\mathbf{k},t)dt \\ &\quad + \frac{\hbar\bar{n}k^2}{m}\delta\theta(\mathbf{k},t)dt + \sqrt{\frac{4\gamma k_B T\bar{n}}{\hbar}}dW_1(\mathbf{k},t), \end{aligned} \tag{4.30}$$

$$\begin{aligned} d\delta\theta(\mathbf{k},t) &= -\frac{g}{\hbar}\delta n(\mathbf{k},t)dt - \frac{\mathcal{M}\hbar\bar{n}k}{m}\delta\theta(\mathbf{k},t)dt - \frac{\hbar k^2}{4m\bar{n}}\delta n(\mathbf{k},t)dt \\ &\quad - \frac{\gamma\hbar k^2}{2m}\delta\theta(\mathbf{k},t)dt + \sqrt{\frac{2\mathcal{M}k_B T}{\hbar k}}dW_3(\mathbf{k},t) + \sqrt{\frac{\gamma k_B T}{\hbar\bar{n}}}dW_2(\mathbf{k},t). \end{aligned} \tag{4.31}$$

or in vector SDE notation

$$d\delta\mathbf{x}(\mathbf{k},t) = -\mathbf{A}(\mathbf{k})\delta\mathbf{x}(\mathbf{k},t)dt + \mathbf{B}(\mathbf{k})d\mathbf{W}(\mathbf{k},t) \tag{4.32}$$

where

$$\delta\mathbf{x}(\mathbf{k},t) = \begin{bmatrix} \delta n(\mathbf{k},t) \\ \\ \delta\theta(\mathbf{k},t) \end{bmatrix}, \quad d\mathbf{W}(\mathbf{k},t) = \begin{bmatrix} dW_1(\mathbf{k},t) \\ \\ dW_2(\mathbf{k},t) \\ \\ dW_3(\mathbf{k},t) \end{bmatrix}, \tag{4.33}$$

the complex Wiener processes are independent with correlations

$$\langle dW_i(\mathbf{k},t)dW_j^*(\mathbf{k}',t)\rangle = \delta(\mathbf{k}-\mathbf{k}')\delta_{ij}dt, \tag{4.34}$$

with drift matrix

$$\mathbf{A}(\mathbf{k}) = \begin{bmatrix} \dfrac{2\gamma\mu}{\hbar} + \dfrac{\gamma\hbar k^2}{2m} & -\dfrac{\hbar\bar{n}k^2}{m} \\ \\ \dfrac{g}{\hbar} + \dfrac{\hbar k^2}{4m\bar{n}} & \dfrac{\mathcal{M}\hbar\bar{n}k}{m} + \dfrac{\gamma\hbar k^2}{2m} \end{bmatrix}, \tag{4.35}$$

and diffusion matrix

$$\mathbf{B}(\mathbf{k}) = \sqrt{\frac{2k_BT}{\hbar}} \begin{bmatrix} \sqrt{2\bar{n}\gamma} & 0 & 0 \\ 0 & \sqrt{\frac{\gamma}{2\bar{n}}} & \sqrt{\frac{\mathcal{M}}{k}} \end{bmatrix}. \tag{4.36}$$

Equations (4.32)-(4.36) give a complete description of the stochastic dynamics of linearized fluctuations. In what follows we study the fluctuation properties in detail for a specific set of parameters, focussing on steady-state fluctuation spectra and the link to Bogoliubov dispersion for density fluctuations.

4.3 Fluctuation properties

In this section we consider the fluctuation properties that may be discerned from the linearized equation of motion (4.32) using standard stochastic methods [272]. For the purposes of visualizing these properties, we must choose some appropriate parameters. We first find physically consistent parameters for a large harmonically trapped system using the Hartree-Fock parameter estimation scheme [2], then take the values at the trap centre as an estimate of appropriate parameters for our homogeneous system.

4.3.1 Parameters

We first find physically consistent parameters for a large ($N_T = 10^6$) harmonically trapped ($\omega = 2\pi \times 10$ Hz) system of ^{87}Rb atoms at temperature $T = 0.75T_c$ using the Hartree-Fock parameter estimation scheme [2]. We then consider a new homogeneous box system with length chosen to be the Thomas-Fermi radius of the harmonic trap $L = R_{\rm TF} = 21.3\,\mu$m. The parameter estimation gives the chemical potential $\mu = 1.30\times10^{-31}$J ($\mu/k_B = 9.42\,$nK) and temperature $T = 33.8\,$nK. The background particle density, healing length, and speed of sound are chosen to be the values at the centre of the harmonic trap giving $\bar{n} = 2.54\,\mu\text{m}^{-3}$, $\xi = 0.770\,\mu$m, and $c = 948\,\mu\text{m}\,\text{s}^{-1}$ respectively. The total number of particles in the coherent region is then $N = 2.47 \times 10^5$, and the number-damping and energy-damping rates are $\gamma = 4.4\times10^{-4}$ and $\mathcal{M} = 0.0038\,\mu\text{m}^2 = 1.68\times10^{-5}\xi^2$ respectively. For a finite system, the experimentally meaningful values of k are limited[1] above by the

[1]By this we mean that there is little relevant interesting physics outside this regime; the $\mathbf{k}$ values outside this range can in principle be probed.

healing length

$$k_\xi = \frac{2\pi}{\xi} \tag{4.37}$$

and below by the system size

$$k_L = \frac{2\pi}{L}. \tag{4.38}$$

For our homogeneous box system these upper and lower limits are $k_\xi = 8.16\,\mu\mathrm{m}^{-1} = 2\pi\xi^{-1}$ and $k_L = 0.294\,\mu\mathrm{m}^{-1} = 0.226\xi^{-1}$ respectively.

4.3.2 Dispersion and damping

Here we neglect the noise in order to obtain the dispersion relation describing the relation between wavenumber, energy, and dissipation rate. We will then use this non-stochastic description as a reference point for understanding the role of noise in the system. Neglecting the noise, we find the deterministic equation

$$\frac{\partial}{\partial t}\delta\mathbf{x}(\mathbf{k},t) = -\mathbf{A}(\mathbf{k})\delta\mathbf{x}(\mathbf{k},t). \tag{4.39}$$

As is usual for such calculations, we assume the time dependence is given by

$$\delta\mathbf{x}(\mathbf{k},t) = \delta\mathbf{x}(\mathbf{k})e^{-i\epsilon(\mathbf{k})t/\hbar} \tag{4.40}$$

where $\epsilon(\mathbf{k})$ is the dispersion relation. Then

$$\left(\mathbf{A}(\mathbf{k}) - i\epsilon(\mathbf{k})/\hbar\right)\delta\mathbf{x}(\mathbf{k}) = 0, \tag{4.41}$$

and we can find the dispersion relation by solving the characteristic equation

$$|\mathbf{A}(\mathbf{k}) - i\epsilon(\mathbf{k})/\hbar| = 0, \tag{4.42}$$

giving

$$\epsilon(\mathbf{k}) \equiv \epsilon(k) = \sqrt{\frac{\hbar^2k^2}{2m}\left(\frac{\hbar^2k^2}{2m} + 2g\bar{n}\right) - \hbar^2\Gamma(k)^2} - i\hbar\Gamma(k) \tag{4.43}$$

where we have identified the momentum dependent damping rate

$$\Gamma(k) = \frac{\gamma}{\hbar}\left(g\bar{n} + \frac{\hbar^2 k^2}{2m}\right) + \frac{\mathcal{M}\hbar\bar{n}k}{2m}, \tag{4.44}$$

containing distinct terms due to number-damping and energy-damping respectively. In the limit of small damping rate, the dispersion takes the usual form

$$\epsilon(k) \approx \sqrt{\frac{\hbar^2 k^2}{2m}\left(\frac{\hbar^2 k^2}{2m} + 2g\bar{n}\right)}, \tag{4.45}$$

and there is a clear distinction between the phonon-like behaviour at low k

$$\epsilon_{\mathrm{PH}}(k) = \sqrt{\frac{g\bar{n}}{m}}\hbar k = cp \tag{4.46}$$

and the quasiparticle-like behaviour at high k

$$\epsilon_{\mathrm{QP}}(k) = \frac{\hbar^2 k^2}{2m} + g\bar{n}. \tag{4.47}$$

We can decompose the damping rate into contributions from the two reservoir interaction processes

$$\begin{aligned}
\Gamma(k) &= \Gamma_\gamma(k) + \Gamma_\varepsilon(k) && (4.48)\\
\Gamma_\gamma(k) &= \frac{\gamma}{\hbar}\left(g\bar{n} + \frac{\hbar^2 k^2}{2m}\right) && (4.49)\\
\Gamma_\varepsilon(k) &= \frac{\mathcal{M}\hbar\bar{n}k}{2m} && (4.50)
\end{aligned}$$

There is a clear distinction between the contributions due to energy-damping and number-damping; the number-damping is quadratic in the momentum while energy-damping is linear in the momentum. We can find where the relative contributions of each process are significant by solving the quadratic equation $\Gamma_\gamma(k) = \Gamma_\varepsilon(k)$. The two solutions are

$$k = \frac{\mathcal{M}\bar{n}}{2\gamma}\left(1 \pm \sqrt{1 - \frac{8gm\gamma^2}{\hbar^2\mathcal{M}^2\bar{n}}}\right). \tag{4.51}$$

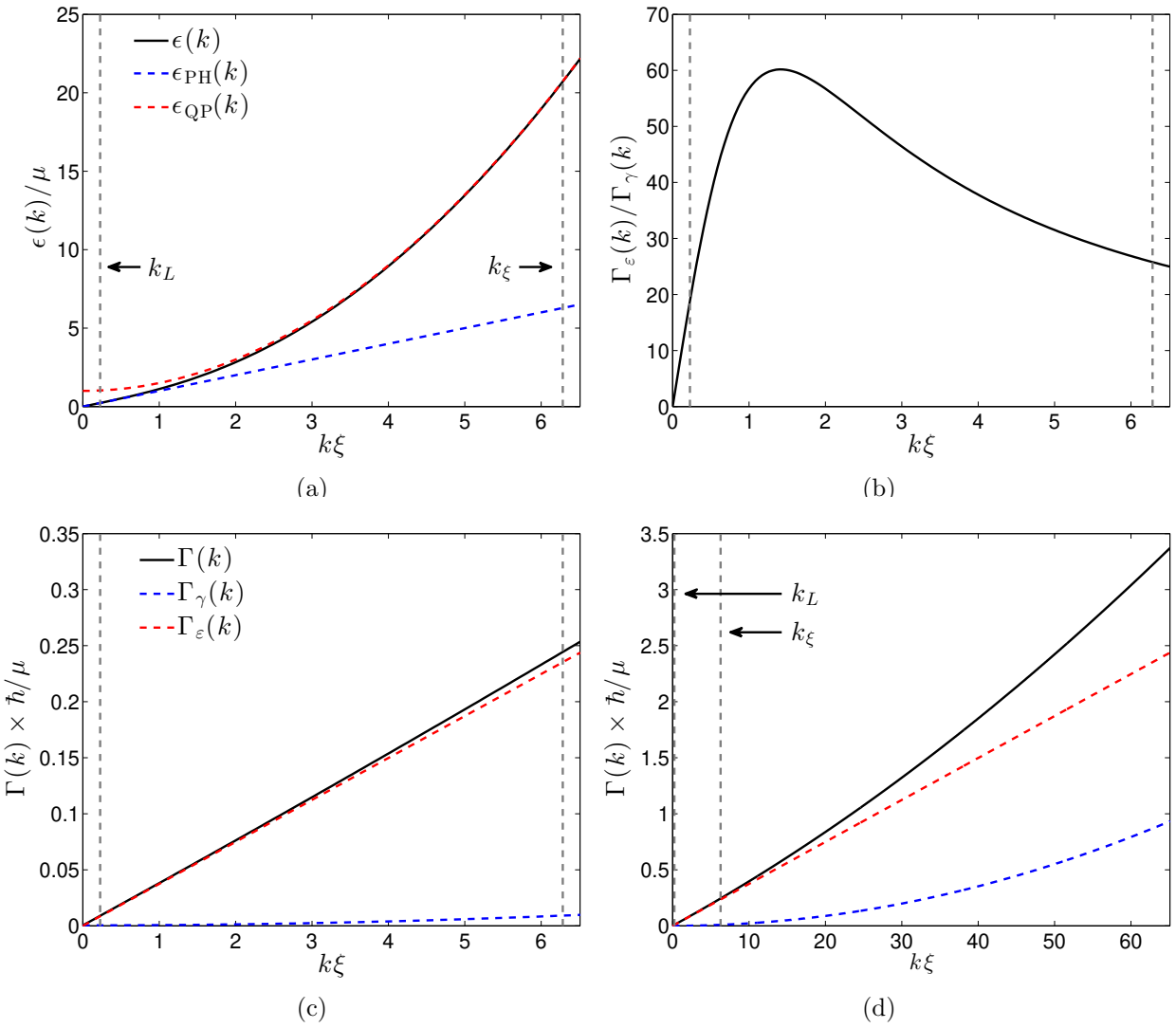

Figure 4.1: (a) The total dispersion relation (4.43), phonon dispersion relation (4.46), and quasiparticle dispersion relation (4.47). (b) The ratio of the energy-damping (4.50) and number-damping (4.49) contributions to the mode damping. (c) The total mode damping (4.44), and the energy-damping (4.50) and number-damping (4.49) contributions for low k. (d) The total mode damping (4.44), and the energy-damping (4.50) and number-damping (4.49) contributions for high k. We have also indicated the upper (k_ξ) and lower (k_L) limits on physically relevant k by dashed gray vertical lines.

For all parameters we have looked at, the second term in the square root is much smaller than unity, so we may approximate the solutions as

$$k_1 \approx \frac{2gm\gamma}{\hbar^2\mathcal{M}}, \quad k_2 \approx \frac{\mathcal{M}\bar{n}}{\gamma}. \tag{4.52}$$

Hence there are three regimes:

i) The low k, or large length scale regime, given by $k < k_1$. Here the number-damping process dominates the total mode damping due to the constant term in (4.49).

ii) The intermediate k, or intermediate length scale regime, given by $k_1 < k < k_2$. Here the energy-damping process dominates the total mode damping due to the linear k term (4.50).

iii) The high k, or short length scale regime, given by $k_2 < k$. Here the number-damping process again dominates the total mode damping due to the quadratic term in (4.49).

There is a point within the intermediate k region where the relative contribution of the energy-damping process is at its highest, which we denote k_ε. It is easy to show that this occurs at $k_\varepsilon\xi \equiv \sqrt{2}$.

The easily accessible regime for many experiments involves k values at longer wavelengths. However, important physics also occurs near $k\xi = 1$, for example in vortex-sound interactions. Values of $k \gg k_\xi$ corresponding to high energy are difficult to both resolve and excite. For these reasons, here we focus on the regime of wave numbers $k_L < k < k_\xi$, accounting for much of the physically interesting and accessible length scales in Bose-Einstein condensates. The dispersion and damping curves are shown in Fig. 4.1. For our parameters the damping regime separators are $k_1 = 0.0235\,\xi^{-1} \ll k_L$ and $k_2 = 170\,\xi^{-1} \gg k_\xi$, small and large enough respectively that we are unable to show them in Fig. 4.1 without obscuring the relevant features. The physically relevant region lies entirely within the intermediate k regime, and so for our parameters we expect the damping of excitations to be dominated by energy-damping.

4.3.3 Stationary properties

Here we consider the stationary properties of the k-space density and phase fluctuations. In the literature it is standard to include a subscript to indicate that we are interested in

fluctuations around the steady-state

$$\delta\mathbf{x}(\mathbf{k},t) \longrightarrow \delta\mathbf{x}_s(\mathbf{k},t). \tag{4.53}$$

Variance

The stationary covariance matrix $\sigma(\mathbf{k})$ is defined by

$$\sigma(\mathbf{k}) = \int d^3\mathbf{k}' \left\langle \delta\mathbf{x}_s(\mathbf{k},t)\delta\mathbf{x}_s^\dagger(\mathbf{k}',t)\right\rangle \tag{4.54}$$

and can be calculated using [272]

$$\sigma(\mathbf{k}) = \frac{\mathrm{Det}\left(\mathbf{A}(\mathbf{k})\right)\mathbf{B}(\mathbf{k})\mathbf{B}^{\mathrm{T}}(\mathbf{k}) + \left[\mathbf{A}(\mathbf{k}) - \mathrm{Tr}\left(\mathbf{A}(\mathbf{k})\right)\right]\mathbf{B}(\mathbf{k})\mathbf{B}^{\mathrm{T}}(\mathbf{k})\left[\mathbf{A}(\mathbf{k}) - \mathrm{Tr}\left(\mathbf{A}(\mathbf{k})\right)\right]^{\mathrm{T}}}{2\mathrm{Tr}\left(\mathbf{A}(\mathbf{k})\right)\mathrm{Det}\left(\mathbf{A}(\mathbf{k})\right)}. \tag{4.55}$$

From this we find that the variances of density and phase fluctuations are

$$\sigma_{11}(\mathbf{k}) \equiv \int d^3\mathbf{k}' \left\langle \delta n_s(\mathbf{k},t)\delta n_s^\dagger(\mathbf{k}',t)\right\rangle = \frac{4k_BTm\bar{n}}{\hbar^2k^2+4m\mu}, \tag{4.56}$$

$$\sigma_{22}(\mathbf{k}) \equiv \int d^3\mathbf{k}' \left\langle \delta\theta_s(\mathbf{k},t)\delta\theta_s^\dagger(\mathbf{k}',t)\right\rangle = \frac{k_BTm}{\bar{n}\hbar^2k^2} \tag{4.57}$$

respectively, while the covariances are zero

$$\sigma_{12}(\mathbf{k}) \equiv \int d^3\mathbf{k}' \left\langle \delta n_s(\mathbf{k},t)\delta\theta_s^\dagger(\mathbf{k}',t)\right\rangle = 0, \tag{4.58}$$

$$\sigma_{21}(\mathbf{k}) \equiv \int d^3\mathbf{k}' \left\langle \delta\theta_s(\mathbf{k},t)\delta n_s^\dagger(\mathbf{k}',t)\right\rangle = 0. \tag{4.59}$$

The steady-state variances have no dependence on either of the damping rates. This is to be expected, as it is a general property of statistical ensembles that the equilibrium ensemble cannot depend on the detailed values of the reservoir coupling parameters, but rather can only depend on the type of reservoir coupling (grand canonical, canonical, microcanonical). The density-density variance has a well-defined low-k limit, while the phase-phase variance diverges as k tends to zero. In any physical system, there is an

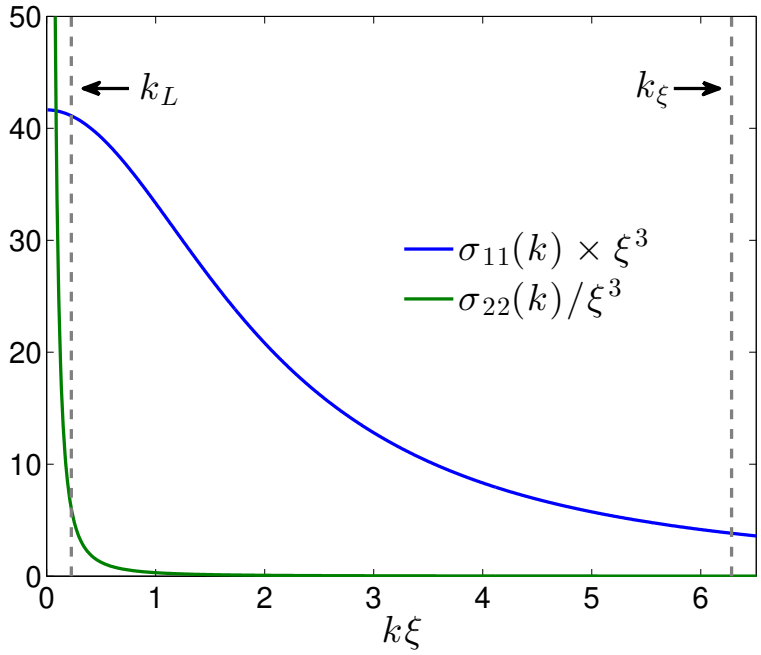

Figure 4.2: The density-density (4.56) $\sigma_{11}(\mathbf{k})$ and phase-phase variances (4.57) $\sigma_{22}(\mathbf{k})$. Also shown by the dashed grey vertical lines are the effective upper and lower k values (4.37) and (4.38).

effective lower limit to k imposed by the system size[2], so in practice the phase variance will saturate at $mk_BT/(\bar{n}\hbar^2k_L^2)$. The k-dependence of the variances are shown in Fig. 4.2, demonstrating these properties.

Spectrum matrix

The spectrum matrix is defined as the temporal Fourier transform of the two-time correlation matrix $G(\mathbf{k}, \tau)$

$$S(\mathbf{k}, \Omega) = \frac{1}{2\pi} \int_{\infty}^{\infty} d\tau G(\mathbf{k}, \tau) e^{i\omega\tau} \tag{4.60}$$

where

$$G(\mathbf{k}, \tau) = \lim_{t\to\infty} \int d^3\mathbf{k}' \, \langle \delta\mathbf{x}_s(\mathbf{k}, t) \delta\mathbf{x}_s^\dagger(\mathbf{k}', t+\tau) \rangle. \tag{4.61}$$

[2]The divergence does imply that there can be no phase coherence in the limit of an infinitely large system. However whether this is an appropriate conclusion is up for debate, as a rigorous application of the thermodynamic limit would need to be considered, especially with respect to the projected formalism which we have thus far neglected.

For a vector stochastic differential equation of the form (4.32)[3] the spectrum matrix may be obtained from [272]

$$S(\mathbf{k},\Omega) = \frac{1}{2\pi}\left(\mathbf{A}(\mathbf{k}) + i\Omega\right)^{-1}\mathbf{B}(\mathbf{k})\mathbf{B}^{\mathrm{T}}(\mathbf{k})\left(\mathbf{A}^{\mathrm{T}}(\mathbf{k}) - i\Omega\right)^{-1}. \tag{4.62}$$

The full result for the spectrum matrix is rather unwieldy, but there is a common factor in each of the elements, so defining

$$\begin{aligned} S_F(\mathbf{k},\Omega)^{-1} &= 16\pi m^2\left(k^2\bar{n}\Omega^2\mathcal{M}\hbar^4(\gamma k + \bar{n}\mathcal{M}) + m^2\left(4\gamma^2\mu^2\Omega^2 + \Omega^4\hbar^2\right)\right) \\ &\quad +8\pi\left(\gamma^2 - 1\right)k^2m^2\hbar^2\left(k^2\Omega^2\hbar^2 + 4\mu m\Omega^2\right) \\ &\quad +\pi\left(k^6\hbar^6 + 8k^4\mu m\hbar^4 + 16k^2\mu^2m^2\hbar^2\right)\left(\gamma^2 k + k + 2\gamma\bar{n}\mathcal{M}\right)^2 \end{aligned} \tag{4.63}$$

we can then express the full steady state power spectra as

$$\frac{S_{11}(\mathbf{k},\Omega)}{S_F(\mathbf{k},\Omega)} = 8k_BTm^2\bar{n}\hbar\left(\hbar^2k^2(\gamma k + 2\mathcal{M}\bar{n})\left(\gamma^2 k + k + 2\gamma\mathcal{M}\bar{n}\right) + 4\gamma m^2\Omega^2\right), \tag{4.64}$$

$$\frac{S_{12}(\mathbf{k},\Omega)}{S_F(\mathbf{k},\Omega)} = -16ik_BTm^3\Omega\left(\hbar^2k(\gamma k + \mathcal{M}\bar{n}) + 2\gamma\mu m\right), \tag{4.65}$$

$$\begin{aligned} \frac{S_{22}(\mathbf{k},\Omega)}{S_F(\mathbf{k},\Omega)} = \frac{2k_BTm^2}{\bar{n}\hbar k}\Big(&4m^2\Omega^2\hbar^2(\gamma k + 2\bar{n}\mathcal{M}) \\ &+\left(\gamma^2 k + k + 2\gamma\bar{n}\mathcal{M}\right)\left(\gamma k^4\hbar^4 + 8\gamma k^2\mu m\hbar^2 + 16\gamma\mu^2m^2\right)\Big), \end{aligned} \tag{4.66}$$

where S_{11} is the density-density fluctuation spectra[4], S_{12} is the density-phase fluctuation spectra, and S_{22} is the phase-phase fluctuation spectra.

To investigate the roles of the two damping processes, we linearize the full fluctuation spectra with respect to the (small) rates γ and $\mathcal{M}$ and decompose this into number-damping and energy-damping contributions

$$S(\mathbf{k},\Omega) \approx S^{\gamma}(\mathbf{k},\Omega) + S^{\varepsilon}(\mathbf{k},\Omega). \tag{4.67}$$

[3] That is, a vector Ornstein-Uhlenbeck process.

[4] The spectra of density-density fluctuations in $\mathbf{k}$-space is equivalent to the *dynamic structure factor*.

The leading order number-damping contribution is

$$S^{\gamma}(\mathbf{k},\Omega) = \frac{2\gamma k_B T m^2}{\bar{n}\hbar\pi\left(\hbar^3 k^4 + 4m\hbar\left(k^2\mu - m\Omega^2\right)\right)^2} \times \begin{pmatrix} 4\bar{n}^2\hbar^2\left(\hbar^2 k^4 + 4m^2\Omega^2\right) & -8im\bar{n}\hbar\Omega\left(\hbar^2 k^2 + 2m\mu\right) \\ 8im\bar{n}\hbar\Omega\left(\hbar^2 k^2 + 2m\mu\right) & \hbar^4 k^4 + 4m\hbar^2\left(2\mu k^2 + m\Omega^2\right) + 16m^2\mu^2 \end{pmatrix} \tag{4.68}$$

and the leading order energy-damping contribution is

$$S^{\varepsilon}(\mathbf{k},\Omega) = \frac{16\mathcal{M}k_B T m^2}{\hbar\pi k\left(\hbar^2 k^4 + 4m\mu k^2 - 4m^2\Omega^2\right)^2} \begin{pmatrix} \bar{n}^2\hbar^2 k^4 & -im\bar{n}\hbar\Omega k^2 \\ im\bar{n}\hbar\Omega k^2 & m^2\Omega^2 \end{pmatrix}. \tag{4.69}$$

For the purposes of comparison, we also construct the ratio of these

$$\frac{S^{\varepsilon}(\mathbf{k},\Omega)}{S^{\gamma}(\mathbf{k},\Omega)} = \frac{\mathcal{M}\bar{n}\hbar^2}{\gamma} \begin{pmatrix} \dfrac{2k^3}{\hbar^2 k^4 + 4m^2\Omega^2} & \dfrac{k}{k^2\hbar^2 + 2m\mu} \\ \dfrac{k}{k^2\hbar^2 + 2m\mu} & \dfrac{8m^2\Omega^2}{k\left(k^4\hbar^4 + 4m\left(2\mu k^2 + m\Omega^2\right)\hbar^2 + 16m^2\mu^2\right)} \end{pmatrix}, \tag{4.70}$$

where where have performed the division component-wise.

The density-density fluctuation spectra is shown in Fig. 4.3(a). Of immediate note is that the fluctuation spectra is always strongly peaked about the dispersion relation (4.43), an expected result but still an important check of consistency. Of more relevance to our investigation of the significance of the two damping processes is the ratio of the linear energy-damping contribution to the linear number-damping contribution (4.70). This ratio is shown in Fig. 4.3(b), where it is clear that the energy-damping contribution dominates over the majority of the space. In particular, the region where the number-damping contribution becomes larger, in the area to the left of the black line in Fig. 4.3(b), is significantly removed from where the spectra is peaked, so the fluctuation spectra have low amplitude in this region anyway. To directly compare the leading order damping contributions to the full fluctuation spectra, we consider each at constant k for varying Ω, or constant Ω for

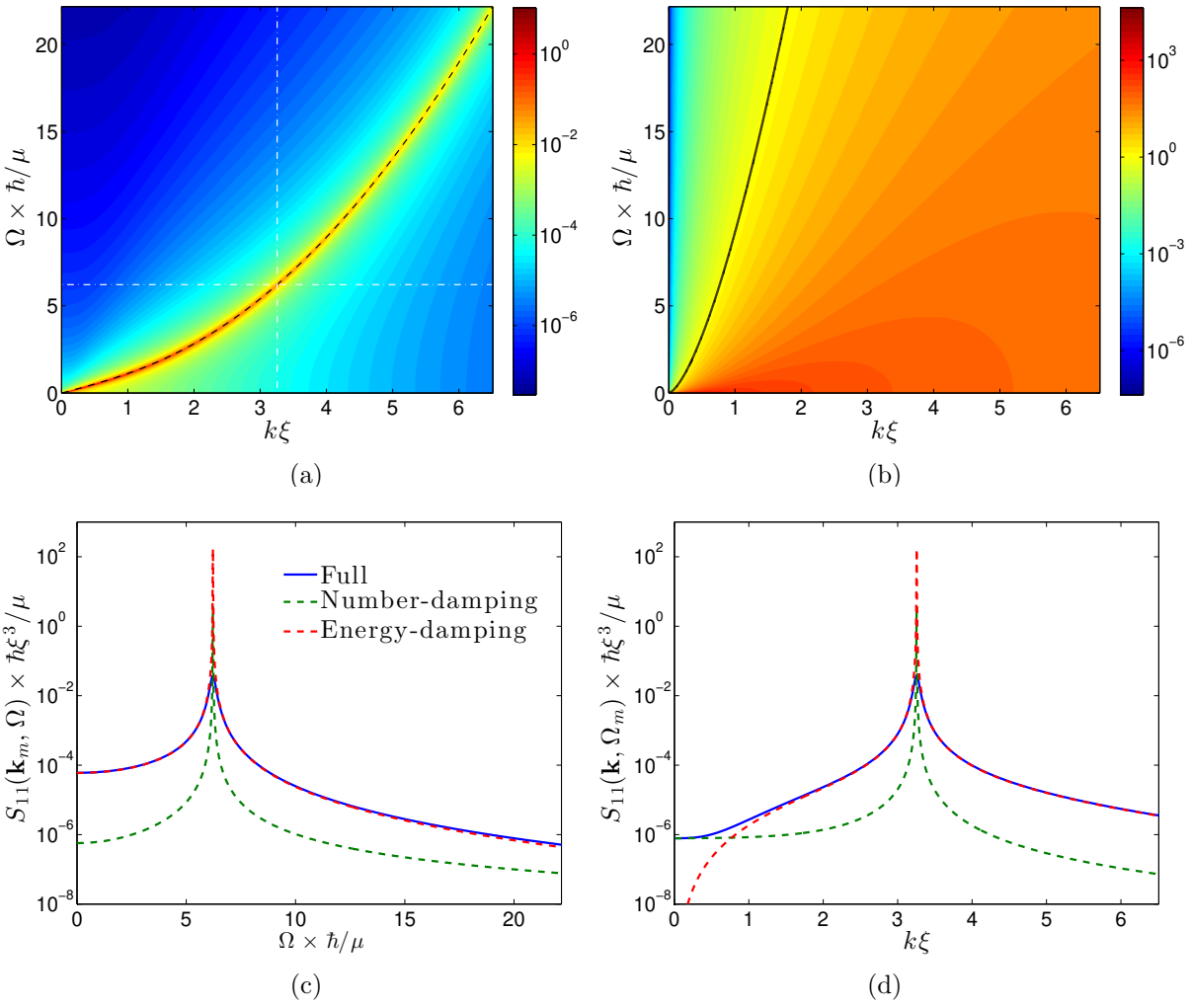

Figure 4.3: (a) The density-density fluctuation spectra (4.64); the black dashed line is the dispersion relation (4.43) and the white dash-dot line are the slices shown in (c) and (d) at Ω_m and k_m. (b) The ratio of the linear contributions (4.68) and (4.69); the black line is where the ratio is unity. (c) The leading damping contributions (4.68) and (4.69), and full spectra (4.64) at Ω_m. (d) The leading damping contributions (4.68) and (4.69), and full spectra (4.64) at k_m.

varying k. We choose the constant k value to lie halfway between k_L and k_ξ, giving a value of

$$k_m = \frac{k_L + k_\xi}{2} = 3.25\xi^{-1}. \tag{4.71}$$

The constant Ω is then chosen to be the value of the dispersion relation (4.43) at k_m

$$\hbar\Omega_m = \epsilon(k_m) = 6.22\mu. \tag{4.72}$$

In Fig. 4.3(c) we show the fluctuation spectra (4.64) and leading order damping contributions (4.68) and (4.69) at $k = k_m$, while in Fig. 4.3(d), we show these at $\Omega = \Omega_m$. We see from these that the energy-damping contribution closely approximates the full fluctuation spectra, while the number-damping contributes very little. Again we see that the spectra is peaked about the dispersion relation (4.43), however the height of the peak is larger for both the leading order damping contributions than the full spectra.

Similar properties can be seen in the phase-phase fluctuation spectra shown in Fig. 4.4(a). As expected the spectra is again strongly peaked about the dispersion relation (4.43), and the energy-damping contribution dominates over the number-damping contribution as shown specifically in Fig. 4.4(b). In this case the small region where number-damping becomes dominant is at low frequency Ω, for all wavenumber k, while in the density-density fluctuation spectra this occurred at low wavenumber for all frequency. In both cases, however, the result of note is that the energy-damping is the largest contributor around the peak of the spectra. In Fig. 4.4(c) and Fig. 4.4(d) we show the fluctuation spectra (4.66) and leading order damping contributions (4.68) and (4.69) at $k = k_m$ and $\Omega = \Omega_m$ respectively. Once again the energy-damping contribution closely approximates the full spectra while the number-damping is largely negligible, and the peak of both leading order damping contributions is larger than the true peak.

We see similar features once more in the density-phase fluctuation spectra shown in Fig. 4.5(a), with a peak about the dispersion relation (4.43). In this case, the ratio of the two contributions (4.70) has no dependence on the frequency Ω; for the density-density and phase-phase fluctuation spectra the ratio had dependence on both Ω and k. The ratio is thus easily visualized in Fig. 4.5(b). The ratio goes to zero at both low and high k, with a peak that can easily be shown to occur at $k_\varepsilon\xi = \sqrt{2}$; this is the same behaviour that was seen in the ratio of damping contributions in Fig. 4.1(b). Over the physically relevant range, the energy-damping contribution is larger than the number-damping contribution

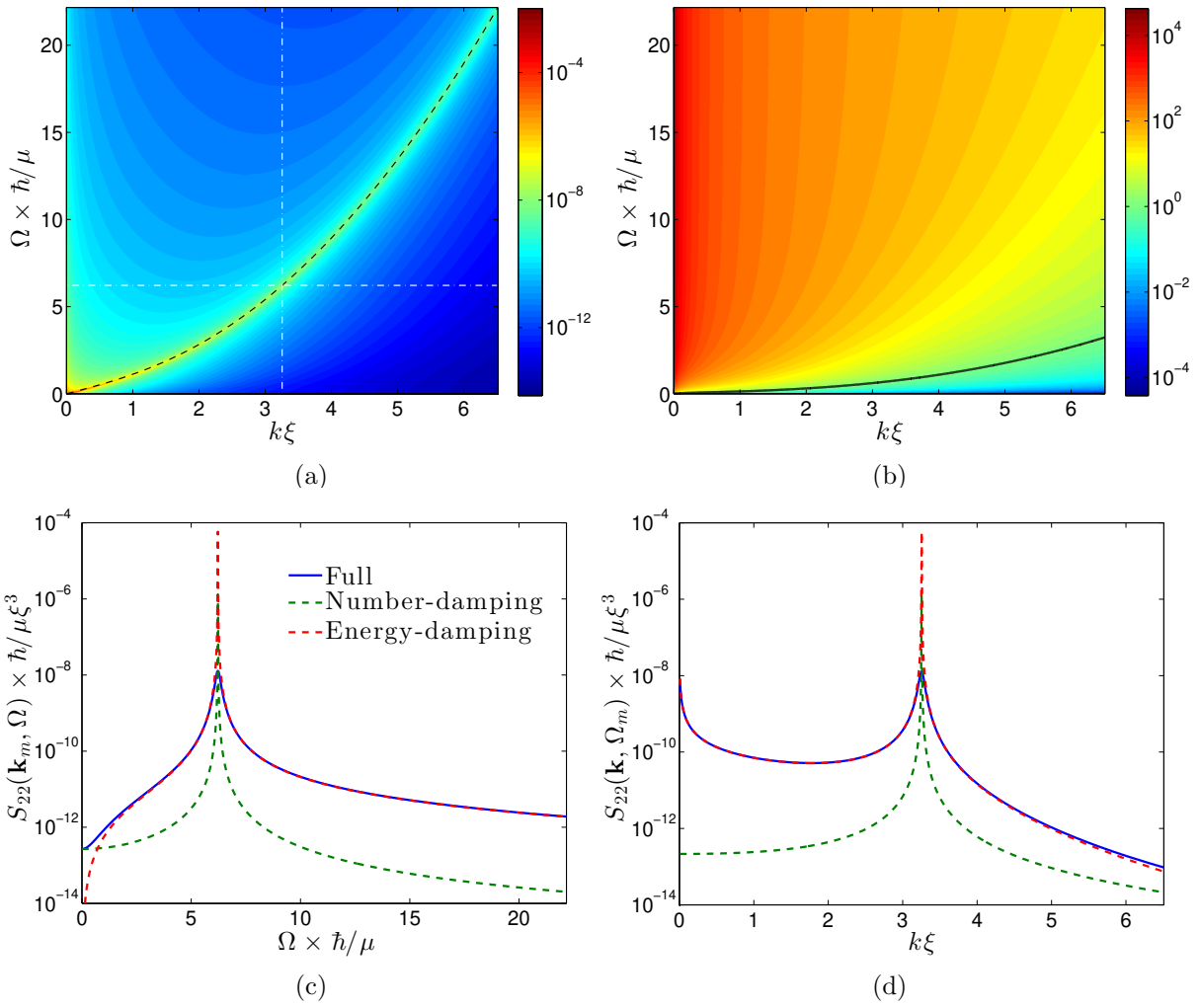

Figure 4.4: (a) The phase-phase fluctuation spectra (4.66); the black dashed line is the dispersion relation (4.43) and the white dash-dot line are the slices shown in (c) and (d) at Ω_m and k_m. (b) The ratio of the linear contributions (4.68) and (4.69); the black line is where the ratio is unity. (c) The leading damping contributions (4.68) and (4.69), and full spectra (4.66) at Ω_m. (d) The leading damping contributions (4.68) and (4.69), and full spectra (4.66) at k_m.

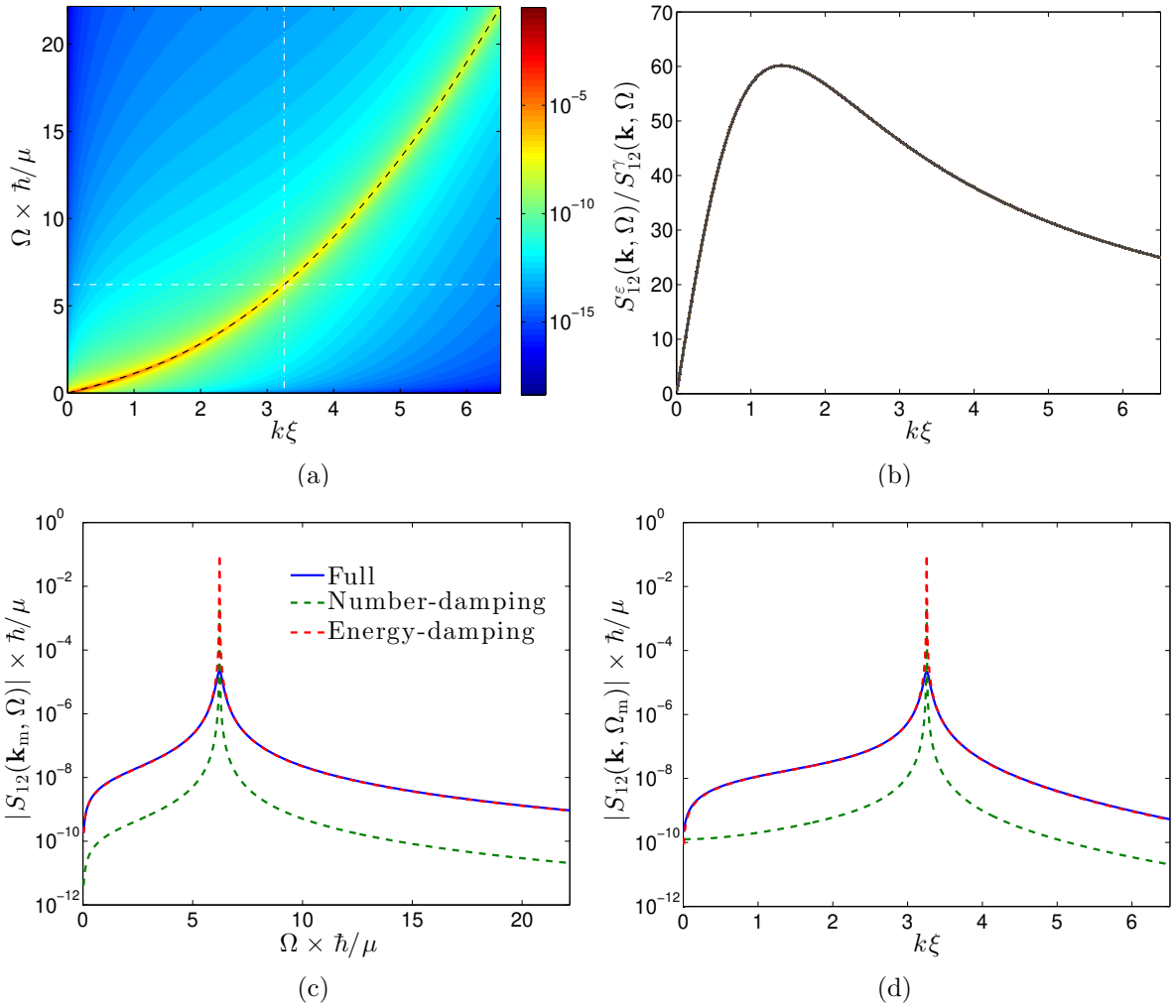

Figure 4.5: (a) The density-phase fluctuation spectra (4.65); the black dashed line is the dispersion relation (4.43) and the white dash-dot line are the slices shown in (c) and (d) at Ω_m and k_m. (b) The ratio of the linear contributions (4.68) and (4.69); the black line is where the ratio is unity. (c) The leading damping contributions (4.68) and (4.69), and full spectra (4.65) at Ω_m. (d) The leading damping contributions (4.68) and (4.69), and full spectra (4.65) at k_m.

by an order of magnitude. In Fig. 4.5(c) and Fig. 4.5(d) we show the fluctuation spectra (4.65) and leading order damping contributions (4.68) and (4.69) at $k = k_m$ and $\Omega = \Omega_m$ respectively. The observed features are consistent with the previous two cases, with the energy-damping contribution closely approximating the full spectra while the number-damping contributing very little, and the peak of both leading order damping contributions being larger than the true peak.

4.4 Conclusions

In this chapter we have performed a linear fluctuation analysis of the SPGPE for a 3D homogeneous system, including both the number-damping and energy-damping reservoir interaction processes. To our knowledge this is the first instance such an analysis has been done that includes the energy-damping process. Using standard stochastic methods we obtained the dispersion relation, momentum dependent damping rate, and momentum space fluctuation spectra. The dispersion relation shows the usual phonon-like and quasiparticle-like regimes familiar from Bogoliubov analysis. The distinct nature of the two reservoir interaction processes are apparent in the momentum dependent damping rate as they have different momentum dependence; the number-damping term is quadratic in the momentum, while the energy-damping term is linear in the momentum. This implies that energy-damping is the dominant damping process over a significant range of length scales. Indeed, we see that the ratio of energy-damping to number-damping contributions to the mode damping is at least an order of magnitude greater than unity over the experimentally accessible range of length scales, and exhibits a peak at $k_\varepsilon \xi = \sqrt{2}$. The momentum space fluctuation spectra is strongly peaked about the Bogoliubov dispersion relation, as would be expected. When taking the linear contributions from energy-damping and number-damping, we found that the fluctuation spectra is typically dominated by the energy-damping contribution. Our results strongly suggest that the energy-damping reservoir interaction process is significant when considering the properties of a finite-temperature 3D homogeneous Bose gas in equilibrium. These predictions can be tested numerically by solving the SPGPE in a 3D box, however the development of code for solving such a system is itself a non-trivial task, and is a topic for future work. Furthermore, increasing control in BEC confinement [279, 280] also means that direct experimental tests in a box trap are now possible. It could also be possible to use a local density approximation to extend this approach to smoothly varying trapped systems.

Chapter 5

Stochastic Ehrenfest relations

5.1 Introduction

Numerical solutions of the Stochastic Projected Gross-Pitaevskii equation (SPGPE) have been shown to give results that agree qualitatively and quantitatively with experiments [71,121]. However solving the full SPGPE is in general very computationally intensive, even for single trajectories, and large ensembles of trajectories are usually required to obtain any meaningful results. Of course, a much quicker route to making predictions is to use analytic solutions of the SPGPE. Unfortunately explicit analytic dynamical or equilibrium solutions for the full complex field are few and far between.

In many systems we may already know that the system will only access a limited set of states, to some reasonable approximation. A system in equilibrium with its surroundings is highly unlikely to change to a state too far from the steady state. Furthermore, particular types of excitations on top of an equilibrium system are often able to be described by only a few parameters. For example, an approximately Thomas-Fermi condensate in a quasi-1D trap is unlikely to stray too far from being Thomas-Fermi, even in contact with a thermal cloud. We may then consider the excitations on top of the equilibrium, such as "sloshing" (Kohn-like modes of the condensate) and "breathing" (expansion and contraction of the condensate). These excitations can be (approximately) parameterised by the expectation of position and momentum, or the square of position and momentum respectively. If we can construct a stochastic differential equation for these low order moments, it may be much more simple than the SPGPE due to the elimination of the spatial degree of freedom, and may even admit analytic solutions.

An earlier implementation of this method was used in a previous work [150] to describe motion of a matter wave bright soliton in a condensed quasi-1D bose gas moving through a thermal cloud of a second component; this was done by obtaining a stochastic equation of motion for the field momentum. In this chapter we take a more general approach and derive stochastic collective equations for matter wave moments of the SPGPE including the

effects of both number-damping and energy-damping, which we refer to as the *stochastic Ehrenfest relations*; a previous work has found Ehrenfest relations for the ensemble averages of the moments for a number-damped system [281]. The chapter is structured as follows. In Section 5.2 we recap the standard Ehrenfest relations. In Section 5.3 we show how Ito's change of variables formula can be applied to the SPGPE. In Section 5.4 we derive the stochastic Ehrenfest relations, stochastic differential equations for moments of the SPGPE, and demonstrate the simpler form that results when the moment is the expectation of a one-body operator. In Section 5.5 we consider the effect of corrective terms arising from the projector via the simple example of a quasi-1D Thomas-Fermi system, showing that these terms can generally be neglected. We conclude in Section 5.6.

5.2 Ehrenfest relations

5.2.1 Ehrenfest's theorem

Ehrefest's theorem [282] as it is generally stated

$$\frac{d}{dt}\langle\hat{\mathbf{r}}\rangle = \frac{1}{m}\langle\hat{\mathbf{p}}\rangle \tag{5.1}$$

$$\frac{d}{dt}\langle\hat{\mathbf{p}}\rangle = -\langle\nabla V(\mathbf{r})\rangle \tag{5.2}$$

relates the time derivative of the position $\hat{\mathbf{r}}$ and momentum $\hat{\mathbf{p}}$ expectation values to the expectation of the force $F(\mathbf{r}) = -\nabla V(\mathbf{r})$ on a massive particle moving in a potential. These *Ehrenfest relations* suggest that the motion of the particle obey Newton's second law in an average sense, though one should not then expect that the averages $\langle\hat{\mathbf{r}}\rangle$ and $\langle\hat{\mathbf{p}}\rangle$ will follow classical trajectories. In fact, only the special case of a harmonic potential will result in the classical particle motion and expectation of the quantum particle motion coinciding exactly. For a general potential, the classical and quantum trajectories will approximately coincide if the wave function is very localised [283]. The Ehrenfest relations are a special case of a more general result that relates the time derivative of the expectation of a general quantum mechanical operator $\hat{A}$ with the Hamiltonian operator $\hat{H} \equiv \hat{\mathbf{p}}^2/2m + V(\mathbf{r})$ [284]

$$\frac{d}{dt}\langle\hat{A}\rangle = -\frac{i}{\hbar}\left\langle\left[\hat{A},\hat{H}\right]\right\rangle + \left\langle\frac{\partial\hat{A}}{\partial t}\right\rangle, \tag{5.3}$$

where the second term arises due to any explicit time dependence of the operator. When working in the Heisenberg picture this result is immediate, however for our purposes it is useful to consider the Schrodinger picture. Let the expectation of $\hat{A}$ be

$$\langle \hat{A} \rangle = \int d^3\mathbf{r} \psi^*(\mathbf{r}, t) \hat{A} \psi(\mathbf{r}, t) \tag{5.4}$$

where $\psi(x, t)$ obeys the time-dependent Schrodinger equation

$$i\hbar \frac{\partial \psi(\mathbf{r}, t)}{\partial t} = \hat{H} \psi(\mathbf{r}, t). \tag{5.5}$$

Then taking the time derivative of (5.4) and substituting in (5.5) gives the result.

5.2.2 Gross-Pitaevskii equation

It is simple to show that the Ehrenfest relations for the Gross-Pitaevskii equation are identical to those for the Schrodinger equation [285]. Let the expectation of $\hat{A}$ be

$$\langle \hat{A} \rangle = \int d^3\mathbf{r} \psi^*(\mathbf{r}, t) \hat{A} \psi(\mathbf{r}, t) \tag{5.6}$$

where $\psi(x, t)$ now obeys the time-dependent Gross-Pitaevskii equation

$$i\hbar \frac{\partial \psi(\mathbf{r}, t)}{\partial t} = \left(\hat{H}_{\rm sp} + g|\psi(\mathbf{r}, t)|^2 \right) \psi(\mathbf{r}, t). \tag{5.7}$$

Then taking the time derivative of (5.6) gives

$$\frac{d}{dt}\langle \hat{A} \rangle = -\frac{i}{\hbar} \left\langle \left[\hat{A}, \hat{H}_{\rm sp} \right] \right\rangle + \left\langle \frac{\partial \hat{A}}{\partial t} \right\rangle. \tag{5.8}$$

Importantly, the terms containing the non-linearity cancel out; the Ehrenfest theorem for a Gross-Pitaevskii fluid simplifies due to the internal cancellation of all two-body interaction forces.

5.2.3 Damped projected Gross-Pitaevskii equation

Recall the damped projected Gross-Pitaevskii equation

$$i\hbar\frac{\partial\psi(\mathbf{r},t)}{\partial t} = \mathcal{P}\left\{(1-i\gamma)(L-\mu)\psi(\mathbf{r},t)\right\} \tag{5.9}$$

with L the Gross-Pitaevskii operator

$$L\psi(\mathbf{r},t) = \left(-\frac{\hbar^2\nabla^2}{2m} + V(\mathbf{r},t) + g|\psi(\mathbf{r},t)|^2\right)\psi(\mathbf{r},t). \tag{5.10}$$

The external potential is decomposed into a time invariant part $V(\mathbf{r})$ and a time dependent part $\delta V(\mathbf{r},t)$; the time invariant part defines the single-particle Hamiltonian

$$H_{\rm sp} = -\frac{\hbar^2\nabla^2}{2m} + V(\mathbf{r}). \tag{5.11}$$

The eigenstates $\phi_n(\mathbf{r})$ of the single-particle Hamiltonian ($H_{\rm sp}\phi_n(\mathbf{r}) = \epsilon_n\phi_n(\mathbf{r})$) are chosen to be the basis states for the system. The Ehrenfest relations for the damped projected Gross-Pitaevskii equation are [281]

$$\frac{d\langle\mathbf{r}\rangle_W}{dt} = \frac{\langle\mathbf{p}\rangle_W}{m} + \frac{2\gamma}{\hbar}{\rm Re}\langle\mathbf{r}\left(\mu-L\right)\rangle_W + \frac{2\gamma k_BT}{\hbar}{\rm Tr}\left(\hat{\mathcal{P}}\hat{\mathbf{r}}\right) + Q_{\mathbf{r}} \tag{5.12}$$

$$\frac{d\langle\mathbf{p}\rangle_W}{dt} = -\langle\nabla V(\mathbf{r},t)\rangle_W + \frac{2\gamma}{\hbar}{\rm Re}\langle\mathbf{p}\left(\mu-L\right)\rangle_W + \frac{2\gamma k_BT}{\hbar}{\rm Tr}\left(\mathcal{P}\hat{\mathbf{p}}\right) + Q_{\mathbf{p}} \tag{5.13}$$

$$\frac{d\langle\mathbf{l}\rangle_W}{dt} = -\frac{i}{\hbar}\langle\mathbf{l}V(\mathbf{r},t)\rangle_W + \frac{2\gamma}{\hbar}{\rm Re}\langle\mathbf{l}\left(\mu-L\right)\rangle_W + \frac{2\gamma k_BT}{\hbar}{\rm Tr}\left(\hat{\mathcal{P}}\hat{\mathbf{l}}\right) + Q_{\mathbf{l}} \tag{5.14}$$

$$\frac{d\langle H\rangle_W}{dt} = \left\langle\frac{\partial\delta V(\mathbf{r},t)}{\partial t}\right\rangle_W + \frac{2\gamma}{\hbar}{\rm Re}\langle L\left(\mu-L\right)\rangle_W + \frac{2\gamma k_BT}{\hbar}\left\langle{\rm Tr}\left(\hat{\mathcal{P}}L\right)\right\rangle_W \tag{5.15}$$

$$\frac{d\langle N\rangle_W}{dt} = \frac{2\gamma}{\hbar}\langle\mu-L\rangle_W + \frac{2\gamma k_BT}{\hbar}{\rm Tr}\left(\hat{\mathcal{P}}\right) \tag{5.16}$$

where the corrective projector terms are

$$Q_A = \frac{1}{\hbar}2{\rm Im}\left\{\langle F_A\rangle_W\right\} + \frac{\gamma}{\hbar}{\rm Re}\left\{\langle F_A\rangle_W\right\} \tag{5.17}$$

with

$$F_A\psi(\mathbf{r}) \equiv \left(\delta V(\mathbf{r},t) + g|\psi(\mathbf{r})|^2\right)\mathcal{Q}\left\{A\psi(\mathbf{r})\right\} \tag{5.18}$$

for $A \in \{\mathbf{r}, \mathbf{p}, \mathbf{l}\}$. The angled brackets again represent the expectation of the operator over the field (5.6), while the subscript W indicates that the Wigner ensemble average has also been taken. With the exception of the nonlinear part in (5.15), the trace terms are given by

$$\mathrm{Tr}\left(\hat{\mathcal{P}}\hat{A}\right) = \sum_{n\in\mathbf{C}} \int d^3\mathbf{r}\phi_n^*(\mathbf{r})\hat{A}\phi_n(\mathbf{r}). \tag{5.19}$$

The nonlinear part in (5.15) is

$$\left\langle \mathrm{Tr}\left(\hat{\mathcal{P}}g|\psi(\mathbf{r})|^2\right)\right\rangle_W = g\int d^3\mathbf{r}\langle\psi^*(\mathbf{r})\psi(\mathbf{r})\rangle_W\delta(\mathbf{r},\mathbf{r}), \tag{5.20}$$

which has a well-defined value in the projected theory. If we take the non-projected limit ($\epsilon_{\mathrm{cut}} \to \infty$) then an ultraviolet divergence arises due to the $\delta(0)$. It is apparent that the value of these trace terms is dependent on the single-particle basis being used.

5.3 Ito change of variables

In this section we show how we can obtain a stochastic differential equation of motion for an arbitrary matter wave moment from the SPGPE. This is done by extending the Ito change of variables method to projected functional calculus. In order to use this method, we must first recast the SPGPE into the Ito form, rather than the usual Stratonovich form. This requires a revisit to the Fokker-Planck equation for the Wigner quasi-probability distribution, and a reordering of projected functional derivatives before again mapping the Fokker-Planck equation to an equivalent stochastic differential equation for the classical field.

5.3.1 Ito stochastic projected Gross-Pitaevskii equation

Recall that the stochastic projected Gross-Pitaevskii equation (SPGPE) is a stochastic differential equation (SDE) in Stratonovich form

$$\begin{aligned}(\mathbf{S})\, d\psi(\mathbf{r},t) = \mathcal{P}\Big\{ &-\frac{i}{\hbar}(1-i\gamma)(L-\mu)\psi(\mathbf{r},t)dt \\ &-\frac{i}{\hbar}V_\varepsilon(\mathbf{r},t)\psi(\mathbf{r},t)dt + dW(\mathbf{r},t) + i\psi(\mathbf{r},t)dU(\mathbf{r},t)\Big\}\end{aligned} \tag{5.21}$$

that is given by a mapping from the Fokker-Planck equation (FPE)

$$\begin{aligned}\frac{\partial W[\psi,\psi^*]}{\partial t} &= \int d^3\mathbf{r}\left[-\frac{\bar{\delta}}{\bar{\delta}\psi(\mathbf{r})}\left(-\frac{i}{\hbar}\left(1-i\gamma\right)\left(L-\mu\right)\psi(\mathbf{r},t)\right)+\text{h.c.}\right]W[\psi,\psi^*]\\ &+\int d^3\mathbf{r}\left[-\frac{\bar{\delta}}{\bar{\delta}\psi(\mathbf{r})}\left(-\frac{i}{\hbar}V_\varepsilon(\mathbf{r},t)\psi(\mathbf{r},t)\right)+\text{h.c.}\right]W[\psi,\psi^*]\\ &+\frac{\gamma k_B T}{\hbar}\int d^3\mathbf{r}\left[\frac{\bar{\delta}^{(2)}}{\bar{\delta}\psi(\mathbf{r})\bar{\delta}\psi^*(\mathbf{r})}+\text{h.c.}\right]W[\psi,\psi^*]\\ &+\frac{k_B T}{\hbar}\int d^3\mathbf{r}\int d^3\mathbf{r}'\varepsilon(\mathbf{r}-\mathbf{r}')\left[\frac{\bar{\delta}}{\bar{\delta}\psi(\mathbf{r})}\psi(\mathbf{r})\frac{\bar{\delta}}{\bar{\delta}\psi^*(\mathbf{r}')}\psi^*(\mathbf{r}')+\text{h.c.}\right]W[\psi,\psi^*]\\ &-\frac{k_B T}{\hbar}\int d^3\mathbf{r}\int d^3\mathbf{r}'\varepsilon(\mathbf{r}-\mathbf{r}')\left[\frac{\bar{\delta}}{\bar{\delta}\psi(\mathbf{r})}\psi(\mathbf{r})\frac{\bar{\delta}}{\bar{\delta}\psi(\mathbf{r}')}\psi(\mathbf{r}')+\text{h.c.}\right]W[\psi,\psi^*].\end{aligned} \tag{5.22}$$

The projector restricts the evolution to the coherent region consisting of the M single-particle modes with energy less than the cutoff ϵ_{cut}. Given a functional $A[\psi,\psi^*,t]$ of the field ψ we can find an equivalent SDE for the functional using Ito's formula [272], however this requires that the original SDE is in Ito form rather than Stratonovich form. The SPGPE being in Stratonovich form is a consequence of the mixed ordering of functional derivatives and fields in the latter two lines of (5.22). To map to an SDE in the Ito form, these must be altered such that all instances of functional derivatives precede any instances of the field. Using

$$\psi(\mathbf{r})\frac{\bar{\delta}}{\bar{\delta}\psi(\mathbf{r}')}\psi(\mathbf{r}')W[\psi,\psi^*]=\frac{\bar{\delta}}{\bar{\delta}\psi(\mathbf{r}')}\psi(\mathbf{r})\psi(\mathbf{r}')W[\psi,\psi^*]-\delta(\mathbf{r},\mathbf{r}')\psi(\mathbf{r}')W[\psi,\psi^*], \tag{5.23}$$

allows us to manipulate the FPE (5.22) such that the functional derivatives and fields are in the desired order, leading to

$$\begin{aligned}\frac{\partial W[\psi,\psi^*]}{\partial t} &= \int d^3\mathbf{r}\left[-\frac{\bar{\delta}}{\bar{\delta}\psi(\mathbf{r})}\left(-\frac{i}{\hbar}\left(1-i\gamma\right)\left(L-\mu\right)\psi(\mathbf{r},t)-\frac{i}{\hbar}V_\varepsilon(\mathbf{r},t)\psi(\mathbf{r},t)\right.\right.\\ &\left.\left.-\frac{k_BT}{\hbar}\int d^3\mathbf{r}'\varepsilon(\mathbf{r}-\mathbf{r}')\delta(\mathbf{r},\mathbf{r}')\psi(\mathbf{r}')\right)+\text{h.c.}\right]W[\psi,\psi^*]\\ &+\frac{\gamma k_BT}{\hbar}\int d^3\mathbf{r}\left[\frac{\bar{\delta}^{(2)}}{\bar{\delta}\psi(\mathbf{r})\bar{\delta}\psi^*(\mathbf{r})}+\text{h.c.}\right]W[\psi,\psi^*]\\ &+\frac{k_BT}{\hbar}\int d^3\mathbf{r}\int d^3\mathbf{r}'\varepsilon(\mathbf{r}-\mathbf{r}')\left[\frac{\bar{\delta}^{(2)}}{\bar{\delta}\psi(\mathbf{r})\bar{\delta}\psi^*(\mathbf{r}')}\psi(\mathbf{r})\psi^*(\mathbf{r}')+\text{h.c.}\right]W[\psi,\psi^*]\\ &-\frac{k_BT}{\hbar}\int d^3\mathbf{r}\int d^3\mathbf{r}'\varepsilon(\mathbf{r}-\mathbf{r}')\left[\frac{\bar{\delta}^{(2)}}{\bar{\delta}\psi(\mathbf{r})\bar{\delta}\psi^*(\mathbf{r}')}\psi(\mathbf{r})\psi(\mathbf{r}')+\text{h.c.},\right]W[\psi,\psi^*]\end{aligned} \tag{5.24}$$

where the Stratonovich correction is given in the second line. The Ito form[1] of the SPGPE is thus

$$\begin{aligned}(\mathbf{I})d\psi(\mathbf{r},t) &= \mathcal{P}\left\{-\frac{i}{\hbar}\left(1-i\gamma\right)\left(L-\mu\right)\psi(\mathbf{r},t)dt-\frac{i}{\hbar}V_\varepsilon(\mathbf{r},t)\psi(\mathbf{r},t)dt\right.\\ &\left.-\frac{k_BT}{\hbar}\int d^3\mathbf{r}'\varepsilon(\mathbf{r}-\mathbf{r}')\delta(\mathbf{r},\mathbf{r}')\psi(\mathbf{r}')dt+dW(\mathbf{r},t)+i\psi(\mathbf{r},t)dU(\mathbf{r},t)\right\}.\end{aligned} \tag{5.25}$$

The change in form has resulted in a correction in the deterministic part of the SPGPE, which we refer to as the *Stratonovich correction*

$$d\psi_S(\mathbf{r},t)=-\frac{k_BT}{\hbar}\mathcal{P}\left\{\int d^3\mathbf{r}'\varepsilon(\mathbf{r}-\mathbf{r}')\delta(\mathbf{r},\mathbf{r}')\psi(\mathbf{r}')\right\}dt. \tag{5.26}$$

5.3.2 Ito change of variables

Consider an n-dimensional vector $\mathbf{x}(t)$ satisfying the (Ito) stochastic differential equation

$$(\mathbf{I})d\mathbf{x}(t)=\boldsymbol{\mathcal{A}}(\mathbf{x},t)dt+\boldsymbol{\mathcal{B}}(\mathbf{x},t)d\mathbf{W}(t), \tag{5.27}$$

[1] We denote this by the inclusion of (**I**).

where $\mathbf{x}(t)$, the $n \times n$ drift matrix $\boldsymbol{\mathcal{A}}(\mathbf{x},t)$, the $n \times m$ diffusion matrix $\boldsymbol{\mathcal{B}}(\mathbf{x},t)$, and the m-dimensional noise vector $d\mathbf{W}(t)$ are all real-valued[2]. The stochastic differential equation describing an arbitrary function of $\mathbf{x}(t)$, $f[\mathbf{x}(t)]$, is given by Ito's formula for change of variables, obtained by expanding $df[\mathbf{x}(t)]$ to second order in $d\mathbf{W}(t)$ and retaining only terms of order dt. The resulting stochastic differential equation is

$$\begin{aligned}(\mathbf{I})df[\mathbf{x}(t)] &= \left\{\sum_i \mathcal{A}_i(\mathbf{x},t)\partial_i f[\mathbf{x}(t)] + \frac{1}{2}\sum_{i,j}\left[\boldsymbol{\mathcal{B}}(\mathbf{x},t)\boldsymbol{\mathcal{B}}(\mathbf{x},t)^T\right]_{ij}\partial_i\partial_j f[\mathbf{x}(t)]\right\}dt \\ &\quad + \sum_{i,j}\mathcal{B}_{ij}(\mathbf{x},t)\partial_i f[\mathbf{x}(t)]dW_j(t). \end{aligned} \tag{5.28}$$

The extension of this to the Ito SPGPE is an application of functional calculus. Consider a functional $A[\psi,\psi^*,t]$ of the complex field ψ, and recall the definition of the projected functional derivatives (3.128) and (3.129). The change of variables formula is then

$$\begin{aligned}(\mathbf{I})dA[\psi,\psi^*,t] &= \frac{\partial A[\psi,\psi^*,t]}{\partial t}dt + \int d^3\mathbf{r}\left[\frac{\bar{\delta}A[\psi,\psi^*,t]}{\bar{\delta}\psi(\mathbf{r})}(I)d\psi(\mathbf{r}) + \text{h.c.}\right] \\ &\quad + \int d^3\mathbf{r}\int d^3\mathbf{r}'\left[\frac{\bar{\delta}^{(2)}A[\psi,\psi^*,t]}{\bar{\delta}\psi^*(\mathbf{r}')\bar{\delta}\psi(\mathbf{r})}\delta(\mathbf{r},\mathbf{r}') + \text{h.c.}\right]\frac{\gamma k_B T}{\hbar}dt \\ &\quad + \int d^3\mathbf{r}\int d^3\mathbf{r}'\varepsilon(\mathbf{r}-\mathbf{r}')\left[\frac{\bar{\delta}^{(2)}A[\psi,\psi^*,t]}{\bar{\delta}\psi(\mathbf{r})\bar{\delta}\psi^*(\mathbf{r}')}\psi(\mathbf{r})\psi^*(\mathbf{r}') + \text{h.c.}\right]\frac{k_B T}{\hbar}dt \\ &\quad - \int d^3\mathbf{r}\int d^3\mathbf{r}'\varepsilon(\mathbf{r}-\mathbf{r}')\left[\frac{\bar{\delta}^{(2)}A[\psi,\psi^*,t]}{\bar{\delta}\psi(\mathbf{r})\bar{\delta}\psi(\mathbf{r}')}\psi(\mathbf{r})\psi(\mathbf{r}') + \text{h.c.}\right]\frac{k_B T}{\hbar}dt, \end{aligned} \tag{5.29}$$

with $(\mathbf{I})d\psi(\mathbf{r})$ the Ito form of the SPGPE (5.25).

Equation (5.29) expresses the Ito change of variables for projected functional calculus applied to the SPGPE. In the next section we apply this general statement to obtain stochastic equations of motion for moments of the stochastic matter wave field.

5.4 Stochastic Ehrenfest relations

In this section we derive equations of motion for moments of the classical field by evaluating (5.29), which we refer to as stochastic Ehrenfest relations. We first consider the most general case, making no assumptions about the nature of the moment. We then consider

[2]The dimensionality of the vector $\mathbf{x}$ and the noise vector $d\mathbf{W}(t)$ need not be the same.

the simpler, but still significant, case of one-body operators. In this case the connection between these equations and the usual statement of the Ehrenfest relations becomes clear. We finish by explicitly showing the stochastic Ehrenfest relations for several commonly considered moments of the classical field.

5.4.1 General matter wave moment

Evaluating (5.29) gives

$$\begin{aligned}(\mathbf{I})dA[\psi,\psi^*,t] \;=\; & \frac{\partial A[\psi,\psi^*,t]}{\partial t}dt+\frac{2}{\hbar}\mathrm{Im}\left\{\int d^3\mathbf{r}\frac{\bar{\delta}A[\psi,\psi^*,t]}{\bar{\delta}\psi(\mathbf{r})}(L-\mu)\psi(\mathbf{r})\right\}dt\\
&-\frac{2\gamma}{\hbar}\mathrm{Re}\left\{\int d^3\mathbf{r}\frac{\bar{\delta}A[\psi,\psi^*,t]}{\bar{\delta}\psi(\mathbf{r})}(L-\mu)\psi(\mathbf{r})\right\}dt\\
&-2\mathcal{M}\int d^3\mathbf{k}k^{-1}\mathcal{F}\left[\mathrm{Im}\left\{\frac{\bar{\delta}A[\psi,\psi^*,t]}{\bar{\delta}\psi(\mathbf{r})}\psi(\mathbf{r})\right\}\right]^*\mathcal{F}\left[\nabla\cdot\mathbf{j}(\mathbf{r})\right]dt\\
&+dW_\gamma^A(t)+dW_\varepsilon^A(t)\\
&+\frac{\gamma k_BT}{\hbar}\int d^3\mathbf{r}\left\{\frac{\bar{\delta}^{(2)}A[\psi,\psi^*,t]}{\bar{\delta}\psi^*(\mathbf{r})\bar{\delta}\psi(\mathbf{r})}+\mathrm{h.c.}\right\}dt\\
&-\frac{k_BT}{\hbar}\int d^3\mathbf{r}\int d^3\mathbf{r}'\left[\frac{\bar{\delta}A[\psi,\psi^*,t]}{\bar{\delta}\psi(\mathbf{r})}\delta(\mathbf{r},\mathbf{r}')\psi(\mathbf{r}')+\mathrm{h.c.}\right]\varepsilon(\mathbf{r}-\mathbf{r}')dt\\
&+\frac{k_BT}{\hbar}\int d^3\mathbf{r}\int d^3\mathbf{r}'\left[\frac{\bar{\delta}^{(2)}A[\psi,\psi^*,t]}{\bar{\delta}\psi^*(\mathbf{r}')\bar{\delta}\psi(\mathbf{r})}\psi^*(\mathbf{r}')\psi(\mathbf{r})+\mathrm{h.c.}\right]\varepsilon(\mathbf{r}-\mathbf{r}')dt\\
&-\frac{k_BT}{\hbar}\int d^3\mathbf{r}\int d^3\mathbf{r}'\left[\frac{\bar{\delta}^{(2)}A[\psi,\psi^*,t]}{\bar{\delta}\psi(\mathbf{r}')\bar{\delta}\psi(\mathbf{r})}\psi(\mathbf{r}')\psi(\mathbf{r})+\mathrm{h.c.}\right]\varepsilon(\mathbf{r}-\mathbf{r}')dt.\end{aligned} \tag{5.30}$$

The two noises are independent

$$\langle dW_\gamma^A(t)dW_\varepsilon^A(t)\rangle\equiv 0 \tag{5.31}$$

with correlations

$$\langle dW_\gamma^A(t)dW_\gamma^A(t)\rangle\equiv\frac{4\gamma k_BT}{\hbar}\mathrm{Re}\left\{\int d^3\mathbf{r}\int d^3\mathbf{r}'\frac{\bar{\delta}A[\psi,\psi^*,t]}{\bar{\delta}\psi(\mathbf{r})}\frac{\bar{\delta}A[\psi,\psi^*,t]}{\bar{\delta}\psi^*(\mathbf{r}')}\delta(\mathbf{r},\mathbf{r}')\right\}dt, \tag{5.32}$$

$$\langle dW_\varepsilon^A(t)dW_\varepsilon^A(t)\rangle\equiv\frac{8\mathcal{M}k_BT}{\hbar}\int d^3\mathbf{k}\,k^{-1}\left|\mathcal{F}\left[\mathrm{Im}\left\{\frac{\bar{\delta}A[\psi,\psi^*,t]}{\bar{\delta}\psi(\mathbf{r})}\psi(\mathbf{r})\right\}\right]\right|^2dt. \tag{5.33}$$

It will be useful to rewrite this as an equation of motion with regular functional derivatives and cutoff terms due to the projector. To this end, we use the identity

$$\frac{\bar{\delta}A}{\bar{\delta}\psi(\mathbf{r})} = \frac{\delta A}{\delta\psi(\mathbf{r})} - \int d^3\mathbf{u}\langle\mathbf{u}|\hat{\mathcal{Q}}|\mathbf{r}\rangle\frac{\delta A}{\delta\psi(\mathbf{u})}. \tag{5.34}$$

The equation of motion is then

$$\begin{aligned}
(\mathbf{I})dA[\psi,\psi^*,t] &= \frac{\partial A[\psi,\psi^*,t]}{\partial t}dt + \frac{2}{\hbar}\mathrm{Im}\left\{\int d^3\mathbf{r}\frac{\delta A[\psi,\psi^*,t]}{\delta\psi(\mathbf{r})}(L-\mu)\psi(\mathbf{r})\right\}dt + Q_A^H \\
&\quad -\frac{2\gamma}{\hbar}\mathrm{Re}\left\{\int d^3\mathbf{r}\frac{\delta A[\psi,\psi^*,t]}{\delta\psi(\mathbf{r})}(L-\mu)\psi(\mathbf{r})\right\}dt + Q_A^\gamma \\
&\quad -2\mathcal{M}\int d^3\mathbf{k}\, k^{-1}\mathcal{F}\left[\mathrm{Im}\left\{\frac{\delta A[\psi,\psi^*,t]}{\delta\psi^*(\mathbf{r})}\psi^*(\mathbf{r})\right\}\right]^*\mathcal{F}\left[\nabla\cdot\mathbf{j}(\mathbf{r})\right]dt + Q_A^\varepsilon \\
&\quad +dW_\gamma^A(t) + dW_\varepsilon^A(t) \\
&\quad +\frac{2\gamma k_B T}{\hbar}\mathrm{Re}\left\{\int d^3\mathbf{r}\int d^3\mathbf{u}\;\delta(\mathbf{u},\mathbf{r})\frac{\delta^{(2)}A[\psi,\psi^*,t]}{\delta\psi^*(\mathbf{r})\delta\psi(\mathbf{u})}\right\}dt + T_A^\varepsilon,
\end{aligned} \tag{5.35}$$

where the noise correlations are

$$\langle dW_\gamma^A(t)dW_\gamma^A(t)\rangle = \left(\frac{4\gamma k_B T}{\hbar}\int d^3\mathbf{r}\left|\frac{\delta A[\psi,\psi^*,t]}{\delta\psi(\mathbf{r})}\right|^2 + D_A^\gamma\right)dt, \tag{5.36}$$

$$\langle dW_\varepsilon^A(t)dW_\varepsilon^A(t)\rangle = \left(\frac{8\mathcal{M}k_B T}{\hbar}\int d^3\mathbf{k}\, k^{-1}\left|\mathcal{F}\left[\mathrm{Im}\left\{\frac{\delta A[\psi,\psi^*,t]}{\delta\psi(\mathbf{r})}\psi(\mathbf{r})\right\}\right]\right|^2 + D_A^\varepsilon\right)dt, \tag{5.37}$$

and we have defined the Hamiltonian, number-damping, and energy-damping drift cutoff terms

$$Q_A^H = -\frac{2}{\hbar}\mathrm{Im}\left\{\int d^3\mathbf{r}\int d^3\mathbf{u}\langle\mathbf{u}|\hat{\mathcal{Q}}|\mathbf{r}\rangle\frac{\delta A[\psi,\psi^*,t]}{\delta\psi(\mathbf{u})}\left(gn(\mathbf{r})+\delta V(\mathbf{r},t)\right)\psi(\mathbf{r})\right\}dt \tag{5.38}$$

$$Q_A^\gamma = \frac{2\gamma}{\hbar}\mathrm{Re}\left\{\int d^3\mathbf{r}\int d^3\mathbf{u}\langle\mathbf{u}|\hat{\mathcal{Q}}|\mathbf{r}\rangle\frac{\delta A[\psi,\psi^*,t]}{\delta\psi(\mathbf{u})}\left(gn(\mathbf{r})+\delta V(\mathbf{r},t)\right)\psi(\mathbf{r})\right\}dt \tag{5.39}$$

$$Q_A^\varepsilon = 2\mathcal{M}\int d^3\mathbf{k}\, k^{-1}\mathcal{F}\left[\mathrm{Im}\left\{\int d^3\mathbf{u}\langle\mathbf{u}|\hat{\mathcal{Q}}|\mathbf{r}\rangle\frac{\delta A[\psi,\psi^*,t]}{\delta\psi(\mathbf{u})}\psi(\mathbf{r})\right\}\right]^*\mathcal{F}\left[\nabla\cdot\mathbf{j}(\mathbf{r})\right]dt, \tag{5.40}$$

the number-damping, and energy-damping diffusion cutoff terms

$$D_A^{\gamma} = -\frac{4\gamma k_B T}{\hbar}\mathrm{Re}\left\{\int d^3\mathbf{r}\int d^3\mathbf{u}\langle\mathbf{u}|\hat{\mathcal{Q}}|\mathbf{r}\rangle\frac{\delta A[\psi,\psi^*,t]}{\delta\psi(\mathbf{u})}\frac{\delta A[\psi,\psi^*,t]}{\delta\psi^*(\mathbf{r})}\right\} \tag{5.41}$$

$$\begin{aligned} D_A^{\varepsilon} = {} & \frac{8\mathcal{M}k_B T}{\hbar}\int d^3\mathbf{k}\,k^{-1}\Bigg(\left|\mathcal{F}\left[\mathrm{Im}\left\{\int d^3\mathbf{u}\langle\mathbf{u}|\hat{\mathcal{Q}}|\mathbf{r}\rangle\frac{\delta A[\psi,\psi^*,t]}{\delta\psi(\mathbf{u})}\psi(\mathbf{r})\right\}\right]\right|^2 \\ & -2\mathrm{Re}\left\{\mathcal{F}\left[\mathrm{Im}\left\{\int d^3\mathbf{u}\langle\mathbf{u}|\hat{\mathcal{Q}}|\mathbf{r}\rangle\frac{\delta A[\psi,\psi^*,t]}{\delta\psi(\mathbf{u})}\psi(\mathbf{r})\right\}\right]\mathcal{F}\left[\mathrm{Im}\frac{\delta A[\psi,\psi^*,t]}{\delta\psi(\mathbf{r})}\psi(\mathbf{r})\right]^*\right\}\Bigg), \end{aligned} \tag{5.42}$$

and the epsilon term

$$\begin{aligned} T_A^{\varepsilon} = {} & -\frac{k_B T}{\hbar}\int d^3\mathbf{r}\int d^3\mathbf{r}'\left[\frac{\bar{\delta}A[\psi,\psi^*,t]}{\bar{\delta}\psi(\mathbf{r})}\delta(\mathbf{r},\mathbf{r}')\psi(\mathbf{r}')+\mathrm{h.c.}\right]\varepsilon(\mathbf{r}-\mathbf{r}')dt \\ & +\frac{k_B T}{\hbar}\int d^3\mathbf{r}\int d^3\mathbf{r}'\left[\frac{\bar{\delta}^{(2)}A[\psi,\psi^*,t]}{\bar{\delta}\psi^*(\mathbf{r}')\bar{\delta}\psi(\mathbf{r})}\psi^*(\mathbf{r}')\psi(\mathbf{r})+\mathrm{h.c.}\right]\varepsilon(\mathbf{r}-\mathbf{r}')dt \\ & -\frac{k_B T}{\hbar}\int d^3\mathbf{r}\int d^3\mathbf{r}'\left[\frac{\bar{\delta}^{(2)}A[\psi,\psi^*,t]}{\bar{\delta}\psi(\mathbf{r}')\bar{\delta}\psi(\mathbf{r})}\psi(\mathbf{r}')\psi(\mathbf{r})+\mathrm{h.c.}\right]\varepsilon(\mathbf{r}-\mathbf{r}')dt. \end{aligned} \tag{5.43}$$

The number-damping and energy-damping each have a corresponding drift, diffusion, and trace[3] term.

5.4.2 One-body operators

With knowledge of a particular matter wave moment, we can use (5.42) to obtain the corresponding stochastic equation of motion. However, we can obtain a simpler form if we restrict our attention to one-body operators, which is a restriction that still includes a number of useful moments and is thus a useful restriction with some practical advantages. Consider a moment that is the expectation of a one-body operator

$$A[\psi,\psi^*,t] = \langle\psi|\hat{A}|\psi\rangle = \int d^3\mathbf{r}\langle\psi|\hat{A}|\mathbf{r}\rangle\psi(\mathbf{r}), \tag{5.44}$$

[3]We refer to dA^{ε} loosely as the energy-damping trace term, despite the fact it is not strictly a trace; it is the energy-damping counterpart to the number-damping trace term, which is a true trace.

where the operator $\hat{A}$ is independent of ψ, ψ^*. The non-zero projected functional derivatives are

$$\frac{\bar{\delta}A[\psi,\psi^*,t]}{\bar{\delta}\psi(\mathbf{r})} = \langle\psi|\hat{\mathcal{P}}\hat{A}\hat{\mathcal{P}}|\mathbf{r}\rangle = \frac{\delta A_{\mathcal{P}}[\psi,\psi^*,t]}{\delta\psi(\mathbf{r})}, \tag{5.45}$$

$$\frac{\bar{\delta}^{(2)}A[\psi,\psi^*,t]}{\bar{\delta}\psi^*(\mathbf{r}')\bar{\delta}\psi(\mathbf{r})} = \langle\mathbf{r}'|\hat{\mathcal{P}}\hat{A}\hat{\mathcal{P}}|\mathbf{r}\rangle = \frac{\delta^{(2)}A_{\mathcal{P}}[\psi,\psi^*,t]}{\delta\psi^*(\mathbf{r}')\delta\psi(\mathbf{r})}, \tag{5.46}$$

where we have defined the *totally projected operator* $\hat{A}_{\mathcal{P}} \equiv \hat{\mathcal{P}}\hat{A}\hat{\mathcal{P}}$. Importantly, for such operators the projected functional derivatives corresponding to the operator $\hat{A}$ are equivalent to the regular functional derivatives of the totally projected operator $\hat{A}_{\mathcal{P}}$; this makes the equation of motion simple to construct. The SDE of the moment A is

$$\begin{aligned}
(\mathbf{I})dA(t) = &\left\langle\frac{\partial\hat{A}_{\mathcal{P}}}{\partial t}\right\rangle dt + \frac{1}{i\hbar}\left\langle\left[\hat{A}_{\mathcal{P}},\hat{H}_{\mathrm{sp}}\right]\right\rangle dt \\
&+\frac{2}{\hbar}\mathrm{Im}\left\{\int d^3\mathbf{r}\langle\psi|\hat{A}_{\mathcal{P}}|\mathbf{r}\rangle(gn(\mathbf{r})+\delta V(\mathbf{r},t))\psi(\mathbf{r})\right\}dt \\
&-\frac{2\gamma}{\hbar}\mathrm{Re}\left\{\int d^3\mathbf{r}\langle\psi|\hat{A}_{\mathcal{P}}|\mathbf{r}\rangle(L-\mu)\psi(\mathbf{r})\right\}dt + \frac{2\gamma k_BT}{\hbar}\mathrm{Tr}\left(\hat{A}_{\mathcal{P}}\right)dt \\
&-2\mathcal{M}\int d^3\mathbf{k}\,k^{-1}\mathcal{F}\left[\mathrm{Im}\left\{\langle\psi|\hat{A}_{\mathcal{P}}|\mathbf{r}\rangle\psi(\mathbf{r})\right\}\right]^*\mathcal{F}\left[\nabla\cdot\mathbf{j}(\mathbf{r})\right]dt + T_A^{\varepsilon} \\
&+dW_{\gamma}^{A}(t) + dW_{\varepsilon}^{A}(t)
\end{aligned} \tag{5.47}$$

where the noise correlations are

$$\langle dW_{\gamma}^{A}(t)dW_{\gamma}^{A}(t)\rangle = \frac{4\gamma k_BT}{\hbar}\left\langle\hat{A}_{\mathcal{P}}^2\right\rangle dt, \tag{5.48}$$

$$\langle dW_{\varepsilon}^{A}(t)dW_{\varepsilon}^{A}(t)\rangle = \frac{8\mathcal{M}k_BT}{\hbar}\int d^3\mathbf{k}\,k^{-1}\left|\mathcal{F}\left[\mathrm{Im}\left\{\langle\psi|\hat{A}_{\mathcal{P}}|\mathbf{r}\rangle\psi(\mathbf{r})\right\}\right]\right|^2 dt, \tag{5.49}$$

and the epsilon term is

$$\begin{aligned}
T_A^{\varepsilon} = &-\frac{k_BT}{\hbar}\int d^3\mathbf{r}\int d^3\mathbf{r}'\left[\delta(\mathbf{r},\mathbf{r}')\psi(\mathbf{r}')\langle\psi|\hat{A}_{\mathcal{P}}|\mathbf{r}\rangle + \mathrm{h.c.}\right]\varepsilon(\mathbf{r}-\mathbf{r}')dt \\
&+\frac{k_BT}{\hbar}\int d^3\mathbf{r}\int d^3\mathbf{r}'\left[\langle\mathbf{r}|\hat{A}_{\mathcal{P}}|\mathbf{r}'\rangle\psi(\mathbf{r}')\psi^*(\mathbf{r}) + \mathrm{h.c.}\right]\varepsilon(\mathbf{r}-\mathbf{r}')dt.
\end{aligned} \tag{5.50}$$

As with (5.30), it will be useful to rewrite this as an equation of motion where the effect of the projectors are more explicit. To this end, we use that $\hat{\mathcal{P}} \equiv 1 - \hat{\mathcal{Q}}$, so the SDE of the

moment A can then be written as

$$\begin{aligned}(\mathbf{I})dA(t) &= \left\langle \frac{\partial \hat{A}}{\partial t} \right\rangle dt + \frac{1}{i\hbar}\left\langle \left[\hat{A}, \hat{H}_{\rm sp}\right] \right\rangle dt \\ &+\frac{2}{\hbar}{\rm Im}\left\{ \int d^3\mathbf{r} \langle\psi|\hat{A}|\mathbf{r}\rangle (gn(\mathbf{r}) + \delta V(\mathbf{r},t))\psi(\mathbf{r}) \right\} dt \\ &-\frac{2\gamma}{\hbar}{\rm Re}\left\{ \int d^3\mathbf{r} \langle\psi|\hat{A}|\mathbf{r}\rangle (L-\mu)\psi(\mathbf{r}) \right\} dt + \frac{2\gamma k_B T}{\hbar}{\rm Tr}\left(\hat{A}\hat{\mathcal{P}}\right) dt \\ &-2\mathcal{M}\int d^3\mathbf{k}\, k^{-1} \mathcal{F}\left[{\rm Im}\left\{ \langle\psi|\hat{A}|\mathbf{r}\rangle\psi(\mathbf{r}) \right\} \right]^* \mathcal{F}\left[\nabla\cdot\mathbf{j}(\mathbf{r})\right] dt \\ &+dW_\gamma^A(t) + dW_\varepsilon^A(t) \\ &+T_A^\varepsilon + Q_A^H + Q_A^\gamma + Q_A^\varepsilon \end{aligned} \tag{5.51}$$

where the noise correlations are

$$\langle dW_\gamma^A(t) dW_\gamma^A(t)\rangle = \left(\frac{4\gamma k_B T}{\hbar}\left\langle \hat{A}^2 \right\rangle + D_A^\gamma \right) dt, \tag{5.52}$$

$$\langle dW_\varepsilon^A(t) dW_\varepsilon^A(t)\rangle = \left(\frac{8\mathcal{M}k_B T}{\hbar}\int d^3\mathbf{k}\, k^{-1} \left| \mathcal{F}\left[{\rm Im}\left\{ \langle\psi|\hat{A}|\mathbf{r}\rangle\psi(\mathbf{r}) \right\} \right] \right|^2 + D_A^\varepsilon \right) dt, \tag{5.53}$$

the Hamiltonian, number-damping, and energy-damping drift cutoff terms are now given by

$$Q_A^H = -\frac{2}{\hbar}{\rm Im}\left\{ \int d^3\mathbf{r} \langle\psi|\hat{A}\hat{\mathcal{Q}}|\mathbf{r}\rangle (gn(\mathbf{r}) + \delta V(\mathbf{r},t))\psi(\mathbf{r}) \right\} dt \tag{5.54}$$

$$Q_A^\gamma = \frac{2\gamma}{\hbar}{\rm Re}\left\{ \int d^3\mathbf{r} \langle\psi|\hat{A}\hat{\mathcal{Q}}|\mathbf{r}\rangle (gn(\mathbf{r}) + \delta V(\mathbf{r},t))\psi(\mathbf{r}) \right\} dt \tag{5.55}$$

$$Q_A^\varepsilon = 2\mathcal{M}\int d^3\mathbf{k}\, k^{-1} \mathcal{F}\left[{\rm Im}\left\{ \langle\psi|\hat{A}\hat{\mathcal{Q}}|\mathbf{r}\rangle\psi(\mathbf{r}) \right\} \right]^* \mathcal{F}\left[\nabla\cdot\mathbf{j}(\mathbf{r})\right] dt \tag{5.56}$$

the number-damping and energy-damping diffusion cutoff terms are

$$D_A^\gamma = -\frac{4\gamma k_B T}{\hbar}\langle \hat{A}\hat{\mathcal{Q}}\hat{A}\rangle \tag{5.57}$$

$$D_A^\varepsilon = \frac{8\mathcal{M}k_B T}{\hbar}\int d^3\mathbf{k}\, k^{-1}\Bigg(\left|\mathcal{F}\left[\mathrm{Im}\langle\psi|\hat{A}\hat{\mathcal{Q}}|\mathbf{r}\rangle\psi(\mathbf{r})\right]\right|^2 - 2\mathrm{Re}\left\{\mathcal{F}\left[\mathrm{Im}\left\{\langle\psi|\hat{A}\hat{\mathcal{Q}}|\mathbf{r}\rangle\psi(\mathbf{r})\right\}\right]\mathcal{F}\left[\mathrm{Im}\left\{\langle\psi|\hat{A}|\mathbf{r}\rangle\psi(\mathbf{r})\right\}\right]^*\right\}\Bigg) \tag{5.58}$$

and the epsilon term is

$$T_A^\varepsilon = -\frac{k_B T}{\hbar}dt\int d^3\mathbf{r}\int d^3\mathbf{r}'\langle\psi|\hat{A}\hat{\mathcal{P}}|\mathbf{r}\rangle\delta(\mathbf{r},\mathbf{r}')\psi(\mathbf{r}')\varepsilon(\mathbf{r}-\mathbf{r}') + \mathrm{h.c.} + \frac{k_B T}{\hbar}dt\int d^3\mathbf{r}\int d^3\mathbf{r}'\langle\mathbf{r}|\hat{\mathcal{P}}\hat{A}\hat{\mathcal{P}}|\mathbf{r}'\rangle\psi^*(\mathbf{r})\psi(\mathbf{r}')\varepsilon(\mathbf{r}-\mathbf{r}') + \mathrm{h.c.}. \tag{5.59}$$

We have expressed (5.51) in a way that shows the presence of the commutator $[\hat{A}, \hat{H}_{\mathrm{sp}}]$ so as to make the connection between this equation and the general Ehrenfest theorem clear.

5.4.3 Noise correlations for multiple moments

When considering more than one moment, one must take care when considering the noise terms that arise. Let $B = B[\psi, \psi^*, t]$ be another moment of the SPGPE with evolution described by (5.30). The correlations between the noises corresponding to A and the noises corresponding to B are

$$\langle dW_\gamma^A(t) dW_\gamma^B(t)\rangle = \frac{4\gamma k_B T}{\hbar}\mathrm{Re}\int d^3\mathbf{r}\int d^3\mathbf{r}'\frac{\bar{\delta}A[\psi,\psi^*,t]}{\bar{\delta}\psi(\mathbf{r})}\frac{\bar{\delta}B[\psi,\psi^*,t]}{\bar{\delta}\psi^*(\mathbf{r}')}\delta(\mathbf{r},\mathbf{r}')dt \tag{5.60}$$

$$\langle dW_\varepsilon^A(t) dW_\varepsilon^B(t)\rangle = \frac{8\mathcal{M}k_B T}{\hbar}\int d^3\mathbf{k}\, k^{-1}\mathcal{F}\left[\mathrm{Im}\left\{\frac{\bar{\delta}A[\psi,\psi^*,t]}{\bar{\delta}\psi(\mathbf{r})}\psi(\mathbf{r},t)\right\}\right]^* \times\mathcal{F}\left[\mathrm{Im}\left\{\frac{\bar{\delta}B[\psi,\psi^*,t]}{\bar{\delta}\psi(\mathbf{r})}\psi(\mathbf{r},t)\right\}\right]dt \tag{5.61}$$

for number-damping and energy-damping respectively.

One-body operator

For moments that are the expectation of a one-body operator the correlations are

$$\langle dW_\gamma^A(t) dW_\gamma^B(t)\rangle = \frac{4\gamma k_B T}{\hbar}\mathrm{Re}\langle \hat{A}\hat{\mathcal{P}}\hat{B}\rangle dt \tag{5.62}$$

$$\langle dW_\varepsilon^A(t) dW_\varepsilon^B(t)\rangle = \frac{8\mathcal{M}k_B T}{\hbar}\int d^3\mathbf{k}\, k^{-1}\mathcal{F}\left[\mathrm{Im}\left\{\langle\psi|\hat{A}\hat{\mathcal{P}}|\mathbf{r}\rangle\psi(\mathbf{r},t)\right\}\right]^* \times\mathcal{F}\left[\mathrm{Im}\left\{\langle\psi|\hat{B}\hat{\mathcal{P}}|\mathbf{r}\rangle\psi(\mathbf{r},t)\right\}\right] dt \tag{5.63}$$

for number-damping and energy-damping respectively.

5.4.4 Stochastic Ehrenfest relations

Now that we have a general form of the stochastic Ehrenfest relations (5.59), we consider some useful special cases of operators. We consider the expectations of position $\mathbf{R} \equiv \langle\hat{\mathbf{r}}\rangle$, momentum $\mathbf{P} \equiv \langle\hat{\mathbf{p}}\rangle$, angular momentum $\mathbf{L} \equiv \langle\hat{\mathbf{l}}\rangle$, grand canonical energy $K \equiv E - \mu N$,

and coherent region particle number N. The equations of motion for these moments are

$$
\begin{aligned}
(\mathbf{I})dR_j(t) &= \frac{1}{m}P_j(t)dt - \frac{2\gamma}{\hbar}\mathrm{Re}\left\langle \hat{r}_j(L-\mu)\right\rangle dt + \frac{2\gamma k_B T}{\hbar}\mathrm{Tr}\left(\hat{r}_j\hat{\mathcal{P}}\right)dt \\
&\quad + dW_\gamma^{R_j}(t) + dW_\varepsilon^{R_j}(t) \\
&\quad + Q_{r_j}^H + Q_{r_j}^\gamma + Q_{r_j}^\varepsilon + T_{r_j}^\varepsilon + \sqrt{D_{r_j}^\varepsilon}dW_{j2}(t) \qquad (5.64) \\
(\mathbf{I})dP_j(t) &= -\left\langle \partial_j V(\mathbf{r},t)\right\rangle dt - \frac{2\gamma}{\hbar}\mathrm{Re}\left\langle \hat{p}_j(L-\mu)\right\rangle dt + \frac{2\gamma k_B T}{\hbar}\mathrm{Tr}\left(\hat{p}_j\hat{\mathcal{P}}\right)dt \\
&\quad - \hbar\mathcal{M}\int d^3\mathbf{k}\, k^{-1}\mathcal{F}\left[\partial_j n(\mathbf{r})\right]^*\mathcal{F}\left[\nabla\cdot\mathbf{j}(\mathbf{r})\right]dt \\
&\quad + dW_\gamma^{P_j}(t) + dW_\varepsilon^{P_j}(t) \\
&\quad + Q_{p_j}^H + Q_{p_j}^\gamma + Q_{p_j}^\varepsilon + T_{p_j}^\varepsilon \qquad (5.65) \\
(\mathbf{I})dL_j(t) &= -\left\langle \left(r_{j+1}\partial_{j-1} - r_{j-1}\partial_{j+1}\right)V(\mathbf{r},t)\right\rangle dt - \frac{2\gamma}{\hbar}\mathrm{Re}\left\langle \hat{l}_j(L-\mu)\right\rangle dt \\
&\quad + \frac{2\gamma k_B T}{\hbar}\mathrm{Tr}\left(\hat{l}_j\hat{\mathcal{P}}\right)dt \\
&\quad - \hbar\mathcal{M}\int d^3\mathbf{k}k^{-1}\mathcal{F}\left[\left(r_{j+1}\partial_{j-1} - r_{j-1}\partial_{j+1}\right)n(\mathbf{r})\right]^*\mathcal{F}\left[\nabla\cdot\mathbf{j}(\mathbf{r})\right]dt \\
&\quad + dW_\gamma^{L_j}(t) + dW_\varepsilon^{L_j}(t) \\
&\quad + Q_{l_j}^H + Q_{l_j}^\gamma + Q_{l_j}^\varepsilon + T_{l_j}^\varepsilon \qquad (5.66) \\
(\mathbf{I})dK(t) &= \left\langle \frac{\partial V(\mathbf{r},t)}{\partial t}\right\rangle dt - \frac{2\gamma}{\hbar}\mathrm{Re}\left\langle (L-\mu)^2\right\rangle dt + \frac{2\gamma k_B T}{\hbar}\mathrm{Tr}\left(\hat{\mathcal{P}}\,(L-\mu)\,\hat{\mathcal{P}}\right)dt \\
&\quad - \hbar\mathcal{M}\int d^3\mathbf{k}k^{-1}\left|\mathcal{F}\left[\nabla\cdot\mathbf{j}(\mathbf{r})\right]\right|^2 dt \\
&\quad + dW_\gamma^K(t) + dW_\varepsilon^K(t) \\
&\quad + Q_K^H + Q_K^\gamma + Q_K^\varepsilon + T_K^\varepsilon \qquad (5.67) \\
(\mathbf{I})dN(t) &= -\frac{2\gamma}{\hbar}\mathrm{Re}\langle(L-\mu)\rangle dt + \frac{2\gamma k_B T M}{\hbar}dt + dW_\gamma^N(t), \qquad (5.68)
\end{aligned}
$$

where M is the number of single-particle modes in the coherent region. These *stochastic Ehrenfest relations* are our main result[4]. The cutoff terms are all consistently accounted for, in general contributing additional damping and diffusion. However, provided the basis of projection is properly chosen, their effect is typically only a small correction. Testing whether such terms are negligible provides a useful consistency test for a well chosen cutoff. Neglecting energy-damping and averaging over the noise leads us back to the (non-

[4]Note in these equations we have used the index $j \in \{1,2,3\}$ to denote a general cartesian coordinate. This is cyclic, so e.g. if $j = 3$, then $j + 1 = 1$.

stochastic) Ehrenfest relations for the number-damped SPGPE as found in [281][5].

5.5 Cutoff terms

The terms given by (5.54)-(5.59) are collectively referred to as the *cutoff terms*, as they are explicitly dependent on the projector. Their presence greatly restricts any analytic progress being made using the stochastic Ehrenfest relations. Fortunately, in most cases these terms are small enough to be neglected. We provide an example of a system where neglecting these terms is valid: the centre of mass motion of a finite-temperature harmonically trapped quasi-1D system described using a Thomas-Fermi ansatz.

5.5.1 1D Thomas-Fermi ansatz

For the quasi-1D system we use the dimensionally reduced SPGPE [286]

$$(\mathbf{S})\, d\psi(x,t) = \mathcal{P}\Big\{ -\frac{i}{\hbar}\left(1-i\gamma\right)\left(L-\mu_1\right)\psi(x,t)dt \\ -\frac{i}{\hbar}V_\varepsilon(x,t)\psi(x,t)dt + dW(x,t) + i\psi(x,t)dU(x,t)\Big\}, \quad (5.69)$$

relating to a system with external trapping potential

$$V(\mathbf{r}) = \frac{1}{2}m\omega^2 x^2 + \frac{1}{2}m\omega_\perp^2\left(y^2+z^2\right) \quad (5.70)$$

where the transverse trapping is much tighter than the longitudinal trapping ($\omega_\perp \gg \omega$). The 1D SPGPE explicitly includes the 1D GPE operator

$$L\psi(x,t) = \left(-\frac{\hbar^2}{2m}\frac{\partial^2}{\partial x^2} + V(x) + g_1|\psi(x,t)|^2\right)\psi(x,t), \quad (5.71)$$

and the 1D effective energy damping potential

$$V_\varepsilon(x,t) = -\hbar\int dx'\varepsilon_1(x-x')\frac{\partial}{\partial x'}j(x',t), \quad (5.72)$$

[5] In [281] the energy equation is missing the projector correction.

defined in terms of the 1D probability current

$$j(x,t) = \frac{i\hbar}{2m}\left[\psi(x,t)\frac{\partial}{\partial x}\psi^*(x,t) - \psi^*(x,t)\frac{\partial}{\partial x}\psi(x,t)\right], \tag{5.73}$$

and the 1D epsilon function

$$\varepsilon(x) = \frac{\mathcal{M}}{2\pi}\int dk e^{ikx} S_1(k), \tag{5.74}$$

which itself is determined by the 1D scattering kernel

$$S_1(k) = \frac{1}{\sqrt{8\pi\sigma^2}} G\left(\frac{|k|\sigma}{\sqrt{2}}\right), \tag{5.75}$$

where $G(q) \equiv e^{q^2}\,\mathrm{erfc}(q)$ is the scaled complementary error function and $\sigma \equiv \sqrt{\hbar/(m\omega_\perp)}$ is the transverse harmonic oscillator length scale. Here we have the 1D interaction parameter $g_1 = 2\hbar\omega_\perp a_s$ and chemical potential $\mu_1 = \mu - \hbar\omega_\perp$. The transverse trapping is assumed to be strong enough that the transverse dynamics of the coherent region are suppressed, allowing an effective 1D representation to be found, but weak enough that the thermal cloud retains 3D characteristics. The reservoir interaction parameters $\mathcal{M}$ and γ are therefore unchanged from the 3D case. Further discussion on this point, and the low dimensional SPGPE in general, can be found in [286].

We use as an ansatz for the coherent region wave function the Thomas-Fermi state with variable centre of mass position and momentum

$$\psi(x) = \sqrt{\frac{\mu_1}{g_1}}\sqrt{1 - \frac{(x-x(t))^2}{R^2}}\exp\left[\frac{ip(t)x}{\hbar}\right] H\left(R - |x - x(t)|\right), \tag{5.76}$$

with $H(x)$ the Heaviside step function, $R = \sqrt{2\mu_1/m\omega^2}$ the Thomas-Fermi radius, ω the harmonic trapping frequency, $x(t)$ the centre of mass position, and $p(t)$ the centre of mass momentum. Useful quantities for comparing with numerics include the probability current

$$j(x,t) = \frac{\mu_1 p(t)}{g_1 m}\left(1 - \frac{(x-x(t))^2}{R^2}\right) H\left(R - |x - x(t)|\right), \tag{5.77}$$

its divergence

$$\partial_x j(x,t) = -\frac{2\mu_1 p(t)}{g_1 m}\frac{(x-x(t))}{R^2} H\left(R-|x-x(t)|\right), \tag{5.78}$$

and the Fourier transform of the divergence

$$\mathcal{F}\left[\frac{\partial}{\partial x} j(x,t)\right] = -ie^{-ikx(t)}\sqrt{\frac{2}{\pi}}\frac{2\mu_1 p(t)}{g_1 m}\frac{kR\cos(kR)-\sin(kR)}{k^2R^2}. \tag{5.79}$$

As we are considering a harmonically trapped system, we use the harmonic oscillator state basis to represent the system. In this basis, the number-damping trace terms for position and momentum (in (5.64) and (5.65)) are zero:

$$\mathrm{Tr}\left(\hat{x}\hat{\mathcal{P}}\right) = \mathrm{Tr}\left(\hat{p}\hat{\mathcal{P}}\right) = 0. \tag{5.80}$$

5.5.2 Equations of motion

Substituting (5.76) into the stochastic Ehrenfest relations for position (5.64) and momentum (5.65) leads to a pair of coupled stochastic differential equations for the centre of mass position and momentum

$$\begin{aligned}(\mathbf{I})dx(t) &= \frac{1}{m}p(t)dt - \frac{\gamma m\omega^2}{\hbar}x(t)^3dt - 2\Lambda_\gamma x(t)dt + dW_\gamma^x(t) \\ &\quad + dW_\varepsilon^x(t) + q_x^H + q_x^\gamma + q_x^\varepsilon + t_x^\varepsilon, \qquad (5.81)\\ (\mathbf{I})dp(t) &= -m\omega^2 x(t)dt - \frac{\gamma m\omega^2}{\hbar}x(t)^2p(t)dt - 2\Lambda_\varepsilon p(t)dt + dW_\varepsilon^p(t) \\ &\quad + dW_\gamma^p(t) + q_p^H + q_p^\gamma + q_p^\varepsilon + t_p^\varepsilon, \qquad (5.82)\end{aligned}$$

where the noise correlations are

$$\begin{aligned}\langle dW_\gamma^x(t)dW_\gamma^x(t)\rangle &= \left(\frac{\mathcal{D}_\gamma}{m^2\omega^4} + \frac{4\gamma k_B T x(t)^2}{N\hbar} + d_x^\gamma\right)dt, \qquad (5.83)\\ \langle dW_\gamma^p(t)dW_\gamma^p(t)\rangle &= d_p^\gamma dt, \qquad (5.84)\\ \langle dW_\gamma^x(t)dW_\gamma^p(t)\rangle &= -\frac{4\mu_1\gamma k_B T}{g_1\hbar}p(t)x(t)dt, \qquad (5.85)\\ \langle dW_\varepsilon^x(t)dW_\varepsilon^x(t)\rangle &= d_x^\varepsilon dt, \qquad (5.86)\\ \langle dW_\varepsilon^p(t)dW_\varepsilon^p(t)\rangle &= \left(m^2\mathcal{D}_\varepsilon + d_p^\varepsilon\right)dt, \qquad (5.87)\\ \langle dW_\varepsilon^x(t)dW_\varepsilon^p(t)\rangle &= d_{x,p}^\varepsilon dt, \qquad (5.88)\end{aligned}$$

and we have identified the number-damping drift and diffusion constants

$$\Lambda_\gamma = \frac{2\gamma\mu_1}{5\hbar}, \qquad \mathcal{D}_\gamma = \frac{4m\omega^2 k_B T}{N}\Lambda_\gamma, \tag{5.89}$$

the energy-damping drift and diffusion constants

$$\Lambda_\varepsilon = \frac{3\omega\mathcal{M}\hbar\sqrt{\mu_1}}{\pi g_1 R^4\sqrt{2m}}\int dk S_1(k)\frac{(\sin(kR)-kR\cos(kR))^2}{k^4}, \qquad \mathcal{D}_\varepsilon = \frac{4k_B T}{mN_{\rm TF}}\Lambda_\varepsilon, \tag{5.90}$$

and the cutoff terms have all been scaled by N^{-1}, apart from the diffusion cutoff terms which have been scaled by N^{-2}, to eliminate common factors of N. Using

$$\langle\psi|\hat{x}\hat{\mathcal{Q}}|x\rangle = \sqrt{\frac{\hbar(n_{\rm cut}+1)}{2m\omega}}\alpha^*_{n_{\rm cut}}(t)\phi^*_{n_{\rm cut}+1}(x), \tag{5.91}$$

$$\langle\psi|\hat{p}\hat{\mathcal{Q}}|x\rangle = -i\sqrt{\frac{\hbar m\omega(n_{\rm cut}+1)}{2}}\alpha^*_{n_{\rm cut}}(t)\phi^*_{n_{\rm cut}+1}(x), \tag{5.92}$$

the cutoff terms are

$$q^H_x = -\frac{g_1}{N}\sqrt{\frac{2(n_{\rm cut}+1)}{\hbar m\omega}}{\rm Im}\left\{\alpha^*_{n_{\rm cut}}(t)\int dx\phi^*_{n_{\rm cut}+1}(x)\psi(x)n(x)\right\}, \tag{5.93}$$

$$q^\gamma_x = \frac{g_1\gamma}{N}\sqrt{\frac{2(n_{\rm cut}+1)}{\hbar m\omega}}{\rm Re}\left\{\alpha^*_{n_{\rm cut}}(t)\int dx\phi^*_{n_{\rm cut}+1}(x)\psi(x)n(x)\right\}, \tag{5.94}$$

$$q^\varepsilon_x = \frac{\mathcal{M}}{N}\sqrt{\frac{2\hbar(n_{\rm cut}+1)}{m\omega}}\int dk\, S_1(k)\mathcal{F}\left[{\rm Im}\left\{\alpha^*_{n_{\rm cut}}(t)\phi^*_{n_{\rm cut}+1}(x)\psi(x)\right\}\right]^*\mathcal{F}\left[\partial_x j(x)\right], \tag{5.95}$$

$$d^\gamma_x = -\frac{2\gamma k_B T(n_{\rm cut}+1)}{N^2 m\omega}\left|\alpha_{n_{\rm cut}}(t)\right|^2, \tag{5.96}$$

$$d^\varepsilon_x = \frac{4\mathcal{M}k_B T(n_{\rm cut}+1)}{N^2 m\omega}\int dk S_1(k)\left|\mathcal{F}\left[{\rm Im}\left\{\alpha^*_{n_{\rm cut}}(t)\phi^*_{n_{\rm cut}+1}(x)\psi(x)\right\}\right]\right|^2, \tag{5.97}$$

$$\begin{aligned} t^\varepsilon_x = &-\frac{k_B T}{N\hbar}\int dx\int dx'\langle\psi|\hat{x}\hat{\mathcal{P}}|x\rangle\delta(x,x')\psi(x')\varepsilon(x-x') + {\rm h.c.} \\ &+\frac{k_B T}{N\hbar}\int dx\int dx'\langle x|\hat{\mathcal{P}}\hat{x}\hat{\mathcal{P}}|x'\rangle\psi^*(x)\psi(x')\varepsilon(x-x') + {\rm h.c.}, \end{aligned} \tag{5.98}$$

for position, and

$$q_p^H = \frac{g_1}{N}\sqrt{\frac{2m\omega(n_{\rm cut}+1)}{\hbar}}{\rm Re}\left\{\alpha^*_{n_{\rm cut}}(t)\int dx\phi^*_{n_{\rm cut}+1}(x)\psi(x)n(x)\right\}, \tag{5.99}$$

$$q_p^\gamma = \frac{g_1\gamma}{N}\sqrt{\frac{2m\omega(n_{\rm cut}+1)}{\hbar}}{\rm Im}\left\{\alpha^*_{n_{\rm cut}}(t)\int dx\phi^*_{n_{\rm cut}+1}(x)\psi(x)n(x)\right\}, \tag{5.100}$$

$$q_p^\varepsilon = -\frac{\mathcal{M}}{N}\sqrt{2\hbar m\omega(n_{\rm cut}+1)}\int dk\, S_1(k)\mathcal{F}\left[{\rm Re}\left\{\alpha^*_{n_{\rm cut}}(t)\phi^*_{n_{\rm cut}+1}(x)\psi(x)\right\}\right]^*\mathcal{F}\left[\partial_x j(x)\right], \tag{5.101}$$

$$d_p^\gamma = -\frac{2\gamma m\omega k_B T(n_{\rm cut}+1)}{N^2}\left|\alpha_{n_{\rm cut}}(t)\right|^2, \tag{5.102}$$

$$d_p^\varepsilon = \frac{4\mathcal{M}k_BT}{N^2}\int dk S_1(k)\Bigg(m\omega(n_{\rm cut}+1)\left|\mathcal{F}\left[{\rm Re}\left\{\alpha^*_{n_{\rm cut}}(t)\phi^*_{n_{\rm cut}+1}(x)\psi(x)\right\}\right]\right|^2 + \sqrt{8\hbar m\omega(n_{\rm cut}+1)}{\rm Re}\left\{\mathcal{F}\left[{\rm Re}\left\{\alpha^*_{n_{\rm cut}}(t)\phi^*_{n_{\rm cut}+1}(x)\psi(x)\right\}\right]\mathcal{F}\left[\partial_x n(x)\right]^*\right\}\Bigg), \tag{5.103}$$

$$t_p^\varepsilon = -\frac{k_BT}{N\hbar}\int dx\int dx'\langle\psi|\hat{p}\hat{\mathcal{P}}|x\rangle\delta(x,x')\psi(x')\varepsilon(x-x') + {\rm h.c.} + \frac{k_BT}{N\hbar}\int dx\int dx'\langle x|\hat{\mathcal{P}}\hat{p}\hat{\mathcal{P}}|x'\rangle\psi^*(x)\psi(x')\varepsilon(x-x') + {\rm h.c.}, \tag{5.104}$$

for momentum. Additionally, the cutoff term for the position-momentum energy-damping noise correlations is

$$d_{x,p}^\varepsilon = -4\mathcal{M}k_BT\sqrt{\frac{\hbar(n_c+1)}{2m\omega}}\int d^3\mathbf{k}\,k^{-1}\mathcal{F}\left[{\rm Im}\left\{\alpha^*_{n_{\rm cut}}(t)\phi^*_{n_{\rm cut}+1}(x)\psi(x)\right\}\right]^* \times\left[\mathcal{F}\left[\partial_x n(x)\right]+\sqrt{2m\omega\hbar(n_c+1)}\mathcal{F}\left[{\rm Re}\left\{\alpha^*_{n_{\rm cut}}(t)\phi^*_{n_{\rm cut}+1}(x)\psi(x)\right\}\right]\right]dt. \tag{5.105}$$

We restrict our attention to small values of $x(t)$ and $p(t)$, retaining terms only linear in these variables, which allows us to write the coupled equations of motion as a single equation of motion for the dimensionless complex variable

$$z(t) = \sqrt{\frac{m\omega}{2\hbar}}x(t) + \frac{i}{\sqrt{2\hbar m\omega}}p(t) \equiv \langle\hat{a}\rangle \tag{5.106}$$

where $\hat{a}$ is the usual ladder operator for a quantum harmonic oscillator. The equation of motion is then

$$\begin{aligned}(\mathbf{I})dz(t) &= -i\omega z dt - (\Lambda_\gamma + \Lambda_\varepsilon) z dt - (\Lambda_\gamma - \Lambda_\varepsilon)\bar{z} dt \\ &\quad + dW^z_{\gamma,1}(t) + dW^z_{\varepsilon,1}(t) + dW^z_{\gamma,2}(t) + dW^z_{\varepsilon,2}(t) \\ &\quad + q^H_z + q^\varepsilon_z + q^\gamma_z + dz^\varepsilon \end{aligned} \tag{5.107}$$

where the cutoff terms are

$$q^H_z = \frac{ig_1}{\hbar N}\sqrt{n_{\rm cut}+1}\alpha^*_{n_{\rm cut}}(t)\int dx \phi^*_{n_{\rm cut}+1}(x)\psi(x)n(x), \tag{5.108}$$

$$q^\gamma_z = \frac{\gamma g_1}{\hbar N}\sqrt{n_{\rm cut}+1}\alpha^*_{n_{\rm cut}}(t)\int dx \phi^*_{n_{\rm cut}+1}(x)\psi(x)n(x), \tag{5.109}$$

$$q^\varepsilon_z = -\frac{i\mathcal{M}}{N}\sqrt{n_{\rm cut}+1}\alpha^*_{n_{\rm cut}}(t)\int dk\, S_1(k)\mathcal{F}\left[\phi_{n_{\rm cut}+1}(x)\psi^*(x)\right]^*\mathcal{F}\left[\partial_x j(x)\right], \tag{5.110}$$

$$\begin{aligned} t^\varepsilon_z &= -\frac{k_B T}{N\hbar}\int dx \int dx' \langle\psi|\hat{z}\hat{\mathcal{P}}|x\rangle\delta(x,x')\psi(x')\varepsilon(x-x') + \text{h.c.} \\ &\quad + \frac{k_B T}{N\hbar}\int dx \int dx' \langle x|\hat{\mathcal{P}}\hat{z}\hat{\mathcal{P}}|x'\rangle\psi^*(x)\psi(x')\varepsilon(x-x') + \text{h.c.}, \end{aligned} \tag{5.111}$$

and the noises have correlations

$$\langle dW^z_{\gamma,1}(t)dW^z_{\gamma,1}(t)\rangle = \frac{m\omega}{2\hbar}\langle dW^x_\gamma(t)dW^x_\gamma(t)\rangle = \frac{m\omega}{2\hbar}\left(\frac{\mathcal{D}_\gamma}{m^2\omega^4} + d^\gamma_x\right)dt, \tag{5.112}$$

$$\langle dW^z_{\gamma,2}(t)dW^z_{\gamma,2}(t)\rangle = -\frac{1}{2\hbar m\omega}\langle dW^p_\gamma(t)dW^p_\gamma(t)\rangle = -\frac{1}{2\hbar m\omega}d^\gamma_p dt, \tag{5.113}$$

$$\langle dW^z_{\gamma,1}(t)dW^z_{\gamma,2}(t)\rangle = \frac{i}{2\hbar}\langle dW^x_\gamma(t)dW^p_\gamma(t)\rangle = 0, \tag{5.114}$$

$$\langle dW^z_{\varepsilon,1}(t)dW^z_{\varepsilon,1}(t)\rangle = \frac{m\omega}{2\hbar}\langle dW^x_\varepsilon(t)dW^x_\varepsilon(t)\rangle = \frac{m\omega}{2\hbar}d^\varepsilon_x dt, \tag{5.115}$$

$$\langle dW^z_{\varepsilon,2}(t)dW^z_{\varepsilon 2}(t)\rangle = -\frac{1}{2\hbar m\omega}\langle dW^p_\varepsilon(t)dW^p_\varepsilon(t)\rangle = -\frac{1}{2\hbar m\omega}\left(m^2\mathcal{D}_\varepsilon + d^\varepsilon_p\right)dt, \tag{5.116}$$

$$\langle dW^z_{\varepsilon,1}(t)dW^z_{\varepsilon 2}(t)\rangle = \frac{i}{2\hbar}\langle dW^x_\varepsilon(t)dW^p_\varepsilon(t)\rangle = \frac{i}{2\hbar}d^\varepsilon_{x,p}dt. \tag{5.117}$$

Using the properties of the epsilon function we can rewrite t_z^ε as

$$\begin{aligned} t_z^\varepsilon &= -\frac{\mathcal{M}k_BT}{N\hbar}\sum_{n\in\mathbf{C}}\int dkS_1(k)\mathcal{F}\left[\phi_n^*(x)\sum_{l\in\mathbf{C}}\sqrt{l+1}\phi_{l+1}(x)\right]^*\mathcal{F}\left[\phi_n^*(x)\psi(x)\right]+\text{h.c.} \\ &\quad+\frac{\mathcal{M}k_BT}{N\hbar}\sum_{n\in\mathbf{C}}\sqrt{n+1}\int dkS_1(k)\mathcal{F}\left[\phi_n^*(x)\psi(x)\right]^*\mathcal{F}\left[\phi_{n+1}^*(x)\psi(x)\right]+\text{h.c.}, \quad (5.118) \end{aligned}$$

a more useful form for constructing t_z^ε numerically.

5.5.3 Cutoff term magnitudes

With the exception of the epsilon correction (5.111), all the cutoff terms are a result of mode mixing between the highest energy coherent mode and the lowest energy incoherent mode. In the limit of the energy cutoff being very high, it is easy to see that all the cutoff terms go to zero. We expect the integrals involving the overlap of the lowest energy incoherent mode $\phi_{n_{\text{cut}}+1}(x)$ and the coherent field wave function $\psi(x)$ to be small, as $\phi_{n_{\text{cut}}+1}(x)$ is highly oscillatory and the mode population is invariably small for a well-chosen cutoff. We claim that for a well-chosen cutoff the cutoff terms are small enough such that they may be neglected, and we justify this in two ways. Firstly, we consider the magnitude of a selection of the cutoff terms by calculating them numerically. Second, we consider the analytic solutions that can be found by neglecting the cutoff terms and show that these agree well with simulations of the 1D SPGPE.

Magnitude calculations

When considering the cutoff terms involving mode mixing at the cutoff (i.e. all except the epsilon correction), we note that only the Hamiltonian cutoff term q_z^H (5.108) does not have one of the damping rates as a multiplying factor. As the damping rates have a typical value several orders of magnitude less than unity, it is reasonable to expect that of all these terms, the Hamiltonian cutoff term will be the largest. If we show that q_z^H is small enough to be neglected then we can reason that the remaining cutoff terms are smaller still and so can certainly be neglected also.

The epsilon term t_z^ε (5.111) is distinct from the other terms, as it is not a result of mode mixing at the cutoff. We expect the two terms in the epsilon term to almost cancel, as it is clear this is the case in the limit that the projector becomes the identity. This is an important result of the earlier step where we found that writing the SPGPE in Ito

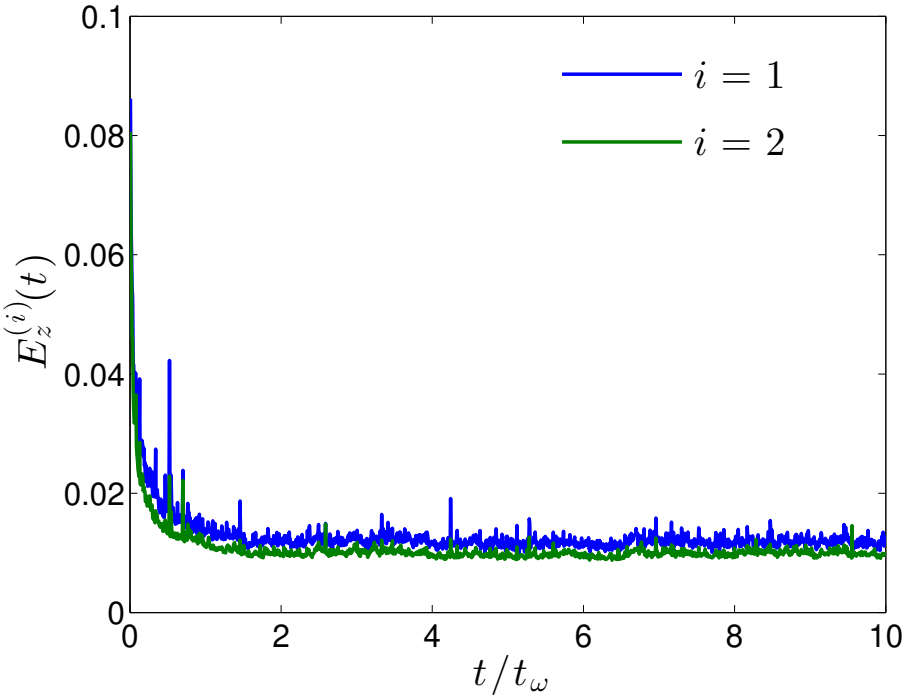

Figure 5.1: The mean relative cutoff term magnitudes (5.119) for q_z^H (blue) and t_z^ε (green) over time determined numerically for an ensemble of 1000 trajectories.

form resulted in an extra term; without this extra term the epsilon term would in general be non-negligible, and in fact diverges in the infinite cutoff limit. We thus monitor the magnitudes of q_z^H and t_z^ε over the course of an ensemble of numerical trajectories.

We define the relative cutoff term magnitudes by

$$E_z^{(1)}(t) = \left|\frac{q_z^H(t)}{\dot{z}(t)}\right|, \quad E_z^{(2)}(t) = \left|\frac{t_z^\varepsilon(t)}{\dot{z}(t)}\right|, \tag{5.119}$$

noting that $|\dot{z}(t)|$ is strictly non-zero for harmonic motion. If these values remain significantly less than unity, then we may conclude that the effects of the cutoff terms are negligible. We perform simulations of the 1D SPGPE with the initial condition given by (5.76) with $x(0) = p(0) = 0$. We choose parameters such that the effects of energy-damping and number-damping are of similar significance; we note that in general one of the damping processes may dominate over the other in a physical system. While in principle we could find a set of parameters that match a particular experimental system, our goal here is not to make predictions about experimental observations but rather to investigate whether we

can make analytic predictions for solutions of the SPGPE using the stochastic Ehrenfest relations. We use a chemical potential of $\mu_1 = 100\hbar\omega$, an energy cutoff of $\epsilon_{\rm cut} = 500\hbar\omega$, a temperature of $T = 500\hbar\omega/k_B$, an interaction strength of $g = 0.01\hbar\omega a_\omega$, an energy-damping rate of $\mathcal{M} = 0.0005a_\omega^2$, and a number-damping rate of $\gamma = 0.001$. Timescales are considered in units of the harmonic oscillator time period $t_\omega \equiv 2\pi/\omega$.

The relative cutoff term magnitudes are shown in Fig. 5.1, where the initial state is (5.76) with $x(0) = p(0) = 0$ and we have taken an ensemble average over 1000 trajectories. While the magnitudes can reach as high as ~ 0.1 early in the dynamics, we see that once the system has equilibrated they obtain a steady-state of roughly ~ 0.01.

Analytic solutions

If we neglect the cutoff terms, we can then write the coupled differential equation as a vector SDE representing an Ornstein-Uhlenbeck process

$$d\mathbf{u}(t) = -\mathbf{\Lambda}\mathbf{u}(t)dt + \mathbf{B}d\mathbf{W}(t) \tag{5.120}$$

where

$$\mathbf{u}(t) = \begin{bmatrix} x(t) \\ p(t) \end{bmatrix}, \tag{5.121}$$

$$\mathbf{\Lambda} = \begin{bmatrix} 2\Lambda_\gamma & -1/m \\ m\omega^2 & 2\Lambda_\varepsilon \end{bmatrix}, \quad \mathbf{B} = \begin{bmatrix} \sqrt{\dfrac{\mathcal{D}_\gamma}{m^2\omega^4}} & 0 \\ 0 & \sqrt{m^2\mathcal{D}_\varepsilon} \end{bmatrix}, \tag{5.122}$$

are the drift and diffusion matrices respectively, and

$$d\mathbf{W}(t) = \begin{bmatrix} dW_1(t) \\ dW_2(t) \end{bmatrix} \tag{5.123}$$

is a vector of independent Wiener processes with correlations[6]

$$\langle dW_n(t) dW_m(t) \rangle = \delta_{mn} dt. \tag{5.124}$$

The vector SDE representing an Ornstein-Uhlenbeck process admits the analytic solution

$$\mathbf{u}(t) = \exp\left[-\mathbf{\Lambda} t\right] \mathbf{u}(0) + \int_0^t \exp\left[-\mathbf{\Lambda}(t-t')\right] \mathbf{B} d\mathbf{W}(t'), \tag{5.125}$$

where we have assumed the initial state $\mathbf{u}(0)$ to be deterministic. The mean undergoes exponential decay

$$\langle \mathbf{u}(t) \rangle = \exp\left[-\mathbf{\Lambda} t\right] \mathbf{u}(0). \tag{5.126}$$

We perform simulations for an ensemble of 500 trajectories with an initial displacement of $x(0) = 0.2R$ to test the exponential decay rate. For a system with $x(0) = x_0$ and $p(0) = 0$, the centre of mass position over time is given by

$$\langle x(t) \rangle = x_0 e^{-(\Lambda_\gamma + \Lambda_\varepsilon)t} \left[\cos\left(\omega_{\gamma\varepsilon} t\right) + \frac{|\Lambda_\gamma - \Lambda_\varepsilon|}{\omega_{\gamma\varepsilon}} \sin\left(\omega_{\gamma\varepsilon} t\right) \right], \tag{5.127}$$

where we have defined the new frequency

$$\omega_{\gamma\varepsilon} = \sqrt{\omega^2 - (\Lambda_\gamma - \Lambda_\varepsilon)^2}. \tag{5.128}$$

The result of this is shown in Fig. 5.2, where we see that the analytically predicted decay rate agrees well with the numeric data.

We also consider the steady-state correlations given by

$$\mathbf{G}(\tau) \equiv \lim_{t\to\infty} \left\langle \left[\mathbf{u}(t) - \langle \mathbf{u}(t) \rangle\right] \left[\mathbf{u}(t+\tau) - \langle \mathbf{u}(t+\tau) \rangle\right]^T \right\rangle, \tag{5.129}$$

and the steady-state spectra given by

$$\mathbf{S}(\omega) = \frac{1}{2\pi} (\mathbf{\Lambda} + i\Omega)^{-1} \mathbf{B}\mathbf{B}^\intercal (\mathbf{\Lambda}^\intercal - i\Omega)^{-1}. \tag{5.130}$$

The steady-state correlations for position-position, momentum-momentum, and momentum-

[6] Note that the correlations between the position and momentum noises are either nonlinear in $x(t)$ and $p(t)$ (5.85), or given by a cutoff term (5.88). Therefore, in the regime we are considering these correlations are small and we are able to approximate the noises as being independent.

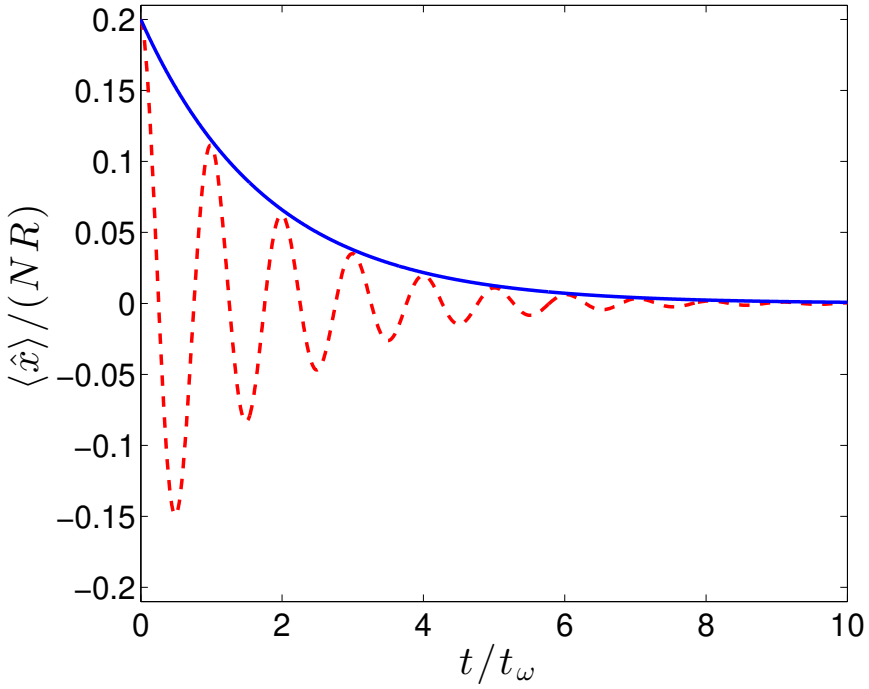

Figure 5.2: Mean centre of mass position for 500 trajectories with an initial displacement $x(0) = 0.2R$, showing the numeric result from simulations of the 1D SPGPE (dashed red) and the predicted exponential decay envelope from (5.127) (solid blue).

position are

$$G_{xx}(\tau) = -\frac{k_B T}{Nm}\frac{1}{\omega\omega_{\gamma\varepsilon}} e^{-(\Lambda_\gamma+\Lambda_\varepsilon)|\tau|}\sin\left(\omega_{\gamma\varepsilon}|\tau| - \sin^{-1}\left(\frac{\omega_{\gamma\varepsilon}}{\omega}\right)\right), \tag{5.131}$$

$$G_{pp}(\tau) = \frac{mk_B T}{N}\frac{\omega}{\omega_{\gamma\varepsilon}} e^{-(\Lambda_\gamma+\Lambda_\varepsilon)|\tau|}\sin\left(\omega_{\gamma\varepsilon}|\tau| + \sin^{-1}\left(\frac{\omega_{\gamma\varepsilon}}{\omega}\right)\right), \tag{5.132}$$

$$G_{px}(\tau) = \frac{k_B T}{N}\frac{1}{\omega_{\gamma\varepsilon}} e^{-(\Lambda_\gamma+\Lambda_\varepsilon)|\tau|}\sin\left(\omega_{\gamma\varepsilon}\tau\right) \tag{5.133}$$

respectively. The steady-state spectra for position-position, momentum-momentum, and

momentum-position are

$$S_{xx}(\Omega) = \frac{2k_BT}{N\pi m\omega^2}\frac{\Lambda_\varepsilon(4\Lambda_\gamma\Lambda_\varepsilon+\omega^2)+\Lambda_\gamma\Omega^2}{(4\Lambda_\gamma\Lambda_\varepsilon+\omega^2)^2-2(\omega^2-2(\Lambda_\varepsilon^2+\Lambda_\gamma^2))\Omega^2+\Omega^4} \tag{5.134}$$

$$S_{pp}(\Omega) = \frac{2k_BTm}{N\pi}\frac{\Lambda_\gamma(4\Lambda_\gamma\Lambda_\varepsilon+\omega^2)+\Lambda_\varepsilon\Omega^2}{(4\Lambda_\gamma\Lambda_\varepsilon+\omega^2)^2-2(\omega^2-2(\Lambda_\varepsilon^2+\Lambda_\gamma^2))\Omega^2+\Omega^4} \tag{5.135}$$

$$S_{px}(\Omega) = \frac{2ik_BT}{N\pi}\frac{(\Lambda_\gamma+\Lambda_\varepsilon)\Omega}{(4\Lambda_\gamma\Lambda_\varepsilon+\omega^2)^2-2(\omega^2-2(\Lambda_\varepsilon^2+\Lambda_\gamma^2))\Omega^2+\Omega^4} \tag{5.136}$$

respectively. We compare these analytic solutions with the numerical data used to calculate the variance.

In Fig. 5.3 we show the steady-state correlations for position-position, momentum-momentum, and momentum-position using an ensemble of 5000 trajectories. When calculating the correlations from the numeric data, we have assumed that the system has reached equilibrium after five trap cycles $t = 5t_\omega$, and used ergodic averaging over the remaining time. With respect to the dissipation timescale $(\Lambda_\gamma + \Lambda_\varepsilon)^{-1}$, this is equivalent to $t = 2.78(\Lambda_\gamma + \Lambda_\varepsilon)$. We see that the analytic and numeric results show excellent agreement for short times with differences becoming more pronounced for larger τ. Similarly, the steady-state spectra for position-position, momentum-momentum, and momentum-position are shown in Fig. 5.4, where the numeric spectra are obtained using the Wiener-Khinchin theorem applied to the numeric steady-state correlations. Again we see that the analytic and numeric results show good agreement.

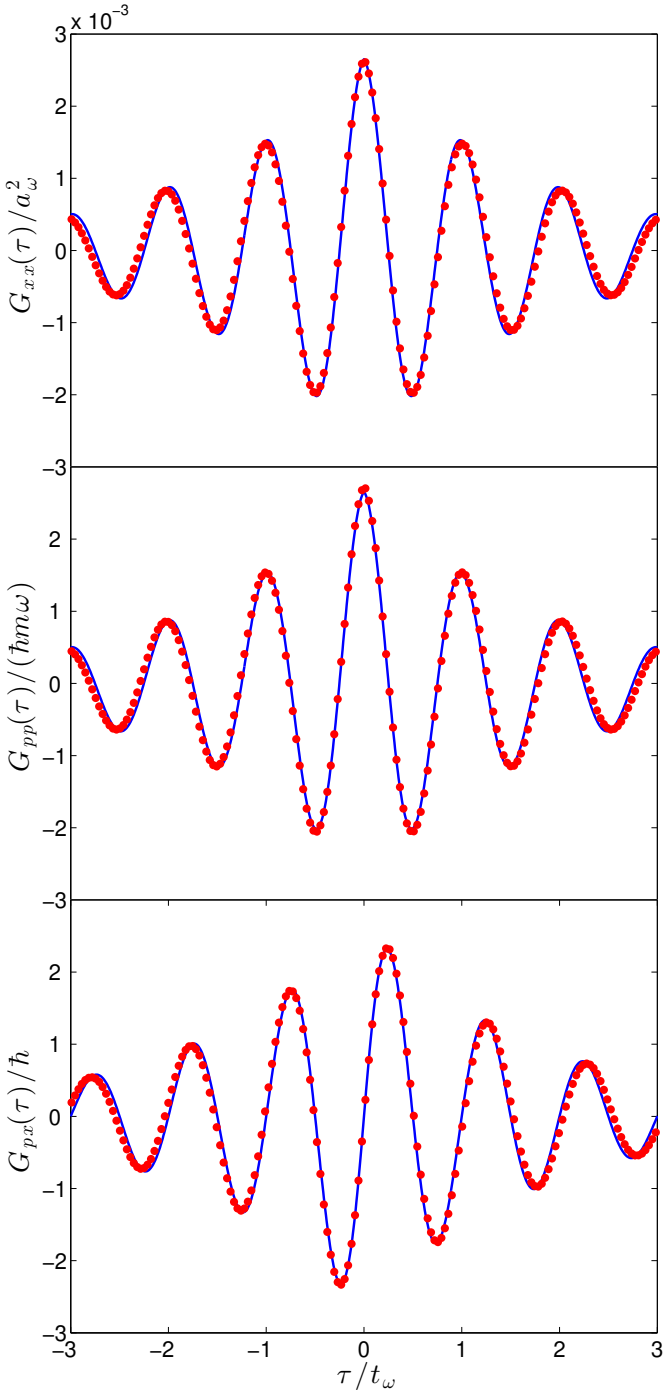

Figure 5.3: Steady-state time correlations for position-position (top), momentum-momentum (middle) and momentum-position (bottom), as determined by numerical solutions of the SPGPE (red dots) and the analytic solutions (solid blue) (5.131)-(5.133).

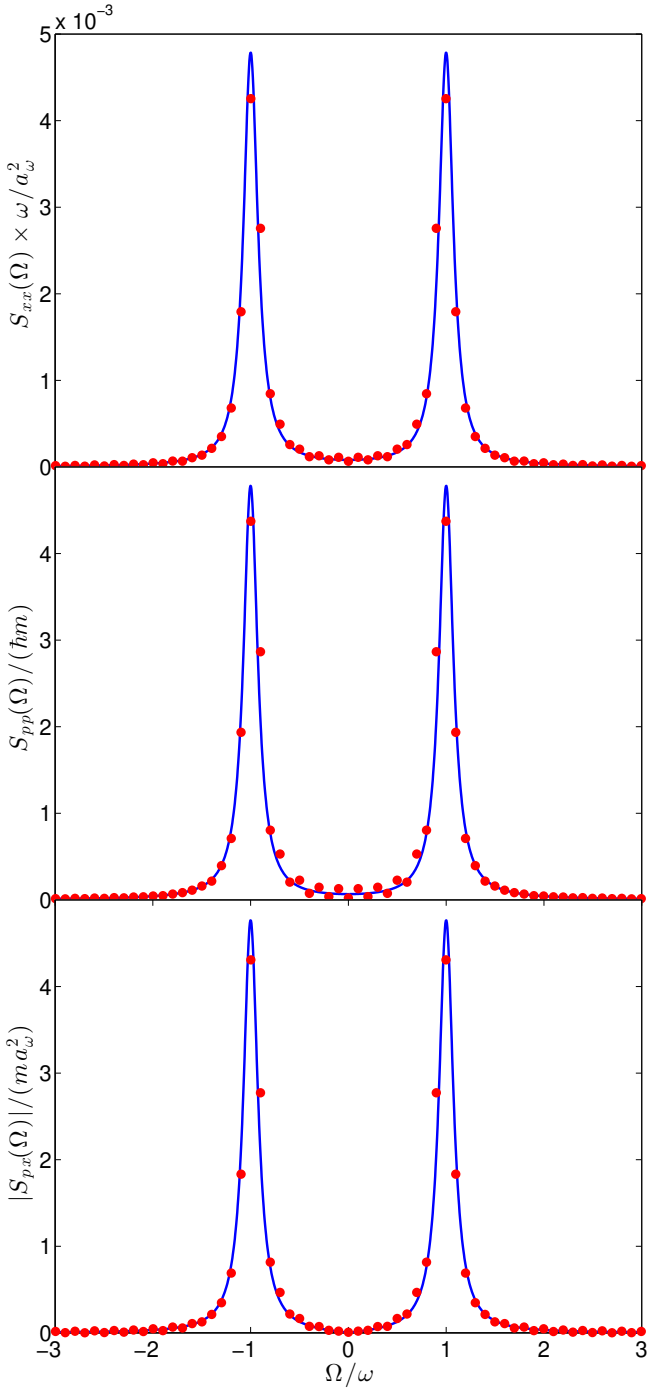

Figure 5.4: Steady-state spectra for position-position (top), momentum-momentum (middle) and momentum-position (bottom), as determined by numerical solutions of the SPGPE (red dots) and the analytic solutions (solid blue) (5.134)-(5.136).

5.6 Conclusions

In this chapter we used stochastic calculus methods to obtain stochastic equations of motion for moments of the classical field in the SPGPE. We refer to these equations of motion as the *stochastic Ehrenfest relations*, as they are the extension of the usual Ehrenfest relations to the SPGPE and involve integrating the stochastic field over its spatial degrees of freedom. Using the example of a quasi-1D Thomas-Fermi system, we have demonstrated that for a well-chosen cutoff the effects of the projector are often small enough to be neglected in an analytic treatment[7]. The stochastic Ehrenfest relations then admit analytic solutions, which we found compared favourably to numeric solutions of the 1D SPGPE. These results suggest that the stochastic Ehrenfest relations may be utilised to attain deeper analytic understanding for a range of systems. In particular they may be used to reveal the particular influence of the respective damping processes for systems where an insightful ansatz for the matter-wave field leads to a reduced description in terms of a small number of effective degrees of freedom.

[7]Note that the cutoff can be neglected only in an analytic treatment; it is still essential that it is included in any numerical implementation.

Chapter 6

Kohn mode oscillations at finite temperature

6.1 Introduction

Historically, when modelling finite-temperature bosonic systems reservoir interactions have been accounted for through the inclusion of the number-damping process only, with the energy-damping process neglected entirely. The combined effect of the two reservoir interactions is often assumed to be encapsulated in a single effective number-damping rate, with any additional effects due to the energy-damping serving only to increase the value of the effective number-damping rate [208, 214]. It is usually suggested that in any system with both processes present, the energy-damping would only be significant when far from equilibrium [106]. Using the stochastic Ehrenfest relations derived in the previous chapter in addition to the Hartree-Fock parameter estimation scheme described in [2], we investigate whether the neglect of the energy-damping reservoir interaction is physically consistent, and how the two reservoir interaction processes may be individually measured in experiments.

In this chapter we apply the stochastic Ehrenfest relations for position and momentum to a degenerate finite-temperature Bose gas confined to an isotropic harmonic trap in the Thomas-Fermi regime. The chapter is structured as follows. In Section 6.2 we briefly recap Kohn's theorem. In Section 6.3 we introduce the system under consideration, presenting the wave function ansatz and subsequent relevant properties. In Section 6.4 we use the stochastic Ehrenfest relations to find a pair of coupled stochastic differential equations describing the centre of mass motion of the classical field. In Section 6.5 we present the analytic solutions to these equations and compare these to results from numeric simulations of the full stochastic projected Gross-Pitaevskii equation. In Section 6.6 we briefly consider the additional effect of including number dynamics in the wave function ansatz. We conclude in Section 6.8.

6.2 Kohn's theorem

Kohn showed that the presence of electron-electron interactions in a bulk three dimensional electron gas does not change the cyclotron resonant frequency [287]. The theorem was extended by Dobson to describe any many-body system with two-body interactions under harmonic confinement [288]. Consider a system of N interacting particles and assume a Hamiltonian of the form

$$\hat{H} = \sum_{i=1}^{N} \sum_{\alpha} \left[\frac{\hat{p}_{i\alpha}^2}{2m} + \frac{1}{2} m \omega_\alpha^2 \hat{r}_{i\alpha}^2 \right] + \sum_{i<j} U(|\mathbf{r}_i - \mathbf{r}_j|), \tag{6.1}$$

where the subscript $\alpha \in \{x, y, z\}$ refers to the coordinate. Define the centre of mass position operator

$$\hat{R}_\alpha = \frac{1}{N} \sum_{i=1}^{N} \hat{r}_{i\alpha}, \tag{6.2}$$

then the Heisenberg equation of motion for the centre of mass position operator is

$$\frac{d\hat{R}_\alpha}{dt} = \frac{1}{i\hbar} \left[\hat{R}_\alpha, \hat{H} \right] = \frac{1}{mN} \hat{P}_\alpha \tag{6.3}$$

where we have also defined the centre of mass momentum operator

$$\hat{P}_\alpha = \sum_{i=1}^{N} \hat{p}_{i\alpha}. \tag{6.4}$$

From (6.3) we find

$$\frac{d^2 \hat{R}_\alpha}{dt^2} + \omega_\alpha^2 \hat{R}_\alpha = 0, \tag{6.5}$$

showing that the centre of mass motion is independent of the detailed form of the two-body potential and undergoes oscillations at the harmonic trapping frequency. Furthermore, one can show that the time-dependent Gross-Pitaevskii equation admits a solution of the form

$$n(\mathbf{r}, t) = n_0(\mathbf{r} - \mathbf{u}(t)), \quad \mathbf{v}(\mathbf{r}, t) = \dot{\mathbf{u}}(t) \tag{6.6}$$

where

$$\frac{d^2u_\alpha(t)}{dt^2} + \omega_\alpha^2 u_\alpha(t) = 0, \tag{6.7}$$

that is, the condensate oscillates rigidly about the centre of the trap.

When considering finite-temperature systems, Kohn's theorem may be violated due to the treatment of the thermal reservoir. If the thermal reservoir is assumed to be time-independent, then oscillations of the low-energy region can be damped via interactions with the reservoir. Hence the separation of the system into a high-energy subspace acting as a stationary thermal reservoir and a low-energy coherent subspace in the SPGPE leads to explicit violation of Kohn's theorem. In this work we use *Kohn mode* to refer to the dipole mode oscillating with the trap frequency; such modes will have finite lifetime when Kohn's theorem does not hold. Systems for which an SPGPE treatment of the Kohn mode is appropriate include those with a thermal reservoir of a distinct component, or where the trapping potential becomes non-harmonic at high energies.

6.3 System

Consider a finite temperature repulsive Bose gas in an isotropic harmonic trap. The natural choice of basis for this system is the Hermite polynomials, which results in the trace term being zero for both position and momentum. We assume a wave function of the form

$$\psi(\mathbf{r}, t) = \psi_{\mathrm{TF}}(\mathbf{r} - \mathbf{r}(t)) \exp\left[\frac{i\mathbf{r}\cdot\mathbf{p}(t)}{\hbar}\right] \tag{6.8}$$

where

$$\psi_{\mathrm{TF}}(\mathbf{r}) = \sqrt{\frac{\mu - V(\mathbf{r})}{g}}, \quad \mu > V(\mathbf{r}) \tag{6.9}$$

is the Thomas-Fermi wave function. This assumes that the particle number stays essentially constant at the Thomas Fermi value

$$N_{\mathrm{TF}} = \frac{16\sqrt{2}\pi\mu^{5/2}}{15gm^{3/2}\omega^3}. \tag{6.10}$$

The position and momentum expectations are

$$R_j(t) \equiv \langle \hat{r}_j \rangle = N_{\rm TF} r_j(t) \tag{6.11}$$

$$P_j(t) \equiv \langle \hat{p}_j \rangle = N_{\rm TF} p_j(t). \tag{6.12}$$

The current divergence is

$$\nabla \cdot \mathbf{j}(\mathbf{r}, t) = \frac{\mu}{g} \left(1 - \frac{(\mathbf{r} - \mathbf{r}(t))^2}{R^2} \right) \frac{\mathbf{r} \cdot \mathbf{p}(t)}{m}, \tag{6.13}$$

which is required for evaluating the energy-damping terms.

6.4 Equation of motion

Kohn's theorem states that the density is unchanged while undergoing oscillations; this can be taken as an approximation when damping is included. We have also taken the Thomas-Fermi approximation, so second derivatives of the wave function are neglected. Applying the stochastic Ehrenfest relations and neglecting cutoff terms as justified in the preceding section, we arrive at

$$\begin{aligned} (\mathbf{I}) dr_j(t) &= \frac{1}{m} p_j(t) dt - \frac{4\gamma\mu}{7\hbar} r_j(t) dt - \frac{\gamma m \omega^2}{\hbar} r_j(t) \sum_i r_i(t)^2 dt \\ &\quad + \sqrt{\frac{8\gamma\mu k_B T}{7\hbar m \omega^2 N_{\rm TF}} + \frac{4\gamma k_B T}{\hbar N_{\rm TF}} r_j(t)^2} dW_{j1}(t), \end{aligned} \tag{6.14}$$

$$\begin{aligned} (\mathbf{I}) dp_j(t) &= -m\omega^2 r_j(t) dt - \frac{\gamma m \omega^2}{\hbar} p_j(t) \sum_i r_i(t)^2 dt - \frac{5\mu\mathcal{M}\hbar}{3\pi g m R} p_j(t) dt \\ &\quad + \sqrt{\frac{10 k_B \mu T \mathcal{M} \hbar}{3\pi g R N_{\rm TF}}} dW_{j2}(t), \end{aligned} \tag{6.15}$$

where $dW_{jn}(t)$ are independent Wiener processes with correlations[1]

$$\langle dW_{jn}(t) dW_{im}(t) \rangle = \delta_{ij} \delta_{mn} dt. \tag{6.16}$$

From (6.15) we see that the number-damping process contributes both linear and third-order damping terms, while the energy-damping contributes a linear term only. As a result

[1] With the cutoff terms neglected, the noises are independent. We thus express them as independent Wiener processes with the norm taken out as a prefactor.

of the third-order terms, the equation of motion for each component of the position and momentum is coupled to the other three components. There is also a multiplicative term in the number-damping noise. If we consider only small displacements, as is the case when the system is in thermal equilibrium, then we obtain an equation of motion where the components are independent:

$$dr_j(t) = \frac{1}{m}p_j(t)dt - \frac{4\gamma\mu}{7\hbar}r_j(t)dt + \sqrt{\frac{8\gamma\mu k_B T}{7\hbar m\omega^2 N_{\rm TF}}}dW_{j1}(t), \tag{6.17}$$

$$dp_j(t) = -m\omega^2 r_j(t)dt - \frac{5\mu\mathcal{M}\hbar}{3\pi gmR}p_j(t)dt + \sqrt{\frac{10k_B\mu T\mathcal{M}\hbar}{3\pi gRN_{\rm TF}}}dW_{j2}(t). \tag{6.18}$$

Identifying the drift and diffusion constants

$$\Lambda_\gamma = \frac{2\gamma\mu}{7\hbar}, \quad \mathcal{D}_\gamma = \frac{4m\omega^2 k_B T}{N_{\rm TF}}\Lambda_\gamma, \quad \Lambda_\varepsilon = \frac{5\mu\mathcal{M}\hbar}{6\pi gmR}, \quad \mathcal{D}_\varepsilon = \frac{4k_B T}{mN_{\rm TF}}\Lambda_\varepsilon \tag{6.19}$$

we can then represent the equation of motion for the system as a vector SDE representing an Ornstein-Uhlenbeck process

$$d\mathbf{u}(t) = -\mathbf{\Lambda}\mathbf{u}(t)dt + \mathbf{B}d\mathbf{W}(t) \tag{6.20}$$

where

$$\mathbf{u}(t) = \begin{bmatrix} r_j(t) \\ p_j(t) \end{bmatrix}, \tag{6.21}$$

$$\mathbf{\Lambda} = \begin{bmatrix} 2\Lambda_\gamma & -1/m \\ m\omega^2 & 2\Lambda_\varepsilon \end{bmatrix}, \quad \mathbf{B} = \begin{bmatrix} \sqrt{\dfrac{\mathcal{D}_\gamma}{m^2\omega^4}} & 0 \\ 0 & \sqrt{m^2\mathcal{D}_\varepsilon} \end{bmatrix}, \tag{6.22}$$

are the drift and diffusion matrices respectively, and

$$d\mathbf{W}(t) = \begin{bmatrix} dW_{j1}(t) \\ dW_{j2}(t) \end{bmatrix} \tag{6.23}$$

is a vector of independent Wiener processes. Alternatively the equation of motion can be written as a stochastic differential equation for the complex variable

$$z_j(t) = \sqrt{\frac{m\omega}{2\hbar}} r_j(t) + \frac{i}{\sqrt{2\hbar m\omega}} p_j(t) \tag{6.24}$$

giving

$$\begin{aligned} dz_j(t) &= -i\omega z_j(t)dt - (\Lambda_\gamma + \Lambda_\varepsilon)\, z_j(t)dt - (\Lambda_\gamma - \Lambda_\varepsilon)\, \bar{z}_j(t)dt \\ &\quad + \frac{1}{\sqrt{2\hbar m\omega}} \left(\sqrt{\frac{\mathcal{D}_\gamma}{\omega^2}} dW_{j1}(t) + i\sqrt{m^2\mathcal{D}_\varepsilon} dW_{j2}(t) \right). \end{aligned} \tag{6.25}$$

This equation represents damped noisy circular motion in the complex plane[2]. If we consider the limit where only one of the damping processes is included, we obtain noisily driven damped harmonic oscillation in the position for energy-damping only

$$\ddot{r_j}(t) + 2\Lambda_\varepsilon \dot{r_j}(t) + \omega^2 r_j(t) = \sqrt{\mathcal{D}_\varepsilon}\vartheta_{j2}(t) \tag{6.26}$$

or momentum for number-damping only

$$\ddot{p_j}(t) + 2\Lambda_\gamma \dot{p_j}(t) + \omega^2 p_j(t) = \sqrt{\mathcal{D}_\gamma}\vartheta_{j1}(t), \tag{6.27}$$

where $\vartheta_{jn}(t)$ are independent white noises with correlations

$$\langle \vartheta_{jn}(t)\vartheta_{im}(t')\rangle = \delta_{ij}\delta_{mn}\delta(t-t'). \tag{6.28}$$

6.5 Results

6.5.1 Analytic solutions

The solution to the vector SDE (6.20) is well known

$$\mathbf{u}(t) = \exp\left[-\mathbf{\Lambda}t\right]\mathbf{u}(0) + \int_0^t \exp\left[-\mathbf{\Lambda}(t-t')\right]\mathbf{B}d\mathbf{W}(t'), \tag{6.29}$$

[2]We note that the second damping coefficient $(\Lambda_\gamma - \Lambda_\varepsilon)$ can take negative values, which at first glance seems to imply the possibility of anomalous growth when $\Lambda_\varepsilon > \Lambda_\gamma$, however it is clear from (6.20) that this is not the case.

and from this can be found many properties of the system. The mean undergoes exponential decay

$$\langle \mathbf{u}(t) \rangle = \exp\left[-\mathbf{\Lambda} t\right] \mathbf{u}(0). \tag{6.30}$$

The correlations are

$$\begin{aligned} \langle \mathbf{u}(t), \mathbf{u}^{\intercal}(s) \rangle &\equiv \langle \left[\mathbf{u}(t) - \langle \mathbf{u}(t) \rangle\right] \left[\mathbf{u}(s) - \langle \mathbf{u}(s) \rangle\right]^{\intercal} \rangle \\ &= \int_0^{\min(t,s)} \exp\left[-\mathbf{\Lambda}(t-t')\right] \mathbf{B}\mathbf{B}^{\intercal} \exp\left[-\mathbf{\Lambda}^{\intercal}(s-t')\right] dt' \end{aligned} \tag{6.31}$$

where we have assumed deterministic initial conditions such that $\langle \mathbf{u}(0), \mathbf{u}^{\intercal}(0) \rangle = 0$. Setting $s = t$ gives the variances

$$\begin{aligned} \boldsymbol{\sigma}(t) &\equiv \langle \mathbf{u}(t), \mathbf{u}^{\intercal}(t) \rangle \\ &= \int_0^{t} \exp\left[-\mathbf{\Lambda}(t-t')\right] \mathbf{B}\mathbf{B}^{\intercal} \exp\left[-\mathbf{\Lambda}^{\intercal}(t-t')\right] dt'. \end{aligned} \tag{6.32}$$

Defining the new frequency

$$\omega_{\gamma\varepsilon} \equiv \sqrt{\omega^2 - (\Lambda_\gamma - \Lambda_\varepsilon)^2}, \tag{6.33}$$

and damping rates

$$\Lambda_p \equiv \Lambda_\gamma + \Lambda_\varepsilon, \quad \Lambda_m \equiv \left|\Lambda_\gamma - \Lambda_\varepsilon\right|, \tag{6.34}$$

the variances are

$$\sigma_{r_j r_j}(t) = \frac{k_B T}{N_{\mathrm{TF}} m \omega^2} \left[1 + e^{-2\Lambda_p t} \left(\frac{\Lambda_m^2}{\omega_{\gamma\varepsilon}^2} \cos\left(2\omega_{\gamma\varepsilon} t\right) + \frac{\Lambda_m}{\omega_{\gamma\varepsilon}} \sin\left(2\omega_{\gamma\varepsilon} t\right) - \frac{\omega^2}{\omega_{\gamma\varepsilon}^2} \right)\right] \tag{6.35}$$

$$\sigma_{p_j p_j}(t) = \frac{m k_B T}{N_{\mathrm{TF}}} \left[1 + e^{-2\Lambda_p t} \left(\frac{\Lambda_m^2}{\omega_{\gamma\varepsilon}^2} \cos\left(2\omega_{\gamma\varepsilon} t\right) - \frac{\Lambda_m}{\omega_{\gamma\varepsilon}} \sin\left(2\omega_{\gamma\varepsilon} t\right) - \frac{\omega^2}{\omega_{\gamma\varepsilon}^2} \right)\right] \tag{6.36}$$

$$\sigma_{p_j r_j}(t) = -\frac{2 k_B T \Lambda_m}{N_{\mathrm{TF}} \omega_{\gamma\varepsilon}^2} e^{-2\Lambda_p t} \sin^2\left(\omega_{\gamma\varepsilon} t\right). \tag{6.37}$$

We note that for all intents and purposes, we expect $\omega_{\gamma\varepsilon} = \omega$ to a high degree of accuracy, as the damping rates Λ_γ and Λ_ε are generally at least an order of magnitude smaller than

the trapping frequency ω. Defining the steady state solution

$$\mathbf{u}_s(t) = \int_{-\infty}^{t} \exp\left[-\mathbf{\Lambda}(t-t')\right] \mathbf{B} d\mathbf{W}(t') \tag{6.38}$$

we find the steady-state correlations

$$\begin{aligned} \mathbf{G}(\tau) &\equiv \langle \mathbf{u}_s(t), \mathbf{u}_s^{\intercal}(t+\tau) \rangle \\ &= \int_{-\infty}^{\min(t,t+\tau)} \exp\left[-\mathbf{\Lambda}(t-t')\right] \mathbf{B}\mathbf{B}^{\intercal} \exp\left[-\mathbf{\Lambda}^{\intercal}(t+\tau-t')\right] dt' \end{aligned} \tag{6.39}$$

and steady-state spectra

$$\mathbf{S}(\omega) = \frac{1}{2\pi}(\mathbf{\Lambda} + i\Omega)^{-1}\mathbf{B}\mathbf{B}^{\intercal}(\mathbf{\Lambda}^{\intercal} - i\Omega)^{-1}. \tag{6.40}$$

The steady-state correlations of the centre of mass position and momentum are

$$G_{r_j r_j}(\tau) = -\frac{k_B T}{Nm} \frac{1}{\omega \omega_{\gamma\varepsilon}} e^{-(\Lambda_\gamma + \Lambda_\varepsilon)|\tau|} \sin\left(\omega_{\gamma\varepsilon}|\tau| - \sin^{-1}\left(\frac{\omega_{\gamma\varepsilon}}{\omega}\right)\right), \tag{6.41}$$

$$G_{p_j p_j}(\tau) = \frac{m k_B T}{N} \frac{\omega}{\omega_{\gamma\varepsilon}} e^{-(\Lambda_\gamma + \Lambda_\varepsilon)|\tau|} \sin\left(\omega_{\gamma\varepsilon}|\tau| + \sin^{-1}\left(\frac{\omega_{\gamma\varepsilon}}{\omega}\right)\right), \tag{6.42}$$

and the steady-state cross-correlation of position and momentum is

$$G_{p_j r_j}(\tau) = \frac{k_B T}{N} \frac{1}{\omega_{\gamma\varepsilon}} e^{-(\Lambda_\gamma + \Lambda_\varepsilon)|\tau|} \sin\left(\omega_{\gamma\varepsilon}\tau\right). \tag{6.43}$$

The exponential decay envelope has a decay rate given by the sum of the two damping rates, as one may naively expect. Interesting is that the modulation of the frequency is given by the difference in the damping rates, such that if both rates were equal then there would be no change in the frequency. This does suggest a potential signature for the presence of both damping processes, though in practice the frequency shift is almost certainly too small to be detected experimentally. The power spectra are

$$S_{r_j r_j}(\Omega) = \frac{2k_B T}{N\pi m\omega^2} \frac{\Lambda_\varepsilon(4\Lambda_\gamma\Lambda_\varepsilon + \omega^2) + \Lambda_\gamma\Omega^2}{(4\Lambda_\gamma\Lambda_\varepsilon + \omega^2)^2 - 2(\omega^2 - 2(\Lambda_\varepsilon^2 + \Lambda_\gamma^2))\Omega^2 + \Omega^4}, \tag{6.44}$$

$$S_{p_j p_j}(\Omega) = \frac{2k_B T m}{N\pi} \frac{\Lambda_\gamma(4\Lambda_\gamma\Lambda_\varepsilon + \omega^2) + \Lambda_\varepsilon\Omega^2}{(4\Lambda_\gamma\Lambda_\varepsilon + \omega^2)^2 - 2(\omega^2 - 2(\Lambda_\varepsilon^2 + \Lambda_\gamma^2))\Omega^2 + \Omega^4}, \tag{6.45}$$

$$S_{p_j r_j}(\Omega) = \frac{2ik_B T}{N\pi} \frac{(\Lambda_\gamma + \Lambda_\varepsilon)\Omega}{(4\Lambda_\gamma\Lambda_\varepsilon + \omega^2)^2 - 2(\omega^2 - 2(\Lambda_\varepsilon^2 + \Lambda_\gamma^2))\Omega^2 + \Omega^4}. \tag{6.46}$$

	N_T								
	10^4			10^5			10^6		
	T/T_c								
	0.65	0.75	0.85	0.65	0.75	0.85	0.65	0.75	0.85
$k_BT/\hbar\omega$	13	15	17	28	33	37	61	71	80
$\epsilon_{\rm cut}/\hbar\omega$	7.9	8.6	9.2	18	19	20	39	42	44
$\mu/\hbar\omega$	3.6	3.2	2.6	9.1	7.9	6.3	23	20	15
$\gamma \times 10^4$	0.80	0.81	0.84	2.0	1.9	1.9	4.9	4.4	4.2
$\mathcal{M}/a_\omega^2 \times 10^4$	3.2	2.9	2.7	3.6	3.1	2.7	4.1	3.3	2.8
$N_{\rm TF}/N_T$	0.60	0.44	0.26	0.61	0.43	0.24	0.58	0.41	0.22

Table 6.1: Table of parameters.

6.5.2 Numeric solutions

We choose for our simulations a trapping frequency of $\omega = 2\pi \times 10$ Hz. We choose physically consistent reservoir parameters for ^{87}Rb atoms using the Hartree-Fock parameter estimation scheme described in [2]. We consider a range of total particle numbers and temperatures from $N_T \in \left[10^4, 10^5, 10^6\right]$ and $T/T_c \in [0.65, 0.75, 0.85]$, giving a total of 9 parameter sets. We summarize the resulting reservoir parameters in Table 6.1. Our initial condition is given by (6.8) with $\mathbf{r}(0) = \mathbf{p}(0) = 0$. We evolve 100 trajectories of this initial state for each set of the reservoir parameters presented in Table 6.1.

In Fig. 6.1 we show the numeric and analytic position-position variances. Generally the steady-state is reasonably well predicted. For $T/T_c = 0.65$ for all values of N_T, the variance appears to be converging to the predicted value, however for $T/T_c = 0.85$, particularly for $N_T = 10^6$, the variance appears to be converging to a somewhat lower than predicted value. The fluctuations can be reduced by using larger ensembles; we chose to explore several parameter sets with relatively small ensembles rather than focus on a single parameter set with a large ensemble. We note that there still a large amount of noise present in the variance. An ensemble of 100 trajectories per parameter set is not all that large, however

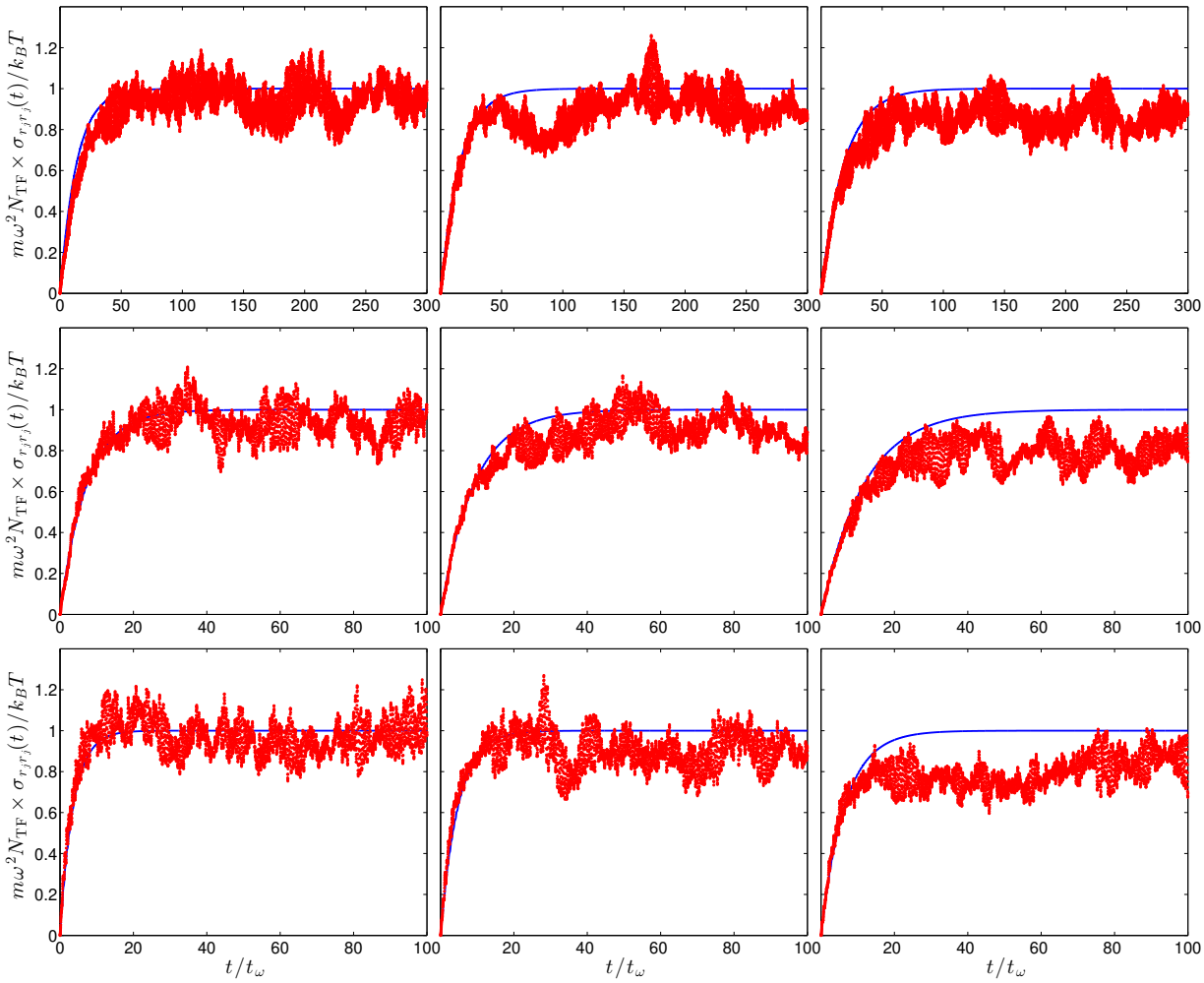

Figure 6.1: Variance of the centre of mass position for our parameter sets, with the analytic expression (6.35) in blue and the numeric data in red. The parameter sets are left column: $T/T_c = 0.65$, middle column: $T/T_c = 0.75$, right column: $T/T_c = 0.85$, top row: $N_T = 10^4$, middle row: $N_T = 10^5$, bottom row: $N_T = 10^6$.

appreciably reducing the noise in the variance would require a significantly larger number of trajectories, ideally at least an order of magnitude, as the error in the variance scales like the square root of the number of trajectories. Noting it took on the order of 10^4 hours of computing time to obtain the initial 100, pursuing this with our current resources for every parameter set is infeasible.

Fig. 6.2 shows the numeric and analytic steady-state position-position correlations. When calculating the correlations from the numeric data, we have assumed that the system

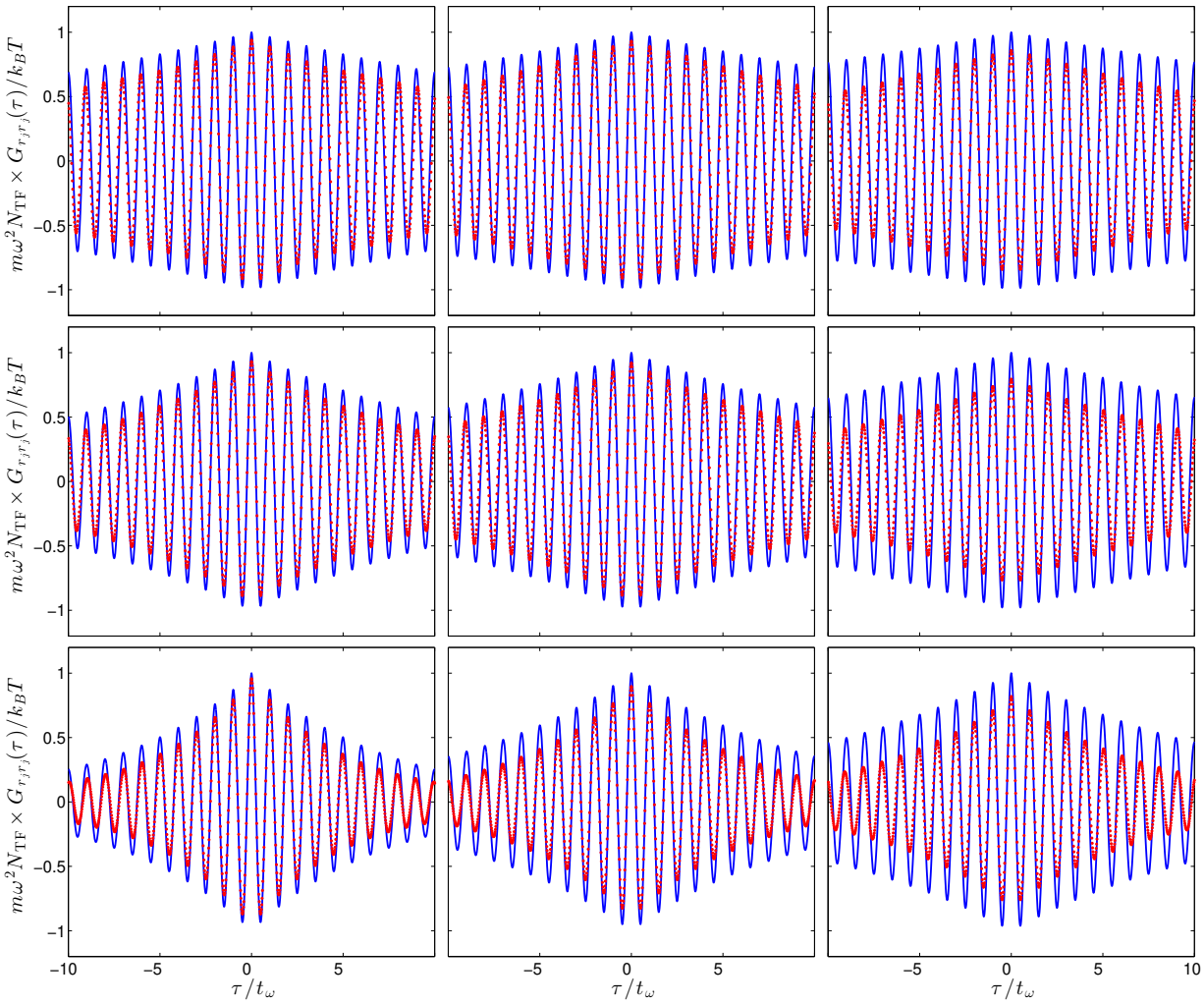

Figure 6.2: Equilibrium centre of mass position correlations for our parameter sets, with the analytic expression (6.41) in blue and the numeric data in red. The parameter sets are left column: $T/T_c = 0.65$, middle column: $T/T_c = 0.75$, right column: $T/T_c = 0.85$, top row: $N_T = 10^4$, middle row: $N_T = 10^5$, bottom row: $N_T = 10^6$.

has reached equilibrium after 150 trap cycles ($t = 150/\omega$) for $N_T = 10^4$, and 50 trap cycles ($t = 50/\omega$) for $N_T = 10^5$ and $N_T = 10^6$. Generally, the agreement between analytic predictions and numeric results worsens for increasing temperature; this is unsurprising as the true wave function departs from the ansatz more at higher temperatures. There does not appear to be any similar trend in the total particle number, with the intermediate value of $N_T = 10^5$ for $T/T_c = 0.65$ showing the best agreement of any parameter set. However, the deterioration in agreement with respect to temperature does appear to be enhanced for

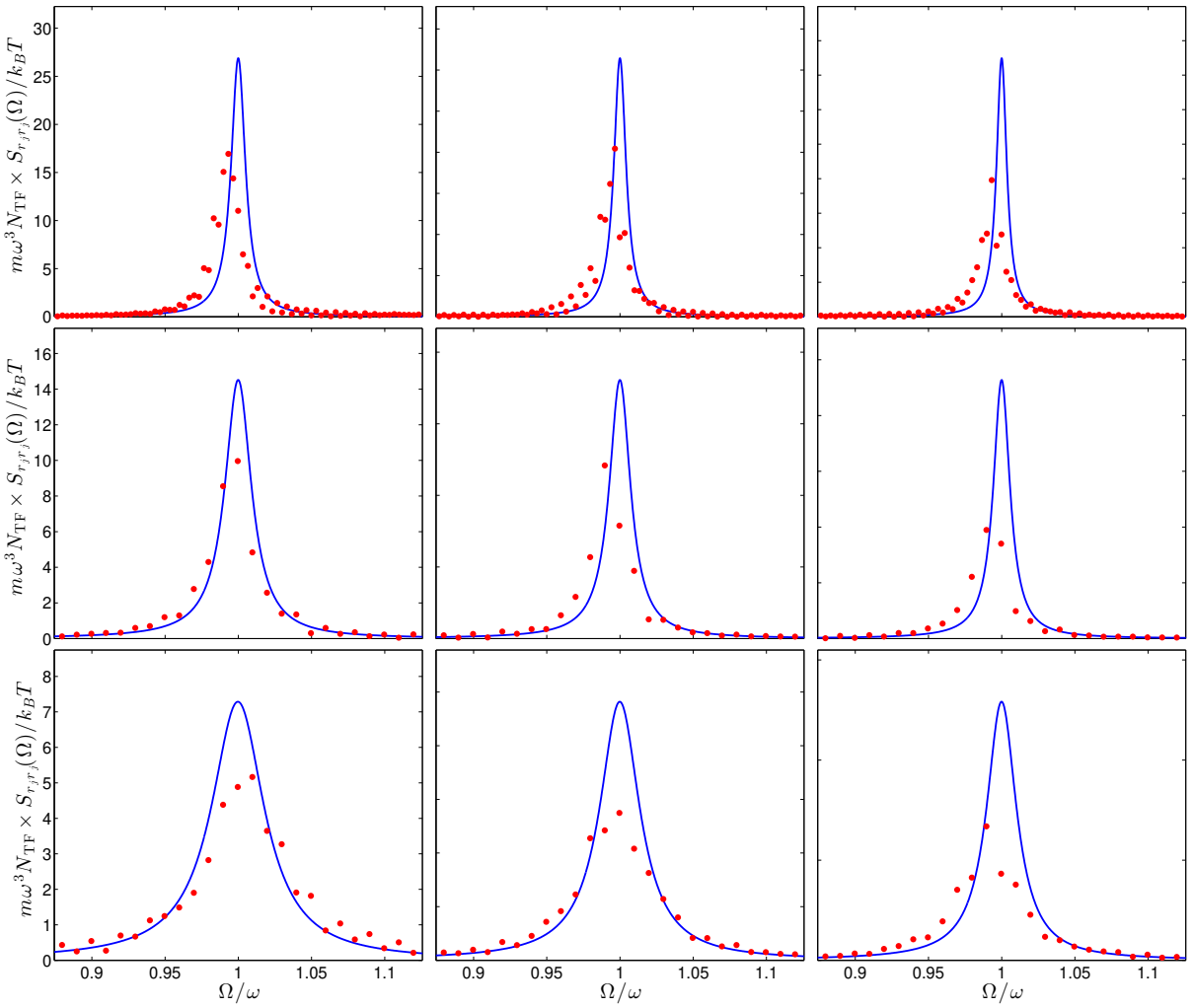

Figure 6.3: Equilibrium centre of mass position spectra for our parameter sets, with the analytic expression (6.44) in blue and the numeric data in red. The parameter sets are left column: $T/T_c = 0.65$, middle column: $T/T_c = 0.75$, right column: $T/T_c = 0.85$, top row: $N_T = 10^4$, middle row: $N_T = 10^5$, bottom row: $N_T = 10^6$.

larger particle number. This disagreement manifests in two aspects; the peak value of the correlation is less than predicted, and the exponential decay envelope has a higher decay rate than predicted.

Finally, in Fig. 6.3 we show the numeric and analytic steady-state position-position spectra, obtained using the Wiener-Khinchin theorem applied to the numeric steady-state correlations. There is some agreement between analytic predictions and numeric results; the line-width appears to be correct and the height of the spectral peak is relatively close

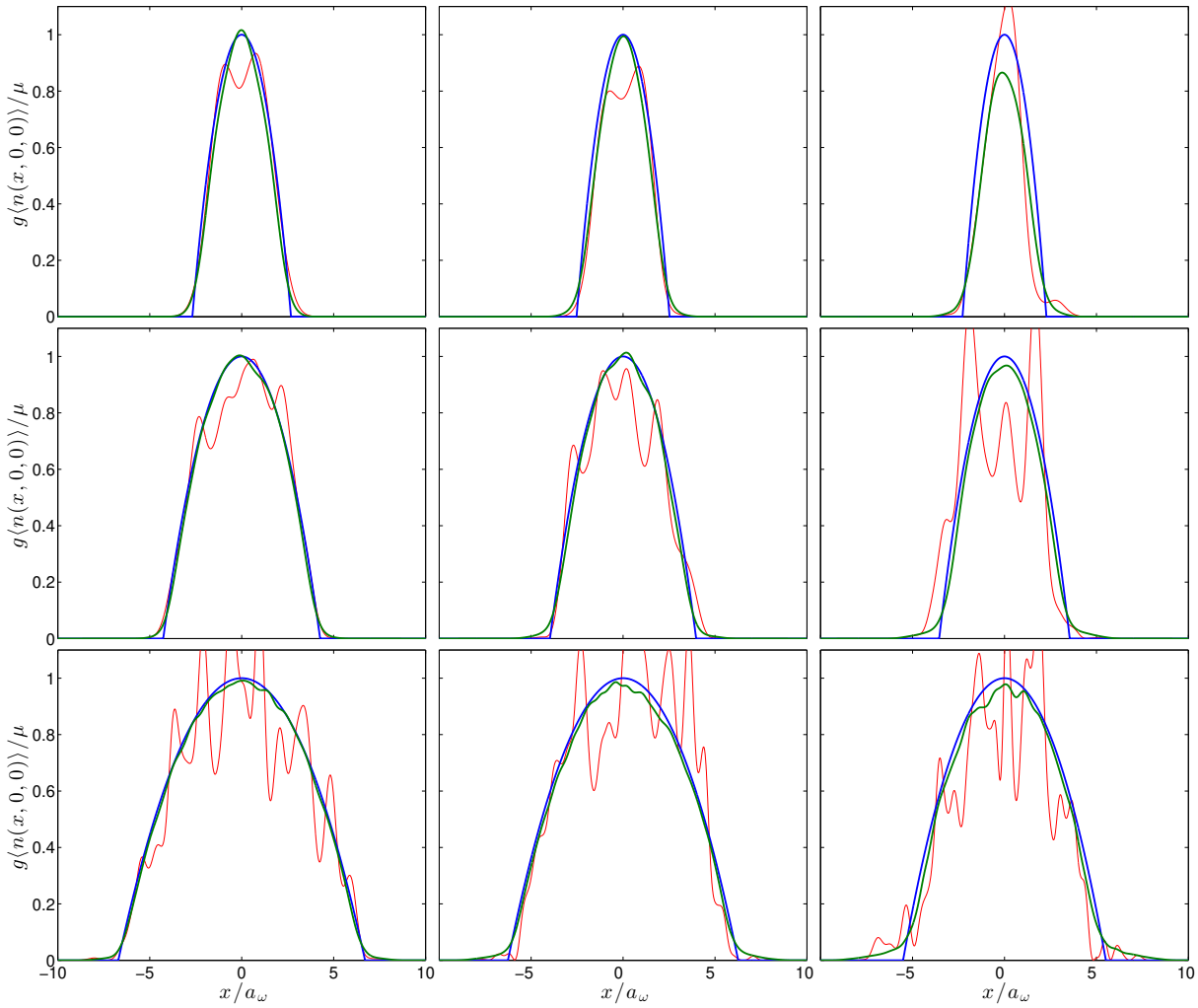

Figure 6.4: x-coordinate cross sections of the scaled system densities with blue given by the ansatz (6.8) and the numeric data in green. The numeric data is the ensemble average of the final densities for each parameter set. Also shown is a single trajectory of the density in red. The parameter sets are left column: $T/T_c = 0.65$, middle column: $T/T_c = 0.75$, right column: $T/T_c = 0.85$, top row: $N_T = 10^4$, middle row: $N_T = 10^5$, bottom row: $N_T = 10^6$.

at least for the lower temperatures. For higher temperatures the height of the numeric spectra is decreased relative to the analytic predictions. The location of the spectral peak also seems to be at a slightly lower frequency than predicted; this may be a result of the higher than predicted decay rate observed in the correlations, and as expected is more pronounced at higher temperatures.

Overall, we see that while we may claim that the numeric results show good agreement with analytic predictions, we would not go so far as to say we have exact quantitative

agreement. This is not surprising, as the wave function ansatz was never expected to be exact when considering finite temperatures. Furthermore, the ansatz does not allow for the number of particles to vary, while the full SPGPE does include particle transfer between coherent region and the thermal cloud. With respect to the two reservoir interaction processes, our results suggest that the two drift rates Λ_γ and Λ_ε to a very good approximation do encapsulate the effect of the reservoir interaction processes on the centre of mass motion of the condensate, and as such a comparison of these drift rates serves well as a comparison of the relative influence of the two processes. In addition, we commented earlier that measuring the frequency shift due to the damping and comparing with the exponential decay envelope could allow one to distinguish between the two damping processes. It is clear from our data that this would not be practical, as the frequency shift is almost certainly too small to be measured accurately in an experiment.

In Fig. 6.4 we show the x-coordinate cross sections of the scaled system densities $g|\psi(x,0,0)|^2/\mu$. Here we have taken the ensemble average of the final densities for each of the parameter sets. This serves as some measure of how well the ansatz (6.8) describes the system. The best agreement is for the $N_T = 10^5$ parameters. For the larger systems of $N_T = 10^6$ there is some apparent depletion at $x = 0$ that departs from the ansatz, while for the smaller systems of $N_T = 10^4$ the numeric solutions seem to be tending away from a Thomas-Fermi state and toward a Gaussian profile. We see from the single trajectory densities that the wave function is departing most significantly from the ansatz for larger particle numbers and higher temperatures. Indeed, given the amount of visible departure of individual densities from the ansatz it is remarkable that the numerical data and analytical predictions agree to such an extent.

6.5.3 Relative importance of damping processes

The effects of the energy-damping and number-damping reservoir interaction processes are represented on equal footing by the two diffusion rates Λ_ε and Λ_γ, in the sense that they manifest in the equation of motion (6.20) in the same fashion. We are therefore in a position where it makes sense to consider the relative importance of the two processes by considering the ratio of the diffusion rates

$$\frac{\Lambda_\varepsilon}{\Lambda_\gamma} = \frac{\mathcal{M}}{\gamma}\frac{35\omega}{48\pi^2 a_s}\sqrt{\frac{m}{2\mu}}. \tag{6.47}$$

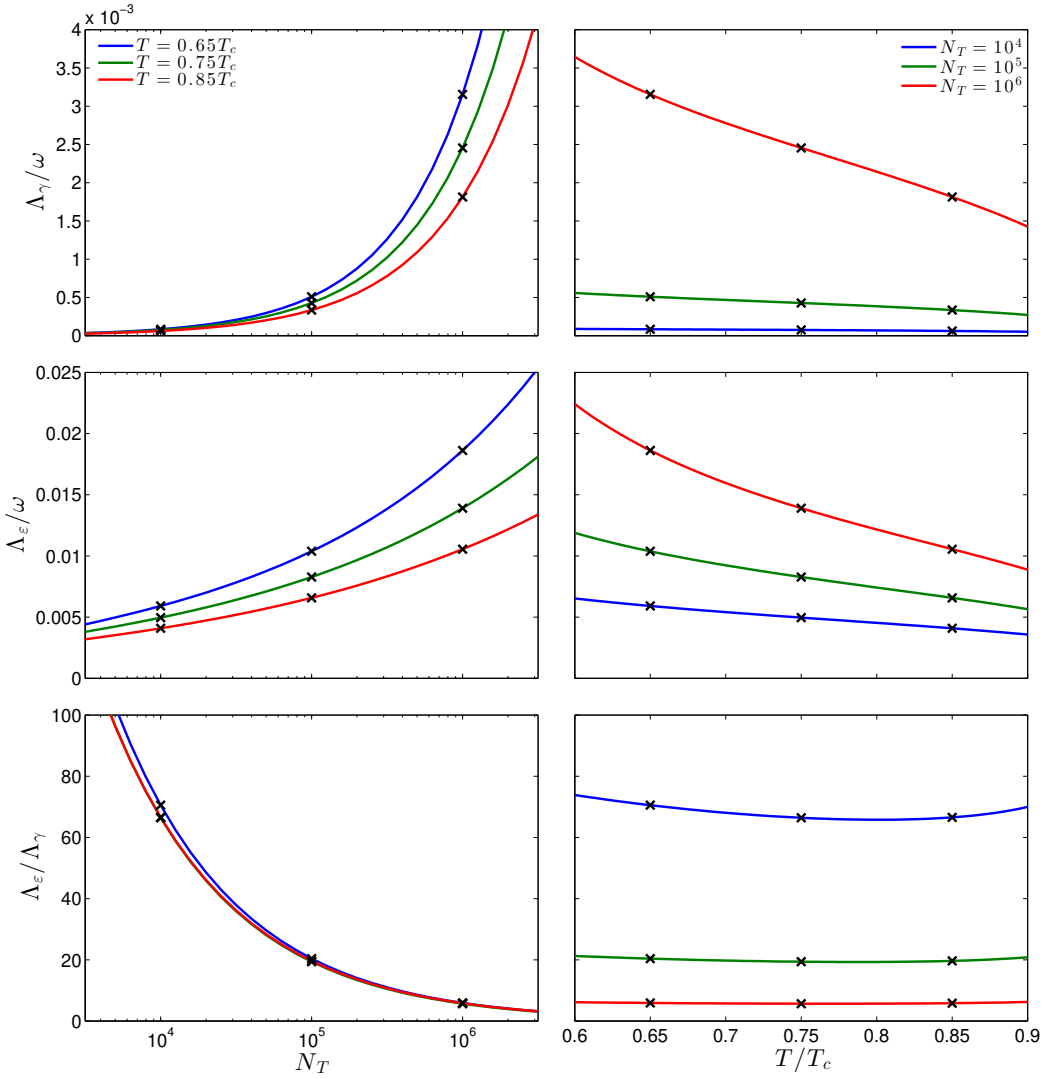

Figure 6.5: The damping rates Λ_γ and Λ_ε (6.19) for a range of total particle number N_T and temperature T/T_c. The black crosses indicate the parameters from Table 6.1.

Recalling the ratio of damping rates from Chapter 3, we get

$$\frac{\Lambda_\varepsilon}{\Lambda_\gamma} \approx \frac{35\hbar^2\omega}{48\Phi_0(\beta\mu)a_s}\sqrt{\frac{2}{m\mu^3}} \tag{6.48}$$

where $\Phi_0(\beta\mu)$ is typically on the order of unity. While not explicitly dependent on temperature, recall that the chemical potential $\mu \equiv \mu(N_T, T)$ is a function of the total particle number N_T and the temperature T, so there is implicit temperature dependence. The ratio indicates that there is scope to tune the relative effects of energy-damping and number-

damping, implicitly by varying the total particle number N_T or temperature T, but also explicitly by tuning the scattering length a_s (by using a Feshbach resonance) or modifying the trapping frequency ω.

In Fig. 6.5, we show the diffusion rates for a range of total particle numbers N_T and temperatures T/T_c, where we have used the Hartree-Fock parameter estimation scheme to obtain the appropriate SPGPE parameters. We see that the energy-damping diffusion rate is always larger than the number-damping rate for the systems we consider. For systems with less particles the energy-damping diffusion rate is dominant, nearing two orders of magnitude larger than the number-damping diffusion rate. For the more populous systems considered the ratio approaches unity, indicating this is a regime where the two damping processes have relatively equal influence. The relative influence of the two processes is largely independent of the system temperature.

6.5.4 Effective phenomenological number-damping constant

It is common when considering finite-temperature systems to parameterise the dissipation rate by a single phenomenological constant, such that the number-damping SPGPE can be applied. Using the Kohn mode damping rates, we can estimate a value for the effective number-damping rate required that most closely approximates the combined effect of both the true number-damping and energy-damping processes by setting

$$\Lambda_{\gamma'} \equiv \Lambda_\gamma + \Lambda_\varepsilon. \tag{6.49}$$

The effective number-damping rate γ' is then

$$\gamma' = \gamma + \frac{35\mathcal{M}\hbar^2 m}{12\pi g m R}. \tag{6.50}$$

In 6.6, we show the effective number-damping rate for a range of total particle numbers N_T and temperatures T/T_c, where we have used the Hartree-Fock parameter estimation scheme to obtain the appropriate SPGPE parameters. The effect number-damping rate is always larger relative to the bare number-damping rate, with the relative value becoming smaller for systems containing more particles; the relative value is largely independent of temperature. For smaller systems ($N_T < 10^4$) the effective number-damping rate can be larger than the bare number-damping rate by two orders of magnitude, while for larger systems ($N_T > 10^6$) the effective number-damping rate is larger only by a factor on the

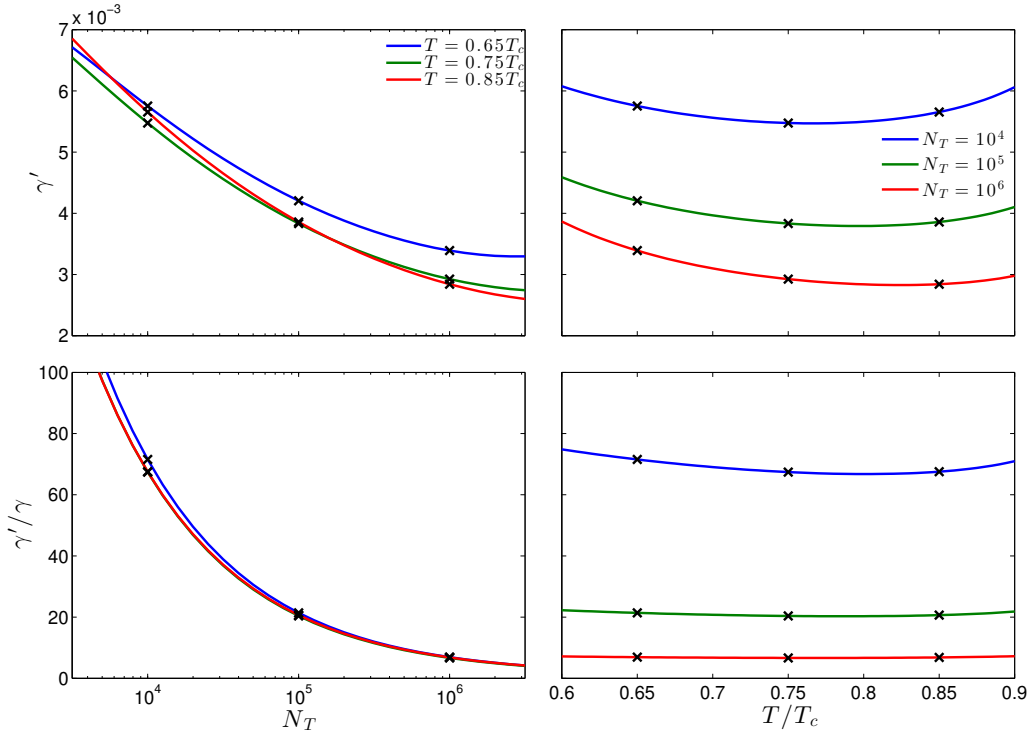

Figure 6.6: The effective number damping rate (6.50) (top) and the ratio of the effective number damping rate to the true number damping rate (bottom) for a range of total particle number N_T and temperature T/T_c. The black crosses indicate the parameters from Table 6.1.

order of unity.

In systems such as the one we have considered, it may be sufficient when making predictions for experiments using the SPGPE to include only the number-damping process with this appropriately modified number-damping rate. For systems where there is number conservation between the thermal cloud and coherent region using a modified number-damping rate is insufficient as it allows particle transfer.

6.6 Number dynamics

Here we briefly consider the effect of variable particle number on the system. Earlier we mentioned that one possible contributor to the partial non-agreement between the numeric simulations of the SPGPE and the analytic predictions for the centre of mass motion was that we had not accounted for potential particle transfer in our ansatz. A presumably

improved ansatz allowing for change in particle number is

$$\psi(\mathbf{r},t)=\sqrt{\frac{\mu_{\rm eff}(t)-\frac{1}{2}m\omega^2(\mathbf{r}-\mathbf{r}(t))^2}{g}}\exp\left[\frac{i\mathbf{r}\cdot\mathbf{p}(t)}{\hbar}\right],\quad \mu_{\rm eff}(t)>\frac{1}{2}m\omega^2(\mathbf{r}-\mathbf{r}(t))^2 \tag{6.51}$$

where

$$\mu_{\rm eff}(t)=\left(\frac{15gm^{3/2}\omega^3N(t)}{16\pi\sqrt{2}}\right)^{2/5}, \tag{6.52}$$

that is, we allow for an instantaneous Thomas-Fermi distribution with dynamical population. The position, momentum, and number are

$$\begin{aligned}
R_j(t) &= N(t)r_j(t) && (6.53)\\
P_k(t) &= N(t)p_k(t) && (6.54)\\
N(t) &= N_{\rm TF}\left(\frac{\mu_{\rm eff}(t)}{\mu}\right)^{5/2}. && (6.55)
\end{aligned}$$

Using the stochastic Ehrenfest relations we can then obtain a set of three coupled equations of motion for $R_j(t)$, $P_k(t)$, and $N(t)$

$$\begin{aligned}
(\mathbf{I})dR_j(t) &= \frac{1}{m}P_j(t)dt+\frac{2\gamma\mu}{7\hbar}\left(7-9\left(\frac{N(t)}{N_{\rm TF}}\right)^{2/5}\right)R_j(t)dt\\
&\quad -\frac{\gamma m\omega^2}{\hbar N(t)^2}\left(\sum_{i=1}^{3}R_i(t)^2\right)R_j(t)dt+dW_\gamma^{R_j}(t) && (6.56)\\
(\mathbf{I})dP_k(t) &= -m\omega^2R_k(t)dt+\frac{2\gamma\mu}{\hbar}\left(1-\left(\frac{N(t)}{N_{\rm TF}}\right)^{2/5}\right)P_k(t)dt\\
&\quad -\frac{\gamma m\omega^2}{\hbar N(t)^2}\left(\sum_{i=1}^{3}R_i(t)^2\right)P_k(t)dt-\frac{16\mathcal{M}\mu^3\hbar}{9g^2m^2\omega^2N(t)}\left(\frac{N(t)}{N_{\rm TF}}\right)^{6/5}P_k(t)dt\\
&\quad +dW_\varepsilon^{P_k}(t) && (6.57)\\
(\mathbf{I})dN(t) &= \frac{2\gamma\mu}{\hbar}\left(1-\left(\frac{N(t)}{N_{\rm TF}}\right)^{2/5}\right)N(t)dt-\frac{m\gamma\omega^2}{\hbar N(t)}\left(\sum_{i=1}^{3}R_i(t)^2\right)\\
&\quad +dW_\gamma^{N}(t), && (6.58)
\end{aligned}$$

where the non-vanishing noise correlations are

$$\langle dW_\gamma^{R_j}(t)dW_\gamma^{R_j}(t)\rangle = \left(\frac{8\gamma k_B T\mu N(t)}{7m\omega^2\hbar}\left(\frac{N(t)}{N_{\rm TF}}\right)^{2/5}+\frac{4\gamma k_B T R_j(t)^2}{\hbar N(t)}\right)dt, \quad (6.59)$$

$$\langle dW_\gamma^{N}(t)dW_\gamma^{N}(t)\rangle = \frac{4\gamma k_B T}{\hbar}N(t)dt, \quad (6.60)$$

$$\langle dW_\varepsilon^{P_k}(t)dW_\varepsilon^{P_k}(t)\rangle = \frac{32\mathcal{M}k_B T\mu^3\hbar}{9g^2m\omega^2}\left(\frac{N(t)}{N_{\rm TF}}\right)^{6/5}dt, \quad (6.61)$$

$$\langle dW_\gamma^{R_j}(t)dW_\gamma^{P_k}(t)\rangle = \frac{4\gamma k_B T}{N\hbar}P_k(t)R_j(t)dt, \quad (6.62)$$

$$\langle dW_\gamma^{N}(t)dW_\gamma^{R_j}(t)\rangle = \frac{4\gamma k_B T}{\hbar}R_j(t)dt, \quad (6.63)$$

$$\langle dW_\gamma^{N}(t)dW_\gamma^{P_k}(t)\rangle = \frac{4\gamma k_B T}{\hbar}P_k(t)dt. \quad (6.64)$$

These equations have a more complicated dependence on time compared to (6.15), as well as significant coupling. Let us again limit our considerations to a system with only small amplitude oscillations away from the origin, as would be the case in equilibrium, so we retain only terms that are at most linear in $P_k(t)$ and $R_j(t)$. The equations of motion are now

$$(\mathbf{I})dR_j(t) = \frac{1}{m}P_j(t)dt+\frac{2\gamma\mu}{7\hbar}\left(7-9\left(\frac{N(t)}{N_{\rm TF}}\right)^{2/5}\right)R_j(t)dt+dW_\gamma^{R_j}(t) \quad (6.65)$$

$$\begin{aligned}(\mathbf{I})dP_k(t) &= -m\omega^2R_k(t)dt-\frac{16\mathcal{M}\mu^3\hbar}{9g^2m^2\omega^2N(t)}\left(\frac{N(t)}{N_{\rm TF}}\right)^{6/5}P_k(t)dt\\ &\quad+\frac{2\gamma\mu}{\hbar}\left(1-\left(\frac{N(t)}{N_{\rm TF}}\right)^{2/5}\right)P_k(t)dt+dW_\varepsilon^{P_k}(t)\end{aligned} \quad (6.66)$$

$$(\mathbf{I})dN(t) = \frac{2\gamma\mu}{\hbar}\left(1-\left(\frac{N(t)}{N_{\rm TF}}\right)^{2/5}\right)N(t)dt+\frac{2\gamma k_B TM}{\hbar}dt+dW_\gamma^{N}(t). \quad (6.67)$$

In this regime, the particle number equation of motion is independent of the position and momentum[3]. Furthermore, the evolution of the particle number has no dependence on the energy-damping rate. This suggests a potential route to distinguish between the two reservoir interaction processes in the same system; the centre of mass motion we have already seen is dominated by the effects of energy-damping, while particle number

[3]The noise in the number equation of motion is still correlated with $P_k(t)$ and $R_j(t)$. However since the norm is independent of these, the evolution of the particle is independent of those.

dynamics are governed only by number-damping. We now consider the properties of the number equation.

6.6.1 Number equation

The particle number equation of motion is

$$(\mathbf{I})dN(t) = \frac{2\gamma\mu}{\hbar}\left(1-\left(\frac{N(t)}{N_{\mathrm{TF}}}\right)^{2/5}\right)N(t)dt + \frac{2\gamma k_B T M}{\hbar}dt + \sqrt{\frac{4\gamma k_B T N(t)}{\hbar}}dW(t), \tag{6.68}$$

where $dW(t)$ is a Wiener process with unit correlations[4]

$$\langle dW(t)dW(t)\rangle = dt. \tag{6.69}$$

If we neglect the latter two terms in (6.68) (the trace and noise terms) as being much smaller than the preceding term, we obtain a deterministic equation which we can solve analytically. Physically this represents the particle number being far from the equilibrium. Letting

$$\alpha = \frac{2\gamma\mu}{\hbar}, \quad \beta = \frac{\alpha}{N_{\mathrm{TF}}^{2/5}}, \tag{6.70}$$

we have the ordinary differential equation

$$\dot{N}(t) \approx \alpha N(t) - \beta N(t)^{7/5}, \tag{6.71}$$

which has the analytic solution

$$N(t) \approx \left(\frac{\alpha N_0^{2/5} e^{2\alpha t/5}}{\alpha + \beta N_0^{2/5}\left(e^{2\alpha t/5}-1\right)}\right)^{5/2} \tag{6.72}$$

where $N_0 \equiv N(0)$. This equation predicts the equilibrium particle number to be just the Thomas-Fermi value N_{TF}, however using (6.72) to predict equilibrium properties is inconsistent with the neglect of the trace and noise terms, as it is precisely when close to equilibrium that we expect these to be significant. Let us assume that in equilibrium the

[4]Since we are no linger considering any cross-correlations, we may as well write the noise as a unit Wiener process with explicit norm.

particle number is not too different from the Thomas-Fermi value, that is

$$\lim_{t\to\infty} N(t) = N_{\rm TF} + N_\gamma(t) \tag{6.73}$$

where $N_\gamma(t)$ is stochastic and small with all moments time-independent. Substituting this into (6.68) and retaining only linear in $N_\gamma(t)$ leads to

$$(\mathbf{I})dN_\gamma(t) \;=\; -\frac{4\gamma\mu}{5\hbar}N_\gamma(t)dt + \frac{2\gamma k_B T M}{\hbar}dt + \sqrt{\frac{4\gamma k_B T}{\hbar}\left(N_{\rm TF}+N_\gamma(t)\right)}dW_{04}(t), \tag{6.74}$$

an Ornstein-Uhlenbeck process with mean value $5k_BTM/2\mu$. The mean particle number in equilibrium is thus predicted to be

$$\bar{N} \;\approx N_{\rm TF} + \frac{5Mk_BT}{2\mu}. \tag{6.75}$$

In our parameter sets, the size of this correction is very small, and is thus neglected.

6.6.2 Linearized Fluctuations

To investigate the steady state properties of the particle number, we write the particle number as $N(t) = \bar{N} + \delta N(t)$, where $\bar{N}$ is the equilibrium particle number, and $\delta N(t)$ is small with zero mean. Then, taking only linear contributions, the equation of motion for $\delta N(t)$ is

$$d\delta N(t) = -\frac{2\gamma\mu}{\hbar}\left(\frac{7}{5}\left(\frac{\bar{N}}{N_{\rm TF}}\right)^{2/5} - 1\right)\delta N(t)dt + \sqrt{\frac{4\gamma k_B T\bar{N}}{\hbar}}dW_{04}(t). \tag{6.76}$$

If we assume that the equilibrium particle number is very close to the Thomas-Fermi particle number, then

$$d\delta N(t) \approx -\frac{4\gamma\mu}{5\hbar}\delta N(t)dt + \sqrt{\frac{4\gamma k_B T\bar{N}}{\hbar}}dW_{04}(t). \tag{6.77}$$

This is then the equation for an Ornstein-Uhlenbeck process, and as such we can easily find the properties analytically. The steady-state time correlation is

$$\langle\delta N(t)\delta N(t+\tau)\rangle = \frac{5k_BT\bar{N}}{2\mu}\exp\left[-\frac{4\gamma\mu}{5\hbar}|\tau|\right], \tag{6.78}$$

or in normalized form

$$g_N(\tau) \equiv \frac{\langle \delta N(t)\delta N(t+\tau)\rangle}{\langle \delta N(t)^2\rangle} = \exp\left[-\frac{4\gamma\mu}{5\hbar}|\tau|\right], \tag{6.79}$$

and the steady-state variance is

$$\langle \delta N(t)^2\rangle = \frac{5k_BT\bar{N}}{2\mu}. \tag{6.80}$$

To check the number dynamics alone, we have performed simulations for a Thomas-Fermi-like initial state with a non-equilibrium particle number. Specifically, we have chosen $\mu_{\rm eff}(0)$ in (6.51) such that the initial particle number is $N_0 = 1.2N_{\rm TF}$. In Fig. 6.7(a) we show evolution of the particle number to equilibrium for several values of the energy-damping rate $\mathcal{M}$ relative to the number-damping rate γ. Each of these is the average of 20 trajectories. Aside from the differing values of $\mathcal{M}$, the parameters used in each trajectory are the same as for the ($N_T = 10^5$, $T/T_c = 0.75$) system considered in the previous section. We see that, as predicted, both the equilibrium particle number and the rate at which the initial particle number evolves to this is independent of the energy-damping rate. The analytic expression (6.72) does not match the numeric data; the equilibrium particle number reached is lower than that predicted. However, using (6.72) but replacing the Thomas-Fermi particle number $N_{\rm TF}$ with the observed equilibrium particle number gives excellent agreement with the numeric data. One might suggest that we could fix things by using $\bar{N}$ as predicted by (6.75), which is reasonable. However $\bar{N}$ is strictly larger than $N_{\rm TF}$, while the observed equilibrium particle number is less. It is clear then that this is not the reason for the discrepancy. It appears that while the predicted equilibrium is incorrect, the rate of approach to the equilibrium is still well predicted by the analytics.

In Fig. 6.7(b) we show the variance in particle number over time. The steady-state of the variance from the numeric results appears to match the prediction from the analytics, exhibiting fluctuations about the value (6.80); a larger number of trajectories would decrease the size of these fluctuations. We also have calculated the steady-state correlations of particle number fluctuations, shown in 6.7(c), for $t = 500t_\omega$, and compared to the analytic prediction (6.79). The numeric data agrees very well with the analytic expression.

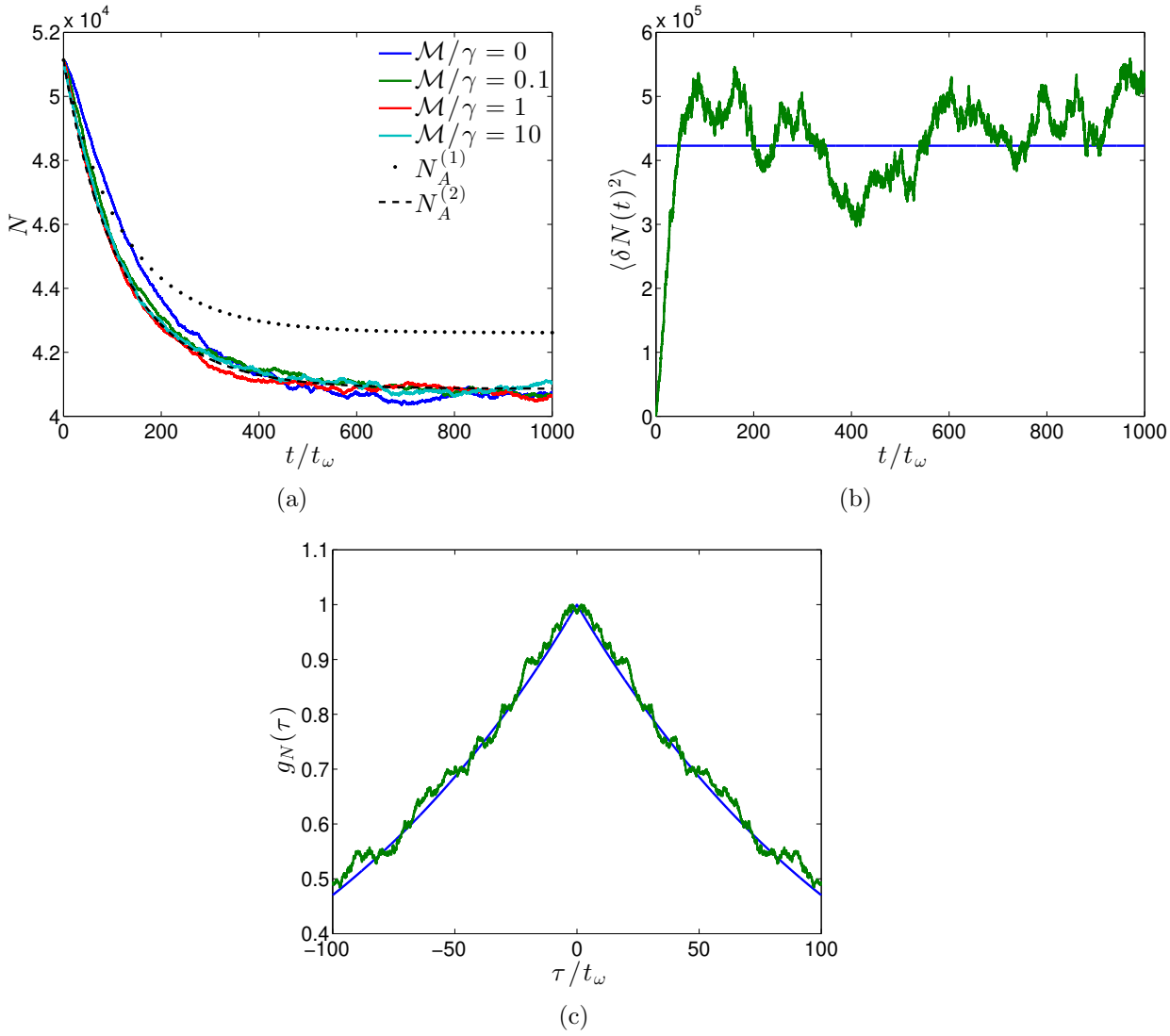

Figure 6.7: (a) Particle number over time for several values of the energy-damping rate $\mathcal{M}$ relative to the number-damping rate γ, taking the mean of 20 trajectories for each (solid coloured lines). Also shown is the analytic expression (6.72) (black dotted line), and (6.72) again but with N_{TF} replaced by the numerically observed equilibrium particle number (black dashed line)(b) Particle number variance over time, showing the numeric result (green) and the predicted steady-state (6.80) (blue) (c) Normalized time correlations for particle number fluctuations at $t = 500t_\omega$, showing the numeric result (green) and the predicted steady-state (6.79).

6.7 Energy-damped system: second component thermal cloud

Earlier we mentioned that one possible contributor to the partial non-agreement between the numeric simulations of the SPGPE and the analytic predictions for the centre of mass motion was that we had not accounted for potential particle transfer in our ansatz. Here we briefly consider a system where this would not be an issue; a highly degenerate component (i.e. effectively no thermal component) in the presence of a distinct thermalized component (i.e effectively no coherent region). This can be achieved in a two-component system at temperature T such that $T_{c,2} \lesssim T \ll T_{c,1}$, where $T_{c,i}$ is the critical temperature for Bose-Einstein condensation of the ith component. This scenario is relevant when using sympathetic cooling to achieve Bose-Einstein condensation. Again assuming small $r_j(t)$ and $p_j(t)$ we have the two equations of motion

$$dr_j(t) = \frac{1}{m} p_j(t) dt \tag{6.81}$$

$$dp_j(t) = -m\omega^2 r_j(t) dt - 2\Lambda_\varepsilon p_j(t) dt + \sqrt{\mathcal{D}_\varepsilon} dW_{j2}(t). \tag{6.82}$$

This can also be represented as a single equation in the Langevin form

$$\ddot{r_j}(t) + 2\Lambda_\varepsilon \dot{r_j}(t) + \omega^2 r_j(t) = \sqrt{\frac{\mathcal{D}_\varepsilon}{m^2}} \vartheta_j(t) \tag{6.83}$$

where $\vartheta_j(t)$ are independent white noises with correlations

$$\langle \vartheta_j(t) \vartheta_i(t') \rangle = \delta_{ij} \delta(t - t'). \tag{6.84}$$

Defining the new frequency

$$\omega_\varepsilon \equiv \sqrt{\omega^2 - \Lambda_\varepsilon^2}, \tag{6.85}$$

the variances are

$$\boldsymbol{\sigma}_{r_j r_j}(t) = \frac{k_B T}{N_{\rm TF} m\omega^2}\left[1 + e^{-2\Lambda_\varepsilon t}\left(\frac{\Lambda_\varepsilon^2}{\omega_\varepsilon^2}\cos\left(2\omega_\varepsilon t\right) + \frac{\Lambda_\varepsilon}{\omega_\varepsilon}\sin\left(2\omega_\varepsilon t\right) - \frac{\omega^2}{\omega_\varepsilon^2}\right)\right] \quad (6.86)$$

$$\boldsymbol{\sigma}_{p_j p_j}(t) = \frac{m k_B T}{N_{\rm TF}}\left[1 + e^{-2\Lambda_\varepsilon t}\left(\frac{\Lambda_\varepsilon^2}{\omega_\varepsilon^2}\cos\left(2\omega_\varepsilon t\right) - \frac{\Lambda_\varepsilon}{\omega_\varepsilon}\sin\left(2\omega_\varepsilon t\right) - \frac{\omega^2}{\omega_\varepsilon^2}\right)\right] \quad (6.87)$$

$$\boldsymbol{\sigma}_{p_j r_j}(t) = -\frac{2k_B T\Lambda_\varepsilon}{N_{\rm TF}\omega_\varepsilon^2} e^{-2\Lambda_\varepsilon t}\sin^2\left(\omega_\varepsilon t\right). \quad (6.88)$$

The steady-state correlations of the centre of mass position-position, momentum-momentum, and position-momentum are

$$G_{r_j r_j}(\tau) = -\frac{k_B T}{Nm}\frac{1}{\omega\omega_\varepsilon} e^{-\Lambda_\varepsilon|\tau|}\sin\left(\omega_\varepsilon|\tau| - \sin^{-1}\left(\frac{\omega_\varepsilon}{\omega}\right)\right), \quad (6.89)$$

$$G_{p_j p_j}(\tau) = \frac{m k_B T}{N}\frac{\omega}{\omega_\varepsilon} e^{-\Lambda_\varepsilon|\tau|}\sin\left(\omega_\varepsilon|\tau| + \sin^{-1}\left(\frac{\omega_\varepsilon}{\omega}\right)\right), \quad (6.90)$$

$$G_{p_j r_j}(\tau) = \frac{k_B T}{N}\frac{1}{\omega_\varepsilon} e^{-\Lambda_\varepsilon|\tau|}\sin\left(\omega_\varepsilon\tau\right). \quad (6.91)$$

while the power spectra are

$$S_{r_j r_j}(\Omega) = \frac{2k_B T}{N\pi m\omega^2}\frac{\Lambda_\varepsilon\omega^2}{\omega^4 - 2(\omega^2 - 2\Lambda_\varepsilon^2)\Omega^2 + \Omega^4}, \quad (6.92)$$

$$S_{p_j p_j}(\Omega) = \frac{2k_B T m}{N\pi}\frac{\Lambda_\varepsilon\Omega^2}{\omega^4 - 2(\omega^2 - 2\Lambda_\varepsilon^2)\Omega^2 + \Omega^4}, \quad (6.93)$$

$$S_{p_j r_j}(\Omega) = \frac{2ik_B T}{N\pi}\frac{\Lambda_\varepsilon\Omega}{\omega^4 - 2(\omega^2 - 2\Lambda_\varepsilon^2)\Omega^2 + \Omega^4}. \quad (6.94)$$

We have performed simulations for the parameter set ($N_T = 10^5$, $T/T_c = 0.75$), given by the central column of Table 6.1, with the one difference that we set $\gamma = 0$. The energy-damping reservoir interaction process is number-conserving, and so the number of particles in the coherent region remains at the Thomas-Fermi value $N_{\rm TF}$. The position-position variance, steady-state correlations, steady-state spectra, and the x-coordinate cross sections of the scaled system density are shown in Fig. 6.8, for an ensemble of 100 trajectories. Comparing these with those for the same parameter set including number-damping, shown as the centre plot in Fig. 6.1, Fig. 6.2, Fig. 6.3, Fig. 6.4 we see that removing the number-damping process has had very little effect on these properties of the system. From this it is clear that the neglect of particle variations in the initial ansatz

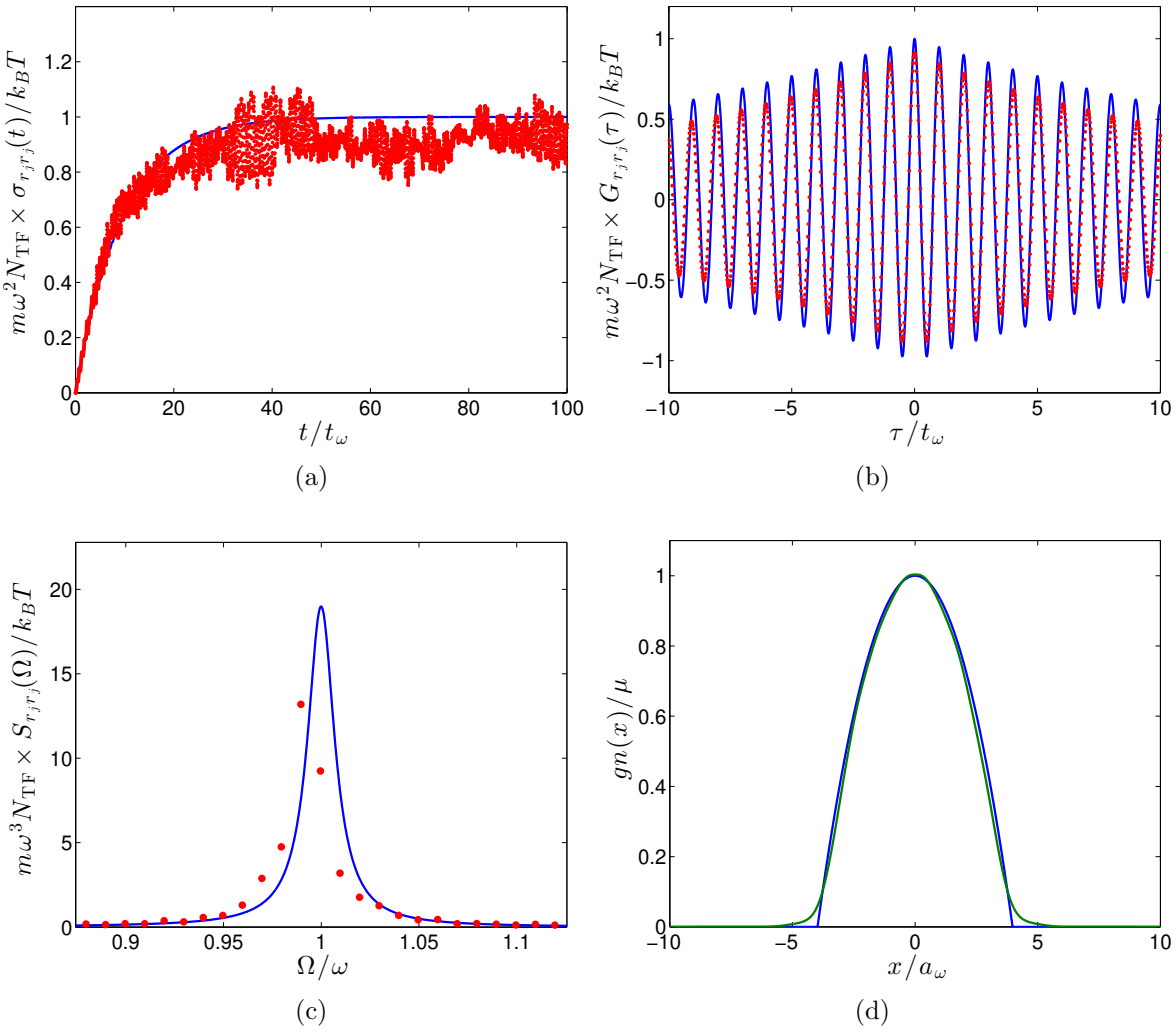

Figure 6.8: (a) Variance of the centre of mass position for the energy-damped system, with the analytic expression (6.86) in blue and the numeric data in red. (b) Equilibrium centre of mass position correlations for ($N_T = 10^5$, $T/T_c = 0.75$, $\gamma = 0$), with the analytic expression (6.89) in blue and the numeric data in red. (c) Equilibrium centre of mass position spectra ($N_T = 10^5$, $T/T_c = 0.75$, $\gamma = 0$), with the analytic expression (6.92) in blue and the numeric data in red. (d) x-coordinate cross sections of the scaled system density with blue given by the ansatz (6.8) and the numeric data in green.

is not the reason for any departure of the numeric data from the analytic predictions for the fully damped systems. We can then conclude that the cause of discrepancies between the analytical predictions and numerical results is the departure of the true wave function from the proposed ansatz.

6.8 Conclusion

In this chapter we considered the centre of mass motion of a finite temperature harmonically trapped degenerate Bose gas in the Thomas-Fermi regime. Using the stochastic Ehrenfest relations derived in Chapter 5, we obtained stochastic equations of motion for the centre of mass position and momentum, finding that they take the form of a vector Ornstein-Uhlenbeck process and thus admit well known analytic solutions. In these equations of motion the influence of the energy-damping reservoir interaction is on the same footing as the number-damping reservoir interaction process, allowing direct comparison of the two. Using the Hartree-Fock parameter estimation scheme developed in [2] we found physically consistent and experimentally obtainable parameters for the system, and used these to directly compare the relative strengths of the two reservoir interaction processes. For the range of temperatures and total particle numbers considered, we found that energy-damping is the dominant reservoir interaction process; when considering the centre of mass motion it would indeed be appropriate to neglect the number-damping entirely. This is in direct conflict with the general argument that energy-damping could only be dominant in highly non-equilibrium systems.

Including number dynamics in the initial ansatz was considered, however the resulting equations of motion are more complex and may not admit analytic solutions. Considering the number dynamics alone, we found that we could predict the rate of particle decay or growth to equilibrium well, but not the actual equilibrium particle number. The steady-state properties of the particle number fluctuations were found to be independent of energy-damping, and analytic predictions agreed well with the numeric data. We therefore have the potential for measuring signatures of the energy-damping process and number-damping process separately in the one system. The observation that number-damping dominates the particle number fluctuations while the energy-damping dominates the centre of mass motion is consistent with the results of the linear fluctuation analysis of Chapter 4, where we saw that the damping of large length scale excitations is mainly due to energy-damping while for small length scale excitations the damping is mainly due to number-damping.

Chapter 7

Stochastic single vortex motion in a disc

7.1 Introduction

In this chapter we consider the application of the stochastic Ehrenfest relations to the motion of a singly quantized vortex in a quasi-2D Bose-Einstein condensate (BEC). It is well known that a vortex in a finite system with a stationary thermal cloud is unstable and will travel to the edge of the system [2, 85, 122, 289]. The nature of a quantum vortex, in particular its topological stability and ability to be clearly imaged, make it an ideal platform for investigating dissipative properties in finite-temperature systems. We specifically consider the influence of the energy-damping reservoir interaction for a vortex confined to a circular hard-walled potential.

This chapter is organised as follows. We start in Section 7.2 with a short background of quantum vortices. In Section 7.3 we introduce the 2D form of the stochastic projected Gross-Pitaevskii equation (SPGPE) as derived in [286]. In Section 7.4 we reintroduce the stochastic Ehrenfest relation for the angular momentum as derived in Chapter 5, and modify it as appropriate to reflect our system. The vortex wave function ansatz is given in Section 7.5, as well as some of its important properties. In Section 7.6 we construct the stochastic differential equation for the motion of the vortex. The properties of this equation of motion are discussed in Section 7.7. We briefly consider the possibility of introducing a rotating thermal cloud in Section 7.8, which can result in the stabilization of the vortex. We comment on the requirements for numeric simulation of this system in Section 7.9, before concluding in Section 7.10.

7.2 Quantum vortices

Vortices are an essential component of fluid dynamics, both in classical and quantum physics, and are intrinsically linked to the nature of fluid turbulence [290–292]. In superfluids, quantum vortices manifest as topological defects with the fluid undergoing irrotational flow about the zero-density vortex core [293, 294]. Quantum vortices are one of the clearest signatures for the presence of superfluidity [11], appearing in a number of systems including superconductors [295], neutron stars [296], and ultra-cold gases [297].

To see how quantum vortices arise, we consider the mean-field description of a Bose-Einstein condensate. Within mean-field theory, the macroscopic wave function of a Bose-Einstein condensate can be written in terms of the particle density $n(\mathbf{r}, t)$ and phase $S(\mathbf{r}, t)$ as per the Madelung transformation [298, 299]

$$\psi(\mathbf{r}, t) = \sqrt{n(\mathbf{r}, t)} e^{iS(\mathbf{r},t)}. \tag{7.1}$$

If we then calculate the current density, we can identify the superfluid velocity by

$$\mathbf{v}(\mathbf{r}, t) = \frac{\hbar}{m} \nabla S(\mathbf{r}, t). \tag{7.2}$$

The phase thus acts as a potential for the velocity, and consequently the superfluid flow is irrotational as $\nabla \times \mathbf{v} = 0$ away from any phase singularities. The flow circulation around a closed path is defined as

$$\Gamma = \oint \mathbf{v} \cdot d\mathbf{l} = \frac{\hbar}{m} \Delta S, \tag{7.3}$$

where ΔS is the accumulated phase around the path. The accumulated phase is independent of the particular path taken due to the irrotational nature of the velocity field. The wave function must be a single valued function, so upon returning to the position $\mathbf{r}$ after traversing the path

$$\psi(\mathbf{r}, t) = \psi(\mathbf{r}, t) e^{i\Delta S}, \tag{7.4}$$

and therefore the change in phase is restricted to

$$\Delta S = 2\pi\kappa, \quad \kappa \in \mathbb{Z}. \tag{7.5}$$

The circulation is thus quantised in units of h/m

$$\Gamma = \kappa \frac{2\pi\hbar}{m} = \kappa \frac{h}{m}, \quad \kappa \in \mathbb{Z} \tag{7.6}$$

where the quantum number κ is the topological winding number of the phase around the integration path. Despite the superfluid flow being irrotational, angular momentum may be supported through the presence of vortices. A vortex is characterised by a zero density core and a non-zero topological winding number about any integration path containing the core. The superfluid flow remains irrotational everywhere except at the vortex core, where a phase singularity emerges as the density vanishes. For a vortex aligned with the z-axis the vorticity is given by a Dirac delta

$$\boldsymbol{\omega}(\mathbf{r}, t) = \nabla \times \mathbf{v}(\mathbf{r}, t) = \kappa \frac{h}{m} \delta^{(2)}(\mathbf{r} - \mathbf{r}_0)\hat{\mathbf{z}} \tag{7.7}$$

where $\mathbf{r}_0$ is the location of the vortex core. The topological winding number κ is the *charge* of the vortex. Vortices of charge $|\kappa| > 1$ in a Gross-Pitaevskii superfluid are unstable, and will rapidly decay into $|\kappa|$ vortices of charge ± 1 [293]. For a comprehensive review on the theory of vortices in trapped dilute Bose-Einstein condensates, we suggest the excellent review by Fetter and Svidzinsky [85].

The motion of quantum vortices is very sensitive to thermal fluctuations and other excitations [294]. Experimental studies on individual quantum vortices in Bose-Einstein condensates have included observations of stability [300, 301], dynamics [302–304], and generation via a rotating thermal cloud [108, 305]. These experiments, along with many others, demonstrate the variety of quantum vortex phenomena that can be observed, and as such the dissipative effects of reservoir interactions on the motion of quantum vortices is an area that requires a clear theoretical description.

The first theoretical studies of dissipative vortex dynamics used the Gross-Pitaevskii equation with additional phenomenological damping [221]. This was used to describe vortex lattice formation [222–224] and gain insight into quantum turbulence [75, 225, 226]. Single vortex decay has been studied using both the damped Gross-Pitaevskii equation [306] and Zaremba-Nikuni-Griffin [259, 260] formalisms. Stochastic Gross-Pitaevskii equations have allowed further study of single vortex decay both analytically [133, 307] and numerically [2, 120]. While there has been much theoretical study of dissipative vortex dynamics there has been little quantitative comparison with experiments. The simple-growth SPGPE was used to model spontaneous vortex formation during a quench [71], but did require a

fitted number-damping rate. Later, the simple-growth SPGPE was used to describe the persistent current formation experiment of Neely *et al* [75] with no fitted parameters [121]. The role of energy-damping in dissipative vortex dynamics has been largely ignored until recently [122], where simulations suggest energy damping may be a significant process.

7.3 Quasi 2D SPGPE

We consider a system with external trapping potential

$$V(\mathbf{r}) = H(R - |\mathbf{r}_\perp|) + \frac{1}{2}m\omega_z^2 z^2 = V(\mathbf{r}_\perp) + \frac{1}{2}m\omega_z^2 z^2, \tag{7.8}$$

where the axial trapping frequency ω_z is such that the axial harmonic oscillator length scale $a_z \equiv \sqrt{\hbar/(m\omega_z)}$ is much less than the disc radius R. The axial trapping is assumed to be strong enough that the transverse dynamics of the coherent region are suppressed, allowing an effective 2D representation to be found, but weak enough that the thermal cloud retains 3D characteristics. The reservoir interaction parameters $\mathcal{M}$ and γ are therefore unchanged from the 3D case, however the detailed form of the energy-damping effective potential is modified. Further discussion on this point, and the low dimensional SPGPE in general, can be found in [286]. For the quasi-2D system, where $\mathbf{r}_\perp \equiv (x, y) \equiv (r, \phi)$, the dimensionally reduced SPGPE [286] is

$$\begin{aligned}(\mathbf{S})\, d\psi(\mathbf{r}_\perp, t) = \mathcal{P}\Big\{ &-\frac{i}{\hbar}(1 - i\gamma)(L - \mu_2)\psi(\mathbf{r}_\perp, t)dt \\ &-\frac{i}{\hbar}V_\varepsilon(\mathbf{r}_\perp, t)\psi(\mathbf{r}_\perp, t)dt + dW(\mathbf{r}_\perp, t) + i\psi(\mathbf{r}, t)dU(\mathbf{r}_\perp, t)\Big\}.\end{aligned} \tag{7.9}$$

The 2D SPGPE explicitly includes the 2D GPE operator

$$L\psi(\mathbf{r}_\perp, t) = \left(-\frac{\hbar^2\nabla_\perp^2}{2m} + V(\mathbf{r}_\perp) + g_2|\psi(\mathbf{r}_\perp, t)|^2\right)\psi(\mathbf{r}_\perp, t), \tag{7.10}$$

and the 2D effective energy damping potential

$$V_\varepsilon(\mathbf{r}_\perp, t) = -\hbar\int d^2\mathbf{r}'_\perp \varepsilon_2(\mathbf{r}_\perp - \mathbf{r}'_\perp)\nabla'_\perp \cdot \mathbf{j}(\mathbf{r}'_\perp, t), \tag{7.11}$$

defined in terms of the 2D probability current

$$\mathbf{j}(\mathbf{r}'_\perp, t) = \frac{i\hbar}{2m}\left[\psi(\mathbf{r}_\perp, t)\nabla_\perp\psi^*(\mathbf{r}_\perp, t) - \psi^*(\mathbf{r}_\perp, t)\nabla_\perp\psi(\mathbf{r}_\perp, t)\right], \tag{7.12}$$

and the 2D epsilon function

$$\varepsilon(\mathbf{r}_\perp) = \frac{\mathcal{M}}{(2\pi)^2}\int d^2\mathbf{k}_\perp e^{i\mathbf{k}_\perp\cdot\mathbf{r}_\perp} S_2(\mathbf{k}_\perp), \tag{7.13}$$

which itself is determined by the 2D scattering kernel

$$S_2(\mathbf{k}_\perp) = S_2(k) = \frac{1}{2\pi}F\left(\frac{(ka_z)^2}{4}\right), \tag{7.14}$$

where $F(q) \equiv e^q K_0(q)$ is the scaled modified Bessel function. Here we have the 2D interaction parameter $g_2 = \sqrt{8\pi}\hbar^2 a_s/(m\sigma)$ and chemical potential $\mu_2 = \mu - \hbar\omega_z/2$.

7.4 Angular momentum equation

We have a quasi-2D system, so we will be considering the z-component of angular momentum given by

$$L_z(t) = \int d^2\mathbf{r}_\perp\psi^*(\mathbf{r}_\perp)(-i\hbar)\left(x\partial_y - y\partial_x\right)\psi(\mathbf{r}_\perp) \tag{7.15}$$

in cartesian coordinates, or

$$L_z(t) = \int d^2\mathbf{r}_\perp\psi^*(\mathbf{r}_\perp)(-i\hbar)\partial_\phi\psi(\mathbf{r}_\perp) \tag{7.16}$$

in cylindrical coordinates, where we have used the shorthand

$$\partial_u \equiv \frac{\partial}{\partial u}. \tag{7.17}$$

The Ehrenfest relation for the z-component of angular momentum in 2D is (5.66)

$$\begin{aligned}(\mathbf{I})dL_z(t) &= -\langle (x\partial_y - y\partial_x)\, V(\mathbf{r}_\perp,t)\rangle\, dt - \frac{2\gamma}{\hbar}\mathrm{Re}\left\langle \hat{l}_z(L-\mu_2)\right\rangle dt \\ &+\frac{2\gamma k_B T}{\hbar}\mathrm{Tr}\left(\hat{l}_z\hat{\mathcal{P}}\right)dt + \sqrt{\frac{4\gamma k_B T}{\hbar}\left\langle \hat{l}_z^2\right\rangle + D_{l_z}^{\gamma}}\, dW_5(t) \\ &-\hbar\mathcal{M}\int d^2\mathbf{k}_\perp S_2(k)\mathcal{F}\left[(x\partial_y - y\partial_x)\, n(\mathbf{r}_\perp)\right]^*\mathcal{F}\left[\nabla_\perp\cdot\mathbf{j}(\mathbf{r}_\perp)\right]dt \\ &+\sqrt{2\hbar\mathcal{M}k_B T\int d^2\mathbf{k}_\perp\, S_2(k)\left|\mathcal{F}\left[(x\partial_y - x\partial_y)\, n(\mathbf{r}_\perp)\right]\right|^2 + D_{l_z}^{\varepsilon}}\, dW_6(t) \\ &+Q_{l_z}^{H} + Q_{l_z}^{\gamma} + Q_{l_z}^{\varepsilon} + dL_z^{\varepsilon}, \end{aligned} \tag{7.18}$$

Following the reasoning of Chapter 5 we assume the effects of the projector corrections are negligible, and assume a choice of basis that results in the trace being zero. Furthermore we consider only the contribution of the energy-damping reservoir interaction, that is we set $\gamma = 0$. This may represent a system that explicitly only has the energy-damping reservoir interaction present, such as a two component system where one component is degenerate while the other is thermalized, or it could be a good approximation in a single-component system where the energy-damping effects are dominant over the number-damping, as was seen in the preceding chapter. The equation of motion for the angular momentum is thus

$$\begin{aligned}(\mathbf{I})dL_z(t) &= -\hbar\mathcal{M}\int d^2\mathbf{k}_\perp S_2(k)\mathcal{F}\left[(x\partial_y - y\partial_x)\, n(\mathbf{r})\right]^*\mathcal{F}\left[\nabla_\perp\cdot\mathbf{j}(\mathbf{r}_\perp)\right]dt \\ &+\sqrt{2\hbar\mathcal{M}k_B T\int d^2\mathbf{k}_\perp\, S_2(k)\left|\mathcal{F}\left[(x\partial_y - y\partial_x)\, n(\mathbf{r}_\perp)\right]\right|^2}\, dW(t) \end{aligned} \tag{7.19}$$

or in cylindrical coordinates

$$\begin{aligned}(\mathbf{I})dL_z(t) &= -\hbar\mathcal{M}\int d^2\mathbf{k}_\perp S_2(k)\mathcal{F}\left[\partial_\phi n(\mathbf{r}_\perp)\right]^*\mathcal{F}\left[\nabla_\perp\cdot\mathbf{j}(\mathbf{r}_\perp)\right]dt \\ &+\sqrt{2\hbar\mathcal{M}k_B T\int d^2\mathbf{k}_\perp\, S_2(k)\left|\mathcal{F}\left[\partial_\phi n(\mathbf{r}_\perp)\right]\right|^2}\, dW(t). \end{aligned} \tag{7.20}$$

Our aim in this chapter is to analytically evaluate the terms in this equation to arrive at an effective equation for the vortex motion.

7.5 System

7.5.1 Wave function

We consider a vortex in a disc trap at the location $\mathbf{r}_0 = (x_0, y_0) = (r_0, \phi_0)$, using the ansatz for the vortex core density from [308] and including an image vortex. The background wave function is homogeneous $\psi_0 \equiv \sqrt{n_0}$ with density $n_0 = \mu_2/g_2$. The ansatz wave function is then

$$\begin{aligned}\psi(\mathbf{r}_\perp) &= \sqrt{n_0}\sqrt{1 - \frac{b^2}{b^2 + (x-x_0)^2 + (y-y_0)^2}} \\ &\quad \times \exp\left[i\kappa \tan^{-1}\left(\frac{y-y_0}{x-x_0}\right)\right] \\ &\quad \times \exp\left[-i\kappa \tan^{-1}\left(\frac{(x_0^2+y_0^2)y - R^2 y_0}{(x_0^2+y_0^2)x - R^2 x_0}\right)\right] \end{aligned} \tag{7.21}$$

where $b = \Lambda^{-1}\xi$, with $\Lambda = 0.8249$ the numerically obtained slope of the dimensionless radial vortex wave function, and $\xi = \hbar/\sqrt{n_0 g_2 m}$ the healing length. From here we proceed in cylindrical coordinates, as the quantity of interest the distance of the vortex from the trap centre r_0. The ansatz wave function is then

$$\begin{aligned}\psi(\mathbf{r}_\perp) &= \sqrt{n_0}\sqrt{1 - \frac{b^2}{b^2 + r^2 - 2rr_0\cos(\phi-\phi_0) + r_0^2}} \\ &\quad \times \exp\left[i\kappa \tan^{-1}\left(\frac{r\sin(\phi) - r_0\sin(\phi_0)}{r\cos(\phi) - r_0\cos(\phi_0)}\right)\right] \\ &\quad \times \exp\left[-i\kappa \tan^{-1}\left(\frac{rr_0\sin(\phi) - R^2\sin(\phi_0)}{rr_0\cos(\phi) - R^2\cos(\phi_0)}\right)\right]. \end{aligned} \tag{7.22}$$

The second phase is that of the image vortex, imposing a hard-wall boundary condition ensuring that the velocity has no radial component at the edge of the trap. We can obtain the ansatz wave function for an ideal point vortex with no core structure by taking $b \to 0$. Noting that vortices of higher charge are unstable, we assume that the vortex is singly charged. Furthermore we assume that the vortex is located close to the disc centre, so we can take linear approximations in r_0/R if needed; at several stages we require this as many of the integrals cannot be evaluated analytically. Hence our approach is able to describe the diffusive instability of a vortex at the centre of the disc, and the early stages of it's

stochastic evolution towards the boundary.

The density is

$$n(\mathbf{r}_\perp) = n_0 \left(1 - \frac{b^2}{b^2 + r^2 - 2rr_0\cos(\phi - \phi_0) + r_0^2}\right), \tag{7.23}$$

the partial derivative with respect to the azimuthal angle ϕ is

$$\partial_\phi n(\mathbf{r}_\perp) = \frac{2b^2 n_0 r r_0 \sin(\phi - \phi_0)}{\left(b^2 + r^2 - 2rr_0\cos(\phi - \phi_0) + r_0^2\right)^2}, \tag{7.24}$$

and the Fourier transform of the azimuthal derivative of density is to first order in r_0/R

$$\mathcal{F}\left[\partial_\phi n(\mathbf{r}_\perp)\right] \approx 2ib^2 n_0 \sin(\phi_0 - \phi_k)\, r_0 \int_0^R \frac{r^2 J_1(kr)}{\left(b^2 + r^2\right)^2}\, dr. \tag{7.25}$$

7.5.2 Current

The coherent region current is

$$\begin{aligned}\mathbf{j}(\mathbf{r}_\perp) \;=\; & \frac{\kappa n_0 r_0 \hbar \left(R^2 - r_0^2\right)\left(r^2 - R^2\right)\sin(\phi - \phi_0)}{m\left(b^2 + r^2 - 2rr_0\cos(\phi - \phi_0) + r_0^2\right)\left(rr_0\left(rr_0 - 2R^2\cos(\phi - \phi_0)\right) + R^4\right)}\hat{\mathbf{r}} \\ & + \frac{\kappa n_0 \hbar \left(R^2 - r_0^2\right)\left(rr_0^2 - r_0\left(r^2 + R^2\right)\cos(\phi - \phi_0) + rR^2\right)}{m\left(b^2 + r^2 - 2rr_0\cos(\phi - \phi_0) + r_0^2\right)\left(rr_0\left(rr_0 - 2R^2\cos(\phi - \phi_0)\right) + R^4\right)}\hat{\boldsymbol{\phi}},\end{aligned} \tag{7.26}$$

the current divergence is

$$\nabla_\perp \cdot \mathbf{j}(\mathbf{r}_\perp) = \frac{2b^2 \kappa n_0 r r_0 \hbar \left(R^2 - r_0^2\right)\sin(\phi - \phi_0)}{m\left(b^2 + r^2 - 2rr_0\cos(\phi - \phi_0) + r_0^2\right)^2\left(rr_0\left(rr_0 - 2R^2\cos(\phi - \phi_0)\right) + R^4\right)}, \tag{7.27}$$

and the Fourier transform of the current divergence is to first order in r_0/R

$$\mathcal{F}\left[\nabla_\perp \cdot \mathbf{j}(\mathbf{r}_\perp)\right] \approx \frac{2ib^2 \kappa \hbar n_0}{mR^2}\sin(\phi_0 - \phi_k)\, r_0 \int_0^R \frac{r^2 J_1(kr)}{\left(b^2 + r^2\right)^2}\, dr. \tag{7.28}$$

Note that the same integral appears in both the Fourier transform of the azimuthal derivative of density and the Fourier transform of the current divergence.

7.5.3 Angular momentum

The angular momentum density is

$$l_z(\mathbf{r}_\perp) = \frac{\kappa n_0 r\hbar\left(R^2 - r_0^2\right)\left(rr_0^2 - r_0\left(r^2+R^2\right)\cos\left(\phi-\phi_0\right) + rR^2\right)}{\left(b^2 + r^2 - 2rr_0\cos\left(\phi-\phi_0\right) + r_0^2\right)\left(rr_0\left(rr_0 - 2R^2\cos\left(\phi-\phi_0\right)\right) + R^4\right)}, \quad (7.29)$$

to second order in the radial vortex location the angular momentum is

$$\begin{aligned} L_z(r_0) &\approx \pi\kappa n_0\hbar\left(R^2 - b^2\log\left(1+\frac{R^2}{b^2}\right)\right) \\ &\quad \pi\kappa n_0\hbar r_0^2\left(\frac{b^2}{R^2}\log\left(1+\frac{R^2}{b^2}\right) + \frac{\left(R^4 - b^2R^2 - b^4\right)}{\left(b^2+R^2\right)^2}\right), \end{aligned} \quad (7.30)$$

and so the differential with respect to the radial vortex location is

$$\begin{aligned} dL_z &\approx -2\pi\kappa n_0 r_0\hbar\left(\frac{b^2}{R^2}\log\left(1+\frac{R^2}{b^2}\right) + \frac{\left(R^4 - b^2R^2 - b^4\right)}{\left(b^2+R^2\right)^2}\right)dr_0 & (7.31) \\ &= -g(b/R)2\pi\kappa\hbar n_0 r_0 dr_0, & (7.32) \end{aligned}$$

where

$$g(x) = x^2\log\left(1+\frac{1}{x^2}\right) + \frac{1-x^2-x^4}{\left(x^2+1\right)^2} \quad (7.33)$$

goes to unity in the limit of an ideal vortex.

7.6 Equation of motion

We now have all the components needed to construct the equation of motion for the vortex radial position. Keeping all quantities to lowest possible order in r_0/R that are nonzero we have

$$\begin{aligned} dr_0 &\approx \frac{2b^4 n_0\hbar\mathcal{M}}{g(b/R)mR^2}r_0\int dk\, kS_2(k)\left(\int_0^R dr\frac{r^2J_1(kr)}{\left(b^2+r^2\right)^2}\right)^2 dt \\ &\quad -\sqrt{\frac{2b^4\mathcal{M}k_BT}{g(b/R)^2\pi\hbar}\int dk\, kS_2(k)\left(\int_0^R dr\frac{r^2J_1(kr)}{\left(b^2+r^2\right)^2}\right)^2}dW(t). \end{aligned} \quad (7.34)$$

Recasting this in a dimensionless form based on the radius of the disc, we let

$$\zeta = \frac{r_0}{R}, \quad s = \frac{b}{R}, \quad q = kR, \quad u = \frac{r}{R}, \tag{7.35}$$

then

$$\begin{aligned} d\zeta &\approx \frac{2s^4 n_0 \hbar \mathcal{M}}{g(s) m R^2} \int dq\, q S_2(q/R) \left(\int_0^1 du \frac{u^2 J_1(qu)}{(s^2+u^2)^2} \right)^2 \zeta dt \\ &+ \sqrt{\frac{2s^4 \mathcal{M} k_B T}{g(s)^2 \pi \hbar R^2} \int dq\, q S_2(q/R) \left(\int_0^1 du \frac{u^2 J_1(qu)}{(s^2+u^2)^2} \right)^2} dW(t) \end{aligned} \tag{7.36}$$

where we have made the noise term positive as we are free to make the replacement $dW(t) \to -dW(t)$. We may write this as

$$d\zeta \approx \Gamma \zeta dt + \sqrt{\mathcal{D}} dW(t) \tag{7.37}$$

where

$$\Gamma = \frac{2s^4 n_0 \hbar \mathcal{M}}{g(s) m R^2} \int dq\, q S_2(q/R) \left(\int_0^1 du \frac{u^2 J_1(qu)}{(s^2+u^2)^2} \right)^2, \quad \mathcal{D} = \frac{\Gamma m k_B T}{g(s) n_0 \pi \hbar^2}. \tag{7.38}$$

It is clear from the form of the equation that the vortex undergoes exponential growth in the radial position. Importantly there is no dependence on the sign of the vortex charge, as we expect since this should only affect the azimuthal direction that the vortex moves.

7.7 Analysis

As the coefficients are time-independent, the solution to (7.37) is readily found to be

$$\zeta(t) = \zeta(0) e^{\Gamma t} + \sqrt{\mathcal{D}} \int_0^t e^{\Gamma(t-t')} dW(t'). \tag{7.39}$$

As would be expected the vortex undergoes noisy exponential growth, and the long-time limit is simply that the vortex leaves the condensate, by annihilating with its image at the boundary. Since (7.37) is an Ito equation, the variance is readily found to be

$$\sigma_\zeta^2(t) = \frac{\mathcal{D}}{\Gamma} \left(e^{2\Gamma t} - 1 \right). \tag{7.40}$$

The steady-state properties are trivial - the vortex leaves the disc and the variance diverges. There are two properties we can investigate. First, the decay rate can be checked. Second, the presence of noise can cause a stabilising effect on the vortex, potentially causing a larger mean lifetime than would be expected.

When considering the vortex location, we can treat the origin $\zeta = 0$ as a reflecting barrier, as if the vortex crosses the origin it remains in the disc, while the disc edge $\zeta = 1$ can be treated as an absorbing barrier, such that if the vortex reaches the disc edge it leaves the disc and does not return. Since we have restricted ourselves to small values of ζ, we cannot consider the motion of the vortex all the way to the boundary, and so we instead consider a smaller region defined by $\zeta = \zeta_f$ with $\zeta_f < 1$. We can assume $\zeta = \zeta_f$ to be an absorbing barrier, as the vortex can exit the region by traversing this radius. The *mean first passage time* of a particle initially at $x \in (a, b)$ is defined as the average time at which the particle first leaves the interval (a, b). For the case of a a reflecting barrier, b an absorbing barrier, and $a < b$, the first passage time $T(x)$ for a particle whose motion is governed by the Fokker-Planck equation

$$\partial_t p(x,t) = -\partial_x \left(A(x)p(x,t)\right) + \frac{1}{2}B(x)\partial_x^2 p(x,t), \tag{7.41}$$

is given by [272]

$$T(x) = 2\int_x^b \frac{dy}{\eta(y)} \int_a^y \frac{\eta(z)}{B(z)}, \tag{7.42}$$

where

$$\eta(x) \equiv \exp\left\{\int_0^x dx' \left[2A(x')/B(x')\right]\right\}. \tag{7.43}$$

Thus for the disc-vortex system, we have

$$x = \zeta, \quad a = 0, \quad b = \zeta_f, \quad \eta(x) = \exp\left\{\frac{\Gamma}{\mathcal{D}}x^2\right\}, \tag{7.44}$$

which gives the mean first passage time to exit the circular region of radius ζ_f as

$$T(\zeta) = \frac{1}{\mathcal{D}}\left[\zeta_f^2\, {}_2F_2\left(1,1;\frac{3}{2},2;-\frac{\Gamma}{\mathcal{D}}\zeta_f^2\right) - \zeta^2\, {}_2F_2\left(1,1;\frac{3}{2},2;-\frac{\Gamma}{\mathcal{D}}\zeta^2\right)\right], \tag{7.45}$$

where ${}_pF_q(a_1, a_2, ..., a_p; b_1, b_2, ..., b_q; , z)$ is the generalized hypergeometric function. In the

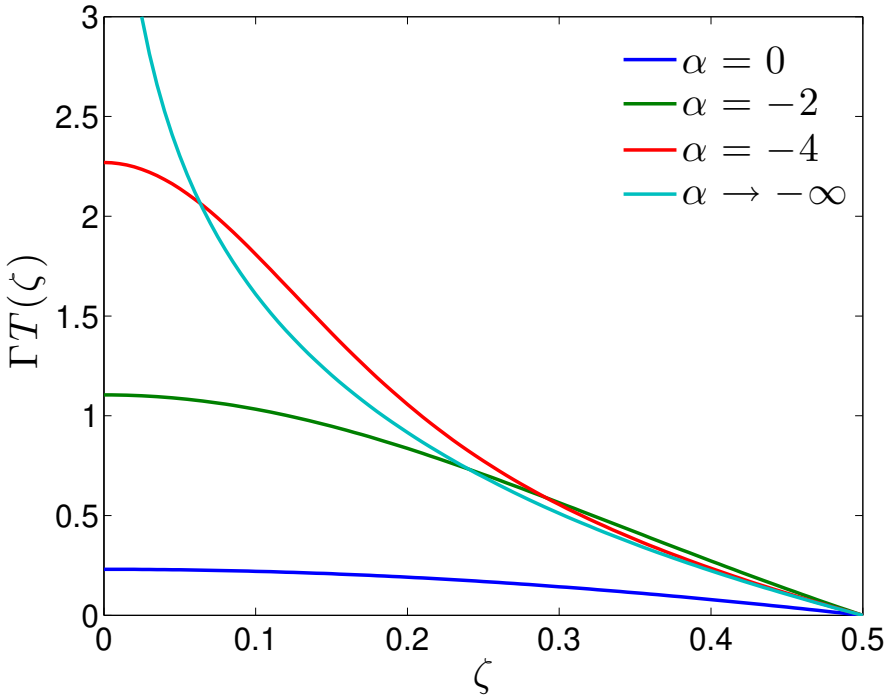

Figure 7.1: Mean scaled vortex lifetime $\Gamma T(\zeta)$ for exiting a circular region of radius $\zeta_f = 0.5$, for several values of α, Equation (7.47).

limit of zero diffusion

$$T_0(\zeta) \equiv \lim_{\mathcal{D}\to 0} T(\zeta) = \frac{1}{\Gamma} \ln\left(\frac{\zeta_f}{\zeta}\right), \tag{7.46}$$

which can also be obtained by inverting the noise-free deterministic solution of (7.37). Note that the scaled mean first passage time $\Gamma T(\zeta)$ depends on the drift Γ and diffusion $\mathcal{D}$ only through the ratio $\mathcal{D}/\Gamma$. We therefore define the parameter α

$$\alpha \equiv \ln\left(\frac{\mathcal{D}}{\Gamma}\right) = \ln\left(\sqrt{\frac{8}{\pi}}\frac{k_B T}{\mu_2}\frac{a_s}{a_z}\right) \tag{7.47}$$

as the difference in magnitude between the drift and diffusion. Now the limit of zero diffusion, and thus the deterministic solution, corresponds to $\alpha \to -\infty$.

An immediate consequence of the noise is that the vortex has a finite lifetime regardless of the initial displacement. For the quiet system $\mathcal{D} = 0$ the lifetime diverges as the initial displacement goes to zero, indicating that a vortex initially at the centre of the disc can only decay in the presence of noise, a consequence of the cylindrical symmetry. The finite

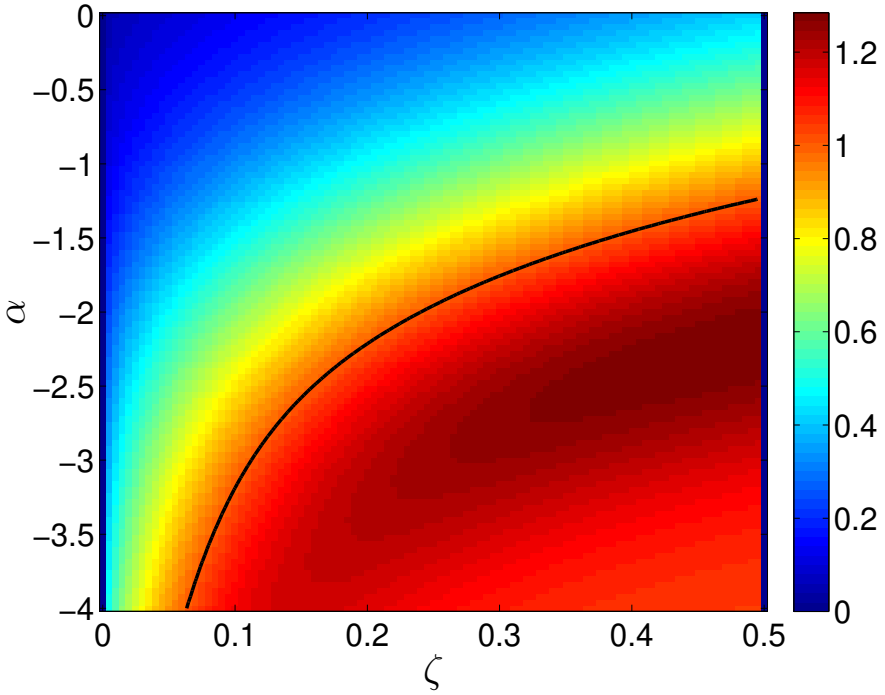

Figure 7.2: Ratio of vortex lifetime to quiet vortex lifetime $T(\zeta)/T_0(\zeta)$ (7.49) for exiting a circular region of radius $\zeta_f = 0.5$. The black line indicates where the ratio is unity.

lifetime of a central vortex in a noisy system have previously been derived [309][1].

In Fig. 7.1 we show the expected vortex lifetime scaled by Γ for several values of α. We see that, depending on the exact value of α, there are initial displacements where the presence of noise serves to *increase* the lifetime. To make this clearer, we look at the ratio of the vortex lifetime to the quiet vortex lifetime

$$\frac{T(\zeta)}{T_0(\zeta)} = \frac{\Gamma}{\mathcal{D}} \frac{\zeta_f^2\, {}_2F_2\left(1,1;\tfrac{3}{2},2;-\tfrac{\Gamma}{\mathcal{D}}\zeta_f^2\right) - \zeta^2\, {}_2F_2\left(1,1;\tfrac{3}{2},2;-\tfrac{\Gamma}{\mathcal{D}}\zeta^2\right)}{\ln\left(\frac{\zeta_f}{\zeta}\right)} \tag{7.48}$$

$$= e^{-\alpha} \frac{\zeta_f^2\, {}_2F_2\left(1,1;\tfrac{3}{2},2;-e^{-\alpha}\zeta_f^2\right) - \zeta^2\, {}_2F_2\left(1,1;\tfrac{3}{2},2;-e^{-\alpha}\zeta^2\right)}{\ln\left(\frac{\zeta_f}{\zeta}\right)}. \tag{7.49}$$

The ratio is shown in Fig. 7.2, where we see that there is a significant region where the noisy vortex lifetime is enhanced relative to the quiet case. In fact, the region where the noise results in the lifetime for an intermediately displaced vortex being reduced is most

[1] This analysis was in the context of a very weakly interacting system in a harmonic trap with number-damping only, preventing a direct comparison with our results.

likely difficult to access, as it requires the diffusion constant to be essentially the same magnitude as the drift constant, whereas the drift constant would generally be expected to be larger than the diffusion constant by at least an order of magnitude. For example, using the trap centre values of the experiment in [310] gives ranges for $\exp(\alpha)$ of $0.016 - 0.045$, for α given by Equation (7.47). This enhanced lifetime can be expected if the noise causes the vortex to deviate significantly from an outward spiral path, effectively exploring more of the disc before reaching the boundary.

7.8 Rotating thermal cloud

The potential behaviour of a vortex becomes more rich when considering a rotating thermal cloud. Assume the thermal cloud is rotating at frequency Ω. The reservoir theory is then naturally formulated in the frame rotating with the thermal cloud. The angular momentum we should look at is

$$\begin{aligned} \hat{L}'_z &= \hat{L}_z - L_{\text{disc}} && (7.50)\\ &= \hat{L}_z - \frac{1}{2}\pi m n_0 \Omega R^4, && (7.51) \end{aligned}$$

which is just the angular momentum in the non-rotating frame with an additional constant. The current picks up a rigid-body rotation term

$$\begin{aligned} \mathbf{j}_\Omega(\mathbf{r}_\perp) &= n(\mathbf{r}_\perp)\left(\mathbf{v}(\mathbf{r}_\perp) - \boldsymbol{\Omega}\times\mathbf{r}\right) && (7.52)\\ &= n(\mathbf{r}_\perp)\left(\mathbf{v}(\mathbf{r}_\perp) - \Omega r\hat{\boldsymbol{\phi}}\right), && (7.53) \end{aligned}$$

then the stochastic Ehrenfest relation for angular momentum is

$$\begin{aligned} (\mathbf{I})dL'_z(t) &= -\hbar\mathcal{M}\int d^2\mathbf{k}_\perp S_2(k)\mathcal{F}\left[\partial_\phi n(\mathbf{r}_\perp)\right]^*\mathcal{F}\left[\nabla_\perp\cdot\mathbf{j}(\mathbf{r}_\perp) - \nabla_\perp\cdot(\Omega r n(\mathbf{r})\hat{\boldsymbol{\phi}})\right]dt \\ &\quad + \sqrt{2\hbar\mathcal{M}k_BT\int d^2\mathbf{k}_\perp\, S_2(k)\left|\mathcal{F}\left[\partial_\phi n(\mathbf{r}_\perp)\right]\right|^2}dW(t). \qquad (7.54) \end{aligned}$$

This leads to an equation of motion for the vortex of

$$\begin{aligned} dr_0 &\approx \frac{2b^4 n_0 \mathcal{M}}{g(b/R)}\left(\frac{\hbar}{mR^2}-\kappa\Omega\right) r_0 \int dk\, kS_2(k)\left(\int_0^R dr \frac{r^2 J_1(kr)}{\left(b^2+r^2\right)^2}\right)^2 dt \\ &\quad -\sqrt{\frac{2b^4\mathcal{M}k_B T}{g(b/R)^2\pi\hbar}\int dk\, kS_2(k)\left(\int_0^R dr \frac{r^2 J_1(kr)}{\left(b^2+r^2\right)^2}\right)^2} dW(t), \end{aligned} \tag{7.55}$$

or, in terms of the rates found earlier and in the dimensionless form with respect to the disc radius,

$$d\zeta \approx \frac{\kappa m R^2}{\hbar}\Gamma\left(\Omega_m-\Omega\right)\zeta dt + \sqrt{\mathcal{D}}dW(t), \tag{7.56}$$

where we have defined the rotation threshold Ω_m

$$\Omega_m = \frac{\hbar}{\kappa m R^2}. \tag{7.57}$$

The rotation threshold Ω_m is rotation frequency at which the energy landscape gives a metastable state for the vortex to exist at the disc centre. The presence of the vortex sign $\kappa = \pm 1$ indicates which direction the thermal cloud should be rotated to stabilize a vortex of charge κ. For a vortex near the disc centre, the introduction of rotation to the thermal cloud at first serves to decrease the rate at which the vortex moves away from the centre. If the rotation frequency passes the threshold $\Omega > \Omega_m$, the vortex will instead move toward the disc centre, with further increasing rotation only serving to increase the rate at which this happens. In reality of course there are other factors at play, most pointedly that when the rotation frequency increases ever more vortices will form, leading at sufficiently rapid rotation to a regular Abrikosov lattice; this is well beyond the regime we have considered.

For small rotation frequencies the equation of motion becomes that of an Ornstein-Uhlenbeck process, and one can then measure the steady-state properties of the vortex as it moves in a stochastic fashion about the centre of the disc. For example, the steady-state correlations of the vortex position are

$$\lim_{t\to\infty}\langle\zeta(t)\zeta(t+\tau)\rangle = \frac{\hbar^2}{2mR^2}\frac{\mathcal{D}}{\Gamma\left(\Omega-\Omega_m\right)}\exp\left[-\frac{mR^2}{\hbar}\Gamma\left(\Omega-\Omega_m\right)|\tau|\right], \tag{7.58}$$

where we have assumed $\Omega > \Omega_m$ and let $\kappa = 1$. This shows the expected behaviour, where the vortex will show less variance in position about the disc centre with increasing rotation

rate. Performing a more complex analysis, rather than considering only small displacements from the disc centre, may be able to reveal the presence of the energy barrier separating the energy minimum at $r_0 = 0$ with the energy minimum at the boundary $r_0 = R$. One may then be able to investigate the possibility of the vortex traversing the barrier using the stochastic analysis of first passage times; this is an example of thermally assisted barrier crossing.

A careful assessment of the regime of validity for our linearization approach would require numerical simulations of the SPGPE in a basis appropriate for implementing an energy cutoff in the hard-wall confining potential.

7.9 Numeric requirements

Accurately propagating the SPGPE requires code that is built upon an appropriate single-particle basis, allowing a physically consistent energy cutoff to be chosen. For a harmonic trap the single-particle solutions are the Hermite polynomials with Gaussian weighting, allowing the use of Gauss-Hermite quadrature for efficient and accurate numeric integration.

The single-particle solutions to the 2D Schrodinger equation in a disc trap of radius R are

$$\phi_{lj}(\mathbf{r}_\perp) = A_{lj} J_l\left(\sqrt{\frac{2mE_{lj}}{\hbar^2}} r\right) e^{il\phi}, \quad l, j \in \mathbb{Z} \tag{7.59}$$

where $J_l(\rho)$ are the Bessel functions of the first kind, and the quantized energies E_{lj} are

$$E_{lj} = \frac{\hbar^2}{2m} \frac{x_{lj}^2}{R^2} \tag{7.60}$$

with x_{lj} the jth zero of the Bessel function of order l. The energies and consequently the normalisation A_{lj} are unable to be determined analytically.

A faithful numerical implementation of the 2D SPGPE in the disc trap would need to follow the general idea of the method presented in appendix F. However we would no longer be able to use Gauss-Hermite quadrature as there is no exponential weighting on the basis functions. Thus writing code to solve the 2D SPGPE in a disc trap is a highly non-trivial task[2], and is outside the scope of this thesis. As such we leave the vortex here, with the brief

[2]In principle numerical propagation of the 2D SPGPE in a disc trap can be implemented using a Fourier-Bessel quadrature.

analytic treatment we have presented, hopefully to be revisited when appropriate code for numeric analysis has been developed. A somewhat less faithful numerical implementation of the 2D SPGPE in the disc trap could use the Fourier basis [311].

7.10 Conclusions

In this chapter we have considered the motion of a singly-charged quantum vortex in a quasi-2D system. We would expect a large system with a single decaying vortex to remain close to particle equilibrium. We thus assumed a quasi-2D system where the dissipative effects are dominated by the energy-damping reservoir interaction process; we have seen in Chapter 6 that this can be the case for a system in particle equilibrium. To our knowledge, this is the first analytic treatment of vortex motion subject to the energy-damping reservoir interaction. Using the angular momentum stochastic Ehrenfest relation of Chapter 5, we derived a stochastic equation of motion for the location of the vortex within the disc. The vortex was found to migrate to the disc boundary exponentially in time when the noise was neglected, but that the presence of noise could either reduce or enhance the vortex lifetime. When including a rotating thermal cloud we saw that the vortex could be stabilized at the disc centre, with the equation of motion taking the form of a Ornstein-Uhlenbeck process when the rotation frequency exceeded the critical value Ω_m (7.57). While other methods, such as considering the energy landscape of the vortex explicitly, can also predict the emergence of vortex stability, the use of the stochastic Ehrenfest relations allows for analysis of the steady-state stochastic properties of the vortex as it undergoes temperature-induced fluctuations about the disc centre.

Chapter 8

Conclusions

8.1 Summary

The SPGPE has seen many applications since it was originally developed by Gardiner and Davis [146] in 2003, however these have largely been restricted to the number-damping sub-theory where the energy-damping reservoir interactions are neglected. With the recent numerical implementation of the energy-damping reservoir interaction terms by Rooney *et al* [1], the range of applications of the SPGPE has been widened even further, though the question of whether the energy-damping process is significant enough to warrant inclusion has remained open. In this thesis we have demonstrated that the effects of the energy-damping reservoir interaction can be comparable to and even dominant over those due to the more commonly studied number-damping reservoir interaction. The importance of energy-damping appears particularly pronounced for systems near particle equilibrium with the reservoir.

In Chapter 4 we have provided the first linear fluctuation analysis of the SPGPE that includes both the energy-damping reservoir interaction process and all noise terms. The dispersion relation is the usual Bogoliubov dispersion (4.43), with a modification due to a momentum dependent damping (4.44). The damping consists of a number-damping contribution and an energy-damping contribution, each with distinct momentum dependence, indicating that each damping process is significant in a regime of wave numbers corresponding to a distinct range of length scales. The fluctuation spectra (4.64)-(4.66) were found to be peaked about the dispersion relation, with the largest contribution to the width coming from the energy-damping reservoir interaction process.

In Chapter 5 we have derived stochastic differential equations of motion for matter wave moments of the SPGPE, which we call the stochastic Ehrenfest relations (5.64)-(5.68). In general these include drift and diffusion terms due to each of the reservoir interaction processes, as well as terms that arise due to mixing of modes at the energy cutoff. Investigating using a toy model of a quasi-1D Thomas-Fermi system in a harmonic

trap, we showed that for a well-chosen cutoff the terms due to the energy cutoff are small compared to the overall motion of the centre of mass. These terms may thus be neglected for the purposes of analysis, and the resulting stochastic differential equations admit analytic solutions. These analytic solutions compared favourably with numerical simulations of the 1D SPGPE, further validating the neglect of the energy cutoff terms. The stochastic Ehrenfest relations then provide a powerful tool for understanding the SPGPE, among other things allowing a quantitative comparison of the two reservoir interaction processes for specific systems.

In Chapter 6 we analysed a 3D isotropic Bose-Einstein condensate in a harmonic trap in the Thomas-Fermi regime using the stochastic Ehrenfest relations. The centre of mass motion of the system was found to be described by a vector Ornstein-Uhlenbeck process (6.20), with the reservoir interactions providing drift and diffusion on top of the usual Kohn oscillations of the system. Analytic solutions of these equations were compared with numerical solutions of the SPGPE, confirming the predicted motion. The energy-damping and number-damping individual reservoir interactions manifested as individual drift and diffusion terms, allowing a direct comparison of the effect each has on the centre of mass motion. Using the Hartree-Fock parameter estimation scheme of [2], we showed that the energy-damping has a much greater influence on the steady-state properties of the centre of mass motion than the number-damping, to the point where in some of the considered systems the number-damping could be neglected entirely. The steady-state properties of particle number, however, were found to be entirely due to the number-damping process. The two reservoir interaction processes thus have distinct and potentially experimentally measurable influences on the system. The results suggest a separation of ensembles for the system moments, with the centre of mass motion effectively described by a canonical ensemble while the particle number is described by the expected grand canonical ensemble.

In Chapter 7 we considered the motion of a singly quantized vortex in a quasi-2D system confined to a disc trap under the influence of the energy-damping reservoir interaction. To our knowledge this is the first analytic treatment of vortex motion under the energy-damping reservoir interaction; previous works have at most included only the number-damping process [309]. Using the stochastic Ehrenfest relation for angular momentum we found a stochastic equation of motion for the vortex location that admitted analytic solutions (7.37). When noise is neglected the vortex leaves the system exponentially fast, however retaining the noise can enhance the vortex lifetime. It was found that including a rotating thermal cloud can lead to stabilisation of the vortex, with the vortex moving

toward the disc centre rather than to the boundary for rotation above some threshold. The equation of motion then becomes that of a Ornstein-Uhlenbeck process (7.56), and the steady-state stochastic motion of the vortex near the disc centre was analysed.

Our main aims for this research was twofold. Firstly we wanted to generalize the method of [150] and apply it to other systems, leading to our general formulation of stochastic Ehrenfest relations. Secondly we wanted to focus on the energy-damping reservoir interaction, as this has generally been neglected. The two formed a synthesis, as applying the stochastic Ehrenfest relations to the system in Chapter 6 revealed that the energy-damping reservoir interaction may be dominant in some regimes. We thus suggest the following broad conclusions to this work. The stochastic Ehrenfest relations provide a powerful platform for analysing a variety of systems, with great potential for experimental predictions without the need for computationally intensive simulations, and the ability to see what effect the reservoir interactions will have more clearly. As for the energy-damping reservoir interaction, our results suggest that it is indeed an important factor in the finite temperature degenerate Bose gas system, and in general it must be accounted for when analysing such systems. In particular, the energy-damping reservoir interaction is of greatest significance for systems close to particle equilibrium, where number-damping becomes relatively unimportant. This regime is of interest for many finite-temperature Bose-Einstein condensate systems.

8.2 Outlook

We have developed a method of analysing finite temperature degenerate Bose gas system that could see a wide range of applications. A suggested non-trivial and interesting application of the stochastic Ehrenfest relations is the motion of a dark soliton in a quasi-1D system, in either a ring geometry or a harmonic trap. An in-depth analysis of the regime where the projector corrections are negligible, and the effect they have on the system when they become significant, is also an important task.

Testing the predictions of Chapter 6 experimentally is an obvious next step. As suggested earlier, measurements of the centre of mass motion and particle number may be able to distinguish clearly between the number-damping and energy-damping reservoir interaction processes, and could also verify the energy-damping dominance for the centre of mass motion. The system itself is not particularly novel, and can almost certainly be easily realized by a number of experimental groups. The difficulties in this task are more likely

to lie in obtaining sufficiently well-resolved long-time data of the position, momentum, and particle number of the system.

New code is required for numerical testing of the fluctuation analysis predictions of Chapter 4 and the disc vortex predictions of Chapter 7. While the code for propagating a system using the basis of single particle solutions of a harmonic trap has been implemented and well tested, for a general confining geometry this is a highly non-trivial task. There is currently code in development for the numeric propagation of the SPGPE in the relatively new programming language Julia that will go a long way toward achieving this.

Further investigation of the energy-damping process would almost certainly be a fruitful endeavour. There may be many more scenarios where this oft-neglected reservoir interaction potentially plays an important role, such as in spinor systems, the Kibble-Zurek mechanism of defect formation, coarsening dynamics in quenched systems, and the coupling of vortices to sound waves. The energy-damping process is indeed a potential explanation for many experimental open questions, including the energy damping anomaly in spin-1 [312], and persistent current decay via thermally activated phase slips [72, 313–316].

Appendix A

Forward-scattering Hamiltonian

Recall the definition of the coherent region super-operator

$$\mathcal{L}_{\mathbf{C}} \equiv \mathcal{L}_0 + \mathcal{P}\mathcal{L}_{\rm int}\mathcal{P} \tag{A.1}$$

where

$$\mathcal{L}_{\rm int}\rho = -\frac{i}{\hbar}\left[\hat{H}_{\rm int}, \rho\right], \tag{A.2}$$

with

$$\hat{H}_{\rm int} = \hat{H}^{(1)}_{\rm int} + \hat{H}^{(2)}_{\rm int} + \hat{H}^{(3)}_{\rm int} \tag{A.3}$$

the interaction Hamiltonian, decomposed into terms with similar number of occurrences of the coherent region field operator

$$\hat{H}^{(1)}_{\rm int} = g\int d^3\mathbf{r}\left[\hat{\psi}^\dagger(\mathbf{r})\hat{\phi}^\dagger(\mathbf{r})\hat{\phi}(\mathbf{r})\hat{\phi}(\mathbf{r}) + \hat{\phi}^\dagger(\mathbf{r})\hat{\phi}^\dagger(\mathbf{r})\hat{\phi}(\mathbf{r})\hat{\psi}(\mathbf{r})\right], \tag{A.4}$$

$$\hat{H}^{(2)}_{\rm int} = \frac{g}{2}\int d^3\mathbf{r}\left[\hat{\psi}^\dagger(\mathbf{r})\hat{\psi}^\dagger(\mathbf{r})\hat{\phi}(\mathbf{r})\hat{\phi}(\mathbf{r}) + \hat{\phi}^\dagger(\mathbf{r})\hat{\phi}^\dagger(\mathbf{r})\hat{\psi}(\mathbf{r})\hat{\psi}(\mathbf{r}) + 4\hat{\psi}^\dagger(\mathbf{r})\hat{\phi}^\dagger(\mathbf{r})\hat{\phi}(\mathbf{r})\hat{\psi}(\mathbf{r})\right], \tag{A.5}$$

$$\hat{H}^{(3)}_{\rm int} = g\int d^3\mathbf{r}\left[\hat{\phi}^\dagger(\mathbf{r})\hat{\psi}^\dagger(\mathbf{r})\hat{\psi}(\mathbf{r})\hat{\psi}(\mathbf{r}) + \hat{\psi}^\dagger(\mathbf{r})\hat{\psi}^\dagger(\mathbf{r})\hat{\psi}(\mathbf{r})\hat{\phi}(\mathbf{r})\right]. \tag{A.6}$$

The projection operator $\mathcal{P}$ takes the uncorrelated part of the density matrix

$$\mathcal{P}\rho = \rho_{\mathbf{I}} \otimes \rho_{\mathbf{C}} = \rho_{\mathbf{I}} \otimes \mathrm{Tr}_{\mathbf{I}}\left(\rho\right). \tag{A.7}$$

Appendix A. Forward-scattering Hamiltonian

Define $\mathcal{L}_F \equiv \mathcal{P}\mathcal{L}_{\rm int}\mathcal{P}$ as the forward-scattering super-operator with corresponding forward-scattering Hamiltonian $\hat{H}_F$ defined by

$$\mathcal{L}_F\rho = -\frac{i}{\hbar}\left[\hat{H}_F, \rho\right], \tag{A.8}$$

giving mean-field contribution to evolution of the coherent region due to scattering from the incoherent region. The forward-scattering Hamiltonian in principle then consists of

$$\hat{H}_F = \hat{H}_F^{(1)} + \hat{H}_F^{(2)} + \hat{H}_F^{(3)} \tag{A.9}$$

where again we have decomposed into terms with similar number of occurrences of the coherent region field operator

$$\hat{H}_F^{(1)} = g\int d^3\mathbf{r}\left[\langle\hat{\phi}^\dagger(\mathbf{r})\hat{\phi}(\mathbf{r})\hat{\phi}(\mathbf{r})\rangle\hat{\psi}^\dagger(\mathbf{r})\hat{\phi}^\dagger(\mathbf{r}) + \langle\hat{\phi}^\dagger(\mathbf{r})\hat{\phi}^\dagger(\mathbf{r})\hat{\phi}(\mathbf{r})\rangle\hat{\psi}(\mathbf{r})\right], \tag{A.10}$$

$$\hat{H}_F^{(2)} = \frac{g}{2}\int d^3\mathbf{r}\left[\langle\hat{\phi}(\mathbf{r})\hat{\phi}(\mathbf{r})\rangle\hat{\psi}^\dagger(\mathbf{r})\hat{\psi}^\dagger(\mathbf{r}) + \langle\hat{\phi}^\dagger(\mathbf{r})\hat{\phi}^\dagger(\mathbf{r})\rangle\hat{\psi}(\mathbf{r})\hat{\psi}(\mathbf{r}) + 4\langle\hat{\phi}^\dagger(\mathbf{r})\hat{\phi}(\mathbf{r})\rangle\hat{\psi}^\dagger(\mathbf{r})\hat{\psi}(\mathbf{r})\right], \tag{A.11}$$

$$\hat{H}_F^{(3)} = g\int d^3\mathbf{r}\left[\langle\hat{\phi}^\dagger(\mathbf{r})\rangle\hat{\psi}^\dagger(\mathbf{r})\hat{\psi}(\mathbf{r})\hat{\psi}(\mathbf{r}) + \langle\hat{\phi}(\mathbf{r})\rangle\hat{\psi}^\dagger(\mathbf{r})\hat{\psi}^\dagger(\mathbf{r})\hat{\psi}(\mathbf{r})\right]. \tag{A.12}$$

where we have used

$$\langle\hat{\mathcal{R}}[\hat{\phi}^\dagger(\mathbf{r}), \hat{\phi}(\mathbf{r})]\rangle = {\rm Tr}_{\mathbf{I}}\left[\hat{\mathcal{R}}[\hat{\phi}^\dagger(\mathbf{r}), \hat{\phi}(\mathbf{r})]\rho_{\mathbf{I}}\right], \tag{A.13}$$

with $\hat{\mathcal{R}}[\hat{\phi}^\dagger(\mathbf{r}), \hat{\phi}(\mathbf{r})]$ a product of the incoherent field operators. We neglect the anomalous averages $\langle\hat{\phi}(\mathbf{r})\hat{\phi}(\mathbf{r})\rangle$ and $\langle\hat{\phi}^\dagger(\mathbf{r})\hat{\phi}^\dagger(\mathbf{r})\rangle$ in (A.11). Also (A.10) and (A.12) are zero since $\hat{\phi}(\mathbf{r})$ is quantum Gaussian and thus $\langle\hat{\phi}(\mathbf{r})\rangle = 0$. Thus the forward-scattering Hamiltonian is

$$\hat{H}_F = 2g\int d^3\mathbf{r}\, n_{\mathbf{I}}(\mathbf{r})\hat{\psi}^\dagger(\mathbf{r})\hat{\psi}(\mathbf{r}), \tag{A.14}$$

where we have identified the incoherent region density

$$n_{\mathbf{I}}(\mathbf{r}) = {\rm Tr}_{\mathbf{I}}\left[\rho_{\mathbf{I}}\hat{\phi}^\dagger(\mathbf{r})\hat{\phi}(\mathbf{r})\right] = \langle\hat{\phi}^\dagger(\mathbf{r})\hat{\phi}(\mathbf{r})\rangle. \tag{A.15}$$

Appendix B

Reservoir interaction terms

Here we evaluate the terms of the form

$$\mathrm{Tr}_{\mathbf{I}}\left[\left\{\mathcal{P}\mathcal{L}_{\mathbf{IC}}\int_{-\infty}^{0}d\tau e^{-(\mathcal{L}_{\mathbf{C}}+\mathcal{L}_{\mathbf{I}})\tau}\mathcal{L}_{\mathbf{IC}}\right\}\rho_{\mathbf{C}}\otimes\rho_{\mathbf{I}}\right]. \tag{B.1}$$

B.1 Cross-terms

We define the cross-terms as

$$\dot{\rho}_{\mathbf{C}}|_{(i,j)} \;=\; \mathrm{Tr}_{\mathbf{I}}\left[\left\{\mathcal{P}\mathcal{L}_{\mathbf{IC}}^{(i)}\int_{-\infty}^{0}d\tau e^{-(\mathcal{L}_{\mathbf{C}}+\mathcal{L}_{\mathbf{I}})\tau}\mathcal{Q}\mathcal{L}_{\mathbf{IC}}^{(j)}\right\}\rho_{\mathbf{C}}\otimes\rho_{\mathbf{I}}\right]. \tag{B.2}$$

It is simple to see that the cross-terms $\dot{\rho}_{\mathbf{C}}|_{(1,2)}$ and $\dot{\rho}_{\mathbf{C}}|_{(2,3)}$ are both zero; since there is an odd number of occurrences of the incoherent region field operator the Hartree-Fock factorization will always result in the average of a single operator $\langle\hat{\phi}\rangle$ or $\langle\hat{\phi}^{\dagger}\rangle$ which are equal to zero. Furthermore, for the only remaining cross-term $\dot{\rho}_{\mathbf{C}}|_{(1,3)}$, the Hartee-Fock factorization will always result in a term like $\langle\hat{\phi}^{\dagger}(\mathbf{r}',\tau)\hat{\phi}(\mathbf{r}',\tau)\rangle$ which do not conserve energy. Thus all cross-terms are neglected.

B.2 One-field terms

Consider the first order term

$$\dot{\rho}_{\mathbf{C}}|_{(1)} \;=\; \mathrm{Tr}_{\mathbf{I}}\left[\left\{\mathcal{P}\mathcal{L}_{\mathbf{IC}}^{(1)}\int_{-\infty}^{0}d\tau\exp\left[-(\mathcal{L}_{\mathbf{C}}+\mathcal{L}_{\mathbf{I}})\tau\right]\mathcal{L}_{\mathbf{IC}}^{(1)}\right\}\rho_{\mathbf{C}}\otimes\rho_{\mathbf{I}}\right]. \tag{B.3}$$

First note that since

$$e^{-(\mathcal{L}_{\mathbf{C}}+\mathcal{L}_{\mathbf{I}})\tau}g = e^{i\hat{H}_{\mathbf{C}}\tau/\hbar}e^{i\hat{H}_{\mathbf{I}}\tau/\hbar}ge^{-i\hat{H}_{\mathbf{C}}\tau/\hbar}e^{-i\hat{H}_{\mathbf{I}}\tau/\hbar}. \tag{B.4}$$

and

$$\hat{\psi}(\mathbf{r},t) = e^{i\hat{H}_{\mathbf{C}}t/\hbar}\hat{\psi}(\mathbf{r})e^{-i\hat{H}_{\mathbf{C}}t/\hbar} = e^{-\mathcal{L}_{\mathbf{C}}t}\hat{\psi}(\mathbf{r}) \tag{B.5}$$

$$\hat{\phi}(\mathbf{r},t) = e^{i\hat{H}_{\mathbf{I}}t/\hbar}\hat{\phi}(\mathbf{r})e^{-i\hat{H}_{\mathbf{I}}t/\hbar} = e^{-\mathcal{L}_{\mathbf{I}}t}\hat{\phi}(\mathbf{r}) \tag{B.6}$$

we have that

$$\begin{aligned} e^{-(\mathcal{L}_{\mathbf{C}}+\mathcal{L}_{\mathbf{I}})\tau}\mathcal{L}^{(1)}_{\text{int}}\rho_{\mathbf{C}}\otimes\rho_{\mathbf{I}} = & -\frac{i}{\hbar}g\int d^3\mathbf{r}'\left[\hat{\psi}^\dagger(\mathbf{r}',\tau)\hat{\phi}^\dagger(\mathbf{r}',\tau)\hat{\phi}(\mathbf{r}',\tau)\hat{\phi}(\mathbf{r}',\tau),\rho_{\mathbf{C}}\otimes\rho_{\mathbf{I}}\right] \\ & -\frac{i}{\hbar}g\int d^3\mathbf{r}'\left[\hat{\phi}^\dagger(\mathbf{r}',\tau)\hat{\phi}^\dagger(\mathbf{r}',\tau)\hat{\phi}(\mathbf{r}',\tau)\hat{\psi}(\mathbf{r}',\tau),\rho_{\mathbf{C}}\otimes\rho_{\mathbf{I}}\right] \end{aligned} \tag{B.7}$$

Then, exploiting the cyclical nature of the trace

$$\text{Tr}\left[\hat{A}\hat{B}\hat{C}\right] = \text{Tr}\left[\hat{C}\hat{A}\hat{B}\right] = \text{Tr}\left[\hat{B}\hat{C}\hat{A}\right], \tag{B.8}$$

using (A.13), and noting that averages of the form e.g.

$$\left\langle\hat{\phi}^\dagger(\mathbf{r},0)\hat{\phi}(\mathbf{r},0)\hat{\phi}(\mathbf{r},0)\hat{\phi}^\dagger(\mathbf{r}',\tau)\hat{\phi}(\mathbf{r}',\tau)\hat{\phi}(\mathbf{r}',\tau)\right\rangle \tag{B.9}$$

where there are not equal occurrences of $\hat{\phi}^\dagger$ and $\hat{\phi}$ may be safely neglected as every term in the Hartree-Fock factorization [267] will contain an anomalous average $\langle\hat{\phi}\hat{\phi}\rangle$ or $\langle\hat{\phi}^\dagger\hat{\phi}^\dagger\rangle$, we find

$$\begin{aligned} \dot{\rho}_{\mathbf{C}}|_{(1)} = & \frac{g^2}{\hbar^2}\int d^3\mathbf{r}\int d^3\mathbf{r}'\int_{-\infty}^{0}d\tau\Big\{ \\ & \langle\hat{\phi}^\dagger(\mathbf{r}',\tau)\hat{\phi}^\dagger(\mathbf{r}',\tau)\hat{\phi}(\mathbf{r}',\tau)\hat{\phi}^\dagger(\mathbf{r},0)\hat{\phi}(\mathbf{r},0)\hat{\phi}(\mathbf{r},0)\rangle\left[\hat{\psi}^\dagger(\mathbf{r},0),\rho_{\mathbf{C}}\hat{\psi}(\mathbf{r}',\tau)\right] \\ & +\langle\hat{\phi}^\dagger(\mathbf{r}',\tau)\hat{\phi}(\mathbf{r}',\tau)\hat{\phi}(\mathbf{r}',\tau)\hat{\phi}^\dagger(\mathbf{r},0)\hat{\phi}^\dagger(\mathbf{r},0)\hat{\phi}(\mathbf{r},0)\rangle\left[\hat{\psi}(\mathbf{r},0),\rho_{\mathbf{C}}\hat{\psi}^\dagger(\mathbf{r}',\tau)\right] \\ & +\langle\hat{\phi}^\dagger(\mathbf{r},0)\hat{\phi}^\dagger(\mathbf{r},0)\hat{\phi}(\mathbf{r},0)\hat{\phi}^\dagger(\mathbf{r}',\tau)\hat{\phi}(\mathbf{r}',\tau)\hat{\phi}(\mathbf{r}',\tau)\rangle\left[\hat{\psi}^\dagger(\mathbf{r}',\tau)\rho_{\mathbf{C}},\hat{\psi}(\mathbf{r},0)\right] \\ & +\langle\hat{\phi}^\dagger(\mathbf{r},0)\hat{\phi}(\mathbf{r},0)\hat{\phi}(\mathbf{r},0)\hat{\phi}^\dagger(\mathbf{r}',\tau)\hat{\phi}^\dagger(\mathbf{r}',\tau)\hat{\phi}(\mathbf{r}',\tau)\rangle\left[\hat{\psi}(\mathbf{r}',\tau)\rho_{\mathbf{C}},\hat{\psi}^\dagger(\mathbf{r},0)\right]\Big\}. \end{aligned} \tag{B.10}$$

B.3 Two-field terms

Consider the second order term

$$\dot{\rho}_{\mathbf{C}}|_{(2)} = \mathrm{Tr}_{\mathbf{I}}\left[\left\{\mathcal{P}\mathcal{L}^{(2)}_{\mathbf{IC}}\int_{-\infty}^{0} d\tau \exp\left[-(\mathcal{L}_{\mathbf{C}}+\mathcal{L}_{\mathbf{I}})\tau\right]\mathcal{L}^{(2)}_{\mathbf{IC}}\right\}\rho_{\mathbf{C}}\otimes\rho_{\mathbf{I}}\right]. \tag{B.11}$$

Following the same reasoning as in B.2, with the additional observation that commutators of the form e.g.

$$\left[\hat{\psi}^{\dagger}(\mathbf{r},0)\hat{\psi}^{\dagger}(\mathbf{r},0),\rho_{\mathbf{C}}\hat{\psi}(\mathbf{r}',\tau)\rho_{\mathbf{C}}\hat{\psi}(\mathbf{r}',\tau)\right] \tag{B.12}$$

where coherent field operators appear twice in succession may be safely neglected due to the presence of the anomalous field operator pairings $\hat{\psi}\hat{\psi}$ or $\hat{\psi}^{\dagger}\hat{\psi}^{\dagger}$, gives the result

$$\begin{aligned}\dot{\rho}_{\mathbf{C}}|_{(2)} = \frac{4g^2}{\hbar^2}\int d^3\mathbf{r}\int d^3\mathbf{r}'\int_{-\infty}^{0} d\tau\Big\{ & \\ \langle\hat{\phi}^{\dagger}(\mathbf{r}',\tau)\hat{\phi}(\mathbf{r}',\tau)\hat{\phi}^{\dagger}(\mathbf{r},0)\hat{\phi}(\mathbf{r},0)\rangle\left[\hat{n}(\mathbf{r},0),\rho_{\mathbf{C}}\hat{n}(\mathbf{r}',\tau)\right] & \\ +\langle\hat{\phi}^{\dagger}(\mathbf{r},0)\hat{\phi}(\mathbf{r},0)\hat{\phi}^{\dagger}(\mathbf{r}',\tau)\hat{\phi}(\mathbf{r}',\tau)\rangle\left[\hat{n}(\mathbf{r}',\tau)\rho_{\mathbf{C}},\hat{n}(\mathbf{r},0)\right]\Big\} &\end{aligned} \tag{B.13}$$

where we have introduced the coherent region number density operator

$$\hat{n}(\mathbf{r},t) = \hat{\psi}^{\dagger}(\mathbf{r},t)\hat{\psi}(\mathbf{r},t). \tag{B.14}$$

B.4 Three-field terms

Consider the third order term

$$\dot{\rho}_{\mathbf{C}}|_{(3)} = \mathrm{Tr}_{\mathbf{I}}\left[\left\{\mathcal{P}\mathcal{L}^{(3)}_{\mathbf{IC}}\int_{-\infty}^{0} d\tau \exp\left[-(\mathcal{L}_{\mathbf{C}}+\mathcal{L}_{\mathbf{I}})\tau\right]\mathcal{L}^{(3)}_{\mathbf{IC}}\right\}\rho_{\mathbf{C}}\otimes\rho_{\mathbf{I}}\right]. \tag{B.15}$$

Similar reasoning to the one-field and two-field terms gives

$$\begin{aligned}\dot{\rho}_{\mathbf{C}}|_{(3)} \;=\; & \frac{g^2}{\hbar^2}\int d^3\mathbf{r}\int d^3\mathbf{r}'\int_{-\infty}^{0} d\tau\Big\{ \\ & \langle\hat{\phi}(\mathbf{r},0)\hat{\phi}^\dagger(\mathbf{r}',\tau)\rangle\left[\hat{\psi}^\dagger(\mathbf{r}',\tau)\hat{\psi}(\mathbf{r}',\tau)\hat{\psi}(\mathbf{r}',\tau)\rho_{\mathbf{C}},\hat{\psi}^\dagger(\mathbf{r},0)\hat{\psi}^\dagger(\mathbf{r},0)\hat{\psi}(\mathbf{r},0)\right] \\ & +\langle\hat{\phi}^\dagger(\mathbf{r}',\tau)\hat{\phi}(\mathbf{r},0)\rangle\left[\hat{\psi}^\dagger(\mathbf{r},0)\hat{\psi}^\dagger(\mathbf{r},0)\hat{\psi}(\mathbf{r},0),\rho_{\mathbf{C}}\hat{\psi}^\dagger(\mathbf{r}',\tau)\hat{\psi}(\mathbf{r}',\tau)\hat{\psi}(\mathbf{r}',\tau)\right] \\ & +\langle\hat{\phi}^\dagger(\mathbf{r},0)\hat{\phi}(\mathbf{r}',\tau)\rangle\left[\hat{\psi}^\dagger(\mathbf{r}',\tau)\hat{\psi}^\dagger(\mathbf{r}',\tau)\hat{\psi}(\mathbf{r}',\tau)\rho_{\mathbf{C}},\hat{\psi}^\dagger(\mathbf{r},0)\hat{\psi}(\mathbf{r},0)\hat{\psi}(\mathbf{r},0)\right] \\ & +\langle\hat{\phi}(\mathbf{r}',\tau)\hat{\phi}^\dagger(\mathbf{r},0)\rangle\left[\hat{\psi}^\dagger(\mathbf{r},0)\hat{\psi}(\mathbf{r},0)\hat{\psi}(\mathbf{r},0),\rho_{\mathbf{C}}\hat{\psi}^\dagger(\mathbf{r}',\tau)\hat{\psi}^\dagger(\mathbf{r}',\tau)\hat{\psi}(\mathbf{r}',\tau)\right]\Big\}.\end{aligned} \tag{B.16}$$

Here we have an anomalous field operator pairing $\hat{\psi}\hat{\psi}$ or $\hat{\psi}^\dagger\hat{\psi}^\dagger$ in every term, and thus the entirety of (B.16) is neglected.

Appendix C

Reservoir interaction damping amplitudes

In this appendix we show for completeness how the reservoir rates are derived analytically for a semi-classical reservoir [317].

C.1 Number-damping amplitude

Treating the number-damping as a local process allowed us to write the number-damping amplitude in the form

$$G(\mathbf{u}) \equiv \int d^3\mathbf{v} G^{(+)}(\mathbf{u},\mathbf{v},0). \tag{C.1}$$

Noting that the Bose-Einstein distribution can be expanded as

$$W(\mathbf{r},\mathbf{k}) = \frac{1}{e^{\beta(\hbar\omega(\mathbf{r},\mathbf{k})-\mu)}-1} = \sum_{n=1}^{\infty} e^{n\beta(\mu-\hbar\omega(\mathbf{r},\mathbf{k}))} \tag{C.2}$$

and performing the spatial integral leads to

$$\begin{aligned} G(\mathbf{u}) &= \frac{g^2}{(2\pi)^5\hbar^2}\sum_{p=0}^{\infty}\sum_{q=1}^{\infty}\sum_{r=1}^{\infty} e^{\beta(\mu-V(\mathbf{u}))(p+q+r)} \int_{\mathbf{I}} d^3\mathbf{k}_1 \int_{\mathbf{I}} d^3\mathbf{k}_2 \int_{\mathbf{I}} d^3\mathbf{k}_3\, \delta^{(3)}\left(\mathbf{k}_1-\mathbf{k}_2-\mathbf{k}_3\right) \\ &\quad \times\delta\left(\frac{\hbar}{2m}\left(\mathbf{k}_1^2-\mathbf{k}_2^2-\mathbf{k}_3^3\right)-V(\mathbf{u})/\hbar\right) e^{-\left(p\mathbf{k}_1^2+q\mathbf{k}_2^2+r\mathbf{k}_3^3\right)\beta\hbar^2/2m}. \end{aligned} \tag{C.3}$$

The first delta function gives $\mathbf{k}_1 = \mathbf{k}_2 + \mathbf{k}_3$, so

$$\begin{aligned} G(\mathbf{u}) &= \frac{g^2}{(2\pi)^5\hbar^2}\sum_{p=0}^{\infty}\sum_{q=1}^{\infty}\sum_{r=1}^{\infty} e^{\beta(\mu-V(\mathbf{u}))(p+q+r)}\int_{\mathbf{I}} d^3\mathbf{k}_2\int_{\mathbf{I}} d^3\mathbf{k}_3\delta\left(\frac{\hbar}{m}\mathbf{k}_2\cdot\mathbf{k}_3 - V(\mathbf{u})/\hbar\right) \\ &\quad\times e^{-\left(p(\mathbf{k}_2+\mathbf{k}_3)^2+q\mathbf{k}_2^2+r\mathbf{k}_3^3\right)\beta\hbar^2/2m}\Theta\left(\frac{\hbar^2}{2m}(\mathbf{k}_2+\mathbf{k}_3)^2 + V(\mathbf{u}) - \epsilon_{\text{cut}}\right), \end{aligned} \tag{C.4}$$

where $\Theta(x)$ is the Heaviside step function, which ensures that the integration is restricted to the incoherent region. We can write this in terms of the relative angle α between $\mathbf{k}_2$ and $\mathbf{k}_3$

$$\begin{aligned} G(\mathbf{u}) &= \frac{g^2}{(2\pi)^5\hbar^2}\sum_{p=0}^{\infty}\sum_{q=1}^{\infty}\sum_{r=1}^{\infty} e^{\beta(\mu-V(\mathbf{u}))(p+q+r)}\int_{\mathbf{I}} d^3\mathbf{k}_2\int_{\mathbf{I}} d^3\mathbf{k}_3\delta\left(\frac{\hbar}{m}k_2k_3\cos\alpha - V(\mathbf{u})/\hbar\right) \\ &\quad\times e^{-\left(2pk_2k_3\cos\alpha+(p+q)k_2^2+(p+r)k_3^3\right)\beta\hbar^2/2m} \\ &\quad\times\Theta\left(\frac{\hbar^2}{2m}(k_2^2+k_3^2+2k_2k_3\cos\alpha) + V(\mathbf{u}) - \epsilon_{\text{cut}}\right). \end{aligned} \tag{C.5}$$

We choose the $\mathbf{k}_2$ and $\mathbf{k}_3$ z-axes to coincide, such that $\alpha = \theta_{k2}$, allowing us to perform all the angular integration:

$$\begin{aligned} G(\mathbf{u}) &= \frac{g^2}{(2\pi)^5\hbar^2}\frac{8m\pi^2}{\hbar}\sum_{p=0}^{\infty}\sum_{q=1}^{\infty}\sum_{r=1}^{\infty} e^{\beta(\mu-V(\mathbf{u}))(p+q+r)}\int_{\mathbf{I}} k_2dk_2\int_{\mathbf{I}} k_3dk_3 \\ &\quad\times e^{-\beta pV(\mathbf{u})}e^{-\left((p+q)k_2^2+(p+r)k_3^2\right)\beta\hbar^2/2m}\Theta\left(\frac{\hbar^2}{2m}(k_2^2+k_3^2) + 2V(\mathbf{u}) - \epsilon_{\text{cut}}\right). \end{aligned} \tag{C.6}$$

Let $s = (p+q)\hbar^2\beta k_2^2/2m$, $t = (p+r)\hbar^2\beta k_3^2/2m$, then the integral takes the form

$$G(\mathbf{u}) = \frac{g^2}{(2\pi)^5\hbar^2}\frac{8m^3\pi^2}{\beta^2\hbar^5}\sum_{p=0}^{\infty}\sum_{q=1}^{\infty}\sum_{r=1}^{\infty}\frac{e^{\beta\mu(p+q+r)}}{(p+q)(p+r)}e^{-\beta V(\mathbf{u})(2p+q+r)}\int_{s_{\min}}^{\infty} dse^{-s}\int_{t_{\min}}^{\infty} dte^{-t}. \tag{C.7}$$

The boundaries of integration are defined by the individual restrictions on k_2 and k_3 to remain in the incoherent region

$$\frac{\hbar^2k_i^2}{2m} \geq \epsilon_{\text{cut}} - V(\mathbf{u}), \quad i = 2, 3 \tag{C.8}$$

giving

$$s \geq (p+q)\beta(\epsilon_{\rm cut} - V(\mathbf{u})), \quad t \geq (p+r)\beta(\epsilon_{\rm cut} - V(\mathbf{u})), \tag{C.9}$$

and the Heaviside function resulting from the restriction on k_1

$$\frac{s}{\beta(p+q)} + \frac{t}{\beta(p+r)} + 2V(\mathbf{u}) - \epsilon_{\rm cut} \geq 0. \tag{C.10}$$

For the moment, let us assume that the former inequalities are the harder restriction, so

$$s_{\rm min} = (p+q)\beta(\epsilon_{\rm cut} - V(\mathbf{u})), \quad t_{\rm min} = (p+r)\beta(\epsilon_{\rm cut} - V(\mathbf{u})). \tag{C.11}$$

Now consider the latter inequality for these values

$$\frac{s_{\rm min}}{\beta(p+q)} + \frac{t_{\rm min}}{\beta(p+r)} + 2V(\mathbf{u}) - \epsilon_{\rm cut} = \epsilon_{\rm cut} > 0, \tag{C.12}$$

so these are the lowest values of s and t that satisfy every inequality. Evaluating the integral then leads to

$$G(\mathbf{u}) \;=\; \frac{g^2}{(2\pi)^5\hbar^2}\frac{8m^3\pi^2}{\beta^2\hbar^5}\sum_{p=0}^{\infty}\sum_{q=1}^{\infty}\sum_{r=1}^{\infty}\frac{e^{\beta\mu(p+q+r)}}{(p+q)(p+r)}e^{-\beta\epsilon_{\rm cut}(2p+q+r)}, \tag{C.13}$$

and we note that we have lost the spatial dependence. Letting $j = p+1$, $k = q-1$, $l = r-1$

$$G(\mathbf{u}) \;=\; \frac{g^2}{(2\pi)^5\hbar^2}\frac{8m^3\pi^2}{\beta^2\hbar^5}\sum_{j=1}^{\infty}\sum_{k=0}^{\infty}\sum_{l=0}^{\infty}\frac{e^{\beta\mu(j+k+l+1)}}{(j+k)(j+l)}e^{-\beta\epsilon_{\rm cut}(2j+k+l)} \tag{C.14}$$

and recalling the definition of the Lerch transcendent $\Phi[z,s,a] = \sum_{k=0}^{\infty} z^k/(a+k)^s$ gives us the final form of the number-damping rate

$$G(\mathbf{u}) = \frac{k_BT}{\hbar}\gamma = \frac{k_BT}{\hbar}\gamma_0\sum_{j=1}^{\infty}\frac{e^{\beta\mu(j+1)}}{e^{2\beta\epsilon_{\rm cut}j}}\Phi\left[\frac{e^{\beta\mu}}{e^{\beta\epsilon_{\rm cut}}}, 1, j\right]^2 \tag{C.15}$$

with $\gamma_0 = 8a_s^2/\lambda_{\rm dB}^2$, where a_s is the s-wave scattering length and $\lambda_{\rm dB} = \sqrt{2\pi\hbar^2/mk_BT}$ is the thermal de Broglie wavelength.

C.2 Energy-damping amplitude

The form of the energy-damping amplitude is obtained by considering the Fourier transform with respect to the relative coordinate $\mathbf{v}$

$$\begin{aligned}\bar{M}(\mathbf{u},\mathbf{q},0) &= \frac{1}{(2\pi)^3}\int d^3\mathbf{v}e^{-i\mathbf{q}\cdot\mathbf{v}}M(\mathbf{u},\mathbf{v},0) &\text{(C.16)}\\ &= \frac{2g^2}{\hbar^2(2\pi)^5}\int_{\mathbf{I}}d^3\mathbf{k}_1\int_{\mathbf{I}}d^3\mathbf{k}_2 W(\mathbf{u},\mathbf{k}_1)\left[1+W(\mathbf{u},\mathbf{k}_2)\right]\delta(\mathbf{k}_1-\mathbf{k}_2-\mathbf{q})\\ &\quad\times\delta(\omega(\mathbf{u},\mathbf{k}_1)-\omega(\mathbf{u},\mathbf{k}_2)). &\text{(C.17)}\end{aligned}$$

The first delta function gives $\mathbf{k}_2=\mathbf{k}-\mathbf{q}$, where we have replaced $\mathbf{k}_1\to\mathbf{k}$, allowing the amplitude to be written as

$$\bar{M}(\mathbf{u},\mathbf{q},0) = \frac{2g^2}{\hbar^2(2\pi)^5}\int_{\mathbf{I}}d^3\mathbf{k}W(\mathbf{u},\mathbf{k})\left[1+W(\mathbf{u},\mathbf{k})\right]\frac{2m}{\hbar}\delta(2\mathbf{k}\cdot\mathbf{q}-\mathbf{q}^2), \quad \text{(C.18)}$$

where we have also used that the second delta function gives $\mathbf{q}^2=2\mathbf{k}\cdot\mathbf{q}$ and so

$$\hbar\omega(\mathbf{u},\mathbf{k}-\mathbf{q})=\frac{\hbar^2\mathbf{k}^2}{2m}+\frac{\hbar^2\mathbf{q}^2}{2m}-\frac{\hbar^2\mathbf{k}\cdot\mathbf{q}}{m}+V(\mathbf{u})=\frac{\hbar^2\mathbf{k}^2}{2m}+V(\mathbf{u})=\hbar\omega(\mathbf{u},\mathbf{k}). \quad \text{(C.19)}$$

We choose the x axis of the $\mathbf{k}$ integration to be parallel to $\mathbf{q}$, so that the delta function gives $k_x=|\mathbf{q}|/2$. Then let

$$e_{\mathbf{k}_\perp}(\mathbf{u},\mathbf{q})=\frac{\hbar^2\left(\mathbf{k}_\perp^2+\mathbf{q}^2/4\right)}{2m}+V(\mathbf{u})\equiv\hbar\omega(\mathbf{u},\mathbf{k}_\perp+\hat{\mathbf{x}}|\mathbf{q}|/2) \quad \text{(C.20)}$$

where $\mathbf{k}_\perp\equiv k_y\hat{\mathbf{y}}+k_z\hat{\mathbf{z}}$. Then

$$\bar{M}(\mathbf{u},\mathbf{q},0) = \frac{2mg^2}{\hbar^3(2\pi)^5|\mathbf{q}|}\int_{\mathbf{I}}d^2\mathbf{k}_\perp f\left(e_{\mathbf{k}_\perp}(\mathbf{u},\mathbf{q})\right)\left[1+f\left(e_{\mathbf{k}_\perp}(\mathbf{u},\mathbf{q})\right)\right], \quad \text{(C.21)}$$

where

$$f(x)=\frac{1}{e^{\beta(x-\mu)}-1}. \quad \text{(C.22)}$$

We change the integration variable to $x \equiv e_{\mathbf{k}_\perp}(\mathbf{u},\mathbf{q})$ using (C.20), with the lower limit of the integral given by $E_{\min}(\mathbf{u},\mathbf{q}) \equiv \max\left(\epsilon_{\rm cut}, V(\mathbf{u}) + \hbar^2\mathbf{k}_\perp^2/8m\right)/k_BT$

$$\bar{M}(\mathbf{u},\mathbf{q},0) = \frac{4\pi m^2 g^2}{\hbar^5(2\pi)^5|\mathbf{q}|}\int_{E_{\min}(\mathbf{u},\mathbf{q})}^{\infty} dx f(x)\left[1+f(x)\right], \tag{C.23}$$

with

$$E_{\min}(\mathbf{u},\mathbf{q}) = \max\left(\epsilon_{\rm cut}, \frac{\hbar^2\mathbf{q}^2}{8m} + V(\mathbf{u})\right). \tag{C.24}$$

Performing the final integral gives

$$\bar{M}(\mathbf{u},\mathbf{q},0) = \frac{4\pi m^2 g^2 k_B T}{\hbar^5(2\pi)^5|\mathbf{q}|}\frac{1}{e^{(E_{\min}(\mathbf{u},\mathbf{q})-\mu)/k_BT}-1} \tag{C.25}$$

and the energy-damping amplitude is then the inverse Fourier transform of this

$$M(\mathbf{u},\mathbf{v},0) = \frac{16\pi a^2 k_B T}{\hbar(2\pi)^3}\int d^3\mathbf{q}\frac{1}{|\mathbf{q}|}\frac{1}{e^{(E_{\min}(\mathbf{u},\mathbf{q})-\mu)/k_BT}-1} \tag{C.26}$$

where we have also used $g \equiv 4\pi\hbar^2 a/m$.

This can be further simplified by considering the conservation of momentum during the scattering event. In a semiclassical description the momenta must satisfy

$$\mathbf{k}_1 + \mathbf{k}_3 = \mathbf{k}_2 + \mathbf{k}_4 \tag{C.27}$$

where $\mathbf{k}_1$ and $\mathbf{k}_2$ are the initial and final wave-vector of the incoherent region particle (as in (C.17)), and $\mathbf{k}_3$ and $\mathbf{k}_4$ are the initial and final wave-vector of the coherent region particle. Since the coherent region particle is in the coherent region, we also have

$$\frac{\hbar^2\mathbf{k}_j^2}{2m} + V(\mathbf{u}) \le \epsilon_{\rm cut}, \quad j = 3,4. \tag{C.28}$$

The momentum transfer in the scattering event also satisfies

$$\mathbf{q} = \mathbf{k}_1 - \mathbf{k}_2 = \mathbf{k}_4 - \mathbf{k}_3, \tag{C.29}$$

and so we have

$$\frac{\hbar^2\mathbf{q}^2}{8m} + V(\mathbf{u}) = \frac{1}{4}\left(\frac{\hbar^2\mathbf{k}_3^2}{2m} + \frac{\hbar^2\mathbf{k}_4^2}{2m} - \frac{\hbar^2\mathbf{k}_3\cdot\mathbf{k}_4}{m}\right) + V(\mathbf{u}) \tag{C.30}$$

$$\leq \frac{1}{4}\left(\frac{\hbar^2\mathbf{k}_3^2}{2m} + \frac{\hbar^2\mathbf{k}_4^2}{2m} + \frac{\hbar^2|\mathbf{k}_3||\mathbf{k}_4|}{m}\right) + V(\mathbf{u}). \tag{C.31}$$

Clearly $2|\mathbf{k}_3||\mathbf{k}_4| \leq \mathbf{k}_3^2 + \mathbf{k}_4^2$, and so

$$\frac{\hbar^2\mathbf{q}^2}{8m} + V(\mathbf{u}) \leq \frac{1}{2}\left(\frac{\hbar^2\mathbf{k}_3^2}{2m} + \frac{\hbar^2\mathbf{k}_4^2}{2m}\right) + V(\mathbf{u}) \tag{C.32}$$

$$\leq \epsilon_{\rm cut}. \tag{C.33}$$

Therefore the value of $E_{\rm min}(\mathbf{u},\mathbf{q}) = \max\left(\epsilon_{\rm cut}, \hbar^2\mathbf{q}^2/8m + V(\mathbf{u})\right)$ is always given by the energy cutoff $E_{\rm min}(\mathbf{u},\mathbf{q}) \equiv \epsilon_{\rm cut}$. The energy-damping amplitude then has no $\mathbf{u}$ dependence, and we write it as

$$M(\mathbf{u},\mathbf{v},0) = \frac{k_B T}{\hbar}\varepsilon(\mathbf{v}) = \frac{k_B T}{\hbar}\varepsilon(\mathbf{r}-\mathbf{r}') \tag{C.34}$$

where

$$\varepsilon(\mathbf{v}) = \frac{\mathcal{M}}{(2\pi)^3}\int d^3\mathbf{q}\frac{e^{i\mathbf{q}\cdot\mathbf{v}}}{|\mathbf{q}|} \tag{C.35}$$

and

$$\mathcal{M} \equiv \frac{16\pi a_s^2}{e^{(\epsilon_{\rm cut}-\mu)/k_B T} - 1}. \tag{C.36}$$

Appendix D

Mapping Fokker-Planck equations to stochastic differential equations

The Fokker-Planck equation (FPE) obtained by a mapping from the master equation (3.106) may be written as

$$\begin{aligned}\frac{\partial W[\psi,\psi^*]}{\partial t} &= \int d^3\mathbf{r}\left[-\frac{\bar{\delta}}{\bar{\delta}\psi(\mathbf{r})}\left(-\frac{i}{\hbar}\left(1-i\gamma\right)\left(L-\mu\right)\psi(\mathbf{r})\right)+\text{h.c.}\right]W[\psi,\psi^*]\\ &+\int d^3\mathbf{r}\left[-\frac{\bar{\delta}}{\bar{\delta}\psi(\mathbf{r})}\left(\frac{i}{\hbar}V_\varepsilon(\mathbf{r})\psi(\mathbf{r})\right)+\text{h.c.}\right]W[\psi,\psi^*]\\ &+\int d^3\mathbf{r}\left[\frac{\gamma k_B T}{\hbar}\frac{\bar{\delta}^{(2)}}{\bar{\delta}\psi(\mathbf{r})\bar{\delta}\psi^*(\mathbf{r})}+\text{h.c.}\right]W[\psi,\psi^*]\\ &+\int d^3\mathbf{r}\int d^3\mathbf{r}'\frac{k_B T}{\hbar}\varepsilon(\mathbf{r}-\mathbf{r}')\left[\frac{\bar{\delta}}{\bar{\delta}\psi(\mathbf{r})}\psi(\mathbf{r})\frac{\bar{\delta}}{\bar{\delta}\psi^*(\mathbf{r}')}\psi^*(\mathbf{r}')+\text{h.c.}\right]W[\psi,\psi^*]\\ &-\int d^3\mathbf{r}\int d^3\mathbf{r}'\frac{k_B T}{\hbar}\varepsilon(\mathbf{r}-\mathbf{r}')\left[\frac{\bar{\delta}}{\bar{\delta}\psi(\mathbf{r})}\psi(\mathbf{r})\frac{\bar{\delta}}{\bar{\delta}\psi(\mathbf{r}')}\psi(\mathbf{r}')+\text{h.c.}\right]W[\psi,\psi^*].\end{aligned} \tag{D.1}$$

Consider a general FPE for a complex field with projected functional derivatives

$$\begin{aligned}\frac{\partial P}{\partial t} &= \int d^D\mathbf{r}\left[-\frac{\bar{\delta}}{\bar{\delta}\psi(\mathbf{r})}A(\psi,\psi^*,t)+\text{h.c.}\right.\\ &+\frac{\bar{\delta}^{(2)}}{\bar{\delta}\psi(\mathbf{r})\bar{\delta}\psi(\mathbf{r})}D_{11}(\psi,\psi^*,t)+\text{h.c.}\\ &\left.+\frac{\bar{\delta}^{(2)}}{\bar{\delta}\psi(\mathbf{r})\bar{\delta}\psi^*(\mathbf{r})}D_{12}(\psi,\psi^*,t)+\text{h.c.}\right]P\end{aligned} \tag{D.2}$$

where $\mathbf{A}=[A,A^*]$ is the drift and $\mathbf{D}=[D_{11},D_{12};D_{12}^*,D_{11}^*]$ is the diffusion matrix. If the diffusion matrix is positive semi-definite it can be factorised as $\mathbf{D}=\mathbf{B}\mathbf{B}^{\mathrm{T}}$, and the FPE

Appendix D. Mapping Fokker-Planck equations to stochastic differential equations

(D.2) can be mapped to the stochastic differential equation (SDE) [272]

$$\begin{bmatrix} d\psi(\mathbf{r},t) \\ d\psi^*(\mathbf{r},t) \end{bmatrix} = \begin{bmatrix} \mathcal{P} & 0 \\ 0 & \mathcal{P}^* \end{bmatrix} \Big(\mathbf{A}(\mathbf{r},t)dt + \mathbf{B}(\mathbf{r},t)\mathbf{dW}(\mathbf{r},t) \Big) \tag{D.3}$$

where $\mathbf{dW}(\mathbf{r},t)$ a vector of noises.

Appendix E

Hartree-Fock parameter estimation scheme for the SPGPE

Here we present the method used to estimate physically consistent parameters for the SPGPE using the the Hartree-Fock parameter estimation scheme [2]. This procedure gives estimates for the chemical potential μ and energy cutoff $\epsilon_{\rm cut}$ given the total atom number N_T and temperature T.

E.1 Hartree-Fock Density of States

The Hartree-Fock density of states for a trapped 3D system is defined by

$$\rho_{\rm HF}(\epsilon) = \int \frac{d^3\mathbf{r}d^3\mathbf{p}}{(2\pi\hbar)^3}\delta\left(\epsilon - E_{\rm HF}(\mathbf{r},\mathbf{p})\right) \tag{E.1}$$

with the energy of a noncondensate atom in the Hartree-Fock approximation given by

$$E_{\rm HF}(\mathbf{r},\mathbf{p}) = \frac{\mathbf{p}^2}{2m} + U(\mathbf{r},t) \tag{E.2}$$

and the potential experienced by noncondensate atoms is

$$U(\mathbf{r},t) = \begin{cases} 2\mu - U_{\rm ext}(\mathbf{r}) & n_c \neq 0 \\ U_{\rm ext}(\mathbf{r}) & n_c = 0. \end{cases} \tag{E.3}$$

The minimum value of this potential is μ and occurs on the boundary of the condensate; in the Thomas-Fermi approximation this is defined by the Thomas-Fermi radii. We can evaluate the integral over momentum space in (E.1) without any knowledge of the potential,

giving the result

$$\rho_{\rm HF}(\epsilon) = \frac{m^{3/2}}{\sqrt{2}\pi^2\hbar^3}\int_{U<\epsilon} d^3\mathbf{r}\sqrt{\epsilon - U(\mathbf{r},t)}. \tag{E.4}$$

E.2 3D Harmonic trap

We redefine the energy scale by shifting it by $U_{\rm min} = \mu$, the minimum of the effective potential $U(\mathbf{r},t)$,

$$\bar{\epsilon} = \epsilon - \mu, \quad \bar{U}(\mathbf{r},t) = U(\mathbf{r},t) - \mu. \tag{E.5}$$

Note that the effective potential is now

$$\bar{U}(\mathbf{r},t) = \begin{cases} \mu - U_{\rm ext}(\mathbf{r}) & n_c \neq 0 \\ -\mu + U_{\rm ext}(\mathbf{r}) & n_c = 0. \end{cases} \tag{E.6}$$

Evaluating the spatial integral then leads to

$$\rho_{\rm HF}(\bar{\epsilon}) = \frac{1}{\pi\left(\hbar\bar{\omega}\right)^3}\left[2\bar{\epsilon}^{3/2}\mu^{1/2} + \left(\bar{\epsilon}+\mu\right)^2\tan^{-1}\left(\sqrt{\frac{\bar{\epsilon}}{\mu}}\right) + \left(\bar{\epsilon}-\mu\right)^2\ln\left(\frac{\sqrt{|\mu-\bar{\epsilon}|}}{\sqrt{\mu}+\sqrt{\bar{\epsilon}}}\right)\right] \tag{E.7}$$

E.3 Estimating SPGPE parameters

The total number of atoms in the system is given by

$$N_T = \int_0^\infty d\bar{\epsilon}\,\rho_{\rm HF}(\bar{\epsilon})n_{\rm BE}(\bar{\epsilon}) + N_0 \tag{E.8}$$

where

$$n_{\rm BE}(\bar{\epsilon}) = \frac{1}{e^{(\bar{\epsilon}-\mu)/k_BT}-1}. \tag{E.9}$$

Given the total atom number N_T and temperature T, (E.8) can be solved numerically to find N_0, and hence μ, using the appropriate Thomas-Fermi chemical potential. For temperatures above T_c the parameter $\mu(T)$ may be found easily using (E.8) with $N_0 = 0$. For the temperature $T = T_c$ the chemical potential is simply $\mu = 0$.

The simplest way to connect the cutoff in our chosen representation $\epsilon_{\rm cut}$ with the cutoff as determined by the Hartree-Fock density of states $\epsilon_{\rm cutHF}$ is to require that the number of modes in the coherent region is the same in either representation.

The Hartree-Fock density of states takes energies relative to the condensate, so from (E.9) with $\mu = 0$ we have

$$\epsilon_{\rm cutHF} = k_B T \ln\left(1 + \frac{1}{n_{\rm cut}}\right) \tag{E.10}$$

valid for $T < T_c$, where $\epsilon_{\rm cutHF}$ is the energy set by the Hartree-Fock density of states at mean occupation $n_{\rm cut}$. The number of states is given by integrating from the minimum energy up to the cutoff. Hence the condition giving $\epsilon_{\rm cut}$ is

$$\int_0^{\varepsilon_{\rm cutHF}} d\bar{\epsilon}\, \rho_{\rm HF}(\bar{\epsilon}) = \int_{\varepsilon_0}^{\epsilon_{\rm cut}} d\epsilon\, \rho_{\rm SP}(\epsilon) \tag{E.11}$$

where ε_0 is the lowest energy in the chosen representation and $\rho_{\rm SP}(\epsilon)$ is the single-particle density of states. For the harmonic system

$$\varepsilon_0 = \frac{\hbar}{2}(\omega_x + \omega_y + \omega_z), \quad \rho_{\rm SP}(\epsilon) = \frac{\epsilon^2}{2(\hbar\bar{\omega})^3}. \tag{E.12}$$

For temperatures above the transition ($T > T_c$) , the single-particle density is applicable so $\epsilon_{\rm cut}$ can be found directly by inverting the Bose-Einstein distribution

$$\epsilon_{\rm cut} = k_B T \ln\left(1 + \frac{1}{n_{\rm cut}}\right) + \mu. \tag{E.13}$$

Appendix F

Numerically solving the SPGPE

In this appendix we present the method we use for numerically solving the full SPGPE. This method was developed by Rooney *et al* for a three-dimensional harmonically trapped system [1], and is an extension of the spectral-Galerkin method previously developed for evaluating the SPGPE number-damping terms [115].

The appendix is organised as follows. In section F.1 we outline the SPGPE formalism in non-dimensional form, as is standard for numerical evolution. In section F.2 we give an outline of the spectral approach, and arrive at the equations of motion for the single-particle mode amplitudes. In section F.3 we review the algorithm used to evaluate the SPGPE energy-damping terms using Gauss-Hermite quadrature. We conclude in section F.4 we briefly discuss the accuracy of the algorithm, as tested in [1].

F.1 Dimensionless SPGPE

In this work, a suitable system of dimensionless units is chosen depending on the nature of the system under consideration. The units of length x_0, time t_0, and energy E_0 are sufficient to fully define the entire system of units. For harmonically trapped systems, harmonic oscillator units

$$x_0 = \sqrt{\frac{\hbar}{m\omega_0}}, \quad t_0 = \frac{1}{\omega_0}, \quad E_0 = \hbar\omega_0, \tag{F.1}$$

for some trapping frequency ω_0. The single-particle Hamiltonian is

$$H_{\rm sp} = -H_0 + \delta V(\mathbf{r}, t) \tag{F.2}$$

where

$$H_0 = -\frac{1}{2}\nabla^2 + \frac{1}{2}\left(\lambda_x^2 x^2 + \lambda_y^2 y^2 + \lambda_z^2 z^2\right) \tag{F.3}$$

defines the basis of the coherent region. Here $\lambda_i = \omega_i/\omega_0$ is the anisotropy in the ith dimension. The classical field is decomposed into

$$\psi(\mathbf{r},t) = \sum_{n\in\mathbf{C}} c_n(t)\phi_n(\mathbf{r}) \tag{F.4}$$

where the $\phi_n(\mathbf{r})$ are eigenfunctions of H_0

$$H_0\phi_n(\mathbf{r}) = \epsilon_n\phi_n(\mathbf{r}). \tag{F.5}$$

The summation covers the coherent region

$$C = \{n : \epsilon_n \leq \epsilon_{\rm cut}\} \tag{F.6}$$

where $\epsilon_{\rm cut}$ is the cutoff energy and n represents all quantum numbers required to completely specify the eigenfunctions of H_0. The SPGPE (3.147)-(3.150) in dimensionless form is

$$(S)d\psi(\mathbf{r},t) = d\psi|_H + d\psi|_\gamma + (S)d\psi|_\varepsilon\,, \tag{F.7}$$

where

$$d\psi|_H = \mathcal{P}\{-i(L-\mu)\psi(\mathbf{r},t)dt\} \tag{F.8}$$

$$d\psi|_\gamma = \mathcal{P}\{-\gamma(L-\mu)\psi(\mathbf{r},t)dt + dW(\mathbf{r},t)\} \tag{F.9}$$

$$(S)d\psi|_\varepsilon = \mathcal{P}\{-iV_\varepsilon(\mathbf{r},t)\psi(\mathbf{r},t)dt + i\psi(\mathbf{r},t)dU(\mathbf{r},t)\} \tag{F.10}$$

respectively. The projector, defined by

$$\mathcal{P}\{F(\mathbf{r})\} = \sum_{n\in\mathbf{C}} \phi_n(\mathbf{r}) \int d^3\mathbf{r}'\phi_n^*(\mathbf{r}')F(\mathbf{r}'), \tag{F.11}$$

formally restricts evolution of the classical field to the coherent region. The first term of the SPGPE (F.8) gives Hamiltonian evolution of the coherent region where

$$L\psi(\mathbf{r},t) = (H_{\rm sp} + C_{\rm NL}|\psi(\mathbf{r},t)|^2)\psi(\mathbf{r},t) \tag{F.12}$$

is the Gross-Pitaevskii operator for the coherent region and the dimensionless interaction parameter is

$$C_{\mathrm{NL}} = \frac{g}{E_0 x_0^3} = \frac{4\pi a_s}{x_0} \tag{F.13}$$

with a_s the s-wave scattering length.

F.1.1 Number-damping terms

The second term of the SPGPE (F.9) gives the number-damping reservoir interaction. The dimensionless parameter γ determines the rate of the number-damping process, and the Gaussian complex noise has the non-zero correlation

$$\langle dW^*(\mathbf{r},t)dW(\mathbf{r}',t)\rangle = 2\gamma T\delta(\mathbf{r},\mathbf{r}')dt, \tag{F.14}$$

with T the dimensionless temperature and

$$\delta(\mathbf{r},\mathbf{r}') = \sum_{n\in\mathbf{C}} \phi_n(\mathbf{r})\phi_n^*(\mathbf{r}') \tag{F.15}$$

the coherent region delta function.

F.1.2 Energy-damping terms

The third term of the SPGPE (F.10) gives the energy-damping reservoir interaction. The process is described by the energy-damping potential

$$V_\varepsilon(\mathbf{r},t) = \int d^3\mathbf{r}'\varepsilon(\mathbf{r}-\mathbf{r}')\nabla'\cdot\mathbf{j}(\mathbf{r}',t) \tag{F.16}$$

where the dimensionless coherent region current is

$$\mathbf{j}(\mathbf{r},t) = \frac{i}{2}\left(\psi(\mathbf{r},t)\nabla\psi^*(\mathbf{r},t) - \psi^*(\mathbf{r},t)\nabla\psi(\mathbf{r},t)\right) \tag{F.17}$$

and the epsilon function is

$$\varepsilon(\mathbf{r}) = \frac{\mathcal{M}}{(2\pi)^3}\int d^3\mathbf{k}\frac{e^{i\mathbf{k}\cdot\mathbf{r}}}{|\mathbf{k}|} \tag{F.18}$$

where

$$\mathcal{M} = \frac{16\pi a_s^2}{x_0^2}\frac{1}{e^{\beta(\epsilon_{\rm cut}-\mu)}-1} \tag{F.19}$$

parameterises the rate of the energy-damping process, somewhat analogous to the parameter γ for number-damping. The energy-damping potential can also be expressed as

$$V_\varepsilon(\mathbf{r},t) = -\mathcal{M}\int d^3\mathbf{k}\frac{e^{i\mathbf{k}\cdot\mathbf{r}}}{(2\pi)^{3/2}}i\hat{\mathbf{k}}\cdot\int d^3\mathbf{r}'\frac{e^{-i\mathbf{k}\cdot\mathbf{r}'}}{(2\pi)^{3/2}}\mathbf{j}(\mathbf{r}',t) \tag{F.20}$$

where $\hat{\mathbf{k}} = \mathbf{k}/|\mathbf{k}|$. The energy-damping potential can thus be evaluated using Fourier transforms

$$V_\varepsilon(\mathbf{r},t) = -\mathcal{M}\mathcal{F}^{-1}\left[i\hat{\mathbf{k}}\cdot\mathcal{F}\left[\mathbf{j}(\mathbf{r}',t)\right]\right] = -i\mathcal{M}\mathcal{F}^{-1}\left[\hat{\mathbf{k}}\cdot\tilde{\mathbf{j}}(\mathbf{k},t)\right]. \tag{F.21}$$

The energy-damping noise is real with non-zero (and non-local) correlation

$$\langle dU(\mathbf{r},t)dU(\mathbf{r}',t)\rangle = 2T\varepsilon(\mathbf{r}-\mathbf{r}')dt. \tag{F.22}$$

The energy-damping noise is more conveniently represented in momentum space. Defining

$$dU(\mathbf{k},t) = \int d^3\mathbf{r}\frac{e^{-i\mathbf{k}\cdot\mathbf{r}}}{(2\pi)^{3/2}}dU(\mathbf{r},t) \tag{F.23}$$

and noting that this may now be complex, we find that the momentum space correlation is given by

$$\begin{aligned}
\langle dU(\mathbf{k},t)dU^*(\mathbf{k}',t)\rangle &= \frac{2\mathcal{M}Tdt}{(2\pi)^3}\int d^3\mathbf{q}\frac{1}{|\mathbf{q}|}\int d^3\mathbf{r}\frac{e^{i(\mathbf{k}-\mathbf{q})\cdot\mathbf{r}}}{(2\pi)^{3/2}}\int d^3\mathbf{r}\frac{e^{-i(\mathbf{k}'-\mathbf{q})\cdot\mathbf{r}'}}{(2\pi)^{3/2}} &\text{(F.24)}\\
&= 2\mathcal{M}Tdt\int d^3\mathbf{q}\frac{1}{|\mathbf{q}|}\delta(\mathbf{k}-\mathbf{q})\delta(\mathbf{k}'-\mathbf{q}) &\text{(F.25)}\\
&= \frac{2\mathcal{M}T}{|\mathbf{k}|}\delta(\mathbf{k}-\mathbf{k}')dt. &\text{(F.26)}
\end{aligned}$$

The energy-damping correlations are local and diagonal in momentum space, which is exploited to obtain a numerical representation. There is an apparent singularity due to the inverse dependence on $|\mathbf{k}|$, however in practice this is not an issue as any finite system has an effective infrared cutoff due to the system size.

F.2 Formal Algorithm

F.2.1 Spectral-Galerkin formalism

We use a spectral Galerkin approach [278] for numerically solving the SPGPE (F.7), exploiting that H_0 is diagonal in the spectral basis and projecting the SPGPE onto this basis. This results in a set of stochastic differential equations for the mode amplitudes of the form

$$\begin{aligned}(S)dc_n &= -i\left[(\epsilon_n-\mu)c_n+G_n+V_n\right]dt \\ &\quad -\gamma\left[(\epsilon_n-\mu)c_n+G_n+V_n\right]dt+dA_n \\ &\quad -i\left[S_n dt+dB_n\right]\end{aligned} \tag{F.27}$$

where the first line represents Hamiltonian evolution $d\psi|_H$, the second line represents number-damping $d\psi|_\gamma$, and the final line represents energy-damping $d\psi|_\varepsilon$. The matrix elements and noises are given by

$$G_n = C_{\rm NL}\int d^3\mathbf{r}\phi_n^*(\mathbf{r})|\psi(\mathbf{r},t)|^2\psi(\mathbf{r},t) \tag{F.28}$$

$$V_n = \int d^3\mathbf{r}\phi_n^*(\mathbf{r})\delta V(\mathbf{r},t)\psi(\mathbf{r},t) \tag{F.29}$$

$$S_n = \int d^3\mathbf{r}\phi_n^*(\mathbf{r})V_\varepsilon(\mathbf{r},t)\psi(\mathbf{r},t) \tag{F.30}$$

$$dA_n = \sqrt{2\gamma T}\left(\frac{du_n+dv_n}{\sqrt{2}}\right) \tag{F.31}$$

$$dB_n = \int d^3\mathbf{r}\phi_n^*(\mathbf{r})\psi(\mathbf{r},t)\sum_m \zeta_m(\mathbf{r})dw_m, \tag{F.32}$$

corresponding to two-body interactions, perturbation potential, energy-damping potential, number-damping noise, and energy-damping noise respectively. For simplicity we neglect the possibility of a perturbation potential by formally setting $\delta V(\mathbf{r},t)\equiv 0$, as it is not a situation that arises in this work[1]. We define the functions $\zeta_m(\mathbf{r})$ later in the chapter. The noises du_n, dv_n, dw_n are independent standard Wiener processes satisfying

$$\langle du_n\rangle = \langle dv_n\rangle = \langle dw_n\rangle = 0 \tag{F.33}$$

$$\langle du_n du_m\rangle = \langle dv_n dv_m\rangle = \langle dw_n dw_m\rangle = \delta_{nm}dt \tag{F.34}$$

[1] We direct the reader to [1] for information on how to implement a perturbation potential

thus giving the required correlations for the noise terms in the SPGPE.

F.2.2 Stochastic time evolution

The main challenged in numerically propagating the SPGPE (F.27) is in the construction of the nonlinear matrix elements (F.28)-(F.32); this is covered in Sec F.3. Once we have those elements, we evolve the SPGPE in time using stochastic integration. Here we briefly describe the stochastic integration method used for temporal integration of the SPGPE.

Full SPGPE

For solving the full SPGPE including all reservoir interactions we use the *weak vector semi-implicit Euler algorithm* [272, 274, 318, 319]; we are unable to use a more efficient algorithm, such as a high order Runge-Kutta method, due to the energy-damping noise being multiplicative. Our equation of motion (F.27) is of the form

$$(S)dc_n = a_n(t, \mathbf{c})dt + dA_n(du_n, dv_n) + dB_n(t, \mathbf{c}, \mathbf{dw}) \tag{F.35}$$

where

$$a_n = -(i+\gamma)[(\epsilon_n - \mu)c_n + G_n] - iS_n. \tag{F.36}$$

The notation $\mathbf{c}$ indicates dependence on the full field ψ where $\{\mathbf{c}\}_n = c_n(t)$. The energy-damping noise has dependence on a vector of Wiener processes where $\{\mathbf{dw}\}_n = dw_n(t)$. The solution is propagated to a set of discrete times $t_j = j\Delta t$ where Δt is the step size, and the solution at t_j is denoted $c_n(t_j) = c_n^{(j)}$. Solutions at sequential times are related by $c_n^{(j+1)} = c_n^{(j)} + \Delta c_n^{(j)}$ where

$$\Delta c_n^{(j)} = a_n(\bar{t}_j, \bar{\mathbf{c}}^{(j)})\Delta t + \Delta A_n(\Delta u_n^{(j)}, \Delta v_n^{(j)}) + \Delta B_n(\bar{t}_j, \bar{\mathbf{c}}^{(j)}, \Delta\bar{\mathbf{w}}^{(j)}), \tag{F.37}$$

with

$$\bar{c}_n^{(j)} = \frac{1}{2}(c_n^{(j)} + c_n^{(j+1)}) \tag{F.38}$$

$$\bar{t}_j = \frac{1}{2}(t_{j+1} + t_j) \tag{F.39}$$

$$\langle \Delta u_m^{(j)} \Delta u_n^{(j)} \rangle = \Delta t\, \delta_{mn} \tag{F.40}$$

$$\langle \Delta v_m^{(j)} \Delta v_n^{(j)} \rangle = \Delta t\, \delta_{mn} \tag{F.41}$$

$$\langle \Delta w_m^{(j)} \Delta w_n^{(j)} \rangle = \Delta t\, \delta_{mn}. \tag{F.42}$$

The noises $\Delta u_n^{(j)}$ are formally defined as

$$\Delta u_n^{(j)} \equiv \int_{t_j}^{t_{j+1}} du_n, \tag{F.43}$$

and $\Delta u_n^{(j)}$ is sampled as a real Gaussian distributed random variable with zero mean and variance Δt. Similarly for $\Delta v_n^{(j)}$ and $\Delta w_n^{(j)}$. These equations are solved iteratively as they are implicit; typically 4 iterations is sufficient to achieve convergence.

Number-damped SPGPE

The number-damped SPGPE

$$d\psi = \mathcal{P}\left\{-(i+\gamma)(L-\mu)\psi dt + dW_\gamma(\mathbf{r},t)\right\} \tag{F.44}$$

has been widely used in previous works, and as such an efficient numerical implementation has been firmly established based on the spectral-Galerkin approach. The equation of motion for the mode amplitudes, found by projecting (F.44) onto the single particle basis, is

$$dc_n = -(i+\gamma)\left[(\epsilon_n - \mu)c_n + G_n\right]dt + dA_n. \tag{F.45}$$

The noise term dA_n is additive and thus we are able to use a more efficient algorithm than the semi-implicit Euler; a stochastic Runge-Kutta method is used, which has improved convergence and stability [274]. The only nonlinear term to be constructed is G_n, and so the number-damped SPGPE can be solved by a fairly simple extension of PGPE solving methods [115, 269, 273, 275].

Energy-damped SPGPE

The energy-damped SPGPE

$$d\psi = -i\mathcal{P}\left\{(L - \mu + V_\varepsilon(\mathbf{r},t))\psi dt - \psi(\mathbf{r},t)dU(\mathbf{r},t)\right\} \tag{F.46}$$

is obtained by neglecting the contributions from number-damping (F.9). Projecting (F.46) onto the single particle basis gives the equation of motion for the mode amplitudes

$$(S)dc_n = -i\left[(\epsilon_n - \mu)c_n + G_n + S_n\right]dt - idB_n. \tag{F.47}$$

The presence of multiplicative noise enforces the use of the semi-implicit Euler algorithm described in the section F.2.2. As the methods for implementing the number-damping terms are relatively simple and thus well understood[2], in this chapter we focus on the implementation of the energy-damped SPGPE, for which a numerical implementation has only been developed more recently [1].

F.3 Energy-damped SPGPE matrix elements

The main challenge in propagating the energy-damping terms numerically is in constructing the nonlinear matrix elements at each time step. Here we describe how this is done in the harmonic oscillator basis, though in principle the single-particle states of any potential can be used as the basis.

F.3.1 Harmonic oscillator basis properties

The eigenstates of the basis Hamiltonian are separable into the 1D basis states

$$\phi_n(\mathbf{r}) = \phi_\alpha^{\lambda_x}(x)\phi_\beta^{\lambda_y}(y)\phi_\gamma^{\lambda_z}(z), \tag{F.48}$$
$$\epsilon_n = \epsilon_\alpha^{\lambda_x} + \epsilon_\beta^{\lambda_y} + \epsilon_\gamma^{\lambda_z}, \tag{F.49}$$
$$c_n(t) = c_{\alpha\beta\gamma}(t). \tag{F.50}$$

[2] examples include but are not limited to Refs. [2, 71, 115, 120, 121, 131, 140, 148]

The $\phi_\alpha^{\lambda_x}(x)$ are eigenstates of the dimensionless 1D harmonic oscillator Hamiltonian

$$\left[-\frac{1}{2}\frac{d^2}{dx^2}+\frac{1}{2}\lambda_x^2 x^2\right]\phi_\alpha^{\lambda_x}(x)=\epsilon_\alpha^{\lambda_x}\phi_\alpha^{\lambda_x}(x) \tag{F.51}$$

and take the form

$$\phi_\alpha^{\lambda_x}(x)=\lambda_x^{1/4}h_\alpha H_\alpha\left(\sqrt{\lambda_x}x\right)e^{-\lambda_x x^2/2} \tag{F.52}$$

where the normalization constant is $h_\alpha=\left[2^\alpha\alpha!\sqrt{\pi}\right]^{-1/2}$ and $H_\alpha(x)$ is the physicists Hermite polynomial of degree α defined by the recurrence relation

$$H_{\alpha+1}(x)=2xH_\alpha(x)-2\alpha H_{\alpha-1}(x),\quad \alpha=1,2,3,... \tag{F.53}$$

with $H_0(x)=1$ and $H_1(x)=2x$. The energy eigenvalue is

$$\epsilon_\alpha^{\lambda_x}=\lambda_x\left(\alpha+\frac{1}{2}\right),\quad \alpha=0,1,2,... \tag{F.54}$$

where we have used Greek subscripts to denote the 1D eigenstates as opposed to the general n for 3D eigenstates. The coherent region is then defined by

$$C=\left\{\alpha,\beta,\gamma:\epsilon_\alpha^{\lambda_x}+\epsilon_\beta^{\lambda_y}+\epsilon_\gamma^{\lambda_z}\leq\epsilon_{\rm cut}\right\}, \tag{F.55}$$

such that there are $M_x=\lfloor(\epsilon_{\rm cut}/\lambda_x+1/2)\rfloor\approx\epsilon_{\rm cut}/\lambda_x$ distinct 1D eigenstates in the x direction and $M_T\approx M_xM_yM_z/6$ total 3D basis states in the coherent region.

From here we will consider the case of an isotropic harmonic trap ($\lambda_x=\lambda_y=\lambda_z=1$) so as to avoid cumbersome notation, however the method is equally applicable to the anisotropic case. All reference to λ is thus dropped from this point on and we consider a system with $M=\lfloor(\epsilon_{\rm cut}+1/2)\rfloor\approx\epsilon_{\rm cut}$ distinct 1D eigenstates in each direction.

An advantage that comes with using a harmonic oscillator basis is the ability to use step operators to represent derivatives exactly in the spectral basis. The step operators are defined by

$$\hat{a}_x^+ = \frac{1}{\sqrt{2}}\left(-\frac{\partial}{\partial x}+x\right), \tag{F.56}$$

$$\hat{a}_x^- = \frac{1}{\sqrt{2}}\left(\frac{\partial}{\partial x}+x\right), \tag{F.57}$$

and so in the spectral basis

$$(\hat{a}_x^+)_{\alpha\beta} = \sqrt{\beta+1}\delta_{\alpha,\beta+1}, \tag{F.58}$$
$$(\hat{a}_x^-)_{\alpha\beta} = \sqrt{\beta}\delta_{\alpha,\beta-1}. \tag{F.59}$$

From this the derivative operator is given exactly in the spectral basis by

$$(\hat{\partial}_x)_{\alpha\beta} = \sqrt{\frac{\beta}{2}}\delta_{\alpha,\beta-1} - \sqrt{\frac{\beta+1}{2}}\delta_{\alpha,\beta+1} \tag{F.60}$$

Similarly we obtain an exact spectral representation for differentiation with respect to both y and z. These are essential in evaluating the energy-damping matrix elements due to the presence of the coherent region current.

F.3.2 Interaction term

Here we outline the method for constructing the nonlinear contact interaction term G_n (F.28) using Gauss-Hermite quadrature. Conveniently, this method is exact for a harmonically trapped system. Using (F.4) and (F.51), we can write the classical field as

$$\psi(\mathbf{r}) = Q(\mathbf{r})e^{-(x^2+y^2+z^2)/2}, \tag{F.61}$$

where

$$Q(\mathbf{r}) = \sum_{\{\alpha\beta\gamma\}\in\mathbf{C}} c_{\alpha\beta\gamma}(t)h_\alpha H_\alpha(x)h_\beta H_\beta(y)h_\gamma H_\gamma(z) \tag{F.62}$$

is a polynomial of maximum degree $M-1$ in each of the coordinates as a result of the energy cutoff. The interaction term (F.28), being fourth order in the field, can be written in the form

$$G_{\alpha\beta\gamma} = \int d^3\mathbf{r}e^{-2(x^2+y^2+z^2)}P_{\alpha\beta\gamma}(\mathbf{r}) \tag{F.63}$$

where

$$P_{\alpha\beta\gamma}(\mathbf{r}) = C_{\mathrm{NL}}h_\alpha H_\alpha(x)h_\beta H_\beta(y)h_\gamma H_\gamma(z)|Q(\mathbf{r})|^2Q(\mathbf{r}) \tag{F.64}$$

is a polynomial of maximum degree $4(M-1)$ in each coordinate. We are able to evaluate (F.63) exactly using Gauss-Hermite quadrature. The general form of the N point Gauss-Hermite quadrature rule is

$$\int_{-\infty}^{\infty} dx W(x) f(x) dx \approx \sum_{j=1}^{N} w_j f(x_j) \tag{F.65}$$

where $W(x)$ is a Gaussian weight function, x_j are the roots of a particular Hermite polynomial dependent on the precise nature of $W(x)$, and w_j are a set of corresponding weights also dependent on $W(x)$. This expression is exact if the function $f(x)$ is a polynomial of maximum degree $2N-1$. Thus the integral (F.63) may be evaluated exactly as

$$G_{\alpha\beta\gamma} = \sum_{ijk} w_i w_j w_k P_{\alpha\beta\gamma}(x_i, x_j, x_k) \tag{F.66}$$

provided $4(M-1) \leq 2N-1$. Thus we require a three-dimensional spatial grid with $2M-1$ points in each coordinate, where $\{x_i\}$ and $\{w_i\}$ are the $2M-1$ roots and weights of the one-dimensional Gauss-Hermite quadrature with weight function $W(x) = e^{-2x^2}$.

F.3.3 Energy-damping effective potential term

Constructing the energy-damping effective potential matrix elements (F.30) requires the use of multiple Fourier transforms. Here we demonstrate how an auxiliary harmonic-oscillator basis is used to perform the Fourier transforms in the spectral representation. This method was first developed for evaluating the dipolar interaction term in the PGPE [275].

The coherent region current (F.17) is given by

$$\mathbf{j}(\mathbf{r}) = j_x(\mathbf{r})\mathbf{e}_x + j_y(\mathbf{r})\mathbf{e}_y + j_z(\mathbf{r})\mathbf{e}_z \tag{F.67}$$

with $\mathbf{e}_u$ the unit vector in the direction $u \in \{x, y, z\}$, and

$$j_u(\mathbf{r}) = \frac{i}{2}\left(\psi(\mathbf{r})\partial_u\psi^*(\mathbf{r}) - \psi^*(\mathbf{r})\partial_u\psi(\mathbf{r})\right), \tag{F.68}$$

which can be calculated exactly using step operators (F.60). Now we introduce our auxil-

iary basis states

$$\chi_\alpha(x) = 2^{1/4} h_\alpha H_\alpha\left(\sqrt{2}x\right) e^{-x^2}, \tag{F.69}$$

which are eigenstates of the harmonic oscillator Hamiltonian with twice the trapping frequency

$$H_{\rm aux} = -\frac{1}{2}\nabla^2 + 2\left(x^2+y^2+z^2\right). \tag{F.70}$$

The auxiliary basis states are related to the spectral basis states by

$$\chi_\alpha(x) = 2^{1/4}\phi_\alpha\left(\sqrt{2}x\right). \tag{F.71}$$

Note that we can write the current as

$$j_u(\mathbf{r}) = R_u(\mathbf{r}) e^{-(x^2+y^2+z^2)} \tag{F.72}$$

with $R_u(\mathbf{r})$ a polynomial of maximum degree $2(M-1)$ in each coordinate. Since the exponential factor in the current is the same as the exponential factor in the auxiliary basis states, we can also express the current as

$$j_u(\mathbf{r}) = \sum_{\alpha\beta\gamma} d^u_{\alpha\beta\gamma}\chi_\alpha(x)\chi_\beta(y)\chi_\gamma(z). \tag{F.73}$$

Since $R_u(\mathbf{r})$ is a polynomial of maximum degree $2(M-1)$ in each coordinate, we need at most $2M-1$ basis states in each coordinate, thus there are $(2M-1)^3 \approx 8M^3$ coefficients $d^u_{\alpha\beta\gamma}$ to calculate. The coefficients are

$$\begin{aligned} d^u_{\alpha\beta\gamma} &= \int d^3\mathbf{r} j_u(\mathbf{r})\chi^*_\alpha(x)\chi^*_\beta(y)\chi^*_\gamma(z) &\text{(F.74)}\\ &= \int d^3\mathbf{r} e^{-2(x^2+y^2+z^2)} Z^u_{\alpha\beta\gamma}(\mathbf{r}), &\text{(F.75)}\end{aligned}$$

where

$$Z^u_{\alpha\beta\gamma}(\mathbf{r}) = j_u(\mathbf{r})\chi^*_\alpha(x)\chi^*_\beta(y)\chi^*_\gamma(z)e^{2(x^2+y^2+z^2)} \tag{F.76}$$

is a polynomial of maximum degree $4(M-1)$ in each coordinate. We now have an integral

of the same form as (F.63), with the same weight function $W(x) = e^{-2x^2}$ and maximum polynomial degree $4(M-1)$, so we can use the same Gauss-Hermite quadrature to integrate (F.75). So

$$d^u_{\alpha\beta\gamma} = \sum_{ijk} w_i w_j w_k Z^u_{\alpha\beta\gamma}(x_i, x_j, x_k), \tag{F.77}$$

where the quadrature roots $\{x_i\}$ and weights $\{w_i\}$ are the same as used for (F.63).

The effective potential (F.21) requires the Fourier transform of each current component. We exploit the fact that the spectral basis states are eigenstates of the Fourier transform operator

$$\tilde{\phi}_\alpha(k_x) = \frac{1}{(2\pi)^{1/2}} \int dx e^{-ik_x x} \phi_\alpha(x) \tag{F.78}$$

$$= (-i)^\alpha \phi_\alpha(k_x), \tag{F.79}$$

and so for the auxiliary basis

$$\tilde{\chi}_\alpha(k_x) = 2^{-1/2}(-i)^\alpha \chi_\alpha\left(k_x/2\right). \tag{F.80}$$

The Fourier transform of the current is then

$$\tilde{j}_u(\mathbf{k}) = 2^{-3/2} \sum_{\alpha\beta\gamma} (-i)^{\alpha+\beta+\gamma} d^u_{\alpha\beta\gamma} \chi_\alpha(k_x/2)\chi_\beta(k_y/2)\chi_\gamma(k_z/2). \tag{F.81}$$

The next step is to evaluate

$$\Phi(\mathbf{k}) = \hat{\mathbf{k}} \cdot \tilde{\mathbf{j}}(\mathbf{k}) = |\mathbf{k}|^{-1} \sum_u k_u \tilde{j}_u(\mathbf{k}), \tag{F.82}$$

and then compute the inverse Fourier transform of this. To this end, we first expand the energy-damping potential $V_\varepsilon(\mathbf{r})$ in the auxiliary basis

$$V_\varepsilon(\mathbf{r}) \approx \sum_{\alpha\beta\gamma} f_{\alpha\beta\gamma} \chi_\alpha(x)\chi_\beta(y)\chi_\gamma(z) \tag{F.83}$$

$$= 2^{3/4} e^{-\left(x^2+y^2+z^2\right)} \sum_{\alpha\beta\gamma} f_{\alpha\beta\gamma} h_\alpha H_\alpha\left(\sqrt{2}x\right) h_\beta H_\beta\left(\sqrt{2}y\right) h_\gamma H_\gamma\left(\sqrt{2}z\right), \tag{F.84}$$

where

$$f_{\alpha\beta\gamma} = -i\mathcal{M}2^{-3/2}(i)^{\alpha+\beta+\gamma}\int d^3\mathbf{k}\chi_\alpha\left(k_x/2\right)\chi_\beta\left(k_y/2\right)\chi_\gamma\left(k_z/2\right)\Phi(\mathbf{k}). \tag{F.85}$$

We can write this as

$$f_{\alpha\beta\gamma} = -i\mathcal{M}\int d^3\mathbf{k}T_{\alpha\beta\gamma}(\mathbf{k})e^{-\left(k_x^2+k_y^2+k_z^2\right)/2} \tag{F.86}$$

where

$$T_{\alpha\beta\gamma}(\mathbf{k}) = 2^{-3/2}(i)^{\alpha+\beta+\gamma}\chi_\alpha\left(k_x/2\right)\chi_\beta\left(k_y/2\right)\chi_\gamma\left(k_z/2\right)\Phi(\mathbf{k})e^{\left(k_x^2+k_y^2+k_z^2\right)/2}. \tag{F.87}$$

We thus have an integral of the form (F.65), with argument k and weight function $W(k) = e^{-k^2/2}$. The integral can thus be found using the quadrature roots $\left\{\bar{k}_i\right\}$ and weights $\{\bar{w}_i\}$ corresponding to $W(k) = e^{-k^2/2}$

$$f_{\alpha\beta\gamma} = -i\mathcal{M}\sum_{ijk}\bar{w}_i\bar{w}_j\bar{w}_k T_{\alpha\beta\gamma}(\bar{k}_i,\bar{k}_j,\bar{k}_k). \tag{F.88}$$

where

$$T_{\alpha\beta\gamma}(\bar{k}_i,\bar{k}_j,\bar{k}_k) = 2^{-3/2}(i)^{\alpha+\beta+\gamma}\chi_\alpha\left(\bar{k}_i/2\right)\chi_\beta\left(\bar{k}_j/2\right)\chi_\gamma\left(\bar{k}_k/2\right)\Phi(\bar{k}_i,\bar{k}_j,\bar{k}_k)e^{\left(\bar{k}_i^2+\bar{k}_j^2+\bar{k}_k^2\right)/2}. \tag{F.89}$$

We point out that due to the presence of the $|\mathbf{k}|^{-1}$ in (F.82), it cannot be represented exactly in the harmonic oscillator basis by a finite number of terms. Thus the quadrature rules used for the integral (F.88) are not exact and consequently the representation of the energy-damping potential $V_\varepsilon(\mathbf{r})$ (F.83) is only an approximation, the accuracy of which will depend on the number of k-grid quadrature points in a non-trivial fashion.

Now that the energy-damping potential is constructed we can construct the matrix elements (F.30)

$$S_{\alpha\beta\gamma} = \int d^3\mathbf{r}e^{-2\left(x^2+y^2+z^2\right)}Y_{\alpha\beta\gamma}(\mathbf{r}) \tag{F.90}$$

where

$$Y_{\alpha\beta\gamma}(\mathbf{r}) = h_\alpha H_\alpha(x)h_\beta H_\beta(y)h_\gamma H_\gamma(z)Q(\mathbf{r})V_\varepsilon(\mathbf{r})e^{x^2+y^2+z^2} \tag{F.91}$$

is a polynomial of maximum degree $4(M-1)$ in each coordinate. We can thus use a quadrature rule for the weight function $W(x) = e^{-2x^2}$ to evaluate this integral using a grid of $2M-1$ points in each coordinate

$$S_{\alpha\beta\gamma} = \sum_{\alpha\beta\gamma} w_i w_j w_k Y_{\alpha\beta\gamma}(x_i, x_j, x_k), \tag{F.92}$$

with $\{x_i\}$ and $\{w_i\}$ the roots and weights corresponding to the weight function $W(x) = e^{-2x^2}$.

F.3.4 Energy-damping noise term

Correlations

We can construct a noise with the appropriate correlations in k-space by

$$dU(\mathbf{k}, t) = \sqrt{\frac{2\mathcal{M}T}{|\mathbf{k}|}} \sum_{\alpha\beta\gamma} dw_{\alpha\beta\gamma} \tilde{\phi}_{\alpha\beta\gamma}(\mathbf{k}), \tag{F.93}$$

where the $dw_{\alpha\beta\gamma}$ are real independent standard Wiener processes

$$\langle dw_{\alpha\beta\gamma} dw_{\alpha'\beta'\gamma'} \rangle = \delta_{\alpha\alpha'}\delta_{\beta\beta'}\delta_{\gamma\gamma'} dt. \tag{F.94}$$

Using (F.79) the phase factors cancel out and we are left with the desired diagonal correlations

$$\langle dU(\mathbf{k}, t) dU^*(\mathbf{k}', t) \rangle = \frac{2\mathcal{M}T}{|\mathbf{k}|} \sum_{\alpha\beta\gamma} (-i)^{\alpha+\beta+\gamma} \phi_{\alpha\beta\gamma}(\mathbf{k}) (-i)^{-(\alpha+\beta+\gamma)} \phi_{\alpha\beta\gamma}(\mathbf{k}') dt \tag{F.95}$$

$$= \frac{2\mathcal{M}T}{|\mathbf{k}|} \delta(\mathbf{k}, \mathbf{k}') dt. \tag{F.96}$$

Matrix elements

In the spectral Galerkin approach the noise takes the form of the matrix elements (F.32); we need to project the noise in position space onto the spectral basis. We start with the

noise in k-space (F.93)

$$dU(\mathbf{r},t) = \int d^3\mathbf{k}\frac{e^{i\mathbf{k}\cdot\mathbf{r}}}{(2\pi)^{3/2}}dU(\mathbf{k},t) \tag{F.97}$$

$$= \sum_{\alpha\beta\gamma}\zeta_{\alpha\beta\gamma}(\mathbf{r})dw_{\alpha\beta\gamma}, \tag{F.98}$$

where

$$\zeta_{\alpha\beta\gamma}(\mathbf{r}) = \int d^3\mathbf{k}\frac{e^{i\mathbf{k}\cdot\mathbf{r}}}{(2\pi)^{3/2}}\Theta_{\alpha\beta\gamma}(\mathbf{k}), \tag{F.99}$$

and we have defined

$$\Theta_{\alpha\beta\gamma}(\mathbf{k}) = \sqrt{\frac{2\mathcal{M}T}{|\mathbf{k}|}}\tilde{\phi}_\alpha(k_x)\tilde{\phi}_\beta(k_y)\tilde{\phi}_\gamma(k_z). \tag{F.100}$$

Our main goal at this point is to construct $\zeta_{\alpha\beta\gamma}(\mathbf{r})$. The latter expression (F.100) can be written as

$$\Theta_{\alpha\beta\gamma}(\mathbf{k}) = X_{\alpha\beta\gamma}(\mathbf{k})e^{-\left(k_x^2+k_y^2+k_z^2\right)/2} \tag{F.101}$$

where

$$X_{\alpha\beta\gamma}(\mathbf{k}) = \sqrt{\frac{2\mathcal{M}T}{|\mathbf{k}|}}(-i)^{\alpha+\beta+\gamma}h_\alpha H_\alpha(k_x)h_\beta H_\beta(k_y)h_\gamma H_\gamma(k_z). \tag{F.102}$$

We can perform the inverse Fourier transform of (F.101) using quadrature rules just as in the previous subsection, however now we do not need to introduce an auxiliary basis as the exponential factor in (F.101) matches that of the standard basis states. We write $\zeta_{\alpha\beta\gamma}(\mathbf{r})$ as the product of a polynomial and exponential

$$\zeta_{\alpha\beta\gamma}(\mathbf{r}) \approx K_{\alpha\beta\gamma}(\mathbf{r})e^{-\left(x^2+y^2+z^2\right)/2} \tag{F.103}$$

where

$$K_{\alpha\beta\gamma}(\mathbf{r}) = n_{\alpha\beta\gamma}h_\alpha H_\alpha(x)h_\beta H_\beta(y)h_\gamma H_\gamma(z) \tag{F.104}$$

is a polynomial of maximum degree $M-1$ in each coordinate, and

$$n_{\alpha\beta\gamma} = \int d^3\mathbf{k}(i)^{\alpha+\beta+\gamma}\phi^*_\alpha(k_x)\phi^*_\beta(k_y)\phi^*_\gamma(k_z)\Theta_{\alpha\beta\gamma}(\mathbf{k}). \tag{F.105}$$

The representation of $\zeta_{\alpha\beta\gamma}(\mathbf{r})$ in (F.103) is only approximate, as $X_{\alpha\beta\gamma}(\mathbf{k})$ cannot be represented as a polynomial of finite degree due to the $|\mathbf{k}|^{-1}$ factor; this is the same as for the energy-damping potential (F.83). We can write $n_{\alpha\beta\gamma}$ as

$$n_{\alpha\beta\gamma} = \int d^3\mathbf{k}U_{\alpha\beta\gamma}(\mathbf{k})e^{-\left(k_x^2+k_y^2+k_z^2\right)} \tag{F.106}$$

with

$$U_{\alpha\beta\gamma}(\mathbf{k}) = (i)^{\alpha+\beta+\gamma}h_\alpha H_\alpha(k_x)h_\beta H_\beta(k_y)h_\gamma H_\gamma(k_z)X_{\alpha\beta\gamma}(\mathbf{k}). \tag{F.107}$$

We can these evaluate (F.106) using Gauss-Hermite quadrature

$$n_{\alpha\beta\gamma} = \sum_{ijk}\tilde{w}_i\tilde{w}_j\tilde{w}_k U_{\alpha\beta\gamma}(\tilde{k}_i,\tilde{k}_j,\tilde{k}_k), \tag{F.108}$$

with $\{\tilde{k}_i\}$ and $\{\tilde{w}_i\}$ the roots and weights corresponding to the weight function $W(k) = e^{-k^2}$. Since (F.103) is not exact, we are again in the situation where the number of k points for optimal accuracy is non-trivial.

The matrix elements (F.32) involve the product of a spectral basis state ϕ, the field ψ, and the function ζ, and so can be represented as

$$dB_{\alpha\beta\gamma} = \int d^3\mathbf{r}e^{-\frac{3}{2}\left(x^2+y^2+z^2\right)}dN_{\alpha\beta\gamma}(\mathbf{r}) \tag{F.109}$$

where

$$dN_{\alpha\beta\gamma}(\mathbf{r}) \;=\; h_\alpha H_\alpha(x)h_\beta H_\beta(y)h_\gamma H_\gamma(z)Q(\mathbf{r},t)\sum_{\kappa\lambda\mu}K_{\kappa\lambda\mu}(\mathbf{r})dw_{\kappa\lambda\mu} \tag{F.110}$$

is a polynomial of maximum degree $3(M-1)$ in each coordinate. The matrix element (F.109) can be evaluated using Gauss-Hermite quadrature

$$dB_{\alpha\beta\gamma} = \sum_{ijk}\hat{w}_i\hat{w}_j\hat{w}_k dN_{\alpha\beta\gamma}(\hat{x}_i,\hat{x}_j,\hat{x}_k), \tag{F.111}$$

with $\{\hat{x}_i\}$ and $\{\hat{w}_i\}$ the $3M/2-1$ roots and weights corresponding to the weight function $W(k) = e^{-3x^2/2}$.

F.3.5 Algorithm summary

We now give a summary of the algorithm used for constructing the energy-damped SPGPE matrix elements. We first construct the deterministic terms, then construct the noise term. The procedure is repeated once for each Euler step.

Deterministic terms G_n and S_n

1. Transform the coherent region field from the spectral representation to the spatial representation using

$$\psi(\mathbf{r_s}) = \sum_{\boldsymbol{\sigma}} U_{\mathbf{s}\boldsymbol{\sigma}} c_{\boldsymbol{\sigma}}, \tag{F.112}$$

where $\boldsymbol{\sigma} = \{\alpha, \beta, \gamma\}$, $\mathbf{r_s} = (x_i, x_j, x_k)$ are the quadrature points associated with the weight function $W(x) = e^{-2x^2}$, $c_{\boldsymbol{\sigma}}$ are the spectral basis coefficients of the field, and $U_{\mathbf{s}\boldsymbol{\sigma}} = U_{i\alpha}U_{j\beta}U_{i\gamma}$ are transformation matrices. The transformation matrices are previously constructed by the spectral basis states evaluated at the quadrature points

$$U_{i\alpha} = \phi_\alpha(x_i). \tag{F.113}$$

2. Find the field derivatives in the spectral representation

$$c'_{x\sigma} = \sum_{\kappa\lambda\mu} \left(\hat{\partial}_x\right)_{\alpha\kappa} \left(\hat{I}_y\right)_{\beta\lambda} \left(\hat{I}_z\right)_{\gamma\mu}, \tag{F.114}$$

$$c'_{y\sigma} = \sum_{\kappa\lambda\mu} \left(\hat{I}_x\right)_{\alpha\kappa} \left(\hat{\partial}_y\right)_{\beta\lambda} \left(\hat{I}_z\right)_{\gamma\mu}, \tag{F.115}$$

$$c'_{z\sigma} = \sum_{\kappa\lambda\mu} \left(\hat{I}_x\right)_{\alpha\kappa} \left(\hat{I}_y\right)_{\beta\lambda} \left(\hat{\partial}_z\right)_{\gamma\mu}, \tag{F.116}$$

where the derivative operators are given by (F.60) and the $\hat{I}_j$ are the identity operators.

3. Transform the field derivatives from the spectral representation to the spatial repre-

sentation

$$\psi'_u(\mathbf{r_s}) \;=\; \sum_{\boldsymbol{\sigma}} U_{\mathbf{s}\boldsymbol{\sigma}} c'_{u\sigma}, \tag{F.117}$$

and use this to construct the spatial representation of the coherent region current (F.67)

$$j_u(\mathbf{r_s}) = \frac{i}{2}\left[\psi(\mathbf{r}_s)\left(\psi'_u(\mathbf{r}_s)\right)^* - \left(\psi(\mathbf{r}_s)\right)^* \psi'_u(\mathbf{r}_s)\right]. \tag{F.118}$$

4. Prepare the weighted current components

$$J_u(\mathbf{r_s}) \;\equiv\; w_{\mathbf{s}} e^{2\mathbf{r_s}^2} j_u(\mathbf{r_s}) \tag{F.119}$$

where $w_{\mathbf{s}} = (w_i, w_j, w_k)$ are the quadrature weights associated with the weight function $W(x) = e^{-2x^2}$.

5. Construct the Fourier transform of each component of the current

$$\tilde{j}_{k_u}(\mathbf{k_t}) = \sum_{\mathbf{s}} W_{\mathbf{st}} J_u(\mathbf{r_s}), \tag{F.120}$$

where the precomputed transformation matrix is

$$W_{ir} = 2^{-1/2} \sum_{\alpha} (-i)^{\alpha} \chi_{\alpha}(k_r/2)\chi_{\alpha}(x_i), \tag{F.121}$$

where the k-space quadrature grid is based on the weight function $W(k) = e^{-k^2/2}$.

6. Project the current onto the unit vector $\hat{\mathbf{k}}$ and multiply by the quadrature weights to form

$$\tilde{\mathcal{F}}(\mathbf{k_t}) = \tilde{w}_{\mathbf{t}} e^{\mathbf{k_t}^2/2} \hat{\mathbf{k}}_{\mathbf{t}} \cdot \tilde{\mathbf{j}}(\mathbf{k_t}). \tag{F.122}$$

7. Take the inverse transform to position space to obtain the energy-damping effective potential

$$V_{\varepsilon}(\mathbf{r_s}) = -i\mathcal{M} \sum_{\mathbf{t}} W^*_{\mathbf{st}} \tilde{\mathcal{F}}(\mathbf{k_t}). \tag{F.123}$$

8. The two-body interaction term and energy-damping effective potential have the same quadrature rules for the final integration, so combine the two into a single integrand and multiply by the quadrature weights

$$g(\mathbf{r_s}) = w_{\mathbf{s}} e^{2\mathbf{r_s}^2} \left[C_{\rm NL}|\psi(\mathbf{r_s})|^2 + V_\varepsilon(\mathbf{r_s})\right] \psi(\mathbf{r_s}). \tag{F.124}$$

9. Taking the inverse transformation of $g(\mathbf{r_s})$ back to the spectral basis gives the desired matrix elements

$$G_{\boldsymbol{\sigma}} + S_{\boldsymbol{\sigma}} = \sum_{\mathbf{s}} U^*_{\mathbf{s}\boldsymbol{\sigma}} g(\mathbf{r_s}). \tag{F.125}$$

Energy-damping noise dB_n

1. Generate $dw_{\boldsymbol{\sigma}}$, the Gaussian distributed random variables.

2. Transform the random variables to Fourier space

$$\Psi(\tilde{\mathbf{k}}_{\mathbf{t}}) = \sum_{\boldsymbol{\sigma}} \tilde{U}_{\mathbf{t}\boldsymbol{\sigma}} dw_{\boldsymbol{\sigma}}, \tag{F.126}$$

   where precomputed transformation matrices are the Fourier transformed spectral basis states

$$\tilde{U}_{\mathbf{t}\boldsymbol{\sigma}} = (-i)^{\alpha+\beta+\gamma} \phi_\alpha(\tilde{k}_u)\phi_\beta(\tilde{k}_v)\phi_\gamma(\tilde{k}_w), \tag{F.127}$$

   where the $\tilde{k}_u$ are the points on the k-space quadrature grid for the weight function $W(k) = e^{-k^2}$.

3. Form the appropriate correlation function in k-space, then construct the inverse Fourier transform

$$f(\hat{\mathbf{r}}_{\mathbf{s}}) = \sum_{\mathbf{t}} X^*_{\mathbf{st}} \sqrt{\frac{2T\mathcal{M}}{|\tilde{\mathbf{k}}_{\mathbf{t}}|}} \Psi(\tilde{\mathbf{k}}_{\mathbf{t}}), \tag{F.128}$$

   where

$$X_{ir} = \sum_{\alpha} (-i)^\alpha \phi_\alpha(\tilde{k}_r)\phi_\alpha(\hat{x}_i), \tag{F.129}$$

where the $\hat{x}_i$ are the points on the position space quadrature grid for the weight function $W(x) = e^{-3x^2/2}$.

4. Transform the classical field to position space

$$\psi(\hat{\mathbf{r}}_\mathbf{s}) = \sum_{\boldsymbol{\sigma}} \hat{U}_{\mathbf{s}\boldsymbol{\sigma}} c_{\boldsymbol{\sigma}}, \tag{F.130}$$

where the precomputed transformation matrices are

$$\hat{U}_{\mathbf{s}\boldsymbol{\sigma}} = \phi_\alpha(\hat{x}_i)\phi_\beta(\hat{x}_j)\phi_\gamma(\hat{x}_k). \tag{F.131}$$

5. Form the integrand with appropriate quadrature weights

$$b(\hat{\mathbf{r}}_\mathbf{s}) = \hat{w}_\mathbf{s} e^{3\mathbf{r}_\mathbf{s}^2/2} \psi(\hat{\mathbf{r}}_\mathbf{s}) f(\hat{\mathbf{r}}_\mathbf{s}). \tag{F.132}$$

6. Taking the inverse transform of $b(\hat{\mathbf{r}}_\mathbf{s})$ back to the spectral basis gives the desired matrix elements

$$dB_{\boldsymbol{\sigma}} = \sum_{\mathbf{s}} \hat{U}_{\mathbf{s}\boldsymbol{\sigma}} b(\hat{\mathbf{r}}_\mathbf{s}). \tag{F.133}$$

F.4 Algorithm accuracy

The accuracy of this algorithm has been extensively tested by Rooney *et al* [1]. Here we briefly summarize the checks performed in that work.

Effective potential and matrix elements

The accuracy of the approximate quadrature sums (F.123) and (F.128) is dependent on the size of the k-space quadrature grid. For these two sums, a minimum of $N_k^0 = 2M - 1$ and $N_{k'}^0 = M - 1$ were assumed for the number of quadrature grid points, and increases on these were considered

$$N_k = N_k^0 + \Delta N_k \tag{F.134}$$
$$N_k' = N_k^{0\prime} + \Delta N_k'. \tag{F.135}$$

The accuracy in constructing the effective potential was investigated using the example of a breathing mode, which has the useful property that the effective potential can be calculated analytically. It was found that the accuracy can indeed be improved by at least an order of magnitude for modest values of ΔN_k, but increasing the number of points without bound does not lead to higher accuracies. That is, there is a ΔN_k that depends on the energy cutoff, that gives maximum possible accuracy, and either increasing or decreasing ΔN_k from there only serves to reduce the accuracy. Furthermore, the accuracy is good for all considered values of ΔN_k, with the relative error between the numerically constructed effective potential and the analytic form never exceeding 10^{-4}. In general, the accuracy increases for increasing energy cutoff.

The accuracy in constructing the matrix elements (F.28)-(F.32) was tested for a high-energy randomized state. For the combination of all nonlinear matrix elements $G_{\boldsymbol{\sigma}} + S_{\boldsymbol{\sigma}} + dB_{\boldsymbol{\sigma}}$ both approximate quadrature sums come into play, so testing against both ΔN_k and $\Delta N'_k$ is required. These tests saw that the accuracy in constructing the nonlinear matrix elements increases for increasing either of ΔN_k and $\Delta N'_k$. Again, the accuracy also improves for increasing energy cutoff. The accuracy is generally very good regardless of the values of ΔN_k and $\Delta N'_k$; even for $\Delta N_k = \Delta N'_k = 0$ the relative error between the algorithm and another more accurate method is much less than 10^{-2}.

Propagation convergence

The convergence properties of the algorithm was tested by considering evolution of an initial random state from $t = 0$ to $t = \tau$ for one trap cycle ($\tau = 2\pi$). The accuracy is dependent on both the k-space quadrature grid sizes ΔN_k and $\Delta N'_k$ and the time step size Δt. The accuracy was quantified by considering the ensemble averages of the relative change in normalization δN, relative change in energy δE, relative change in individual mode amplitudes $\delta c_{\boldsymbol{\sigma}}$, and relative difference of all mode amplitudes δX.

For testing convergence with respect to Δt the reference k-space quadrature grids were used, so $\Delta N_k = \Delta N'_k = 0$. The measures of δN and δE represent measures of weak convergence [272]. These measures showed good convergence with Δt, with the relative error in both normalization and energy less than 1% for all values of Δt considered. The other two measures $\delta c_{\boldsymbol{\sigma}}$ and δX represent measures of strong convergence [272]. Good convergence was seen for these measures also, however only the lower values of Δt achieved an accuracy of less than 1%. These measurements of δN, δE, $\delta c_{\boldsymbol{\sigma}}$, and δX showed that the rate of convergence is at least as fast as for the strong vector semi-implicit Euler

method [272], thus justifying the use of the weak vector semi-implicit Euler method in propagation of the SPGPE.

For testing convergence with respect to ΔN_k and $\Delta N'_k$, a time step of $\Delta t = 0.001$ was used, a value that showed accuracy of less than 1% when testing convergence with respect to Δt. Increasing the k-space quadrature grid sizes had no effect on δN, and resulted in increasing accuracy for δE and δX. All values of ΔN_k and $\Delta N'_k$ considered resulted in excellent accuracy over the propagation time, and modifying these values had only a minor influence on the overall accuracy when compared to modifying the time step Δt.

References

[1] S. J. Rooney, P. B. Blakie, and A. S. Bradley, "Numerical method for the stochastic projected Gross-Pitaevskii equation," *Physical Review E*, vol. 89, p. 013302, Jan. 2014.

[2] S. J. Rooney, A. S. Bradley, and P. B. Blakie, "Decay of a quantum vortex: Test of nonequilibrium theories for warm Bose-Einstein condensates," *Physical Review A*, vol. 81, p. 023630, Feb. 2010.

[3] S. N. Bose, "Plancks Gesetz und Lichtquantenhypothese," *Zeitschrift für Physik*, vol. 26, pp. 178–181, Dec. 1924.

[4] A. Einstein, "Quantentheorie des einatomigen idealen Gases," *Sitzungsberichte der Preussischen Akademie der Wissenschaften*, vol. 22, p. 261, 1924.

[5] A. Einstein, "Quantentheorie des einatomigen idealen Gases. Zweite Abhandlung," *Sitzungsberichte der Preussischen Akademie der Wissenschaften*, vol. 1, p. 3, 1925.

[6] A. Einstein, "Zur Quantentheorie des idealen gases," *Sitzungsberichte der Preussischen Akademie der Wissenschaften*, vol. 3, p. 18, 1925.

[7] P. Kapitza, "Viscosity of Liquid Helium below the λ-Point," *Nature*, vol. 141, p. 74, Jan. 1938.

[8] J. F. Allen and A. D. Misener, "Flow of Liquid Helium II," *Nature*, vol. 141, p. 75, Jan. 1938.

[9] F. London, "The λ-Phenomenon of Liquid Helium and the Bose-Einstein Degeneracy," *Nature*, vol. 141, pp. 643–644, Apr. 1938.

[10] J. F. Allen and H. Jones, "New Phenomena Connected with Heat Flow in Helium II," *Nature*, vol. 141, pp. 243–244, Feb. 1938.

[11] W. F. Vinen, "The Detection of Single Quanta of Circulation in Liquid Helium II," in *Proceedings of the Royal Society of London. Series A*, pp. 218–236, Feb. 1961.

[12] B. V. Rollin and F. Simon, "On the "film" phenomenon of liquid helium II," *Physica*, vol. 6, pp. 219–230, Feb. 1939.

[13] L. Onsager, "Statistical hydrodynamics," *Il Nuovo Cimento*, vol. 6, pp. 279–287, Mar. 1949.

[14] R. P. Feynman, "Application of Quantum Mechanics to Liquid Helium," *Progress in Low Temperature Physics*, vol. 1, p. 17, 1955.

[15] O. Penrose and L. Onsager, "Bose-Einstein Condensation and Liquid Helium," *Physical Review*, vol. 104, pp. 576–584, Nov. 1956.

[16] A. J. Leggett, "Superfluidity," *Reviews of Modern Physics*, vol. 71, pp. S318–S323, Mar. 1999.

[17] S. Chu, "Nobel Lecture: The manipulation of neutral particles," *Reviews of Modern Physics*, vol. 70, pp. 685–706, July 1998.

[18] C. N. Cohen-Tannoudji, "Nobel Lecture: Manipulating atoms with photons," *Reviews of Modern Physics*, vol. 70, pp. 707–719, July 1998.

[19] W. D. Phillips, "Nobel Lecture: Laser cooling and trapping of neutral atoms," *Reviews of Modern Physics*, vol. 70, pp. 721–741, July 1998.

[20] M. H. Anderson, J. R. Ensher, M. R. Matthews, C. E. Wieman, and E. A. Cornell, "Observation of Bose-Einstein Condensation in a Dilute Atomic Vapor," *Science*, vol. 269, no. 5221, pp. 198–201, 1995.

[21] K. B. Davis, M. O. Mewes, M. R. Andrews, N. J. van Druten, D. S. Durfee, D. M. Kurn, and W. Ketterle, "Bose-Einstein Condensation in a Gas of Sodium Atoms," *Physical Review Letters*, vol. 75, no. 22, pp. 3969–3973, 1995.

[22] C. C. Bradley, C. A. Sackett, J. J. Tollett, and R. G. Hulet, "Evidence of Bose-Einstein Condensation in an Atomic Gas with Attractive Interactions," *Physical Review Letters*, vol. 75, no. 9, pp. 1687–1690, 1995.

[23] D. G. Fried, T. C. Killian, L. Willmann, D. Landhuis, S. C. Moss, D. Kleppner, and T. J. Greytak, "Bose-Einstein condensation of atomic hydrogen," *Physical Review Letters*, vol. 81, no. 18, pp. 3811–3814, 1998.

[24] S. L. Cornish, N. R. Claussen, J. L. Roberts, E. A. Cornell, and C. E. Wieman, "Stable Rb-85 Bose-Einstein condensates with widely tunable interactions," *Physical Review Letters*, vol. 85, no. 9, pp. 1795–1798, 2000.

[25] A. Robert, O. Sirjean, A. Browaeys, J. Poupard, S. Nowak, D. Boiron, C. I. Westbrook, and A. Aspect, "A Bose-Einstein condensate of metastable atoms," *Science*, vol. 292, no. 5516, pp. 461–464, 2001.

[26] F. P. Dos Santos, J. Leonard, J. M. Wang, C. J. Barrelet, F. Perales, E. Rasel, C. S. Unnikrishnan, M. Leduc, and C. Cohen-Tannoudji, "Bose-Einstein condensation of metastable helium," *Physical Review Letters*, vol. 86, no. 16, pp. 3459–3462, 2001.

[27] G. Modugno, G. Ferrari, G. Roati, R. J. Brecha, A. Simoni, and M. Inguscio, "Bose-Einstein condensation of potassium atoms by sympathetic cooling," *Science*, vol. 294, no. 5545, pp. 1320–1322, 2001.

[28] G. Roati, M. Zaccanti, C. D'Errico, J. Catani, M. Modugno, A. Simoni, M. Inguscio, and G. Modugno, "K39 Bose-Einstein Condensate with Tunable Interactions," *Physical Review Letters*, vol. 99, p. 010403, July 2007.

[29] T. Weber, J. Herbig, M. Mark, H. C. Nagerl, and R. Grimm, "Bose-Einstein condensation of cesium," *Science*, vol. 299, no. 5604, pp. 232–235, 2003.

[30] A. Griesmaier, J. Werner, S. Hensler, J. Stuhler, and T. Pfau, "Bose-Einstein Condensation of Chromium," *Physical Review Letters*, vol. 94, p. 160401, Apr. 2005.

[31] S. Kraft, F. Vogt, O. Appel, F. Riehle, and U. Sterr, "Bose-Einstein Condensation of Alkaline Earth Atoms: 40Ca," *Physical Review Letters*, vol. 103, p. 130401, Sept. 2009.

[32] M. Lu, N. Q. Burdick, S. H. Youn, and B. L. Lev, "Strongly Dipolar Bose-Einstein Condensate of Dysprosium," *Physical Review Letters*, vol. 107, p. 190401, Oct. 2011.

[33] S. Stellmer, M. K. Tey, B. Huang, R. Grimm, and F. Schreck, "Bose-Einstein Condensation of Strontium," *Physical Review Letters*, vol. 103, p. 200401, Nov. 2009.

[34] S. Stellmer, M. K. Tey, R. Grimm, and F. Schreck, "Bose-Einstein condensation of Sr-86," *Physical Review A*, vol. 82, no. 4, 2010.

[35] P. G. Mickelson, Y. N. M. de Escobar, M. Yan, B. J. DeSalvo, and T. C. Killian, "Bose-Einstein condensation of 88Sr through sympathetic cooling with 87Sr," *Physical Review A*, vol. 81, p. 051601, May 2010.

[36] Y. Takasu, K. Maki, K. Komori, T. Takano, K. Honda, M. Kumakura, T. Yabuzaki, and Y. Takahashi, "Spin-singlet Bose-Einstein condensation of two-electron atoms," *Physical Review Letters*, vol. 91, no. 4, 2003.

[37] T. Fukuhara, S. Sugawa, and Y. Takahashi, "Bose-Einstein condensation of an ytterbium isotope," *Physical Review A*, vol. 76, p. 051604, Nov. 2007.

[38] T. Fukuhara, S. Sugawa, Y. Takasu, and Y. Takahashi, "All-optical formation of quantum degenerate mixtures," *Physical Review A*, vol. 79, p. 021601, Feb. 2009.

[39] S. Sugawa, R. Yamazaki, S. Taie, and Y. Takahashi, "Bose-Einstein condensate in gases of rare atomic species," *Physical Review A*, vol. 84, p. 011610, July 2011.

[40] Y. J. Lin, K. Jimenez-Garcia, and I. B. Spielman, "Spin–orbit-coupled Bose–Einstein condensates," *Nature*, vol. 471, pp. 83–86, Mar. 2011.

[41] M. C. Beeler, R. A. Williams, K. Jimenez-Garcia, L. J. LeBlanc, A. R. Perry, and I. B. Spielman, "The spin Hall effect in a quantum gas," *Nature*, vol. 498, pp. 201–204, June 2013.

[42] C. J. Myatt, E. A. Burt, R. W. Ghrist, E. A. Cornell, and C. E. Wieman, "Production of two overlapping Bose-Einstein condensates by sympathetic cooling," *Physical Review Letters*, vol. 78, no. 4, pp. 586–589, 1997.

[43] J. Kasprzak, M. Richard, S. Kundermann, A. Baas, P. Jeambrun, J. M. J. Keeling, F. M. Marchetti, M. H. Szymańska, R. André, J. L. Staehli, V. Savona, P. B. Littlewood, B. Deveaud, and L. S. Dang, "Bose-Einstein condensation of exciton polaritons," *Nature*, vol. 443, pp. 409–414, Sept. 2006.

[44] J. Klaers, J. Schmitt, F. Vewinger, and M. Weitz, "Bose–Einstein condensation of photons in an optical microcavity," *Nature*, vol. 468, pp. 545–548, Nov. 2010.

[45] T. Giamarchi, C. Rüegg, and O. Tchernyshyov, "Bose–Einstein condensation in magnetic insulators," *Nature Physics*, vol. 4, pp. 198–204, Mar. 2008.

[46] C. N. Yang, "Concept of Off-Diagonal Long-Range Order and the Quantum Phases of Liquid He and of Superconductors," *Reviews of Modern Physics*, vol. 34, pp. 694–703, Oct. 1962.

[47] M. R. Andrews, C. G. Townsend, H. J. Miesner, D. S. Durfee, D. M. Kurn, and W. Ketterle, "Observation of Interference Between Two Bose Condensates," *Science*, vol. 275, pp. 637–641, Jan. 1997.

[48] L. Deng, E. W. Hagley, J. Wen, M. Trippenbach, Y. Band, P. S. Julienne, J. E. Simsarian, K. Helmerson, S. L. Rolston, and W. D. Phillips, "Four-wave mixing with matter waves," *Nature*, vol. 398, pp. 218–220, Mar. 1999.

[49] S. Inouye, T. Pfau, S. Gupta, A. P. Chikkatur, A. Görlitz, D. E. Pritchard, and W. Ketterle, "Phase-coherent amplification of atomic matter waves," *Nature*, vol. 402, pp. 641–644, Dec. 1999.

[50] J. Stenger, S. Inouye, A. P. Chikkatur, D. M. Stamper-Kurn, D. E. Pritchard, and W. Ketterle, "Bragg Spectroscopy of a Bose-Einstein Condensate," *Physical Review Letters*, vol. 82, pp. 4569–4573, June 1999.

[51] E. W. Hagley, L. Deng, M. Kozuma, M. Trippenbach, Y. B. Band, M. Edwards, M. Doery, P. S. Julienne, K. Helmerson, S. L. Rolston, and W. D. Phillips, "Measurement of the Coherence of a Bose-Einstein Condensate," *Physical Review Letters*, vol. 83, pp. 3112–3115, Oct. 1999.

[52] I. Bloch, T. W. Hänsch, and T. Esslinger, "Measurement of the spatial coherence of a trapped Bose gas at the phase transition," *Nature*, vol. 403, pp. 166–170, Jan. 2000.

[53] D. Hellweg, L. Cacciapuoti, M. Kottke, T. Schulte, K. Sengstock, W. Ertmer, and J. J. Arlt, "Measurement of the Spatial Correlation Function of Phase Fluctuating Bose-Einstein Condensates," *Physical Review Letters*, vol. 91, p. 010406, July 2003.

[54] I. Bloch, J. Dalibard, and W. Zwerger, "Many-body physics with ultracold gases," *Reviews of Modern Physics*, vol. 80, pp. 885–964, July 2008.

[55] K. Henderson, C. Ryu, C. MacCormick, and M. G. Boshier, "Experimental demonstration of painting arbitrary and dynamic potentials for Bose–Einstein condensates," *New Journal of Physics*, vol. 11, p. 043030, Apr. 2009.

[56] A. Görlitz, J. M. Vogels, A. E. Leanhardt, C. Raman, T. L. Gustavson, J. R. Abo-Shaeer, A. P. Chikkatur, S. Gupta, S. Inouye, T. Rosenband, and W. Ketterle, "Realization of Bose-Einstein Condensates in Lower Dimensions," *Physical Review Letters*, vol. 87, p. 130402, Sept. 2001.

[57] S. Dettmer, D. Hellweg, P. Ryytty, J. J. Arlt, W. Ertmer, K. Sengstock, D. S. Petrov, G. V. Shlyapnikov, H. Kreutzmann, L. Santos, and M. Lewenstein, "Observation of Phase Fluctuations in Elongated Bose-Einstein Condensates," *Physical Review Letters*, vol. 87, p. 160406, Oct. 2001.

[58] J. Esteve, J. B. Trebbia, T. Schumm, A. Aspect, C. I. Westbrook, and I. Bouchoule, "Observations of Density Fluctuations in an Elongated Bose Gas: Ideal Gas and Quasicondensate Regimes," *Physical Review Letters*, vol. 96, p. 130403, Apr. 2006.

[59] C. Ryu, P. W. Blackburn, A. A. Blinova, and M. G. Boshier, "Experimental Realization of Josephson Junctions for an Atom SQUID," *Physical Review Letters*, vol. 111, p. 205301, Nov. 2013.

[60] V. L. Berezinskii, "Destruction of long-range order in one-dimensional and two-dimensional systems possessing a continuous symmetry group. II. Quantum systems," *Soviet Physics, JETP*, vol. 34, no. 3, p. 610, 1972.

[61] J. M. Kosterlitz and D. J. Thouless, "Ordering, metastability and phase transitions in two-dimensional systems," *Journal of Physics C: Solid State Physics*, vol. 6, pp. 1181–1203, Apr. 1973.

[62] S. Stock, Z. Hadzibabic, B. Battelier, M. Cheneau, and J. Dalibard, "Observation of Phase Defects in Quasi-Two-Dimensional Bose-Einstein Condensates," *Physical Review Letters*, vol. 95, p. 190403, Nov. 2005.

[63] P. Krüger, Z. Hadzibabic, and J. Dalibard, "Critical Point of an Interacting Two-Dimensional Atomic Bose Gas," *Physical Review Letters*, vol. 99, p. 040402, July 2007.

[64] Z. Hadzibabic, P. Krüger, M. Cheneau, S. P. Rath, and J. Dalibard, "The trapped two-dimensional Bose gas: from Bose–Einstein condensation to Berezinskii–Kosterlitz–Thouless physics," *New Journal of Physics*, vol. 10, p. 045006, Apr. 2008.

[65] P. Cladé, C. Ryu, A. Ramanathan, K. Helmerson, and W. D. Phillips, "Observation of a 2D Bose Gas: From Thermal to Quasicondensate to Superfluid," *Physical Review Letters*, vol. 102, p. 170401, May 2009.

[66] O. Morsch and M. Oberthaler, "Dynamics of Bose-Einstein condensates in optical lattices," *Reviews of Modern Physics*, vol. 78, pp. 179–215, Feb. 2006.

[67] M. Greiner, O. Mandel, T. Esslinger, T. W. Hänsch, and I. Bloch, "Quantum phase transition from a superfluid to a Mott insulator in a gas of ultracold atoms," *Nature*, vol. 415, pp. 39–44, Jan. 2002.

[68] M. Greiner, O. Mandel, T. W. Hänsch, and I. Bloch, "Collapse and revival of the matter wave field of a Bose–Einstein condensate," *Nature*, vol. 419, pp. 51–54, Sept. 2002.

[69] A. S. Arnold, C. S. Garvie, and E. Riis, "Large magnetic storage ring for Bose-Einstein condensates," *Physical Review A*, vol. 73, p. 041606, Apr. 2006.

[70] C. Ryu, M. F. Andersen, P. Cladé, V. Natarajan, K. Helmerson, and W. D. Phillips, "Observation of Persistent Flow of a Bose-Einstein Condensate in a Toroidal Trap," *Physical Review Letters*, vol. 99, p. 260401, Dec. 2007.

[71] C. N. Weiler, T. W. Neely, D. R. Scherer, A. S. Bradley, M. J. Davis, and B. P. Anderson, "Spontaneous vortices in the formation of Bose–Einstein condensates," *Nature*, vol. 455, pp. 948–951, Oct. 2008.

[72] A. Ramanathan, K. C. Wright, S. R. Muniz, M. Zelan, I. W T Hill, C. J. Lobb, K. Helmerson, W. D. Phillips, and G. K. Campbell, "Superflow in a Toroidal Bose-Einstein Condensate: An Atom Circuit with a Tunable Weak Link," *Physical Review Letters*, vol. 106, p. 130401, Mar. 2011.

[73] C. Ryu, P. W. Blackburn, A. A. Blinova, and M. G. Boshier, "Experimental Realization of Josephson Junctions for an Atom SQUID," *Physical Review Letters*, vol. 111, p. 205301, Nov. 2013.

[74] M. F. Andersen, C. Ryu, P. Cladé, V. Natarajan, A. Vaziri, K. Helmerson, and W. D. Phillips, "Quantized Rotation of Atoms from Photons with Orbital Angular Momentum," *Physical Review Letters*, vol. 97, p. 170406, Oct. 2006.

[75] T. W. Neely, A. S. Bradley, E. C. Samson, S. J. Rooney, E. M. Wright, K. J. H. Law, R. Carretero-González, P. G. Kevrekidis, M. J. Davis, and B. P. Anderson, "Characteristics of Two-Dimensional Quantum Turbulence in a Compressible Superfluid," *Physical Review Letters*, vol. 111, p. 235301, Dec. 2013.

[76] A. L. Gaunt, T. F. Schmidutz, I. Gotlibovych, R. P. Smith, and Z. Hadzibabic, "Bose-Einstein Condensation of Atoms in a Uniform Potential," *Physical Review Letters*, vol. 110, p. 200406, May 2013.

[77] H. J. Miesner, D. M. Stamper-Kurn, M. R. Andrews, D. S. Durfee, S. Inouye, and W. Ketterle, "Bosonic Stimulation in the Formation of a Bose-Einstein Condensate," *Science*, vol. 279, pp. 1005–, Feb. 1998.

[78] M. Köhl, M. J. Davis, C. W. Gardiner, T. W. Hänsch, and T. Esslinger, "Growth of Bose-Einstein Condensates from Thermal Vapor," *Physical Review Letters*, vol. 88, p. 080402, Feb. 2002.

[79] D. S. Jin, J. R. Ensher, M. R. Matthews, C. E. Wieman, and E. A. Cornell, "Collective Excitations of a Bose-Einstein Condensate in a Dilute Gas," *Physical Review Letters*, vol. 77, pp. 420–423, July 1996.

[80] D. S. Jin, M. R. Matthews, J. R. Ensher, C. E. Wieman, and E. A. Cornell, "Temperature-Dependent Damping and Frequency Shifts in Collective Excitations of a Dilute Bose-Einstein Condensate," *Physical Review Letters*, vol. 78, pp. 764–767, Feb. 1997.

[81] D. M. Stamper-Kurn, H. J. Miesner, S. Inouye, M. R. Andrews, and W. Ketterle, "Collisionless and Hydrodynamic Excitations of a Bose-Einstein Condensate," *Physical Review Letters*, vol. 81, pp. 500–503, July 1998.

[82] O. M. Maragò, S. A. Hopkins, J. Arlt, E. Hodby, G. Hechenblaikner, and C. J. Foot, "Observation of the Scissors Mode and Evidence for Superfluidity of a Trapped Bose-Einstein Condensed Gas," *Physical Review Letters*, vol. 84, pp. 2056–2059, Mar. 2000.

[83] O. Maragò, G. Hechenblaikner, E. Hodby, and C. Foot, "Temperature Dependence of Damping and Frequency Shifts of the Scissors Mode of a Trapped Bose-Einstein Condensate," *Physical Review Letters*, vol. 86, pp. 3938–3941, Apr. 2001.

[84] R. Onofrio, D. S. Durfee, C. Raman, M. Köhl, C. E. Kuklewicz, and W. Ketterle, "Surface Excitations of a Bose-Einstein Condensate," *Physical Review Letters*, vol. 84, pp. 810–813, Jan. 2000.

[85] A. L. Fetter and A. A. Svidzinsky, "Vortices in a trapped dilute Bose-Einstein condensate," *Journal of Physics: Condensed Matter*, vol. 13, pp. R135–R194, Mar. 2001.

[86] D. J. Frantzeskakis, "Dark solitons in atomic Bose–Einstein condensates: from theory to experiments," *Journal of Physics A: Mathematical and General*, vol. 43, p. 213001, May 2010.

[87] S. Burger, K. Bongs, S. Dettmer, W. Ertmer, K. Sengstock, A. Sanpera, G. V. Shlyapnikov, and M. Lewenstein, "Dark Solitons in Bose-Einstein Condensates," *Physical Review Letters*, vol. 83, pp. 5198–5201, Dec. 1999.

[88] J. Denschlag, J. E. Simsarian, D. L. Feder, C. W. Clark, L. A. Collins, J. Cubizolles, L. Deng, E. W. Hagley, K. Helmerson, W. P. Reinhardt, S. L. Rolston, B. I. Schneider, and W. D. Phillips, "Generating Solitons by Phase Engineering of a Bose-Einstein Condensate," *Science*, vol. 287, pp. 97–101, Jan. 2000.

[89] Z. Dutton, M. Budde, C. Slowe, and L. V. Hau, "Observation of Quantum Shock Waves Created with Ultra- Compressed Slow Light Pulses in a Bose-Einstein Condensate," *Science*, vol. 293, pp. 663–668, July 2001.

[90] P. Engels and C. Atherton, "Stationary and Nonstationary Fluid Flow of a Bose-Einstein Condensate Through a Penetrable Barrier," *Physical Review Letters*, vol. 99, p. 160405, Oct. 2007.

[91] G. Lamporesi, S. Donadello, S. Serafini, F. Dalfovo, and G. Ferrari, "Spontaneous creation of Kibble–Zurek solitons in a Bose–Einstein condensate," *Nature Physics*, vol. 9, pp. 656–660, Oct. 2013.

[92] C. Becker, S. Stellmer, P. Soltan-Panahi, S. Dörscher, M. Baumert, E.-M. Richter, J. Kronjäger, K. Bongs, and K. Sengstock, "Oscillations and interactions of dark and dark–bright solitons in Bose–Einstein condensates," *Nature Physics*, vol. 4, pp. 496–501, June 2008.

[93] A. Weller, J. P. Ronzheimer, C. Gross, J. Esteve, M. K. Oberthaler, D. J. Frantzeskakis, G. Theocharis, and P. G. Kevrekidis, "Experimental Observation of

Oscillating and Interacting Matter Wave Dark Solitons," *Physical Review Letters*, vol. 101, p. 130401, Sept. 2008.

[94] S. Stellmer, C. Becker, P. Soltan-Panahi, E. M. Richter, S. Dörscher, M. Baumert, J. Kronjäger, K. Bongs, and K. Sengstock, "Collisions of Dark Solitons in Elongated Bose-Einstein Condensates," *Physical Review Letters*, vol. 101, p. 120406, Sept. 2008.

[95] C. Hamner, J. J. Chang, P. Engels, and M. A. Hoefer, "Generation of Dark-Bright Soliton Trains in Superfluid-Superfluid Counterflow," *Physical Review Letters*, vol. 106, p. 065302, Feb. 2011.

[96] C. Hamner, Y. Zhang, J. J. Chang, C. Zhang, and P. Engels, "Phase Winding a Two-Component Bose-Einstein Condensate in an Elongated Trap: Experimental Observation of Moving Magnetic Orders and Dark-Bright Solitons," *Physical Review Letters*, vol. 111, p. 264101, Dec. 2013.

[97] K. E. Strecker, G. B. Partridge, A. G. Truscott, and R. G. Hulet, "Formation and propagation of matter-wave soliton trains," *Nature*, vol. 417, pp. 150–153, May 2002.

[98] L. Khaykovich, F. Schreck, G. Ferrari, T. Bourdel, J. Cubizolles, L. D. Carr, Y. Castin, and C. Salomon, "Formation of a Matter-Wave Bright Soliton," *Science*, vol. 296, pp. 1290–1293, May 2002.

[99] S. L. Cornish, S. T. Thompson, and C. E. Wieman, "Formation of Bright Matter-Wave Solitons during the Collapse of Attractive Bose-Einstein Condensates," *Physical Review Letters*, vol. 96, p. 170401, May 2006.

[100] N. P. Proukakis and B. Jackson, "Finite-temperature models of Bose–Einstein condensation," *Journal of Physics B: Atomic Molecular and Optical Physics*, vol. 41, p. 203002, Oct. 2008.

[101] E. P. Gross, "Structure of a quantized vortex in boson systems," *Il Nuovo Cimento (1955-1965)*, vol. 20, pp. 454–477, May 1961.

[102] L. P. Pitaevskii, "Vortex lines in an imperfect Bose gas," *Soviet Physics, JETP*, vol. 13, no. 2, pp. 451–454, 1961.

[103] P. A. Ruprecht, M. J. Holland, K. Burnett, and M. Edwards, "Time-dependent solution of the nonlinear Schrödinger equation for Bose-condensed trapped neutral atoms," *Physical Review A*, vol. 51, pp. 4704–4711, June 1995.

[104] F. Dalfovo, S. Giorgini, L. P. Pitaevskii, and S. Stringari, "Theory of Bose-Einstein condensation in trapped gases," *Reviews of Modern Physics*, vol. 71, pp. 463–512, Apr. 1999.

[105] T. P. Simula, P. Engels, I. Coddington, V. Schweikhard, E. A. Cornell, and R. J. Ballagh, "Observations on Sound Propagation in Rapidly Rotating Bose-Einstein Condensates," *Physical Review Letters*, vol. 94, p. 080404, Mar. 2005.

[106] P. B. Blakie, A. S. Bradley, M. J. Davis, R. J. Ballagh, and C. W. Gardiner, "Dynamics and statistical mechanics of ultra-cold Bose gases using c-field techniques," *Advances in Physics*, vol. 57, no. 5, pp. 363–455, 2008.

[107] C. Raman, J. R. Abo-Shaeer, J. M. Vogels, K. Xu, and W. Ketterle, "Vortex Nucleation in a Stirred Bose-Einstein Condensate," *Physical Review Letters*, vol. 87, p. 210402, Nov. 2001.

[108] Haljan, P. C., I. Coddington, P. Engels, and E. A. Cornell, "Driving Bose-Einstein-Condensate Vorticity with a Rotating Normal Cloud," *Physical Review Letters*, vol. 87, p. 210403, Nov. 2001.

[109] D. Dagnino, N. Barberán, M. Lewenstein, and J. Dalibard, "Vortex nucleation as a case study of symmetry breaking in quantum systems," *Nature Physics*, vol. 5, pp. 431–437, June 2009.

[110] P. D. Drummond, P. Deuar, and K. V. Kheruntsyan, "Canonical Bose Gas Simulations with Stochastic Gauges," *Physical Review Letters*, vol. 92, p. 040405, Jan. 2004.

[111] V. A. Kashurnikov, N. V. Prokof'ev, and B. V. Svistunov, "Critical Temperature Shift in Weakly Interacting Bose Gas," *Physical Review Letters*, vol. 87, p. 120402, Aug. 2001.

[112] M. J. Davis, S. A. Morgan, and K. Burnett, "Simulations of Bose Fields at Finite Temperature," *Physical Review Letters*, vol. 87, p. 160402, Sept. 2001.

[113] A. Sinatra, C. Lobo, and Y. Castin, "Classical-Field Method for Time Dependent Bose-Einstein Condensed Gases," *Physical Review Letters*, vol. 87, p. 210404, Nov. 2001.

[114] K. Góral, M. Gajda, and K. Rzażewski, "Thermodynamics of an interacting trapped Bose-Einstein gas in the classical field approximation," *Physical Review A*, vol. 66, p. 051602, Nov. 2002.

[115] A. S. Bradley, C. W. Gardiner, and M. J. Davis, "Bose-Einstein condensation from a rotating thermal cloud: Vortex nucleation and lattice formation," *Physical Review A*, vol. 77, p. 033616, Mar. 2008.

[116] B. Damski and W. H. Zurek, "Soliton Creation During a Bose-Einstein Condensation," *Physical Review Letters*, vol. 104, p. 160404, Apr. 2010.

[117] A. Das, J. Sabbatini, and W. H. Zurek, "Winding up superfluid in a torus via Bose Einstein condensation," *Scientific Reports*, vol. 2, p. 352, Apr. 2012.

[118] S.-W. Su, S.-C. Gou, A. Bradley, O. Fialko, and J. Brand, "Kibble-Zurek Scaling and its Breakdown for Spontaneous Generation of Josephson Vortices in Bose-Einstein Condensates," *Physical Review Letters*, vol. 110, p. 215302, May 2013.

[119] R. G. McDonald and A. S. Bradley, "Reservoir interactions during Bose-Einstein condensation: Modified critical scaling in the Kibble-Zurek mechanism of defect formation," *Physical Review A*, vol. 92, p. 033616, Sept. 2015.

[120] S. J. Rooney, P. B. Blakie, B. P. Anderson, and A. S. Bradley, "Suppression of Kelvon-induced decay of quantized vortices in oblate Bose-Einstein condensates," *Physical Review A*, vol. 84, p. 023637, Aug. 2011.

[121] S. J. Rooney, T. W. Neely, B. P. Anderson, and A. S. Bradley, "Persistent-current formation in a high-temperature Bose-Einstein condensate: An experimental test for classical-field theory," *Physical Review A*, vol. 88, p. 063620, Dec. 2013.

[122] S. J. Rooney, A. J. Allen, U. Zülicke, N. P. Proukakis, and A. S. Bradley, "Reservoir interactions of a vortex in a trapped three-dimensional Bose-Einstein condensate," *Physical Review A*, vol. 93, p. 063603, June 2016.

[123] S. P. Cockburn, H. E. Nistazakis, T. P. Horikis, P. G. Kevrekidis, N. P. Proukakis, and D. J. Frantzeskakis, "Matter-Wave Dark Solitons: Stochastic versus Analytical Results," *Physical Review Letters*, vol. 104, p. 174101, Apr. 2010.

[124] S. P. Cockburn, H. E. Nistazakis, T. P. Horikis, P. G. Kevrekidis, N. P. Proukakis, and D. J. Frantzeskakis, "Fluctuating and dissipative dynamics of dark solitons in quasicondensates," *Physical Review A*, vol. 84, p. 043640, Oct. 2011.

[125] M. Wouters and V. Savona, "Stochastic classical field model for polariton condensates," *Physical Review B*, vol. 79, p. 165302, Apr. 2009.

[126] S.-W. Su, C.-H. Hsueh, I.-K. Liu, T.-L. Horng, Y.-C. Tsai, S.-C. Gou, and W. M. Liu, "Spontaneous crystallization of skyrmions and fractional vortices in fast-rotating and rapidly quenched spin-1 Bose-Einstein condensates," *Physical Review A*, vol. 84, p. 023601, Aug. 2011.

[127] S.-W. Su, I.-K. Liu, Y.-C. Tsai, W. M. Liu, and S.-C. Gou, "Crystallized half-skyrmions and inverted half-skyrmions in the condensation of spin-1 Bose gases with spin-orbit coupling," *Physical Review A*, vol. 86, p. 023601, Aug. 2012.

[128] C.-F. Liu and W. M. Liu, "Spin-orbit-coupling-induced half-skyrmion excitations in rotating and rapidly quenched spin-1 Bose-Einstein condensates," *Physical Review A*, vol. 86, p. 033602, Sept. 2012.

[129] C.-F. Liu, H. Fan, Y.-C. Zhang, D.-S. Wang, and W.-M. Liu, "Circular-hyperbolic skyrmion in rotating pseudo-spin-1/2 Bose-Einstein condensates with spin-orbit coupling," *Physical Review A*, vol. 86, p. 053616, Nov. 2012.

[130] S.-W. Song, L. Wen, C.-F. Liu, S.-C. Gou, and W.-M. Liu, "Ground states, solitons and spin textures in spin-1 Bose-Einstein condensates," *Frontiers of Physics*, vol. 8, pp. 302–318, June 2013.

[131] M. C. Garrett, T. M. Wright, and M. J. Davis, "Condensation and quasicondensation in an elongated three-dimensional Bose gas," *Physical Review A*, vol. 87, p. 063611, June 2013.

[132] H. T. C. Stoof and M. J. Bijlsma, "Dynamics of Fluctuating Bose–Einstein Condensates," *Journal of Low Temperature Physics*, vol. 124, no. 3-4, pp. 431–442, 2001.

[133] R. A. Duine and H. T. C. Stoof, "Stochastic dynamics of a trapped Bose-Einstein condensate," *Physical Review A*, vol. 65, p. 013603, Dec. 2001.

[134] N. P. Proukakis, "Interplay of density and phase fluctuations in ultracold one-dimensional Bose gases," *Physical Review A*, vol. 73, p. 023605, Feb. 2006.

[135] N. P. Proukakis, "Spatial correlation functions of one-dimensional Bose gases at equilibrium," *Physical Review A*, vol. 74, p. 053617, Nov. 2006.

[136] N. P. Proukakis, J. Schmiedmayer, and H. T. C. Stoof, "Quasicondensate growth on an atom chip," *Physical Review A*, vol. 73, p. 053603, May 2006.

[137] S. P. Cockburn and N. P. Proukakis, "The stochastic Gross-Pitaevskii equation and some applications," *Laser Physics*, vol. 19, pp. 558–570, Apr. 2009.

[138] S. P. Cockburn, A. Negretti, N. P. Proukakis, and C. Henkel, "Comparison between microscopic methods for finite-temperature Bose gases," *Physical Review A*, vol. 83, p. 043619, Apr. 2011.

[139] S. P. Cockburn, D. Gallucci, and N. P. Proukakis, "Quantitative study of quasi-one-dimensional Bose gas experiments via the stochastic Gross-Pitaevskii equation," *Physical Review A*, vol. 84, p. 023613, Aug. 2011.

[140] M. J. Davis, P. B. Blakie, A. H. van Amerongen, N. J. Van Druten, and K. V. Kheruntsyan, "Yang-Yang thermometry and momentum distribution of a trapped one-dimensional Bose gas," *Physical Review A*, vol. 85, p. 031604, Mar. 2012.

[141] D. Gallucci, S. P. Cockburn, and N. P. Proukakis, "Phase coherence in quasicondensate experiments: An *ab initio* analysis via the stochastic Gross-Pitaevskii equation," *Physical Review A*, vol. 86, p. 013627, July 2012.

[142] S. P. Cockburn and N. P. Proukakis, "*Ab initio* methods for finite-temperature two-dimensional Bose gases," *Physical Review A*, vol. 86, p. 033610, Sept. 2012.

[143] H. Stoof, "Initial stages of Bose-Einstein condensation," *Physical Review Letters*, vol. 78, no. 5, pp. 768–771, 1997.

[144] H. T. C. Stoof, "Coherent Versus Incoherent Dynamics During Bose-Einstein Condensation in Atomic Gases," *Journal of Low Temperature Physics*, vol. 114, no. 1-2, pp. 11–108, 1999.

[145] C. W. Gardiner, J. R. Anglin, and T. I. A. Fudge, "The stochastic Gross-Pitaevskii equation," *Journal of Physics B: Atomic Molecular and Optical Physics*, vol. 35, pp. 1555–1582, Mar. 2002.

[146] C. W. Gardiner and M. J. Davis, "The stochastic Gross-Pitaevskii equation: II," *Journal of Physics B: Atomic Molecular and Optical Physics*, vol. 36, no. 23, pp. 4731–4753, 2003.

[147] A. S. Bradley and C. W. Gardiner, "The stochastic Gross-Pitaevskii equation: III," *arxiv.org/abs/cond-mat/0602162v1*, Feb. 2006.

[148] S. J. Rooney, P. B. Blakie, and A. S. Bradley, "Stochastic projected Gross-Pitaevskii equation," *Physical Review A*, vol. 86, p. 053634, Nov. 2012.

[149] A. S. Bradley and P. B. Blakie, "Stochastic projected Gross-Pitaevskii equation for spinor and multicomponent condensates," *Physical Review A*, vol. 90, p. 023631, Aug. 2014.

[150] R. G. McDonald and A. S. Bradley, "Brownian motion of a matter-wave bright soliton moving through a thermal cloud of distinct atoms," *Physical Review A*, vol. 93, p. 063604, June 2016.

[151] M. J. Steel, M. K. Olsen, L. I. Plimak, P. D. Drummond, S. M. Tan, M. J. Collett, D. F. Walls, and R. Graham, "Dynamical quantum noise in trapped Bose-Einstein condensates," *Physical Review A*, vol. 58, pp. 4824–4835, Dec. 1998.

[152] T. P. Billam, P. Mason, and S. A. Gardiner, "Second-order number-conserving description of nonequilibrium dynamics in finite-temperature Bose-Einstein condensates," *Physical Review A*, vol. 87, p. 033628, Mar. 2013.

[153] A. L. Fetter and J. D. Walecka, *Quantum Theory of Many-particle Systems*. Dover Books on Physics, Dover Publications, 2003.

[154] A. J. Leggett, "Bose-Einstein condensation in the alkali gases: Some fundamental concepts," *Reviews of Modern Physics*, vol. 73, pp. 307–356, Apr. 2001.

[155] L. P. Pitaevskii and S. Stringari, *Bose-Einstein condensation*. Oxford: Oxford University Press, 2002.

[156] C. Pethick and H. Smith, *Bose-Einstein condensation in dilute gases*. Cambridge ; New York: Cambridge University Press, 2nd ed. ed., 2008.

[157] C. W. Gardiner and P. Zoller, *Quantum Noise*. Springer, 2nd edition ed., 1999.

[158] H. J. Carmichael, *Statistical Methods in Quantum Optics 1.* Berlin Heidelberg: Springer-Verlag, 1999.

[159] A. Polkovnikov, "Phase space representation of quantum dynamics," *Annals of Physics*, vol. 325, pp. 1790–1852, Aug. 2010.

[160] P. D. Drummond and C. W. Gardiner, "Generalised P-representations in quantum optics," *Journal of Physics A: Mathematical and General*, vol. 13, pp. 2353–2368, July 1980.

[161] C. W. Gardiner, "Particle-number-conserving Bogoliubov method which demonstrates the validity of the time-dependent Gross-Pitaevskii equation for a highly condensed Bose gas," *Physical Review A*, vol. 56, pp. 1414–1423, Aug. 1997.

[162] Y. Castin and R. Dum, "Low-temperature Bose-Einstein condensates in time-dependent traps: Beyond the U(1) symmetry-breaking approach," *Physical Review A*, vol. 57, pp. 3008–3021, Apr. 1998.

[163] S. A. Morgan, "A gapless theory of Bose-Einstein condensation in dilute gases at finite temperature," *Journal of Physics B: Atomic Molecular and Optical Physics*, vol. 33, no. 19, pp. 3847–3893, 2000.

[164] A. Sinatra, C. Lobo, and Y. Castin, "The truncated Wigner method for Bose-condensed gases: limits of validity and applications," *Journal of Physics B: Atomic Molecular and Optical Physics*, vol. 35, pp. 3599–3631, Aug. 2002.

[165] A. A. Norrie, R. J. Ballagh, and C. W. Gardiner, "Quantum Turbulence in Condensate Collisions: An Application of the Classical Field Method," *Physical Review Letters*, vol. 94, p. 040401, Jan. 2005.

[166] A. A. Norrie, R. J. Ballagh, and C. W. Gardiner, "Quantum turbulence and correlations in Bose-Einstein condensate collisions," *Physical Review A*, vol. 73, p. 043617, Apr. 2006.

[167] A. Polkovnikov, "Quantum corrections to the dynamics of interacting bosons: Beyond the truncated Wigner approximation," *Physical Review A*, vol. 68, p. 053604, Nov. 2003.

[168] A. A. Norrie, R. J. Ballagh, C. W. Gardiner, and A. S. Bradley, "Three-body recombination of ultracold Bose gases using the truncated Wigner method," *Physical Review A*, vol. 73, p. 043618, Apr. 2006.

[169] R. G. Scott, D. A. W. Hutchinson, and C. W. Gardiner, "Disruption of reflecting Bose-Einstein condensates due to interatomic interactions and quantum noise," *Physical Review A*, vol. 74, p. 053605, Nov. 2006.

[170] P. Jain, A. S. Bradley, and C. W. Gardiner, "Quantum de Laval nozzle: Stability and quantum dynamics of sonic horizons in a toroidally trapped Bose gas containing a superflow," *Physical Review A*, vol. 76, p. 023617, Aug. 2007.

[171] R. G. Scott and D. A. W. Hutchinson, "Incoherence of Bose-Einstein condensates at supersonic speeds due to quantum noise," *Physical Review A*, vol. 78, p. 063614, Dec. 2008.

[172] R. G. Scott, T. E. Judd, and T. M. Fromhold, "Exploiting Soliton Decay and Phase Fluctuations in Atom Chip Interferometry of Bose-Einstein Condensates," *Physical Review Letters*, vol. 100, p. 100402, Mar. 2008.

[173] S. Wüster, B. J. Dabrowska-Wüster, A. S. Bradley, M. J. Davis, P. B. Blakie, J. J. Hope, and C. M. Savage, "Quantum depletion of collapsing Bose-Einstein condensates," *Physical Review A*, vol. 75, p. 043611, Apr. 2007.

[174] C. Lobo and A. Sinatra, "Vortex Lattice Formation in Bose-Einstein Condensates," *Physical Review Letters*, vol. 92, p. 020403, Jan. 2004.

[175] T. M. Wright, R. J. Ballagh, A. S. Bradley, P. B. Blakie, and C. W. Gardiner, "Dynamical thermalization and vortex formation in stirred two-dimensional Bose-Einstein condensates," *Physical Review A*, vol. 78, p. 063601, Dec. 2008.

[176] A. D. Martin and J. Ruostekoski, "Quantum and Thermal Effects of Dark Solitons in a One-Dimensional Bose Gas," *Physical Review Letters*, vol. 104, p. 194102, May 2010.

[177] A. D. Martin and J. Ruostekoski, "Nonequilibrium quantum dynamics of atomic dark solitons," *New Journal of Physics*, vol. 12, p. 055018, May 2010.

[178] B. J. Dabrowska-Wüster, S. Wüster, and M. J. Davis, "Dynamical formation and interaction of bright solitary waves and solitons in the collapse of Bose–Einstein condensates with attractive interactions," *New Journal of Physics*, vol. 11, p. 053017, May 2009.

[179] A. D. Martin and J. Ruostekoski, "Quantum dynamics of atomic bright solitons under splitting and recollision, and implications for interferometry," *New Journal of Physics*, vol. 14, p. 043040, Apr. 2012.

[180] J. L. Helm, S. J. Rooney, C. Weiss, and S. A. Gardiner, "Splitting bright matter-wave solitons on narrow potential barriers: Quantum to classical transition and applications to interferometry," *Physical Review A*, vol. 89, p. 033610, Mar. 2014.

[181] B. Gertjerenken, T. P. Billam, C. L. Blackley, C. R. Le Sueur, L. Khaykovich, S. L. Cornish, and C. Weiss, "Generating Mesoscopic Bell States via Collisions of Distinguishable Quantum Bright Solitons," *Physical Review Letters*, vol. 111, p. 100406, Sept. 2013.

[182] R. J. Marshall, G. H. C. New, K. Burnett, and S. Choi, "Exciting, cooling, and vortex trapping in a Bose-condensed gas," *Physical Review A*, vol. 59, pp. 2085–2093, Mar. 1999.

[183] M. J. Davis, R. J. Ballagh, and K. Burnett, "Dynamics of thermal Bose fields in the classical limit," *Journal of Physics B: Atomic Molecular and Optical Physics*, vol. 34, pp. 4487–4512, Nov. 2001.

[184] M. J. Davis, S. A. Morgan, and K. Burnett, "Simulations of thermal Bose fields in the classical limit," *Physical Review A*, vol. 66, p. 053618, Nov. 2002.

[185] B. V. Svistunov, "Highly nonequilibrium Bose condensation in a weakly interacting gas," *Journal of the Moscow Physical Society*, vol. 1, p. 373, 1991.

[186] Y. M. Kagan, B. V. Svistunov, and G. V. Shlyapnikov, "Kinetics of Bose condensation in an interacting Bose gas," *Journal of Experimental and Theoretical Physics*, vol. 101, pp. 528–539, 1992.

[187] Y. M. Kagan and B. V. Svistunov, "Kinetics of the onset of long-range order during Bose condensation in an interacting gas," *Soviet Physics, JETP*, vol. 78, p. 353, 1994.

[188] Y. Kagan and B. V. Svistunov, "Evolution of Correlation Properties and Appearance of Broken Symmetry in the Process of Bose-Einstein Condensation," *Physical Review Letters*, vol. 79, pp. 3331–3334, Nov. 1997.

[189] K. Damle, S. N. Majumdar, and S. Sachdev, "Phase ordering kinetics of the Bose gas," *Physical Review A*, vol. 54, pp. 5037–5041, Dec. 1996.

[190] M. J. Davis and P. B. Blakie, "Critical Temperature of a Trapped Bose Gas: Comparison of Theory and Experiment," *Physical Review Letters*, vol. 96, p. 060404, Feb. 2006.

[191] M. J. Davis and S. A. Morgan, "Microcanonical temperature for a classical field: Application to Bose-Einstein condensation," *Physical Review A*, vol. 68, p. 053615, Nov. 2003.

[192] P. B. Blakie and M. J. Davis, "Projected Gross-Pitaevskii equation for harmonically confined Bose gases at finite temperature," *Physical Review A*, vol. 72, p. 063608, Dec. 2005.

[193] P. B. Blakie and M. J. Davis, "Classical region of a trapped Bose gas," *Journal of Physics B: Atomic Molecular and Optical Physics*, vol. 40, pp. 2043–2053, June 2007.

[194] A. Bezett, E. Toth, and P. B. Blakie, "Two-point correlations of a trapped interacting Bose gas at finite temperature," *Physical Review A*, vol. 77, p. 023602, Feb. 2008.

[195] A. Bezett and P. B. Blakie, "Critical properties of a trapped interacting Bose gas," *Physical Review A*, vol. 79, p. 033611, Mar. 2009.

[196] T. M. Wright, P. B. Blakie, and R. J. Ballagh, "Temporal coherence, anomalous moments, and pairing correlations in the classical-field description of a degenerate Bose gas," *Physical Review A*, vol. 82, p. 013621, July 2010.

[197] T. M. Wright, N. P. Proukakis, and M. J. Davis, "Many-body physics in the classical-field description of a degenerate Bose gas," *Physical Review A*, vol. 84, p. 023608, Aug. 2011.

[198] A. Bezett and P. B. Blakie, "Projected Gross-Pitaevskii equation theory of finite-temperature collective modes for a trapped Bose gas," *Physical Review A*, vol. 79, p. 023602, Feb. 2009.

[199] M. Brewczyk, M. Gajda, and K. Rzażewski, "Classical fields approximation for bosons at nonzero temperatures," *Journal of Physics B: Atomic Molecular and Optical Physics*, vol. 40, pp. R1–R37, Jan. 2007.

[200] T. Karpiuk, M. Brewczyk, M. Gajda, and K. Rzażewski, "Constructing a classical field for a Bose-Einstein condensate in an arbitrary trapping potential: Quadrupole oscillations at nonzero temperatures," *Physical Review A*, vol. 81, p. 013629, Jan. 2010.

[201] T. Karpiuk, P. Deuar, P. Bienias, E. Witkowska, K. Pawłowski, M. Gajda, K. Rzażewski, and M. Brewczyk, "Spontaneous Solitons in the Thermal Equilibrium of a Quasi-1D Bose Gas," *Physical Review Letters*, vol. 109, p. 205302, Nov. 2012.

[202] D. F. Walls and G. J. Milburn, *Quantum Optics*. Springer Berlin Heidelberg, 2nd ed., 2008.

[203] C. W. Gardiner and P. Zoller, "Quantum kinetic theory: A quantum kinetic master equation for condensation of a weakly interacting Bose gas without a trapping potential," *Physical Review A*, vol. 55, pp. 2902–2921, Apr. 1997.

[204] D. Jaksch, C. W. Gardiner, and P. Zoller, "Quantum kinetic theory. II. Simulation of the quantum Boltzmann master equation," *Physical Review A*, vol. 56, pp. 575–586, July 1997.

[205] C. W. Gardiner and P. Zoller, "Quantum kinetic theory. III. Quantum kinetic master equation for strongly condensed trapped systems," *Physical Review A*, vol. 58, pp. 536–556, July 1998.

[206] D. Jaksch, C. W. Gardiner, K. M. Gheri, and P. Zoller, "Quantum kinetic theory. IV. Intensity and amplitude fluctuations of a Bose-Einstein condensate at finite temperature including trap loss," *Physical Review A*, vol. 58, pp. 1450–1464, Aug. 1998.

[207] C. W. Gardiner and P. Zoller, "Quantum kinetic theory.V.Quantum kinetic master equation for mutual interaction of condensate and noncondensate," *Physical Review A*, vol. 61, p. 033601, Feb. 2000.

[208] M. D. Lee and C. W. Gardiner, "Quantum kinetic theory.VI. The growth of a Bose-Einstein condensate," *Physical Review A*, vol. 62, p. 033606, Aug. 2000.

[209] M. J. Davis, C. W. Gardiner, and R. J. Ballagh, "Quantum kinetic theory. VII. The influence of vapor dynamics on condensate growth," *Physical Review A*, vol. 62, p. 063608, Nov. 2000.

[210] C. W. Gardiner, P. Zoller, R. J. Ballagh, and M. J. Davis, "Kinetics of Bose-Einstein Condensation in a Trap," *Physical Review Letters*, vol. 79, pp. 1793–1796, Sept. 1997.

[211] C. W. Gardiner, M. D. Lee, R. J. Ballagh, M. J. Davis, and P. Zoller, "Quantum Kinetic Theory of Condensate Growth: Comparison of Experiment and Theory," *Physical Review Letters*, vol. 81, pp. 5266–5269, Dec. 1998.

[212] L. P. Gorkov, "Microscopic derivation of the Ginzburg-Landau equations in the theory of superconductivity," *Soviet Physics, JETP*, vol. 36(9), p. 1364, 1959.

[213] I. S. Aranson and L. Kramer, "The world of the complex Ginzburg-Landau equation," *Reviews of Modern Physics*, vol. 74, pp. 99–143, Feb. 2002.

[214] J. R. Anglin and W. H. Zurek, "Vortices in the Wake of Rapid Bose-Einstein Condensation," *Physical Review Letters*, vol. 83, pp. 1707–1710, Aug. 1999.

[215] E. B. Linscott and P. B. Blakie, "Thermally activated local collapse of a flattened dipolar condensate," *Physical Review A*, vol. 90, p. 053605, Nov. 2014.

[216] J. Anglin, "Cold, Dilute, Trapped Bosons as an Open Quantum System," *Physical Review Letters*, vol. 79, pp. 6–9, July 1997.

[217] L. Gilz and J. R. Anglin, "Quantum Kinetic Theory of Collisionless Superfluid Internal Convection," *Physical Review Letters*, vol. 107, p. 090601, Aug. 2011.

[218] R. Labouvie, B. Santra, S. Heun, S. Wimberger, and H. Ott, "Negative Differential Conductivity in an Interacting Quantum Gas," *Physical Review Letters*, vol. 115, p. 050601, July 2015.

[219] M. J. Davis, T. M. Wright, P. B. Blakie, A. S. Bradley, R. J. Ballagh, and C. W. Gardiner, "C-Field Methods for Non-Equilibrium Bose Gases," in *Quantum Gases: Finite Temperature and Non-Equilibrium Dynamics* (N. P. Proukakis, S. A. Gardiner, M. J. Davis, and M. H. Szymańska, eds.), p. 163, London: Imperial College Press, 2013.

[220] A. H. van Amerongen, J. J. P. van Es, P. Wicke, K. V. Kheruntsyan, and N. J. Van Druten, "Yang-Yang Thermodynamics on an Atom Chip," *Physical Review Letters*, vol. 100, p. 090402, Mar. 2008.

[221] S. Choi, S. A. Morgan, and K. Burnett, "Phenomenological damping in trapped atomic Bose-Einstein condensates," *Physical Review A*, vol. 57, pp. 4057–4060, May 1998.

[222] M. Tsubota, K. Kasamatsu, and M. Ueda, "Vortex lattice formation in a rotating Bose-Einstein condensate," *Physical Review A*, vol. 65, p. 023603, Jan. 2002.

[223] K. Kasamatsu, M. Tsubota, and M. Ueda, "Nonlinear dynamics of vortex lattice formation in a rotating Bose-Einstein condensate," *Physical Review A*, vol. 67, p. 033610, Mar. 2003.

[224] A. A. Penckwitt, R. J. Ballagh, and C. W. Gardiner, "Nucleation, Growth, and Stabilization of Bose-Einstein Condensate Vortex Lattices," *Physical Review Letters*, vol. 89, p. 260402, Dec. 2002.

[225] T. P. Billam, M. T. Reeves, B. P. Anderson, and A. S. Bradley, "Onsager-Kraichnan Condensation in Decaying Two-Dimensional Quantum Turbulence," *Physical Review Letters*, vol. 112, p. 145301, Apr. 2014.

[226] M. T. Reeves, T. P. Billam, B. P. Anderson, and A. S. Bradley, "Inverse Energy Cascade in Forced Two-Dimensional Quantum Turbulence," *Physical Review Letters*, vol. 110, p. 104501, Mar. 2013.

[227] C.-F. Liu, Y.-M. Yu, S.-C. Gou, and W.-M. Liu, "Vortex chain in anisotropic spin-orbit-coupled spin-1 Bose-Einstein condensates," *Physical Review A*, vol. 87, p. 063630, June 2013.

[228] D. Yan, R. Carretero-González, D. J. Frantzeskakis, P. G. Kevrekidis, N. P. Proukakis, and D. Spirn, "Exploring vortex dynamics in the presence of dissipation: Analytical and numerical results," *Physical Review A*, vol. 89, p. 043613, Apr. 2014.

[229] A. A. Norrie, *A Classical Field Treatment of Colliding Bose-Einstein Condensates*. PhD thesis, University of Otago, 2005.

[230] R. J. Glauber, "Coherent and Incoherent States of the Radiation Field," *Physical Review*, vol. 131, pp. 2766–2788, Sept. 1963.

[231] E. C. Sudarshan, "Equivalence of Semiclassical and Quantum Mechanical Descriptions of Statistical Light Beams," *Physical Review Letters*, vol. 10, pp. 277–279, Apr. 1963.

[232] P. D. Drummond and S. J. Carter, "Quantum-field theory of squeezing in solitons," *Optical Society of America*, vol. 4, pp. 1565–1573, Oct. 1987.

[233] A. Gilchrist, C. W. Gardiner, and P. D. Drummond, "Positive P representation: Application and validity," *Physical Review A*, vol. 55, pp. 3014–3032, Apr. 1997.

[234] P. D. Drummond and J. F. Corney, "Quantum dynamics of evaporatively cooled Bose-Einstein condensates," *Physical Review A*, vol. 60, pp. R2661–R2664, Oct. 1999.

[235] U. V. Poulsen and K. Mølmer, "Positive-P simulations of spin squeezing in a two-component Bose condensate," *Physical Review A*, vol. 64, p. 013616, June 2001.

[236] P. Deuar and P. D. Drummond, "First-principles quantum dynamics in interacting Bose gases: I. The positive P representation," *Journal of Physics A: Mathematical and General*, vol. 39, pp. 1163–1181, Feb. 2006.

[237] U. V. Poulsen and K. Mølmer, "Quantum states of Bose-Einstein condensates formed by molecular dissociation," *Physical Review A*, vol. 63, p. 023604, Feb. 2001.

[238] C. M. Savage, P. E. Schwenn, and K. V. Kheruntsyan, "First-principles quantum simulations of dissociation of molecular condensates: Atom correlations in momentum space," *Physical Review A*, vol. 74, p. 033620, Sept. 2006.

[239] C. M. Savage and K. V. Kheruntsyan, "Spatial Pair Correlations of Atoms in Molecular Dissociation," *Physical Review Letters*, vol. 99, p. 220404, Nov. 2007.

[240] S. L. W. Midgley, S. Wüster, M. K. Olsen, M. J. Davis, and K. V. Kheruntsyan, "Comparative study of dynamical simulation methods for the dissociation of molecular Bose-Einstein condensates," *Physical Review A*, vol. 79, p. 053632, May 2009.

[241] A. Griffin, T. Nikuni, and E. Zaremba, *Bose-Condensed Gases at Finite Temperatures*. Cambridge: Cambridge University Press, 2009.

[242] A. Griffin, "Conserving and gapless approximations for an inhomogeneous Bose gas at finite temperatures," *Physical Review B*, vol. 53, pp. 9341–9347, Apr. 1996.

[243] A. Minguzzi and M. P. Tosi, "Linear density response in the random-phase approximation for confined Bose vapours at finite temperature," *Journal of Physics: Condensed Matter*, vol. 9, pp. 10211–10223, Nov. 1997.

[244] T. R. Kirkpatrick and J. R. Dorfman, "Transport theory for a weakly interacting condensed Bose gas," *Physical Review A*, vol. 28, pp. 2576–2579, Oct. 1983.

[245] U. Eckern, "Relaxation processes in a condensed Bose gas," *Journal of Low Temperature Physics*, vol. 54, pp. 333–359, Feb. 1984.

[246] R. Walser, J. Williams, J. Cooper, and M. Holland, "Quantum kinetic theory for a condensed bosonic gas," *Physical Review A*, vol. 59, pp. 3878–3889, May 1999.

[247] R. Walser, J. Cooper, and M. Holland, "Reversible and irreversible evolution of a condensed bosonic gas," *Physical Review A*, vol. 63, p. 013607, Dec. 2000.

[248] N. P. Proukakis, "Self-consistent quantum kinetics of condensate and non-condensate via a coupled equation of motion formalism," *Journal of Physics B: Atomic Molecular and Optical Physics*, vol. 34, pp. 4737–4755, Dec. 2001.

[249] E. Zaremba, T. Nikuni, and A. Griffin, "Dynamics of Trapped Bose Gases at Finite Temperatures," *Journal of Low Temperature Physics*, vol. 116, no. 3-4, pp. 277–345, 1999.

[250] B. Jackson and E. Zaremba, "Finite-Temperature Simulations of the Scissors Mode in Bose-Einstein Condensed Gases," *Physical Review Letters*, vol. 87, p. 100404, Aug. 2001.

[251] B. Jackson and C. S. Adams, "Damping and revivals of collective oscillations in a finite-temperature model of trapped Bose-Einstein condensation," *Physical Review A*, vol. 63, p. 053606, Apr. 2001.

[252] B. Jackson and E. Zaremba, "Quadrupole Collective Modes in Trapped Finite-Temperature Bose-Einstein Condensates," *Physical Review Letters*, vol. 88, p. 180402, Apr. 2002.

[253] B. Jackson and E. Zaremba, "Modeling Bose-Einstein condensed gases at finite temperatures with N-body simulations," *Physical Review A*, vol. 66, p. 033606, Sept. 2002.

[254] T. Nikuni and A. Griffin, "Landau-Khalatnikov two-fluid hydrodynamics of a trapped Bose gas," *Physical Review A*, vol. 63, p. 033608, Feb. 2001.

[255] T. Nikuni and A. Griffin, "Frequency and damping of hydrodynamic modes in a trapped Bose-condensed gas," *Physical Review A*, vol. 69, p. 023604, Feb. 2004.

[256] J. E. Williams, E. Zaremba, B. Jackson, T. Nikuni, and A. Griffin, "Dynamical Instability of a Condensate Induced by a Rotating Thermal Gas," *Physical Review Letters*, vol. 88, p. 070401, Jan. 2002.

[257] B. Jackson, N. P. Proukakis, and C. F. Barenghi, "Dark-soliton dynamics in Bose-Einstein condensates at finite temperature," *Physical Review A*, vol. 75, p. 051601, May 2007.

[258] B. Jackson, C. F. Barenghi, and N. P. Proukakis, "Matter Wave Solitons at Finite Temperatures," *Journal of Low Temperature Physics*, vol. 148, pp. 387–391, June 2007.

[259] B. Jackson, N. P. Proukakis, C. F. Barenghi, and E. Zaremba, "Finite-temperature vortex dynamics in Bose-Einstein condensates," *Physical Review A*, vol. 79, p. 053615, May 2009.

[260] A. J. Allen, E. Zaremba, C. F. Barenghi, and N. P. Proukakis, "Observable vortex properties in finite-temperature Bose gases," *Physical Review A*, vol. 87, p. 013630, Jan. 2013.

[261] S. A. Gardiner and S. A. Morgan, "Number-conserving approach to a minimal self-consistent treatment of condensate and noncondensate dynamics in a degenerate Bose gas," *Physical Review A*, vol. 75, p. 043621, Apr. 2007.

[262] P. Mason and S. A. Gardiner, "Number-conserving approaches to n-component Bose-Einstein condensates," *Physical Review A*, vol. 89, p. 043617, Apr. 2014.

[263] T. P. Billam and S. A. Gardiner, "Coherence and instability in a driven Bose–Einstein condensate: a fully dynamical number-conserving approach," *New Journal of Physics*, vol. 14, p. 013038, Jan. 2012.

[264] S. A. Morgan, M. Rusch, D. A. W. Hutchinson, and K. Burnett, "Quantitative Test of Thermal Field Theory for Bose-Einstein Condensates," *Physical Review Letters*, vol. 91, p. 250403, Dec. 2003.

[265] T. M. Wright, M. J. Davis, and N. P. Proukakis, "Reconciling the Classical-Field Method with the Beliaev Broken-Symmetry Approach," in *Quantum Gases: Finite Temperature and Non-Equilibrium Dynamics* (N. P. Proukakis, S. A. Gardiner, M. J. Davis, and M. H. Szymańska, eds.), p. 299, Imperial College Press, 2013.

[266] S. Stock, Z. Hadzibabic, B. Battelier, M. Cheneau, and J. Dalibard, "Observation of Phase Defects in Quasi-Two-Dimensional Bose-Einstein Condensates," *Physical Review Letters*, vol. 95, p. 190403, Nov. 2005.

[267] C. Gardiner and P. Zoller, *The Quantum World of Ultra-Cold Atoms and Light*. Book 1: Foundations of Quantum Optics, Imperial College Press, 2014.

[268] M. Naraschewski and R. J. Glauber, "Spatial coherence and density correlations of trapped Bose gases," *Physical Review A*, vol. 59, pp. 4595–4607, June 1999.

[269] A. S. Bradley, *Theoretical investigations of trapped ultra-cold Bose gases: Rotating Bose-Einstein Condensation and Anomolous Segregation*. PhD thesis, Victoria University of Wellington, 2005.

[270] E. Wigner, "On the Quantum Correction For Thermodynamic Equilibrium," *Physical Review*, vol. 40, pp. 749–759, June 1932.

[271] R. Graham, "Statistical Theory of Instabilities in Stationary Nonequilibrium Systems with Applications to Lasers and Nonlinear Optics," in *Springer Tracts in Modern Physics*, pp. 1–97, Berlin, Heidelberg: Springer, Berlin, Heidelberg, 1973.

[272] C. W. Gardiner, *Stochastic Methods*. Springer, 4th edition ed., 2009.

[273] P. B. Blakie, "Numerical method for evolving the projected Gross-Pitaevskii equation," *Physical Review E*, vol. 78, p. 026704, Aug. 2008.

[274] G. N. Milstein and M. V. Tretyakov, *Stochastic Numerics for Mathematical Physics*. Scientific Computation, Springer Berlin Heidelberg, 2013.

[275] P. B. Blakie, C. Ticknor, A. S. Bradley, A. M. Martin, M. J. Davis, and Y. Kawaguchi, "Numerical method for evolving the dipolar projected Gross-Pitaevskii equation," *Physical Review E*, vol. 80, p. 016703, July 2009.

[276] M. J. Bijlsma, E. Zaremba, and H. T. C. Stoof, "Condensate growth in trapped Bose gases," *Physical Review A*, vol. 62, p. 063609, Nov. 2000.

[277] W. Z. Bao and J. Shen, "Fourth-order time-splitting Laguerre-Hermite pseudospectral method for Bose-Einstein condensates," *Siam Journal on Scientific Computing*, vol. 26, no. 6, pp. 2010–2028, 2005.

[278] C. M. Dion and E. Cancès, "Spectral method for the time-dependent Gross-Pitaevskii equation with a harmonic trap," *Physical Review E*, vol. 67, p. 046706, Apr. 2003.

[279] N. Navon, A. L. Gaunt, R. P. Smith, and Z. Hadzibabic, "Critical dynamics of spontaneous symmetry breaking in a homogeneous Bose gas," *Science*, vol. 347, no. 6218, pp. 167–170, 2015.

[280] G. Gauthier, I. Lenton, N. M. Parry, M. Baker, M. J. Davis, H. Rubinsztein-Dunlop, and T. W. Neely, "Direct imaging of a digital-micromirror device for configurable microscopic optical potentials," *Optica*, vol. 3, pp. 1136–1143, Oct. 2016.

[281] A. S. Bradley, P. B. Blakie, and C. W. Gardiner, "Properties of the stochastic Gross–Pitaevskii equation: finite temperature Ehrenfest relations and the optimal plane wave representation," *Journal of Physics B: Atomic Molecular and Optical Physics*, vol. 38, pp. 4259–4280, Dec. 2005.

[282] P. Ehrenfest, "Bemerkung über die angenäherte Gültigkeit der klassischen Mechanik innerhalb der Quantenmechanik," *Zeitschrift für Physik*, vol. 45, pp. 455–457, July 1927.

[283] B. C. Hall, *Quantum Theory for Mathematicians*, vol. 267 of *Graduate Texts in Mathematics*. New York, NY: Springer New York, 2013.

[284] D. J. Griffiths, *Introduction to Quantum Mechanics*. Pearson international edition, Upper Saddle River, NJ: Pearson Prentice Hall, 2nd ed., 2005.

[285] B. M. Caradoc-Davies, *Vortex Dynamics in Bose-Einstein Condensates*. PhD thesis, University of Otago.

[286] A. S. Bradley, S. J. Rooney, and R. G. McDonald, "Low-dimensional stochastic projected Gross-Pitaevskii equation," *Physical Review A*, vol. 92, p. 033631, Sept. 2015.

[287] W. Kohn, "Cyclotron Resonance and De Haas-Van Alphen Oscillations of an Interacting Electron Gas," *Physical Review*, vol. 123, no. 4, pp. 1242–&, 1961.

[288] J. F. Dobson, "Harmonic-Potential Theorem - Implications for Approximate Many-Body Theories," *Physical Review Letters*, vol. 73, no. 16, pp. 2244–2247, 1994.

[289] D. S. Rokhsar, "Vortex stability and persistent currents in trapped Bose gases," *Physical Review Letters*, vol. 79, no. 12, pp. 2164–2167, 1997.

[290] P. Tabeling, "Two-dimensional turbulence: a physicist approach," *Physics Reports*, vol. 362, pp. 1–62, May 2002.

[291] G. Boffetta and R. E. Ecke, "Two-Dimensional Turbulence," *Annual Review of Fluid Mechanics*, vol. 44, pp. 427–451, Dec. 2011.

[292] M. S. Paoletti and D. P. Lathrop, "Quantum Turbulence," *Annual Review of Condensed Matter Physics*, vol. 2, pp. 213–234, Feb. 2011.

[293] R. J. Donnelly, *Quantized Vortices in Helium II*. Cambridge: Cambridge University Press, 1991.

[294] L. M. Pismen, *Vortices in Nonlinear Fields: From Liquid Crystals to Superfluids, from Non-equilibrium Patterns to Cosmic Strings*. Oxford: Clarendon Press, 1999.

[295] G. Blatter, M. V. Feigel'man, V. B. Geshkenbein, A. I. Larkin, and V. M. Vinokur, "Vortices in high-temperature superconductors," *Reviews of Modern Physics*, vol. 66, pp. 1125–1388, Oct. 1994.

[296] B. Link, "Dynamics of Quantum Vorticity in a Random Potential," *Physical Review Letters*, vol. 102, p. 131101, Apr. 2009.

[297] J. R. Abo-Shaeer, C. Raman, J. M. Vogels, and W. Ketterle, "Observation of Vortex Lattices in Bose-Einstein Condensates," *Science*, vol. 292, pp. 476–479, Apr. 2001.

[298] E. Madelung, "Eine anschauliche Deutung der Gleichung von Schrödinger," *Die Naturwissenschaften*, vol. 14, pp. 1004–1004, Nov. 1926.

[299] E. Madelung, "Quantentheorie in hydrodynamischer Form," *Zeitschrift für Physik*, vol. 40, pp. 322–326, Mar. 1927.

[300] Haljan, P. C., B. P. Anderson, I. Coddington, and E. A. Cornell, "Use of Surface-Wave Spectroscopy to Characterize Tilt Modes of a Vortex in a Bose-Einstein Condensate," *Physical Review Letters*, vol. 86, pp. 2922–2925, Apr. 2001.

[301] V. Bretin, P. Rosenbusch, F. Chevy, G. V. Shlyapnikov, and J. Dalibard, "Quadrupole Oscillation of a Single-Vortex Bose-Einstein Condensate: Evidence for Kelvin Modes," *Physical Review Letters*, vol. 90, p. 100403, Mar. 2003.

[302] B. P. Anderson, Haljan, P. C., C. E. Wieman, and E. A. Cornell, "Vortex Precession in Bose-Einstein Condensates: Observations with Filled and Empty Cores," *Physical Review Letters*, vol. 85, pp. 2857–2860, Oct. 2000.

[303] T. W. Neely, E. C. Samson, A. S. Bradley, M. J. Davis, and B. P. Anderson, "Observation of Vortex Dipoles in an Oblate Bose-Einstein Condensate," *Physical Review Letters*, vol. 104, p. 160401, Apr. 2010.

[304] D. V. Freilich, D. M. Bianchi, A. M. Kaufman, T. K. Langin, and D. S. Hall, "Real-Time Dynamics of Single Vortex Lines and Vortex Dipoles in a Bose-Einstein Condensate," *Science*, vol. 329, pp. 1182–, Sept. 2010.

[305] K. W. Madison, F. Chevy, W. Wohlleben, and J. Dalibard, "Vortex Formation in a Stirred Bose-Einstein Condensate," *Physical Review Letters*, vol. 84, pp. 806–809, Jan. 2000.

[306] E. J. M. Madarassy and C. F. Barenghi, "Vortex Dynamics in Trapped Bose-Einstein Condensate," *Journal of Low Temperature Physics*, vol. 152, pp. 122–135, May 2008.

[307] A. S. Bradley and C. W. Gardiner, "Diffusive instability of a vortex in a rotating Bose gas," *arxiv.org/abs/cond-mat/0509592v1*, Sept. 2005.

[308] A. S. Bradley and B. P. Anderson, "Energy Spectra of Vortex Distributions in Two-Dimensional Quantum Turbulence," *Physical Review X*, vol. 2, p. 041001, Oct. 2012.

[309] R. A. Duine, B. W. A. Leurs, and H. T. C. Stoof, "Noisy dynamics of a vortex in a partially Bose-Einstein condensed gas," *Physical Review A*, vol. 69, p. 053623, May 2004.

[310] G. Gauthier, M. T. Reeves, X. Yu, A. S. Bradley, M. Baker, T. A. Bell, H. Rubinsztein-Dunlop, M. J. Davis, and T. W. Neely, "Negative-Temperature Onsager Vortex Clusters in a Quantum Fluid," *arxiv.org/abs/1801.06951v1*, Jan. 2018.

[311] A. J. Groszek, M. J. Davis, and T. P. Simula, "Decaying quantum turbulence in a two-dimensional Bose-Einstein condensate at finite temperature," *arxiv.org/abs/1903.05528v1*, Mar. 2019.

[312] Y. Liu, E. Gomez, S. E. Maxwell, L. D. Turner, E. Tiesinga, and P. D. Lett, "Number Fluctuations and Energy Dissipation in Sodium Spinor Condensates," *Physical Review Letters*, vol. 102, p. 225301, June 2009.

[313] A. C. Mathey, C. W. Clark, and L. Mathey, "Decay of a superfluid current of ultracold atoms in a toroidal trap," *Physical Review A*, vol. 90, p. 023604, Aug. 2014.

[314] A. Kumar, S. Eckel, F. Jendrzejewski, and G. K. Campbell, "Temperature-induced decay of persistent currents in a superfluid ultracold gas," *Physical Review A*, vol. 95, p. 021602, Feb. 2017.

[315] M. Kunimi and I. Danshita, "Thermally activated phase slips of one-dimensional Bose gases in shallow optical lattices," *Physical Review A*, vol. 95, p. 033637, Mar. 2017.

[316] J. Polo, R. Dubessy, P. Pedri, H. Perrin, and A. Minguzzi, "Oscillations and decay of superfluid currents in a one-dimensional Bose gas on a ring," *arxiv.org/abs/1903.09229v1*, Mar. 2019.

[317] A. S. Bradley, C. W. Gardiner, and M. J. Davis, "Bose-Einstein condensation from a rotating thermal cloud: Vortex nucleation and lattice formation," *Physical Review A*, vol. 77, p. 033616, Mar. 2008.

[318] P. D. Drummond and I. K. Mortimer, "Computer simulations of multiplicative stochastic differential equations," *Journal of Computational Physics*, vol. 93, pp. 144–170, Mar. 1991.

[319] M. J. Werner and P. D. Drummond, "Robust Algorithms for Solving Stochastic Partial Differential Equations," *Journal of Computational Physics*, vol. 132, pp. 312–326, Apr. 1997.